uOttawa

L'Université canadienne
Canada's university

FACULTÉ DES ÉTUDES SUPÉRIEURES ET POSTOCTORALES

uOttawa

L'Université canadienne
Canada's university

FACULTY OF GRADUATE AND POSDOCTORAL STUDIES

Togay Ozbakkaloglu

AUTEUR DE LA THÈSE / AUTHOR OF THESIS

Ph.D. (Civil Engineering)

GRADE / DEGREE

Department of Civil Engineering

FACULTÉ, ÉCOLE, DÉPARTEMENT / FACULTY, SCHOOL, DEPARTMENT

Seismic Performance of High-strength Concrete Columns in FRP Stay-in-place Formwork

TITRE DE LA THÈSE / TITLE OF THESIS

Murat Saatcioglu

DIRECTEUR (DIRECTRICE) DE LA THÈSE / THESIS SUPERVISOR

CO-DIRECTEUR (CO-DIRECTRICE) DE LA THÈSE / THESIS CO-SUPERVISOR

EXAMINATEURS (EXAMINATRICES) DE LA THÈSE / THESIS EXAMINERS

David Lau

Beatriz Martin-Perez

Dan Palermo

Sami Rizkalla

Gary W. Slater

LE DOYEN DE LA FACULTÉ DES ÉTUDES SUPÉRIEURES ET POSTDOCTORALES /
DEAN OF THE FACULTY OF GRADUATE AND POSTDOCORAL STUDIES

SEISMIC PERFORMANCE OF HIGH-STRENGTH CONCRETE COLUMNS IN FRP STAY-IN-PLACE FORMWORK

by

Togay Ozbakkaloglu

A thesis submitted to the Faculty of Graduate Studies and Research
in partial fulfillment of the requirements for the degree of
DOCTORATE OF PHILOSOPY
in Civil Engineering*

Department of Civil Engineering
University of Ottawa
Ottawa, Ontario, Canada
September 2005

* The Doctorate of Philosophy Program in Civil Engineering
is a joint program with Carleton University,
administered by the Ottawa-Carleton Institute for Civil Engineering

Your file Votre référence
ISBN: 0-494-11005-8
Our file Notre référence
ISBN: 0-494-11005-8

ABSTRACT

The use of high-strength concrete (HSC), with strengths reaching 130 MPa, has increased in recent years due to its superior performance and strength. Structures are designed and built utilizing HSC, especially in columns of multi-story buildings. However, the use of high-strength concrete (HSC) in seismically active regions poses a major concern because of the brittle nature of the material. The confinement requirements for HSC columns may be prohibitively stringent since they require proportionately greater confinement than columns of normal-strength concrete. An alternative to conventional confinement reinforcement is the use of fibre reinforced polymer (FRP) casings, in the form of a stay-in-place formwork. The use of stay-in-place FRP formwork as concrete confinement reinforcement for HSC columns was investigated. Large scale HSC building columns, encased in FRP casings, were tested under simulated seismic loading. The columns had 270 mm square and circular cross-sections and concrete strengths up to 90 MPa. The casings were manufactured from carbon FRP and epoxy resin. The unique aspects of the test program were the introduction of the corner radius as a test parameter, and the presence of internally placed FRP crossties in square columns, integrally built with column casings to improve the effectiveness of concrete confinement. Results indicate that the deformation capacity of HSC columns can be improved significantly by using FRP casings. The results further indicate that the confinement effectiveness of square columns is significantly affected by the corner radius of casings. Additionally, the confinement efficiency can be improved with the use of FRP crossties. The columns developed inelastic drift capacities of up to 12%, demonstrating the usefulness of FRP stay-in-place formwork in improving deformability of HSC columns.

Fibre-reinforced polymer (FRP) composite casings offer an attractive alternative to conventional reinforcement to enhance strength and deformability of concrete columns. FRP casings can be designed to increase lateral deformability of earthquake resistant columns significantly, while also providing some enhancement of load-carrying capacity. There is a clear need for a design procedure to compute lateral drift capacities of FRP encased square and circular columns. A design approach was developed that incorporates experimentally observed confinement parameters, while also incorporating axial load and lateral drift as design variables. The approach had evolved from a displacement based design procedure developed for concrete columns confined with conventional steel reinforcement. The expression derived as part of the proposed design procedure had been verified against available experimental data.

One of the shortcomings of the current design practice for HSC is the lack of accurate analytical models for strength calculations. Early cover spalling observed in tests and more brittle nature of stress-strain relationship need to be modelled for improved design of HSC columns. While the CSA Standard A23.3-04 provides a rectangular stress block applicable to HSC, it does tend to be over-conservative for certain strength ranges. Furthermore the rectangular stress block specified in ACI 318-05 Building Code for design of reinforced concrete elements was developed on the basis of normal-strength concrete column tests. Applicability of the ACI rectangular stress block to higher strength concretes becomes questionable, especially for members under high levels of axial compression. A new rectangular stress block is developed for a wide range of concrete strengths between 20 MPa and 130 MPa. The proposed stress block is verified against available test data. Column strengths computed using the stress block show good agreement with those recorded experimentally.

ACKNOWLEDGEMENT

I would like to express my gratitude to my advisor, Dr. Murat Saatcioglu, for his guidance and enthusiastic support throughout the course of this study.

Thanks are extended to the technical staff of the Civil Engineering Department of the University of Ottawa for their assistance during the experimental part of this research project.

Finally, I would like to thank my family for their continuous support and patience.

TABLE OF CONTENTS

LIST OF TABLES

LIST OF FIGURES

Chapter 1

Introduction

1.1 GENERAL

The use of high-strength concrete (HSC), with strengths exceeding 40 MPa, has increased in recent years. Concrete strengths of up to 130 MPa have become available in most major metropolitan centers. HSC offers superior performance and economy when used in multi-storey buildings and bridges and forms an attractive alternative to other construction materials. However, HSC poses a major challenge when used in earthquake resistant construction because of its brittle characteristics. Furthermore, new analytical methods are needed for improved design of HSC columns as the extension of methods and procedures developed for normal-strength concrete columns may not be applicable to strength and deformation calculations of these elements.

It is well established that the stress-strain characteristics of concrete change with strength. Therefore, a rectangular stress block established for normal-strength concretes may not be applicable to HSC. This is especially true for HSC columns where compressive stresses dominate the behaviour. It has been shown in the past that the ACI 318 stress block may lead to the overestimation of observed column strength, potentially leading to unsafe designs. It was also observed that the CSA A23.3 stress block, while intended for a wide range of concrete strengths,

can result in unnecessarily conservative results. A new rectangular stress block is needed to compute flexural capacities of HSC columns with sufficient accuracy.

HSC offers improved strength and performance, and hence provides an attractive alternative to normal-strength concrete. However, it creates a challenge for designers, especially for earthquake resistant design, because of its increased brittleness. New and practical techniques are needed to improve ductility of HSC, especially when used in compression members like columns. One approach to solving the problem of brittleness is to confine HSC with a material that is compatible in terms of strength. This implies that a material with higher strength than those used for conventional column confinement may need to be used for seismic design.

An innovative construction material that is being introduced to the construction industry is advanced polymer composites that have a successful history of use in aeronautical and space industries. Fibre reinforced polymers (FRP) have a number of benefits when compared with conventional steel reinforcement, which is widely used in concrete. These benefits can be summarized as follows:

1 High Strength-to-Weight Ratio: Proves to be advantageous in weight sensitive applications.

2 Non-Corrosive: High resistance to chemicals and other corrosive environments.

3 Non-Conductive: Provides excellent electrical and thermal insulation.

4 Good Fatigue Resistance: Performs very well in cyclic loading situations.

5 Good Impact Resistance: Resists sudden and severe point loading.

6 Magnetic Transparency: Not affected by electromagnetic fields; excellent for use in MRI and other types of electronic testing facilities.

7 Dimensionally Stable Under Thermal Loading: Reduced expansion / shrinkage in concrete when subjected to temperature variations.

8 Lightweight: Easily transported and assembled in the field without any need for expensive heavy lifting equipment.

9 Possible incorporation of optical fibre sensors.

Fibre reinforced polymers (FRP) are currently being considered for retrofitting existing concrete columns. FRP also offers potential for use in new construction, especially when used as FRP tubes, which can function as formwork for concrete, while also acting as confinement reinforcement to improve ductility.

1.2 RESEARCH NEEDS

External FRP systems have become increasingly popular in field applications despite limited experimental data available on their seismic performance. Most of the existing research focuses on repair, rehabilitation and retrofit of existing normal-strength concrete columns, overlooking potentials for application to new construction, especially to new HSC columns. On the other hand, multiple functions and effectiveness of FRP stay-in-place formwork offer advantages for use as confinement reinforcement, especially for a brittle material like HSC. Despite its potential, there is lack of research on the topic to develop generalized design methodologies. Furthermore, designing HSC structures requires an accurate representation of concrete stress-strain characteristics, with a representative stress block for ease in design calculations. An improved rectangular stress block is needed for HSC column design. Both strength and deformability of

HSC columns, confined with FRP stay-in-place formwork, need to be researched to develop design and construction techniques that can be substantiated by experimental and analytical evidence.

1.3 OBJECTIVE AND SCOPE

The objective of research, reported in this thesis, is to investigate experimentally and analytically the performance of normal and high strength concrete columns confined by pre-fabricated FRP casings to establish analysis and design techniques for use in structural engineering practice. The scope of research includes experimental and analytical tasks, as outlined below:

1 Literature review on the use of FRP jackets as concrete confinement.
2 Literature review of tests conducted on high-strength concrete columns.
3 Design, construction, and testing of large-scale square and circular concrete columns, confined by pre-fabricated FRP jackets, under reversed cyclic loading.
4 Evaluation of test data to establish the effectiveness of FRP as concrete confinement.
5 Development of a rectangular stress block for flexural strength calculations applicable to high-strength concrete.
6 Development of analytical techniques for analysis of FRP confined concrete columns under seismic loading.

1.4 PRESENTATION OF THESIS

The thesis is presented in the form of a collection of individually written technical papers. Following Chapters 1 and 2; outlining the objective, scope and literature review, Chapters 3 through 6 consist of separate papers on each major task of the overall research program. Chapters 3 and 4 report on the experimental investigation of circular and square FRP encased HSC columns under simulated seismic loading, respectively; Chapter 5 reports on the development of a rectangular stress block for normal and high strength concrete; and Chapter 6 reports on the

analytical investigation for predicting inelastic drift capacities of FRP encased concrete columns. Each of these chapters were written to be stand-alone documents, with individual equation numbers, list of notations and references, as appropriate, following the format required by the journal for which it was written. Conclusions derived in each paper were also included in respective chapters. However, the table and figure numbers have been reformatted for easy access within the thesis, as referenced in "List of Tables" and "List of Figures." Section headings were also renumbered for easy referencing in the "Table of Contents." Chapter 7 is the final chapter, and it provides a summary of conclusions listed at the end of each chapter, and recommendations for future research.

Chapter 2

Literature Review

2.1 GENERAL

The current research project is based on concepts that have been researched individually in the past. These concepts involve; i) the use of HSC as a construction material in building and bridge columns, and ii) confinement of concrete with FRP jackets. The previous research in these areas, as well as in related areas, has been surveyed prior to undertaking the current research program. The previous research on HSC columns and FRP confined concrete columns are reviewed below, in separate sections.

2.2 PREVIOUS RESEARCH ON HIGH-STRENGTH CONCRETE COLUMNS

Extensive experimental and analytical research has been conducted in the past to establish strength and deformability of HSC columns. A large number of column tests were conducted under monotonically increasing eccentric and concentric compression, as well as under simulated seismic loading. The former group of tests were essentially intended to establish the characteristics of confined concrete, while also providing insight into the confinement reinforcement requirements for columns. The latter group was essentially intended to develop design recommendations for earthquake resistant columns, while also used to verify analytical

techniques. The following is a list of previous research programs, with brief explanations of objectives, scope, research parameters and findings.

S. H. Ahmed, and S.P. Shah, 1982

Objective: Study the effect of spiral confinement reinforcement on stress-strain relationship of normal and high-strength concrete.

Scope: 96 normal and high-strength concrete cylinders were tested. 15 of the cylinders had 75 x 300 mm dimensions, the remaining were 75 x 150 mm. Concrete strengths up to 69 MPa were considered with two types of aggregates. There was no longitudinal reinforcement in the specimens.

Test Variables: Concrete strength, aggregate type, spiral pitch, yield strength of spiral reinforcement.

Conclusions: The researches reported that the efficiency of confinement by spiral reinforcement decreased with increased concrete strength. However, ductile behaviour of HSC was achieved when spirals with high yield strength were used sufficiently small pitch provided. It was further reported that the effectiveness of spiral reinforcement, with 413 MPa yield strength, was high for normal-density aggregate concrete, compared to low-density aggregate concrete.

The researches proposed an analytical procedure to predict the stress-strain relationship of confined concrete, based on tri-axial stress-strain curves for plain concrete and stress-strain relationship of confining steel. The researches conducted an analytical investigation using the proposed procedure. It was concluded analytically that as the concrete strength increased the steel stress at peak concrete stress decreased. This was attributed to the small lateral strain of HSC at the peak stress. However, the lateral strain increased rapidly after the peak, producing higher stresses in the spiral steel. It was further reported that, for the same concrete strength, the

stress in spiral steel corresponding to peak concrete stress, was independent of the yield strength. Consequently, increasing the yield strength of spiral steel did not produce beneficial effects on strength enhancement. On the other hand, the use of higher strength steel spirals improved the ductility of confined concrete

H. Mugumura, F. Watanabe, T. Iwashimizu, and R. Mitsueda, 1983

*Objective: The p*rimary objective of this investigation was to establish the effect of lateral confinement on axial ductility of square HSC columns. The researches also wanted to verify their idealized bi-linear stress-strain model, which was originally proposed for confined normal-strength concrete. (Watanabe et al. 1980)

Scope: 18 scaled square columns with concrete strength ranging between 34 MPa and 89 MPa were tested. Columns had a height of 400 mm and a square cross section of 147 x 147 mm. No longitudinal reinforcement provided in any columns. 14 columns were laterally reinforced with circular spirals, having 50 mm spacing and 1390 MPa yield strength. The volumetric ratio of the lateral reinforcement was 2.13%, except for 2 columns, which had 4.26% volumetric ratio.

Test Variables: Concrete strength and volumetric ratio of lateral reinforcement

Conclusions: The researches reported that the ductility of HSC could be significantly improved by using sufficient amount of confinement reinforcement, having high yield strength. The researches also implied that the high volumetric ratio of the lateral reinforcement was most beneficial to ductile behaviour. The stress-strain relationship originally proposed by the researches for normal-strength concrete was modified based on the experimental data obtained in this study.

S. Martinez, A.H. Nilson, and F. O. Slate, 1984

Objectives: The main objective of this study was to establish the differences between behaviour of HSC and normal-strength concrete (NSC).

Scope: 94 normal and high-strength concrete cylinders were tested. Cylinder dimensions were 102 x 203 mm, 102 x 406mm, 127 x 610 mm, and 152 x 610 mm. Concrete strength ranged between 21 MPa and 69 MPa. The specimens were confined with spirals having yield strengths of 379 MPa to 414 MPa. No longitudinal reinforcement was provided in the specimens.

Test Variables: Concrete strength, volumetric ratio of lateral reinforcement, and specimen size.

Conclusions: The researches reported that the compressive strength and ductility of concrete, as well as concrete strain at peak stress all increased with increasing confinement pressures, regardless of unconfined concrete strength. It was also reported the modulus of elasticity of spirally confined cylinders were essentially the same as for unconfined concrete. The spiral steel did not yield in cylinders with HSC. Consequently, it was recommended that the yield strength of spiral steel be limited to 414MPa. It was concluded that the ACI 318-83 building code recommendation provide sufficient strength gain in columns to compensate for spalling of cover up to 83 MPa. However, the decrease in capacity is much higher in HSC columns than in NSC columns. Also shown was the importance of the size effect, since small-scale specimens had higher strengths than comparable larger scale specimens. A stress-strain relationship was developed for confined concrete, based on the test data.

A. Fafitis and S. P. Shah, 1985

Objectives: Objective of the study was to modify the original confinement model, to include HSC

Scope: Researchers carried-out an investigation in order to modify original model proposed by Fafitis and Shah (1985) to include HSC. A computer program was employed using the theoretical procedure, which successfully predicted the other researchers` data. The modification was based on columns tested under concentric loading conducted by Mugumura et al. (1983) and Martinez et al. (1983).

Conclusions: Researchers proposed a relationship, which included concrete strength and confinement pressure as primary confinement parameters.

R. Basset and S. M. Uzumeri, 1986

Objectives: The objective of the investigation was to determine the behaviour of confined high-strength light-weight aggregate concrete (HSLWAC).

Scope: An experimental investigation was conducted on 15 reinforced and 3 unreinforced square columns loaded under monotonically increasing axial compression. The specimens had a cross-sectional core dimension of 305 mm and height of 1956 mm. The concrete strength varied between 37 MPa and 40 MPa. The yield strength of steel ties ranged from 530 MPa to 600 MPa.

Test Variables: The main variables considered in the experimental study included the distribution of longitudinal steel, hoop and crosstie configuration, vertical tie spacing, and amount of longitudinal and transverse reinforcement.

Conclusions: The results indicated that large amount of transverse reinforcement with well-distributed longitudinal reinforcement could improve the brittle behaviour of HSC significantly. The ductility of columns was also improved with increased amount of longitudinal reinforcement. This was attributed to the importance of percentage of longitudinal steel in preventing premature bar buckling. Additionally, increasing the amount of longitudinal

reinforcement increased the portion of load carried by steel, which prevented the sudden drop of load at cover spalling. Minimum longitudinal and transverse reinforcement was recommended to maintain a reasonable level of ductility in columns. It was also reported that the existing concrete confinement models gave unconservative results for HSLWAC, overestimating column ductility.

The ratio of in-place strength to cylinder strength of concrete (k_3) was observed to be 0.98, different from commonly used 0.85. Razvi and Saatcioglu (1994) reported that this ratio varied between 0.85 to 1.0 for high-strength normal-density concrete, and the average value of this variation increased with concrete strength.

Y. K. Yong, M.G. Nour, E. G. Nawy, 1988

Objectives: To study the effect of different transverse and longitudinal reinforcement arrangements on stress-strain relationship of HSC columns.

Scope: 24 square HSC, with the compressive strength ranged from 84 MPa to 94 MPa, were tested. The columns had a cross-sectional dimension of either 152 mm or 133 mm, and a height of 457 mm. The lateral reinforcement consisted of rectilinear ties with a yield strength of 496 MPa.

Test Variables: Volumetric ratio of lateral reinforcement, the longitudinal steel arrangement, and the cover concrete.

Conclusions: The researches reported that ductility of HSC columns significantly improved with proper confinement. The improvement increased with the increase in volumetric ratio of transverse reinforcement. It was reported that the lateral steel did not yield at the first peak load. Columns did not develop any effect of confinement when the tie spacing was increased to cross-

sectional dimension. Hence, it was recommended that the spacing of transverse reinforcement should be less than column cross-sectional dimension. The distribution of longitudinal reinforcement improved ductility of concrete. Consequently, it was recommended to use at least eight bars distributed around the column perimeter. It was further reported that concrete cover did not affect the stress-strain relationship of confined concrete. The available confinement models failed to reproduce descending branches of experimentally obtained stress-strain relationships.

The researches proposed an empirical stress-strain relationship for HSC confined with rectilinear ties. Strength enhancement due to confinement was assumed to be the function of concrete strength, diameter, spacing, volumetric ratio, and yield strength of lateral reinforcement, in addition to the number and diameter of longitudinal reinforcement.

L. Bjerkeli, A. Tomaszewics, and J. Jensen, 1990

Objectives: To study the deformation properties and ductility of HSC. Also studied was the effect of sustained load on HSC.

Scope: An experimental investigation was conducted on HSC with normal-density and low-density aggregates. The cube strengths ranged between 60 MPa and 90 MPa for for low-density aggregate concrete, and between 65 MPa and 115 MPa for normal-density aggregate.

116 columns tested in four series in order to investigate the short-term behaviour of confined and unconfined HSC. Series 1 to 3 consisted of small scale circular and square columns with cross-sectional dimension of 150 mm, where Series 4 consisted of large scale rectangular columns with 300 x 500 x 2000 mm dimensions. Columns with 8-bar and 12-bar arrangements were tested to

sudy the effect of longitudinal reinforcement distribution. The yield strength of transverse reinforcement was 613 MPa for small circular and square columns and it ranged between 506 MPa and 561 MPa for large scale rectangular columns.

Test Variables: Concrete strength, the amount and distribution of confinement steel, the affects of longitudinal reinforcement arrangement, strain rate.

Conclusions: The researches reported that ductility of HSC columns significantly improved with proper confinement. Use of large size longitudinal reinforcement did not produce any beneficial effect on ductility. However the distribution of longitudinal bars had a significant effect on column ductility, showing improvements with increased number of bars. The strain rate varied between 3.33×10^{-6} and 3.3×10^{-7} per second, and no significant effect reported on stress-strain relationship of confined concrete. Confinement effectiveness was reduced with increased concrete strength. The confinement efficiency for normal density concrete, in terms of strength enhancement, was significantly higher than the efficiency for low-density concrete. Behaviour of circular columns confined by circular spirals improved more than similar rectangular columns confined by rectilinear ties.

The researchers introduced a stress-stain relationship for confined normal and low-density concrete. The expression proposed by Martinez et al. (1984) were modified and used in identifying stress-strain relationship. The main parameters considered were concrete strength, section geometry, and confinement pressure.

S. W. Shin, M. Kamara and S. K. Gosh, 1990

Objectives: To investigate the flexural ductility of high-strength concrete members.

Scope: Two series of tests were conducted. The first series consisted of 12 specimens with 150 x 300 mm rectangular cross-section and 3000 mm height. These specimens were tested under monotonically increasing lateral loading and their concrete strength of ranged between 28 MPa and 103 MPa. The specimens of second series had 112.5 x 225 mm cross-section and 3000 mm height. These specimens were tested under reversed cyclic loading and their concrete strength ranged between 35 MPa and 103 MPa. All test specimens were tested under zero axial load.

Test Variables: The main test variables included the concrete strength, longitudinal reinforcement ratio; spacing of lateral reinforcement.

Conclusions: The results of the experimental investigation indicated that the ratio of tension reinforcement to balanced section reinforcement was the most significant factor for flexural ductility. The increase in this ratio resulted in reduced flexural ductility. It was observed that the envelope of load-deflection curves for specimens tested under reversed cyclic loading showed the same features as those tested under monotonically increasing lateral loading. A reduction in load carrying capacity was reported with repetition of cycles at the same deflection level, which was more significant in specimens with higher concrete strength, wider ties spacing, and lower volumetric ratio of transverse reinforcement. The rectangular stress block recommended by the ACI-318 code was found to produce good estimates of flexural capacities, for members with concrete strength up to 103 MPa.

B. V. Rangan, P. Saunders, and E. J. Seng, 1991

Objectives: To study the effects of different amount and type of transverse reinforcement.

Scope: An experimental investigation was conducted on 16 small-scale HSC columns. Concrete compressive strength was 65 MPa in all columns. 10 of these columns had a cross-sectional

dimension of 160 mm and a height of 800 mm, and were tested under concentric loading. The remaining 6 were slender columns with 100 x 100 x 2000 mm dimensions, and were tested under eccentric loading.

Test Variables: The amount and type of lateral steel

Conclusions: It was concluded that the confinement reinforcement did not have any significant effect on load-strain curves, despite the fact that yielding and rupture of confinement reinforcement was observed. This conclusion could be attributed to the low amount of confinement reinforcement used in columns. It was also reported that the experimental data from tests of short columns agreed well with those computed using the current building code.

T. Nagashima, S. Sugano, H. Kimura, A. Ichikawa, 1992

Objectives: To develop an analytical model for confined HSC

Scope: An experimental investigation was conducted on 26 large-scale HSC columns. The columns had a cross-sectional dimension of 225 mm and a height of 716 mm, and were confined with high or ultra-high strength steel.

Test Variables: Concrete strength, amount, yield strength and configuration of confinement reinforcement and yield strength of longitudinal reinforcement.

Conclusions: The researchers reported that ultra-HSC columns with concrete strengths of 120 MPa showed a sudden strength decay at an axial strain around 1% when confinement pressure ($\rho_s f_{yt}$) was less than 18 MPa. The same columns developed strains in excess of 2% when the confinement pressure was higher than 18 MPa. It was reported that longitudinal reinforcement arrangement did not have any significant effects, and columns with 6-bar, 8-bar, and 12-bar arrangements exhibited similar behaviour in terms of strength and ductility.

It was further reported that the strength enhancement due to confinement was independent of plain concrete strength, and was proportional to the square root of the effective confinement capacity. Ductility of confined concrete was directly proportional to the confinement capacity, and inversely proportional to the concrete strength.

The researchers developed an analytical model for confined HSC, based on the test data. The model incorporated the effectively confined concrete area concept for calculation of confined strength.

Y. Itakura, A. Yagenji, 1992

Objectives: To determine the effect of the test parameters on HSC columns.

Scope: An experimental investigation was conducted on 24 HSC square columns. The columns had a cross-sectional dimension of 218 mm and a height of 500 mm. Concrete compressive strength was 74 MPa, and no concrete cover was provided in any of the columns.

Test Variables: Amount, configuration and hook length of confinement reinforcement, and the effect of longitudinal reinforcement.

Conclusions: The researchers reported that the concrete strength was improved vastly by confinement steel. Ties with hook lengths of 6-bar diameter were not as effective as those with 10-bar diameter length. Buckling of longitudinal reinforcement was observed and that caused the fracture of the confinement reinforcement. It was further reported that columns with longitudinal reinforcement were less ductile than those without longitudinal reinforcement.

J. H. Thomsen and J. W. Wallace, 1994

Objectives: To investigate the possibility of using high-strength concrete columns in regions of moderate to high seismic risk.

Scope: An experimental investigation was conducted on 12 small-scale HSC columns, with concrete strengths ranging between 67 MPa and 103 MPa. The specimens had 152 mm square cross-section and either 737 mm or 813 mm height. All columns had eight laterally supported longitudinal reinforcements. Spacing of confinement reinforcement varied between 25 mm and 45 mm, whereas axial load levels ranged between 0% and 20% of their axial load capacity. The yield strength of confinement reinforcement was either 792 MPa or 1275 MPa.

Test Variables: The main variables included the concrete strength; the spacing and yield strength of transverse reinforcement; and the level of axial compression.

Conclusions: The results of the experimental investigation indicated that columns subjected to zero axial load developed lateral drifts in excess of 4% with no significant strength decay. On the other hand, columns subjected to 10% to 20% of their concentric capacity showed stable behaviour up to 2% lateral drift, with subsequent strength degradation. The researchers concluded that the confinement steel requirements of the ACI code were conservative for axial load levels of 0 to 20% of column concentric capacity. It was noted that the use of higher strength steel (1275 MPa vs. 792 MPa) did not affect column deformability, in the drift range of 2% or less. It was also concluded that although the use of high-strength steel could permit using larger tie spacing, buckling of longitudinal reinforcement in such cases should be adequately prevented.

S. A. Sheikh, D. V. Shah, and S.S. Khoury, 1994

Objectives: To investigate the seismic performance of high-strength concrete columns.

Scope: Four HSC columns were tested under axial load and cyclic displacement to simulate seismic loading. The specimens had 305 mm square cross-section, and approximately 2.3 m height. The concrete strength varied between 54 and 59 MPa, and all columns had eight-bar longitudinal reinforcement arrangement. The volumetric ratio of transverse steel ranged from 1.7% to 4.3%, with yield strengths varying between 464 MPa and 507 MPa. Axial load level ranged from 59% to 63 % of the column concentric capacity.

Test Variables: The main test variable was the volumetric ratio of confinement steel.

Conclusions: The results of the experimental investigation were compared with those of normal-strength concrete columns. The comparison indicated that the required amount of confinement reinforcement was proportional to concrete strength. It was reported that the column ductility was proportional to the amount of transverse reinforcement.

O. Bayrak and S. A. Sheikh, 1995

Objectives: To investigate the seismic performance of high-strength concrete columns.

Scope: Five HSC square columns were tested under simulated seismic loading. The specimens had 305 x 305 x 1473 mm dimensions. The concrete strengths of specimens were either 72 MPa or 102 MPa. Spacing of confinement reinforcement varied between 70 mm and 95 mm, whereas the volumetric ratio of transverse reinforcement ranged between 3.15% and 4.29%. Axial load levels considered ranged between 36% and 50% of the column axial-load capacity.

Test Variables: The main variables included the concrete strength; the amount and spacing of transverse reinforcement; and the level of axial load.

Conclusions: The results indicated that HSC column were less ductile than their normal strength counterparts when subjected to the same level of axial compression. Furthermore, the longitudinal reinforcement arrangement reported to have a significant effect on column ductility. The increase in axial load level was observed to reduce column deformability and increase stiffness degradation.

W. Lipien, M. Saatcioglu, 1995

Objectives: Evaluation of the deformability of confined high-strength concrete square columns.

Scope: An experimental investigation was conducted on 10 HSC square columns. The columns had 250 mm square cross-section, and 1640 mm column height. The columns were tested under constant axial compression of up to 28% of section concentric capacity, and incrementally increasing lateral deformation reversals. Test columns were cast using two different concrete mixes. Eight of the columns had a concrete strength of 104 MPa, while the other two columns had a concrete strength of 64 MPa. Longitudinal bars had either eight or twelve bar arrangement. The yield strength of transverse reinforcement ranged between 400 MPa and 1000 MPa. The volumetric ratio of transverse steel for core concrete section ranged between 1.9% and 5.58%, while vertical spacing of transverse steel varied between 45 mm and 62.5 mm.

Test Variables: Concrete strength; yield strength, volumetric ratio and spacing of transverse reinforcement; longitudinal reinforcement arrangement; and axial load level.

Conclusions: The test results indicated that the ductile behaviour of high-strength concrete columns could be achieved if sufficient amount of transverse reinforcement is provided. It was reported that increasing the volumetric ratio of transverse steel and reducing tie spacing resulted in improvement in column ductility. In addition, beneficial effects of high-strength transverse

steel were reported. However, the use of high-strength steel as transverse reinforcement did not have significant effect on column ductility, when the axial load level was low.

D. Baingo, M. Saatcioglu, 1995

Objectives: Evaluation of the deformability of confined high-strength concrete circular columns.

Scope: An experimental investigation was conducted on 9 HSC circular columns. The columns had 250 mm circular cross-section, and 1640 mm column height. The columns were tested under constant axial compression ranging from 22% to 43% of section concentric capacity, and incrementally increasing lateral deformation reversals. Test columns were cast using two different concrete mixes. Seven of the columns had a concrete strength of 90 MPa, while the other two columns had a concrete strength of 60 MPa. Columns either had circular hoops or circular spirals as transverse reinforcement. The yield strength of transverse reinforcement ranged between 400 MPa and 1000 MPa. The volumetric ratio of transverse steel for core concrete section ranged between 1.59% and 3.67%, while vertical spacing of transverse steel varied between 50 mm and 100 mm. Eight of the columns had a clear concrete cover of 10 mm, while the final column did not have any cover.

Test Variables: Concrete strength; type, yield strength, volumetric ratio and spacing of transverse reinforcement; thickness of concrete cover; and axial load level.

Conclusions: The test results indicated that the ductile behaviour of high-strength concrete columns could be achieved if sufficient amount of transverse reinforcement is provided. The results further indicated a superior performance of columns confined with high-strength transverse steel compared to those confined with normal-strength steel. The beneficial effects of high-strength transverse steel were more pronounced for columns subjected to high axial load

levels. Although, spirally confined columns and the columns confined with circular hoops showed similar behaviour, marginally better performance was observed in the spirally reinforced columns at high deformation levels. The concrete cover did not affect the deformability of the test columns for the thickness range considered.

F. Legeron, P. Paultre, 1995

Objectives: Evaluation of the behaviour of HSC square columns.

Scope: An experimental investigation was conducted on 6 HSC square columns. The columns had 305 mm square cross-section, and 2150 mm column height. The columns were tested under constant axial compression ranging from 15% to 40% of section concentric capacity, and incrementally increasing lateral deformation reversals. The concrete strength of test columns ranged between 92.4 MPa and 104.3 MPa. Columns were confined with conventional hoops and ties. The vertical spacing of ties ranged between 60 mm and 130 mm, while the volumetric ratio of transverse steel ranged between 1.96% and 4.26%.

Test Variables: Concrete strength; volumetric ratio and spacing of transverse reinforcement; and axial load level.

Conclusions: The test results indicated that HSC columns having sufficient amount of closely spaced transverse reinforcement demonstrated ductile behaviour. It was concluded that the column ductility was significantly affected by the level of axial load. It was also noted that the ACI and CSA codes were too conservative for HSC columns under the load levels considered in the test program.

H. H. H. Ibrahim and J. G. MacGregor, 1996

Objectives: To investigate the use of the rectangular stress block for high-strength and ultra-high-strength sections.

Scope: An experimental investigation was conducted on 20 eccentrically loaded high and ultra-high strength concrete specimens. The concrete cylinder strength of specimens ranged between 60 MPa and 130 MPa. The test program included two phases. The first phase consisted of 14 C-shaped specimens with a 200 x 300 mm rectangular cross section in the test region. Three of these specimens did not have reinforcement in the test region and 11 had vertical and horizontal reinforcement. The second phase consisted of six C-shaped specimens with a 450 x 240 mm triangular cross-section in the test region.

Test Variables: The main variables included in the test series were the concrete strength; diameter, spacing, and volumetric ratio confinement reinforcement; and the shape of the compression zone.

Conclusions: It was reported that the failure of plain concrete and lightly reinforced sections was very brittle. Columns with a tie spacing equal to the least column dimension failed suddenly when the cover spalled. The researchers concluded that a well-confined HSC section could show a ductile behavior, maintaining the applied loads through large deformations. It was also reported that the shape of the compression zone was an important parameter in determining the ductility of the section. The triangular compression zones exhibited more ductile behavior than the rectangular compression zones.

N. A. Lloyd and B. V. Rangan, 1996

Objectives: The objective of the investigation was to develop an approach to predict the load-deflection behaviour and the failure load of the high-strength concrete columns under eccentric compression.

Scope: An experimental investigation was conducted on 36 HSC columns. The columns either had 300 x 100 mm or 175 x 175 mm cross section, and 1680 mm effective length. Longitudinal reinforcement consisted of four or six deformed bars with 12 mm diameter and 430 MPa yield strength. The concrete cylinder strength ranged between 58 MPa and 97 MPa.

Test Variables: The main variables considered in the experimental study included the concrete strength, amount and distribution of longitudinal reinforcement, and the eccentricity of the axial load.

Conclusions: The results indicated the columns with small load eccentricity failed in a brittle manner. Column with larger load eccentricity were less brittle. Increase in load eccentricity decreased the strength of test columns and increased their midheight deflection at failure. The results of the research had lead to a design method.

S. Razvi, M. Saatcioglu, 1996

Objectives: To determine the effect of the test parameters on square and circular HSC columns.

Scope: An experimental investigation was conducted on 26 square and 20 circular HSC columns. The columns had 250 mm cross-section, and 1500 mm column height, and they were tested under monotonically increasing concentric compression. The concrete strength of test columns ranged between 60 MPa and 124 MPa. Two of the square test columns had plain concrete sections. The yield strength of transverse reinforcement ranged between 400 MPa and 1000

MPa. The volumetric ratio of transverse steel for core concrete section ranged between 0.41% and 4.59%, while vertical spacing of transverse steel varied between 40 mm and 135 mm.

Test Variables: Concrete strength; cross-sectional shape; yield strength, volumetric ratio and spacing of transverse reinforcement; longitudinal reinforcement arrangement; type of transverse reinforcement for circular columns; and the presence of longitudinal reinforcement on circular columns.

Conclusions: The test results indicated that the HSC columns behaved in extremely brittle manner under monotonically increasing concentric compression. It was reported that higher confinement pressure was required for HSC columns to increase column deformability to similar levels observed in normal-strength concrete columns. High confinement pressure could be provided either by increasing the volumetric ratio of transverse reinforcement and/or by using high-strength transverse steel. Confinement efficiency could be improved by reducing the spacing of transverse and/or longitudinal reinforcement. It was reported that circular hoops and circular spirals showed similar confinement behaviour and they both were more effective in confining HSC than rectilinear ties. Longitudinal reinforcement in circular columns had an effect on concrete confinement. Confined HSC columns with closely spaced transverse reinforcement exhibited early spalling of cover concrete.

S. J. Foster and M. M. Attard, 1997

Objectives: To compare the ultimate strength of HSC test columns with strength predictions based on the ACI 318-89 rectangular stress block parameters.

Scope: An experimental investigation was conducted on 68 eccentrically loaded square normal-strength and high-strength columns. The columns had 150 mm cross section, with concrete

strengths ranged between 40 MPa and 90 MPa. The specimens had either 2% or 4% longitudinal reinforcement and ties spacings of 30, 60, or 120 mm. 1680 mm effective length.

Test Variables: The main variables considered in the experimental study included the concrete strength, amount and distribution of longitudinal reinforcement, spacing of transverse reinforcement, and the eccentricity of the axial load.

Conclusions: It was reported that the ductility of reinforced concrete column was dependent on the confinement provided by the transverse reinforcement. The confinement effectiveness was reported to be related to the concrete strength, the tie spacing and configuration, the tie yield strength, the tie diameter, and the amount and arrangement of longitudinal reinforcement. A confinement parameter was defined, and based on this parameter it was reported that higher strength concrete specimens showed considerably lower ductilities than their lower strength counterparts. Strength predictions based on the ACI 318-89 rectangular stress block compared reasonably well with experimental capacities, although lower strengths than calculated occurred for some HSC columns.

Y. Xiao and A. Martirossyan, 1998

Objectives: To investigate the behaviour of high-strength concrete square columns under shear-dominant seismic loading.

Scope: An experimental investigation was conducted on six HSC columns, with concrete strengths varying between 76 MPa and 86 MPa. The specimens had 254 mm square cross-section and they were tested under combined axial load and cyclic shear. Axial load levels ranged between 10% and 20% of the column concentric capacity. Longitudinal reinforcement

ratios ranged between 2.46% to 3.53% and volumetric ratio of transverse reinforcement ranged between 1.63% and 3.67%.

Test Variables: The main variables included the concrete strength; the amount of longitudinal and transverse reinforcement; and the axial load level.

Conclusions: It was reported that the displacement factors of 6 to 8 can be achieved by HSC columns with an axial load below 20% of their concentric capacity and with 2.48-3.52% longitudinal reinforcement ratio, if transverse reinforcements were designed according to the seismic provisions of the ACI 318 code. It was also reported that the shear strength of the HSC columns suffering shear failure were overestimated by the ASCE/ACI 426 recommendation and ACI 318 code approaches by about 10%. Based on the findings of the experimental investigation an equation was proposed for the calculation of shear contribution of HSC.

J. Lee and H. Son, 2000

Objectives: To verify the basic design rules of high-strength concrete columns.

Scope: A total of 32 normal and high strength columns were tested under eccentric loading. The columns either had 210 x 120 mm or 120 x 120 mm cross section. The concrete compressive strength varied from 35 MPa to 93 MPa and the longitudinal steel ratios were between 1.13% and 5.51%.

Test Variables: The main variables included in the test program were the concrete compressive strength, amount of transverse reinforcement, eccentricity, and slenderness ratio.

Conclusions: The researchers had observed spalling of concrete cover in the high-strength concrete specimens. It was reported that the concrete cover spalling zone tended to be larger as concrete strength and the amount of transverse steel increased and as slenderness ratio and initial

eccentricity decreased. The column capacities were compared with those calculated by ACI rectangular stress block and it was found that ACI rectangular stress block overestimated column capacities for the lightly reinforced high-strength concrete specimens. Applicability of two other stress blocks, namely trapezoidal stress block and Ibrahim and McGregor's modified stress block, to HSC columns were investigated. These stress blocks were recommended as a conservative lower bound for design of HSC columns.

F. Legeron and P. Paultre, 2000

Objectives: To evaluate different equations that have been proposed for determination of confinement reinforcement for HSC columns located in seismic zones.

Scope: An experimental investigation was conducted on six HSC columns, with concrete strengths ranging from 92.4 MPa to 104.3 MPa. The columns had 305 mm square cross-section and 2150 mm height. They were subjected to constant axial loads corresponding to target values of 15, 25, and 40% of their concentric capacity and a cyclic horizontal load.

Test Variables: Two main test variables were the level of axial load; and the volumetric ratio of confinement steel.

Conclusions: It was reported that for a ductile behaviour of a column subjected to an axial-load level of less than or equal to 15% of the gross axial-load capacity, approximately 50% of the ACI Code required reinforcement was necessary. It was also reported that for similar levels of deformabilities the columns must be confined very well (more than that required by the ACI Code requirements) when subjected to an axial-load level greater than 40% of the gross axial-load capacity. The researchers concluded that HSC could be used in seismic zones, provided that

it was adequately confined. They suggested additional research to investigate the influence of important parameters including slenderness ratio, stirrups spacing, and size effect.

J. Liu, S. J. Foster, and M. M. Attard, 2000

Objectives: To investigate the ultimate strength and ductility of HSC circular columns confined by steel ties and spirals under static concentric loads, and to study the effect of concrete cover on strength.

Scope: 12 circular columns with 250 mm cross-section were tested under concentric compression. The concrete cylinder strength ranged between 60 MPa and 96 MPa. In all specimens, the longitudinal reinforcement consisted of eight 12mm diameter deformed bars, yielding a reinforcement ratio of 1.8%.

Test Variables: The test variables were the strength of the concrete; the diameter and spacing of the tie and spiral reinforcement; and the concrete cover.

Conclusions: It was reported that for the columns with zero and 15 mm of cover, the capacity increased with an increase in effective confining stress for the well-confined HSC columns. However, that was not the case for the 25 mm cover specimens where the highest load was carried by the specimen with the lowest quantity of confining steel. Based on the findings of the experimental investigation it was concluded that for design, the first peak load (the spalling load) can be taken as 0.85 times the capacity of the concrete section, calculated on the in-place concrete strength plus the capacity of the longitudinal reinforcement.

Y. Xiao, H. W. Yun, 2002

Objectives: Evaluation of the behaviour of full-scale HSC square columns.

Scope: An experimental investigation was conducted on 6 HSC square columns. The columns had 510 mm square cross-section, and 1778 mm column height. The columns were tested under constant axial compression ranging from 20% to 34% of section concentric capacity, and incrementally increasing lateral deformation reversals. The concrete strength of test columns ranged between 62.1 MPa and 64.1 MPa. Columns were confined with conventional ties. The yield strength of transverse reinforcement ranged between 445 MPa and 525 MPa, while the vertical spacing of ties varied between 100 mm and 150 mm.

Test Variables: Yield strength, volumetric ratio and spacing of transverse reinforcement; and axial load level.

Conclusions: The test results indicated that HSC columns with a transverse reinforcement not less than 82% of that specified in the seismic design provisions of ACI 318-99 demonstrated ductile behaviour (6% lateral drift) when the axial load ratio was 20%. Similar columns, however, only achieved a lateral drift ratio of 3% when the axial load was above 30% of the column's axial load capacity. The researchers reported that, for the same transverse reinforcement configuration and testing condition, improved behaviour was observed for the model column with higher-strength transverse reinforcement.

T. Tan and N. Nguyen, 2005

Objectives: To investigate the effect of confinement to the flexural capacity of HSC and the applicability of the rectangular stress block recommended by the ACI code to HSC sections.

Scope: An experimental investigation was conducted on 30 plain and reinforced concrete column specimens with 200 mm square cross-section. The specimens were tested under

concentric or eccentric compression. The volumetric ratio of transverse reinforcement ranged between 0.7% and 2.4%, and the concrete strength varied between 46 MPa and 101 MPa.

Test Variables: The main variables were the concrete strength; amount and arrangement of transverse reinforcement, and the eccentricity of the axial compression.

Conclusions: It was reported that the confinement from lateral reinforcement improved the flexural strength and ductility of reinforced concrete columns. It was also reported that the configuration of the confinement reinforcement had a significant effect on the flexural behaviour of the confined concrete. The researchers found high-strength reinforcement to be more effective than the normal-strength steel for confinement reinforcement of HSC columns. A new set of rectangular stress block parameters were proposed based on the findings of the experimental investigation and available published test data.

2.3 PREVIOUS RESEARCH ON FRP CONFINED CONCRETE COLUMNS

The use of FRP stay-in-place formwork for improved seismic performance of new columns is a relatively new research area that has not been fully explored in the past. Literature review in this chapter, therefore, seeks relevant studies, including those on FRP wrapping of concrete columns as a seismic retrofit strategy.

2.3.1 Previous research on FRP stay-in-place formwork for improved seismic performance

F. Seible, R. Burgueno, M. G. Abdallah, and R. Nuismer, 1996

Objectives: To conduct an experimental feasibility study on concrete filled FRP tubes under simulated seismic loading.

Scope: Three 40% scale models of a prototype circular bridge column were tested as 3.7 m high cantilever columns with a core diameter of 600 mm. One of these specimens was a control column, with 2.66% longitudinal reinforcement ratio, and no FRP tube. The other two columns had carbon FRP tubes, with a thickness of 9.5 mm at column critical section. The tube of one specimen was embedded into the footing for about 0.8 m, whereas the tube of the other specimen was set 24 mm above the footing. The specimen with FRP tube inserted inside the footing had no internal steel reinforcement, whereas the other specimen with FRP tube had the same internal steel reinforcement with the control specimen, but only as starter bars for a length of 0.9 m

Test Variables: The main variables were the type of FRP tubes, and existence of steel reinforcement.

Conclusions: The researchers reported that the specimen with starter bars but no embedment of FRP tube showed a stable hysteretic response up to a displacement ductility of 8, similar to the response of the control specimen. The specimen with embedded FRP tube but no starter bars matched the initial stiffness of the other two specimens. However, the premature failure of the tube due to a combined state of compressive interlaminar shear stresses prevented the specimen from absorbing an equal amount of energy as the ductile columns.

N. C. Gould and T. G. Harmon, 2002

Objectives: To experimentally verify the design expressions used to predict the behavior of confined concrete columns.

Scope: A total of twelve scaled cantilever columns were tested under constant axial load and cyclic shear and flexure. The columns were fabricated by filling FRP tubes, with 180 mm circular cross-section and either 600 mm or 1200 mm height, with concrete. FRP tubes consisted

of glass fibers, oriented at 90 degrees with respect to the longitudinal axis of the column. The specimens were tested under a constant axial compression of either 133 kN or 578 kN, and their concrete strength ranged between 41 MPa to 55 MPa. All columns had 4.2 % longitudinal reinforcement.

Test Variables: The main test variables included the level of axial load, fiber volume ratio of the FRP wrap, and the column height.

Conclusions: It was concluded that wrap strains due to shear, flexure, and axial load could not be treated independently. The researchers reported that columns were able to sustain wrap strains significantly in excess of 0.004 if the wrap volume ratio was sufficiently high. It was also noted that low-cycle fatigue of longitudinal reinforcement was a significant concern for confined concrete columns which typically limited ductility.

Z. Zhu, 2004

Objectives: To investigate the construction feasibility of concrete filled FRP tubes as either cast-in-place or precast members in conjunction with the reinforced concrete footing.

Scope: A total of four specimens were tested under constant axial compression of either 454 kN or 909 kN, and incrementally increasing lateral deformation reversals. One of these specimens was a control column without FRP reinforcement, whereas other three columns were cast-in glass FRP tubes. Three different types of FRP tube-footing connection were considered; cast-in-place reinforced, precast grouted and precast post-tensioned. All specimens had a total height of 3.12 m, which included a 0.61 m high RC footing and 0.53 m high column head. All columns had 310 mm circular cross-section and 55 MPa concrete. The FRP tubes were made of $\pm 55^{o}$ E-glass fibers and epoxy resin with a wall thickness of 5.1 mm.

Test Variables: The main test variable was the type of connection between the FRP tube and the reinforced concrete footing.

Conclusions: The results of the experimental investigation indicated that FRP confined columns performed much better than conventional reinforced concrete columns, in terms of strength and ductility as well as energy absorption capacity, under both hysteretic static load and major earthquake records. The better performance of FRP confined columns was mainly attributed to the confinement by the FRP tube, which prevented spalling of concrete core. It was also noted that the embedment of the tube further improved the performance significantly, as the tube participated effectively in the axial direction. The researcher reported that practices of the precast industry could be easily and effectively implemented for the construction of columns confined by FRP tubes. In comparison to each other, the various FRP tube-footing connections found to perform quite similarly, as long as the FRP tube was properly embedded or implanted into the footing. It was concluded by the researcher that these joints were feasible, constructible, and functional for load transfer between a FRP confined column and its foundation, even at high levels of lateral drift, typical of large earthquakes.

Y. Shao and A. Mirmiran, 2005

Objectives: To investigate the behaviour of concrete filled circular FRP tubes under reversed cyclic loading.

Scope: A total of six specimens were tested as simple span beam columns under constant axial loading and lateral deformation reversals. Three of the tubes were made using centrifuge casting with 12.7 mm thickness, an outside diameter of 305 mm, and the majority of the fibers in the longitudinal direction. The other three tubes were filament wound with a 5.1 mm thickness, an

outside diameter of 322 mm, and ±55° fiber orientation. One specimen for each type of tube had no internal reinforcement, whereas the other two incorporated approximately 1.7% and 2.5% longitudinal reinforcement ratios. The average concrete strength of the specimens were 27.2 MPa and they had a flexural span length of either 2.4 m or 2.7 m. Axial load level ranged from 6% to 10 % of the column concentric capacity.

Test Variables: The main test variables were the type of FRP tubes, and the amount of steel reinforcement.

Conclusions: The researchers reported that thick FRP tubes with the majority of the fibers in the longitudinal direction showed a brittle compression failure resembling that of an over-reinforced concrete member. Thin FRP tubes with off-axis fibers exhibited ductile tension failure, with significant nonlinearity, resembling that of an under-reinforced concrete member. It was also noted that a moderate amount of internal steel reinforcement in the range of 1–2% might further improve the cyclic behavior of members confined by FRP tubes.

2.3.2 Previous research on FRP wrapping of concrete columns as a seismic retrofit strategy

H. Saadatmanesh, M. R. Ehsani, and L. Jin, 1996

Objectives: Evaluation of the behaviour of reinforced concrete columns strengthened with FRP composite straps.

Scope: An experimental investigation was conducted on 5 scaled-down circular columns, which were designed to represent typical pre-1971 designed highway bridge columns. The columns had 305 mm circular cross-section, and approximately 1.8 m column height. The concrete strength of test columns ranged between 36.5 MPa and 38.5 MPa. The columns were tested under constant axial load of 445 kN, and incrementally increasing lateral deformation reversals. Two columns

had continuous longitudinal bars, while the longitudinal bars of the remaining three columns were spliced over a length of 20 bar diameter (254 mm) from the column footing interface. Transverse reinforcement consisted of 3.5 mm stirrups, with a yield strength of 301 MPa, spaced at 89 mm along the column height. Two of the test columns were designed as control specimens and did not have FRP confinement. The other three columns were retrofitted FRP straps by utilizing either active or passive scheme. FRP composite straps consisted of unidirectional glass fibres. The composite straps were 0.8 mm thick and had a yield strength and a modulus of elasticity of 532 MPa and 18.6 GPa, respectively. The strengthened columns were wrapped with six FRP composite straps, within the potential plastic hinge zone of the columns

Test Variables: Existence of lap splices for longitudinal reinforcement; existence and type of FRP confinement.

Conclusions: The test results indicated that FRP confinement significantly improved both strength and deformability of test columns. In particular, the improvement in the displacement ductility of columns having lap splices was notable. It was reported that both passive and active retrofit schemes were comparably effective.

H. Saadatmanesh, M. R. Ehsani, and L. Jin, 1997

Objectives: Evaluation of the behaviour of earthquake damaged reinforced concrete columns repaired with prefabricated FRP wraps.

Scope: An experimental investigation was conducted on 4 scaled-down columns, which were designed to simulate existing seismic deficiencies such as the lack of adequate transverse reinforcement and insufficient development length for starter bars. The height of the columns was 1,898 mm, two of the columns had circular geometry, while the other two had rectangular

geometry. The concrete strength of test columns ranged between 33.4 MPa and 36.6 MPa. The columns were tested under constant axial load of 445 kN, and incrementally increasing lateral deformation reversals. Two columns had continuous longitudinal bars, while the longitudinal bars of the remaining three columns were spliced over a length of 20 bar diameter (254 mm) from the column footing interface. Transverse reinforcement consisted of 3.5 mm stirrups, with a yield strength of 301 MPa. The vertical spacing of ties ranged between 88.9 mm and 114.3 mm, while the volumetric ratio of transverse steel ranged between 1.33% and 1.79%. All columns were initially tested to failure under reversed cyclic loading. The columns were repaired with prefabricated FRP wrap and retested under simulated earthquake loading. FRP composite straps consisted of unidirectional glass fibres. The composite had a yield strength and a modulus of elasticity of 532 MPa and 17.8 GPa, respectively. The circular and rectangular columns were wrapped with six and eight FRP composite straps, respectively, within the potential plastic hinge zone of the columns.

Test Variables: Cross section; longitudinal reinforcement ratio; existence of lap splices for longitudinal reinforcement.

Conclusions: The test results indicated that FRP composite wraps were effective in restoring the flexural strength and ductility capacity of earthquake-damaged concrete columns. It was reported that the stiffness deterioration of repaired columns was lower than that of the corresponding original columns under large reversed cyclic loading.

F. Seible, M. J. N. Priestley,G. A. Hegemier and D. Innamorato, 1997

Objectives: Development, validation and implementation of FRP jacketing system as a new seismic retrofit system for reinforced concrete columns.

Scope: An experimental investigation was conducted on 7 bridge columns, having circular and rectangular geometry. The columns were tested under constant axial load, and incrementally increasing lateral deformation reversals. The concrete compressive strength of test columns was 34.45 MPa. The FRP jacket systems consisted of unidirectional prepeg carbon tow winding system with an epoxy matrix. The composite had a yield strength and a modulus of elasticity of 1300 MPa and 124 GPa, respectively. The test results were compared against previously tested columns, which were confined with conventional steel jackets.

Two rectangular columns had 610 mm x 406 mm cross-section, and 2,438 mm column height, which yielded a clear span of 1,219 mm due to the fixed end conditions. The aspect ratio of those columns was chosen to obtain shear dominant behaviour. Columns were subjected to a constant axial load of 507 kN, and they had continuous longitudinal reinforcement. Test results indicated that, the lateral load displacement ductility of control columns was $\mu = 3$, while it was $\mu = 10$ for FRP jacketed column.

The second pair rectangular columns had 730 mm x 489 mm cross-section, and 3,658 mm column height. Those columns had a clear span equal to the columns height, due to the end conditions, and they were designed as flexure dominant columns. Columns were subjected to constant axial load of 1780 kN, and they had continuous longitudinal reinforcement. Test results indicated that, the lateral load displacement ductility of control columns was $\mu = 3$, while it was $\mu = 7$ for FRP jacketed column.

Three circular columns had 610 mm cross-section, and 3,658 mm column height, which was also equal to the clear span. The longitudinal reinforcement was spliced at the bottom of the column over a length of 20 bar diameter. Each column was subjected to a constant axial load of 1780 kN. Test results indicated debonding of the lap splice after a displacement ductility of $\mu = 5$. It was

later realized by the researchers that the provided jacket thickness was less than the design jacket thickness. A second test was conducted where the column had a slightly higher jacket thickness than that required. The test results of this column indicated that the column developed a ductility ratio of up to $\mu = 10$ without any significant strength decay.

Test Variables: Cross section; shear span; existence of lap splices for longitudinal reinforcement; axial load level.

Conclusions: Researchers concluded that the FRP jacket system could be just as effective structurally as conventional steel jacketing in improving the seismic behaviour of substandard reinforced concrete columns. Researchers also presented a FRP jacket design criteria for various failure modes and column geometries.

Y. Xiao and R. Ma, 1997

Objectives: To evaluate the efficiency of prefabricated composite jackets for seismic retrofit of reinforced concrete bridge columns with lap-spliced longitudinal bars.

Scope: An experimental investigation was conducted on three concrete columns with 610 mm circular cross-section and 2.44 m height. The specimens were tested under a constant axial compression corresponding to 5% of the column concentric capacity, and cyclic horizontal forces. The longitudinal reinforcement consisted of twenty 19.1 mm deformed bars, yielding a reinforcement ratio of 2%. The longitudinal bars were lap-spliced over a length of 20 times the bar diameter near the bottom of the column. One of the specimens was tested as-built and then repaired with four layers of prefabricated composite jacket at column critical section. The remaining two specimens were retrofitted with four and five layer FRP jackets at column critical

section, respectively. Each layer of jackets was prefabricated by unidirectional glass fibre sheets with 90% of the fibres oriented in the circumferential direction.

Test Variables: The main test variable was the amount of FRP reinforcement.

Conclusions: The test results of the as-built column indicated that columns with poor spliced details were vulnerable to premature brittle failure due to the bond deterioration of the lap-spliced bars. The researchers reported that such failure pattern could be delayed using the prefabricated composite jacketing. The retrofitted columns demonstrated significantly improved hysteretic responses, and increased ductility.

S. A. Sheikh, G. Yau, 2002

Objectives: Evaluation of the effectiveness of FRP reinforcement in strengthening deficient columns and repairing damaged columns.

Scope: An experimental investigation was conducted on 12 circular columns. The columns had 356 mm circular cross-section, and 1470 mm column height. The concrete strength of test columns ranged between 39.2 MPa and 44.8 MPa. The columns were tested under constant axial compression ranging from 27% to 54% of section concentric capacity, and incrementally increasing lateral deformation reversals. The test specimens were divided into three groups. The first group consisted of four columns that were conventionally reinforced with longitudinal and spiral steel reinforcement. The second group contained six reinforced concrete columns that were strengthened with carbon fibre-reinforced polymers (CFRP) or glass fibre-reinforced polymers (GFRP) before testing. The last group included two columns that were damaged to a certain extent, repaired with fibre-reinforced polymers (FRP) under axial load, and then tested to failure. U.S. No.3, Grade 60 steel was used for spiral reinforcement. The volumetric ratio of transverse

steel ranged between 0.30% and 1.12%, while vertical spacing of transverse steel varied between 80 mm and 300 mm. The test results were compared against previously tested columns, which were confined with conventional steel reinforcement.

Test Variables: Axial load level; spacing of spirals; presence of column damage; thickness, and type of FRP material.

Conclusions: The test results indicated that the use of CFRP and GFRP resulted in significant improvement in both ductility and strength of test columns. It was reported that, the behaviour of FRP retrofitted columns under simulated earthquake loads matched or exceeded the performance of conventional steel-reinforced columns designed according to the seismic provisions of the ACI Code. The negative effect of high axial load levels on the displacement ductility of columns was reported. Researchers further reported that FRP composites were very effective for the rehabilitation of damaged columns.

R. D. Iacobucci, S. A. Sheikh, and O. Bayrak , 2003

Objectives: Evaluation of the effectiveness of FRP reinforcement in strengthening deficient and repairing damaged square columns.

Scope: An experimental investigation was conducted on 8 square columns, which represented the members of buildings and bridges constructed before 1971. The columns had 305 mm square cross-section, and 1473 mm column height. Corners of all columns were rounded by using concave wood sections with a radius of 16 mm. The concrete strength of test columns ranged between 31.4 MPa and 42.3 MPa. The columns were tested under constant axial compression ranging from 33% to 56% of section concentric capacity, and incrementally increasing lateral deformation reversals. The test specimens were divided into three groups. The first group

consisted of four columns that were conventionally reinforced with longitudinal and spiral steel reinforcement. The second group contained six reinforced concrete columns that were strengthened with carbon fibre-reinforced polymers (CFRP). The last group included two columns that were damaged to a certain extent, repaired with fibre-reinforced polymers (FRP) under axial load, and then tested to failure. The composite sheets were 1.0 mm thick and had a yield strength and a modulus of elasticity of 962 N/mm/layer and 76.35 GPa, respectively. U.S. No.3, Grade 60 steel was used as transverse reinforcement. The volumetric ratio of transverse steel was 0.61%, while vertical spacing of transverse steel was 300 mm within the test zone. The test results were compared against previously tested columns, which were confined with conventional steel reinforcement.

Test Variables: Axial load level; presence of column damage; and number of FRP layers.

Conclusions: The test results indicated that the retrofit of seismically deficient square reinforced concrete columns with CFRP could substantially increase their ductility and improve their seismic resistance. It was reported that, the behaviour of FRP retrofitted deficient columns under simulated earthquake could be superior to the performance of conventional steel-reinforced columns designed according to earthquake building standards. The negative effect of high axial load levels on the displacement ductility of columns was reported. It was concluded that confinement requirements for columns under higher axial loads will be higher than that of lower axial loads to realize similar performance enhancement. Researchers further reported that CFRP repair options can effectively impart ductility and enhanced seismic behaviour to previously damaged columns, although the level of improvement depends on the severity of damage sustained.

M. H. Harajli and A. A. Rteil, 2004

Objectives: To evaluate the seismic performance of reinforced concrete columns designed for gravity load and confined externally with carbon fiber-reinforced polymer sheets.

Scope: An experimental investigation was conducted on a total of 12 rectangular specimens with 150 x 300 mm cross-section and 1050 mm height. The specimens were tested under constant axial compression and incrementally increasing lateral deformation reversals. The concrete strength of columns ranged between 20.3 MPa and 21.9 MPa, whereas the level of axial load, represented by P/f'_cA_g, varied between 0.25 and 0.30. The columns had either 1.5% or 3.0% longitudinal steel reinforcement, with yield strengths ranging between 534 MPa and 565 MPa. The longitudinal bars were lap-spliced over a length of 30 times the bar diameter at the column base. Unidirectional carbon FRP flexible sheets with impregnating epoxy resin were used for external confinement of the specimens. The sheets were applied in either one layer of 300 mm-wide strips or in one 300 mm-wide layer plus three equally spaced 50 mm-wide strips on top of the first layer.

Test Variables: The main test variables included the amount and arrangement of longitudinal reinforcement and external FRP confinement.

Conclusions: It was reported by the researchers that without confinement, the spliced reinforcement at the column base experienced significant bond deterioration under cyclic load, leading to considerable stiffness and strength degradation of the column specimens. The results indicated that wrapping the column critical zone with a relatively small area of carbon FRP sheets increased the bond strength and strength capacity of the columns, significantly reduced concrete spalling and bond deterioration in the column end zone, and resulted, in effect, in considerable improvement in seismic performance of the columns. While increasing the area of

FRP sheets by 50% improved the seismic performance, the improvement was found not to be proportional to the increase in the amount of FRP. The researchers also reported that for the same area of confinement reinforcement per unit length along the spliced column reinforcement in the critical region external confinement by FRP was more effective in improving the seismic performance as compared with confinement by conventional steel reinforcement.

S. N. Bousias, T. C. Triantafillou, M. N. Fardis, L. Spathis, and B. A. O'Regan, 2004

Objectives: To investigate the effectiveness of FRP wraps as concrete confinement of rectangular reinforced concrete column.

Scope: An experimental investigation was conducted on a total of 20 rectangular specimens with 250 x 500 mm cross-section and 1.6 m shear span. To represent nonseismically designed and detailed members, specimens emulated old construction, as far as materials used and lack of earthquake resistant detailing. Longitudinal reinforcement of each column consisted of four 18 mm deformed bars with a yield strength of 560 MPa. The concrete strength of columns ranged between 16.7 MPa and 20.4 MPa. In half of the specimens, salt was added to the mixture at 3% of weight of water. These specimens were tested after 1 m at the bottom of the column had been subjected to accelerated corrosion of the reinforcement. Two types of unidirectional FRP sheets were used for the retrofitting, with different fiber material: Carbon versus Glass. The specimens were tested under constant axial compression and a history of unidirectional deflection cycles along either their strong or weak axis. The level of axial load, represented by P/f'_cA_g, varied between 0.34 and 0.40. One pair of control specimens in each of the two directions of testing was tested without FRP wrapping. One pair of strengthened specimens in each of the two directions

of testing was wrapped with FRP after the initial damage was induced by a preliminary cyclic test that carried the column beyond yielding.

Test Variables: The main test variables included the type of fibres used in FRP sheets, number of FRP sheets, direction of loading with respect to column axis, and the effect of reinforcing bar corrosion.

Conclusions: It was reported by the researchers that deformation capacity and hysteretic response of reinforced concrete columns improved considerably when their nonductile regions were encased in continuous FRP jackets with either carbon or glass fibers. Unretrofitted columns exhibited a gradual loss of lateral and axial load resistance during the cycle that led to failure; after ultimate deformation they retained most of their axial load capacity although losing their lateral load one. Retrofitted columns, however, maintained their axial and lateral load capacities up to the ultimate deformation but lost them abruptly when they failed explosively by rupturing of the FRP wrap. Test observations indicated that changing the type of material (glass fibres versus carbon fibres), while maintaining the same extensional stiffness of the FRP jacket in the circumferential direction, resulted in approximately the same performance. FRP wraps were found to have a larger overall effect for loading in the strong direction of the column. This was confirmed by the columns that failed by fracture of the FRP—the increase in deformation capacity in the strong direction was 90%, versus approximately 55% in the weak direction. It was also reported that the column retrofitted with FRP wraps after being cyclically damaged beyond yielding of the reinforcement exhibited more rapid strength loss and lower deformation capacity when compared with a previously undamaged column. Reinforcing bar corrosion reported to reduce the strength of both retrofitted and unretrofitted columns, despite the fact that the reduction in bar diameter and the loss of cross-sectional area seemed insignificant visually.

M. S. Memon and S. A. Sheikh, 2005

Objectives: To evaluate the effectiveness of glass fibre reinforced polymer (GFRP) wraps in strengthening deficient and repairing damaged square concrete columns.

Scope: An experimental investigation was conducted on 8 square columns, which represented the members of buildings and bridges constructed before 1971. The columns had 305 mm square cross-section, and 1473 mm column height. Corners of all columns were rounded by using concave wood sections with a radius of 16 mm. The concrete strength of test columns ranged between 42.4 MPa and 44.2 MPa. The columns were tested under constant axial compression of either 33% or 56% of section concentric capacity, and incrementally increasing lateral deformation reversals. All columns contained eight 19.5 mm longitudinal bars uniformly distributed around the core, yielding a reinforcement ratio of 2.58%. A glass FRP wrap system was used to retrofit the specimens, with the fibres oriented in the lateral direction.

Test Variables: The main test variables included axial load level, presence of column damage; and number of FRP layers.

Conclusions: It was reported by the researchers that square concrete columns externally retrofitted by glass FRP wraps and tested under simulated seismic loading, showed a pronounced improvement in overall sectional and member behavior over unretrofitted columns. The seismic behavior of columns improved as the number of FRP layers increased. Adverse effects from insufficient lateral steel observed to be eliminated as FRP jackets provided additional confinement to critical sections. The researchers also noted that higher ductility and improved seismic performance can be achieved by retrofitting damaged square concrete columns with glass FRP jackets. The negative effect of high axial load levels on the displacement ductility of columns was reported. It was concluded that confinement requirements for columns under higher

axial loads will be higher than that of lower axial loads to realize similar performance enhancement. It was also noted that the seismic behaviour of deficient columns appropriately retrofitted with GFRP could be made to be superior to the response of columns having sufficient lateral steel content according to seismic provisions of the design codes.

2.4 REFERENCES

Ahmed, S. H., and Shah, S. P. (1982). "Stress-Strain Curves of Comcrete Confined by Spiral Reinforcement." ACI Journal, V.79, No.6, pp. 484-490.

Baingo, D., and Saatcioglu, M. (1995). "Performance of Circular High Strength Concrete Columns under Lateral Load Reversals." Research Report, Department of Civil Engineering, University of Ottawa, Ottawa, Canada.

Basset, R., and Uzumeri, S. M. (1986). "Effect of Confinement on the Behaviour of High-Strength Lightweight Concrete Columns." Canadian Journal of Civil Engineering 13(6): 741-751.

Bayrak, O., and Sheikh, S. A. (1995). "High Strength Concrete Columns Subjected to Earthquake Type Loading." Proc. of the Seventh Canadian Conference on Earthquake Engineering, Montreal, Quebec, pp.477-484.

Bjerkeli, L., Tomaszewics, A., Jensen, J. J. (1990). "Deformation Properties and Ductility of High Strength Concrete." High Strength Concrete, Second International Symposium, ACI SP-121-12, Detroit, pp.215-238.

Bousias, S. N., Triantafillou, T. C., Fardis, M. N., Spathis, L., and O'Regan, B. A. (2004). "Fiber-Reinforced Polymer Retrofitting of Rectangular Reinforced Concrete Columns with or without Corrosion." ACI Structural Journal 101(4): 512-520.

Fafitis, A., and Shah, S. P. (1985). "Predictions of Ultimate Behavior of Confined Columns Subjected to Large Deformations." Journal of the American Concrete Institute 82(4): 423-433.

Foster, S. J., and Attard, M. M. (1997). "Experimental Tests on Eccentrically Loaded High-Strength Concrete Columns." ACI Structural Journal 94(3): 295-303.

Gould, N. C., and Harmon, T. G. (2002). "Confined Concrete Columns Subjected to Axial Load, Cyclic Shear, and Cyclic Flexure - Part II: Experimental Program." ACI Structural Journal 99(1): 42-50.

Harajli, M. H., and Rteil, A. A. (2004). "Effect of Confinement Using Fiber-Reinforced Polymer or Fiber-Reinforced Concrete on Seismic Performance of Gravity Load-Designed Columns." ACI Structural Journal 101(1): 47-56.

Iacobucci, R. D., Sheikh, S. A., and Bayrak, O. (2002) "Retrofit of Square Concrete Columns with Carbon Fiber-Reinforced Polymer for Seismic Resistance." ACI Structural Journal, V. 100, No. 6, pp. 785-794.

Ibrahim, H. H. H., and MacGregor, J. G. (1996). "Tests of Eccentrically Loaded High-Strength Concrete Columns." ACI Structural Journal 93(5): 585-594.

Itakura, Y., and Yagenji, A. (1992) "Compressive Test on High-Strength R/C Columns and their Analysis Based on Energy Concept." Proc. of 10th World Conference on Earthquake Engineering, Madrid, pp. 2599-2602.

Lee, J., Son, H., (2000). "Failure and Strength of High-Strength Concrete Columns Subjected to Eccentric Loads." ACI Structural Journal, 97(1), pp. 75-85.

Légeron, F., and Paultre, P. (1995). "Seismic Behaviour of Columns Made of High-Strength Concrete." Proc. of the Seventh Canadian Conference on Earthquake Engineering, Montreal, Quebec, pp.469-476.

Légeron, F., and Paultre, P. (2000). "Behavior of High-Strength Concrete Columns under Cyclic Flexure and Constant Axial Load." ACI Structural Journal 97(4): 591-601.

Lipien, W., and Saatcioglu, M. (1995) "Ductility of High-Strength Concrete Columns." Research Report, Department of Civil Engineering, University of Ottawa, Ottawa, Canada.

Liu, J., Foster, S. J., and Attard, M. M. (2000). "Strength of Tied High-Strength Concrete Columns Loaded in Concentric Compression." ACI Structural Journal 97(1): 149-156.

Lloyd, N. A., and Rangan, B. V. (1996). "Studies on High-Strength Concrete Columns under Eccentric Compression." ACI Structural Journal 93(6): 631-638.

Martinez, S., Nilson, A. H., and Slate, F. O. (1984). "Spirally Reinforced High-Strength Concrete Columns." ACI Journal, V.81, No.5, pp. 431-442.

Memon, M. S., Sheikh, S. A. (2005). "Seismic Resistance of Square Concrete Columns Retrofitted with Glass Fiber-Reinforced Polymer." ACI Journal, V.102, No.5, pp.774-783.

Mugumura, H., Watanabe, F., Iwashimizu, T., and Mitsueda, R. (1983). "Ductility Improvement of High Strength Concrete by Lateral Confinement." Transactions of the Japan Concrete Institute, Vol.5, pp. 403-410.

Nagashima, T., Sugano, S., Kimura, H., Ichikawa, A. (1992). "Monotonic Axial Compression Tests on Ultra-High-Strength Concrete Tied Columns." Proc. of 10th World Conference on Earthquake Engineering, Madrid, pp. 2983-2988.

Rangan, B. V., Saunders, P., and Seng, E. J. (1991). "Design of High-Strength Concrete Columns." Evaluation and Rehabilitation of Concrete Structures and Innovations in Design, ACI SP 128-52pp. 851-862.

Razvi, S. R., and Saatcioglu, M. (1996). "Tests of High-Strength Concrete Columns under Concentric Loading." Research Report OCEERC 96-03, Ottawa Carleton Earthquake

Engineering Research Center, Department of Civil Engineering, University of Ottawa, Ottawa, Ontario, pp.147.

Saadatmanesh, H., Ehsani, M. R., and Lin, J. (1996). "Seismic Strengthening of Circular Bridge Pier Models with Fiber Composites." ACI Structural Journal 93(6): 639-647.

Saadatmanesh, H., Ehsani, M. R., and Lin, J. (1997). "Seismic Retrofitting of Rectangular Bridge Columns with Composite Straps." Earthquake Spectra 13(2): 281-304.

Seible, F., Burgueño, R., Abdallah, M. G., and Nuismer, R. (1996). "Development of advanced composite carbon shell systems for concrete columns in seismic zones." Proc., 11th World Conf. Earthquake Engineering, Pergamon, Elsevier Science, Oxford, Paper No. 1375.

Seible, F., Priestley, M. J. N., and Hegemier, G.A. and Innamorato, D. (1997). "Seismic Retrofit of RC Columns with Continuous Carbon Fiber Jackets." Journal of Composites for Construction, ASCE, Vol.1, No.2, pp.52-62.

Shao, Y., and Mirmiran, A., (2005). "Experimental Investigation of Cyclic Behavior of Concrete-Filled Fiber Reinforced Polymer Tubes." Journal of composites for Construction, ASCE, 9(3), 263-273.

Sheikh, S. A., Shah, D. V., and Khoury, S. S. (1994). "Confinement of High-Strength Concrete Columns." ACI Structural Journal 91(1): 100-111.

Sheikh, S. A., and Yau, G. (2002). "Seismic Behaviour of Concrete Columns Confined with Steel and Fiber-Reinforced Polymers." ACI Structural Journal, V. 99, No. 1, pp. 72-80.

Shin, S. W., Kamara, M., and Ghosh, S. K. (1990). "Flexural Ductility, Strength Prediction, and Hysteretic Behavior of Ultra-High Strength Concrete Members." High Strength Concrete, Second International Symposium, ACI SP-121-13, Detroit, pp.239-264.

Tan, T., amd Nguyen, N. (2005). "Flexural Behavior of Confined High-Strength Concrete Columns." ACI Structural Journal, V. 102, No. 2, pp.198-205.

Thomsen, J. H., and Wallace, J. W. (1994). "Lateral Load Behavior of Reinforced Concrete Columns Constructed Using High-Strength Materials." ACI Materials Journal 91(5): 605-615.

Xiao, Y., and Ma, R. (1997). "Seismic retrofit of RC circular columns using prefabricated composite jacketing." Journal of Structural Engineering, ASCE, 123(10), 1357–1364.

Xiao, Y., and Martirossyan, A. (1998). "Seismic Performance of High-Strength Concrete Columns." Journal of Structural Engineering 124(3): 241-250.

Xiao, Y., and Yun, H. W. (2002). "Experimental Studies on Full-Scale High-Strength Concrete Columns." ACI Structural Journal, 99(2), pp.199-207

Yong, Y.-K., Nour, M. G. and Nawy, E. G. (1988). "Behavior of Laterally Confined High-Strength Concrete under Axial Loads." Journal of Hydraulic Engineering 114(2): 332-351.

Zhu, Z. (2004). "Joint Construction and Seismic Performance of Concrete-Filled Fiber Reinforced Polymer Tubes." PhD thesis, North Carolina State Univ., Raleigh, N.C.

Chapter 3

Seismic Performance of Circular High-Strength Concrete Columns in FRP Stay-in-Place Formwork

3.1 INTRODUCTION

The use of high-strength concrete (HSC) columns has increased over the last two decades due to the higher strength and improved performance of material relative to concretes of conventional strength. The gain in strength, however, is attained at the expense of deformability. Indeed, HSC columns exhibit brittle behaviour, jeopardizing its use in seismically active regions where seismic energy is expected to be dissipated through significant inelasticity. Inelastic deformability of concrete can be improved by confinement. Properly confined concrete can develop adequate ductility, allowing sufficient lateral deformability without a significant decay in strength. However, the confinement requirements become prohibitively stringent for HSC elements when conventional steel ties, hoops, overlapping hoops and spirals of ordinary grade steel are used, leading to the congestion of the column cage and resulting concrete placement problems. Fibre reinforced polymer (FRP) materials offer an attractive alternative to confine concrete. Extensive research has already been conducted on the application of FRP material for wrapping existing concrete columns. However, the use of FRP sheets for new construction,

especially for HSC columns, is a relatively new concept that is currently being explored. One such application involves the use of FRP casings, in the form of stay-in-place formwork. These FRP casings offer multiple advantages of; i) light and effective formwork with superior handling characteristics, ii) efficient and durable transverse confinement reinforcement with ability to generate high lateral confinement pressure, and iii) protective shell against corrosion, weathering and chemical attacks. The objective of this thesis is to present the findings of an experimental investigation on the effectiveness of circular FRP formwork when used as transverse reinforcement for HSC columns subjected to simulated seismic loading. The study is extended to cover normal strength concrete (NSC) columns for comparison. The performance of columns is also compared with that of companion columns confined with conventional steel reinforcement.

3.2 EXPERIMENTAL PROGRAM

Circular columns, with concrete strengths ranging between 50 MPa and 90 MPa, were cast in carbon FRP casings and tested under a constant axial compression and incrementally increasing lateral deformation reversals. The main test variables included concrete strength, the number of FRP plies, the level of axial load and shear span. Table 3.1 summarizes the geometric properties and test variables considered in the experimental program.

3.2.1 Test Specimens

The specimens represented part of a first-story building column between the footing and point of inflection. They had a 270 mm circular cross-section and either a 1.72 m or a 0.92 m cantilever length, with a 0.56 m high steel loading beam placed on top, resulting in either a 2.0 m or a 1.2 m shear span. All specimens contained eight 16 mm diameter longitudinal bars with a yield

strength (f_y) of 500 MPa resulting in a reinforcement ratio (ρ_l) of 2.79%. The FRP casings had two plies of carbon FRP sheets, except for column RC-1, which had four plies. Figures 3.1 and 3.2 illustrate the geometry and reinforcement arrangements considered in the test program.

3.2.2 Material Properties

Carbon FRP Composite

A carbon fibre polymer composite system was used to manufacture the circular stay-in-place formwork. The thickness of carbon fibre sheet was 0.165 mm/ply, which was increased to 0.8 mm/ply when impregnated with epoxy resin. The fibres were oriented in the circumferential direction to develop hoop tension. The stress-strain relationship of composite material was established by coupon tests and showed linear-elastic behaviour up to the rupturing strength in tension. The capacity of the composite material was established to be approximately 785 MPa based on the fibre content corresponding to 0.8mm/ply. This observation was found to be in agreement with the 3800 MPa fibre strength reported by the manufacturer. Table 3.2 provides the properties of carbon fibres as supplied by the manufacturer. The maximum tensile strain of 1.67% specified by the manufacturer was also in agreement with a large number of strain readings recorded on the composite material. The above values translate into the elastic modulus of 47,000 MPa for the composite material, which is in line with 227,000 MPa reported for the modulus of elasticity of carbon fibres alone.

The manufacturing process involved wrapping FRP sheets around sona tubes of desired diameter and length, followed by the application of epoxy resin as illustrated in Fig. 3.3. The FRP sheets were wrapped one layer at a time with a 100 mm overlap in the direction of fibres to ensure

proper bond, though they were not overlapped along the column height. The number of FRP plies was established based on the results of recent research on the stress-strain behaviour of FRP confined concrete (Miyauchi et al. 1997; Samaan et al. 1998; Spoelstra and Monti 1999; Saafi et al. 1999; Moran and Pantelides 2002; Lam and Teng 2002) while also considering widely accepted confinement models for conventional steel reinforcement (Sheikh and Uzumeri 1980; Mander et al. 1988; Saatcioglu and Razvi 1992). Also considered were the current FRP design guidelines (Buckle and Friedland 1994; ACI 440 2002; CSA S806 2002).

Concrete

Two of the three concrete batches used were HSC, with 90 MPa and 75 MPa strengths attained during the period of column testing. They were designed and ordered from a ready-mixed concrete company. Both mixes consisted of Type 10SF cement (8% Silica fume blended with Normal Portland cement) and crushed limestone with 10 mm maximum size. The water cement ratios used were 0.22 and 0.26 for 90 MPa and 75 MPa concrete mixes, respectively. Strength and workability were the main criteria in mix design, which were achieved by selecting a low water-cement ratio and high cement content. It was necessary to use superplasticizers and retarders to achieve and maintain the desired level of workability. An initial concrete slump of 200 mm was achieved and maintained during casting.

The third batch of concrete was for NSC columns, and was prepared at the Concrete Laboratory of the University of Ottawa. The mix consisted of Normal Portland Cement and crushed limestone with 10 mm maximum size. The water cement ratio was 0.44 and the resulting concrete strength was 50 MPa on the day of column testing. It was necessary to use a small

amount of superplasticizer to achieve and maintain the desired level of workability. An initial concrete slump of 160 mm was achieved and maintained during casting. All specimens were cast vertically and vibrated thoroughly. Cylinder tests were conducted periodically to monitor the strength gain.

Steel Reinforcement

The longitudinal reinforcement consisted of 16 mm diameter deformed bars. They were obtained from the same batch of shipment with 500 MPa yield strength. The stress-strain relationship was established by performing at least three coupon tests. Table 3.3 provides average properties for the reinforcement used, with standard notations; (E_s) as the elastic modulus; (f_y) and (f_u) as stresses at yield and ultimate, respectively; (ε_y), (ε_{sh}), (ε_u), and (ε_r) as strains at yield, onset of strain hardening, ultimate, and rupture, respectively. None of the columns had transverse steel reinforcement, except in the footing where the longitudinal bars were positioned and tied with three hoops and a single tie at the top to keep the bars in place. Mechanical splices were used in Column RC-3 to splice the longitudinal bars at 500 mm from the column footing interface, as illustrated in Fig. 3.4. High strength rebar couplers, designed for extreme tension/compression applications, were used to investigate their applicability to columns under seismic loading. The tensile capacity of couplers was specified by the manufacturer to be in excess of 1.6 times the specified yield strength of standard rebars (60,000 psi or 414 MPa). This corresponds to a capacity of 662 MPa, which is greater than the ultimate tensile capacity (f_u = 620 MPa) of the 16 mm diameter bars used in the current investigation. The tension coupon tests were conducted on mechanically spliced 16 mm bars, and the failure was observed to take place away from the splice region, confirming manufacturer's specification, as shown in Fig. 3.4.

3.2.3 Instrumentation, test setup, and loading program

The columns were instrumented with Linear Variable Displacement Transducers (LVDT) and strain gages to measure horizontal displacements, rotations of the plastic hinge region, anchorage slip, longitudinal strains in the reinforcement and circumferential strains on the FRP formwork. All instrumentation was connected to a data acquisition system and a microcomputer for data recording. The acquisition of strain data on FRP formwork was of particular interest to have a better understanding of the strain profiles on FRP. Therefore, a total number of 29 strain gages were placed on the surface of each FRP casing, oriented in the direction of fibres. They were placed at eight to ten different levels along the height, extending over the bottom 945 mm segment for long columns and 810 mm segment for the short column. The first six layers of gages from the base were place at a spacing of one quarter the cross-sectional dimension along the column height, followed by either one half or full cross-sectional dimension.

Each column was tested under a constant axial compression and incrementally increasing lateral deformation reversals, simulating seismic loading. Three 1000 kN capacity servo-computer-controlled MTS hydraulic actuators were used to apply the loads. Two of the actuators were positioned vertically, one on each side of the column, to apply constant axial compression throughout the test. The third actuator was placed horizontally for the application of lateral deformation reversals. Figure 3.5 illustrates the test setup.

The columns were first subjected to axial compression. HSC columns were tested under either 31% or 34% of their concentric capacity (P_o), while the axial load level (P/P_o) of the NSC

column was 0.47 P_o, where (P_o) was computed using Eq. 1, as 1,580 kN for column RC-1 and 1,480 for all other columns.

$$P_o = 0.85 f'_c (A_g - A_s) + A_s f_y \quad (1)$$

The initial lateral load reversals consisted of three full cycles of 0.5% drift ratio. Subsequent deformation reversals consisted of three cycles at each of 1%, 2%, 3% etc., in the deformation control mode. The lateral deformation reversals continued until the specimen was unable to maintain a significant fraction of its maximum lateral load resistance. The rate of lateral loading was low and the total duration of a typical test was about four to five hours, depending on the deformability of the column.

3.3 TEST RESULTS

3.3.1 Observed Behaviour

All columns had two plies of FRP, except RC-1, which had four plies. They all initially behaved in a similar manner up to 3 % lateral drift ratio. There were no visual signs of damage in any column until the end of 2% lateral drift cycles. Localized changes in FRP color was observed in the plastic hinge region of column RC-4, near the base, starting at 3% drift ratio. This column had a shorter shear span than the others. The discoloration was attributed to the separation of FRP material from concrete as concrete deterioration progressed within the casing. A similar discoloration was observed in other columns with a longer shear span, starting at 4% drift ratio. In longer columns, the regions of discoloration extended towards the tip with increasing lateral drift, reaching up to three times the column cross-sectional dimension of 270 mm. These visual observations were also supported by the transverse strain data recorded on FRP casings. Any increase in displacement beyond 4% drift substantially increased fibre dilatation within the

plastic hinge region. When the testing of Column RC-1 was stopped at 12% drift, there were signs of delamination of FRP up to approximately 800 mm from the column-footing interface, indicating the magnitude of the propagation of plastic hinge region. Column RC-4 failed during the third cycle of 4% lateral drift when a 20 to 30 mm thick strip of fibres ruptured at the column loading-beam interface, followed by the crushing of concrete in this region. This was attributed to stress concentration caused by the spacer block that was placed between the steel loading beam and the column, creating additional bearing stresses on the loading side of the column. At this load stage, there was no sign of significant delamination of fibres within the plastic hinge region, although discoloration in the FRP casing was clearly visible. The strain data indicated transverse strains of approximately 1% in the same region, implying potentially significant distress in column concrete.

Fibre rupturing was the failure mode for columns RC-2 and RC-3. Snapping noise, accompanied by the release of previously built-up pressure in FRP casings resulted in the failure of columns. The most extensive damage occurred within a segment, 150 to 350 mm from the column-footing interface, which coincided with the location of initial fibre rupturing. The shifting of the plastic hinge from the maximum moment section at the column footing interface to a distance 150 mm away was attributed to the confining effect of the footing. Similar observations were previously reported by other researches (Sheikh and Khoury 1993). Figure 3.6 (b) and (c) illustrate the behaviour of hinging regions in columns RC-2 and RC-3. Table 3.4 summarizes the strength values and locations of highly damaged sections for all columns. It may be of interest to note that Column RC-3 with 50 MPa concrete developed approximately the same flexural strength as that

of Column RC-2 with 75 MPa concrete because of the higher level of axial compression applied to the former column.

The FRP casings of columns RC-1 and RC-4 were cut and removed after the test to investigate the condition of concrete inside. Column RC-1, which sustained 12% lateral drift cycles, although did not reveal any sign of serious damage after the removal of FRP, light tapping on concrete by a hammer resulted in the spalling of concrete on loading sides, until the longitudinal reinforcement was exposed. The location of damaged regions was similar in RC-1, RC-2 and RC-3, though the extent of damage was less in RC-1 with 4 plies of FRP, as shown in Fig. 3.6. Similar observations were made for column RC-4 after removing the FRP casing, with a notable difference in the type and the location of damaged regions. The transverse strains recorded along column height indicate higher transverse strains in the low moment region near the tip, as compared to those recorded on all other specimens which showed flexure dominant behaviour. This was attributed to the dominant action of shear stresses in RC-4. Further increase in transverse strains was recorded near the column base due to the flexural compression in confined concrete. The most damaged region in column RC-4 was close to the tip of the column due to the stress concentration effect of the top loading beam, which increased compression in already stressed concrete. This is illustrated in Fig. 3.6(d).

An important observation was made relative to the performance of compression bars under high levels of inelastic deformations. Although no internal transverse steel reinforcement was provided in any of the columns, there was no sign of premature buckling of longitudinal bars until after the columns failed due to the rupturing of FRP and subsequent crushing of concrete.

This indicates that the FRP casing and the 25 mm internal cover concrete provided were able to provide sufficient lateral restraint against bar buckling.

3.3.2 Hysteretic Behaviour

It is generally believed that some strength decay can be tolerated in the columns of multistory multi-bay buildings due to the redundancy in the system. Therefore, the drift ratio corresponding to 20% strength decay beyond peak moment resistance has been adopted as the maximum usable drift, beyond which the column was considered to have failed (Park and Paulay 1975; Saatcioglu 1991). Figure 3.7 illustrates experimentally recorded moment-lateral drift hysteretic relationships. It indicates virtually no strength degradation in any of the columns until the end of testing. In particular, the strength of column RC-1 and RC-2 increased under increasing inelastic deformations up to 11% and 9% lateral drift, respectively. This can be seen in Figs. 3.7(a) and 3.7(b). Testing of Column RC-1 was stopped at 12% lateral drift ratio when the stroke capacity of the horizontal actuator was reached on the pull side, having reached the stroke capacity at 11% drift on the push side. The strain data collected during the last deformation cycle of column RC-1 indicates that the maximum transverse strains recorded are lower than those of RC-2 and RC-3 at failure, suggesting that the specimen could have completed a few additional deformation cycles prior to failure. This is shown in Figs. 3.8(a), 3.8(b) and 3.8(c), where the variation of transverse strains on FRP is plotted for each column. Similar observations can be made for the hysteretic moment-drift relationship for column RC-2 where maximum recorded drifts were 12% and 10% for the pull and push sides, respectively. Once again, the stoke capacity of the actuator was exceeded at 10% drift ratio on the push side, and the column was cycled in the pull direction

near the end of the test, attaining the failure load during the first cycle of 12% drift due to the rupturing of FRP.

The hystereses loops initially indicate typical flexure-dominant (well rounded) curves until after a significant deterioration of concrete has taken place inside the casing. The hysteretic relationships, beyond approximately 7% lateral drift, indicate a gradual increase in the pinching of hystereses loops. The level of pinching has been observed to be quite substantial in column RC-1, which developed up to 12% lateral drift. This behaviour was attributed to increased contribution of shear on the behaviour of damaged concrete, which is reflected on force-deformation relationships as pinching of the loops. An extreme example of the effect of shear on damaged concrete can be seen in Fig. 3.6(b) which depicts a shear-mode deflected shape at the end of testing.

Columns RC-2 and RC-3 failed during the first cycle of 12% and 10% lateral drift ratios, respectively, following the rupturing of fibres within critical regions, as seen in Figs. 3.7(b) and 3.7(c). These columns were identical in every respect except for the concrete strength. Column RC-3 had NSC with f'_c = 50 MPa, in comparison with Column RC-2, which had f'_c = 75 MPa, and hence was expected to have reduced deformability. However, the columns were tested under the same magnitude of axial compression, which resulted in different percentages of column concentric capacity, i.e., 34% P_o for RC-2 and 47% P_o for RC-3. Consequently, RC-3 with NSC was subjected to higher percentage of its concentric capacity, which resulted in reduced deformability. It is interesting to note that the product of $f'_c \cdot (P/P_o)$ was higher for RC-2 than for RC-3. Even then, RC-2 developed higher lateral drift than RC-3, indicating that the

detrimental effect of axial compression on inelastic deformability was higher than that of concrete strength.

The strains recorded on column RC-4 confirm the earlier observation that the column failure was triggered by the crushing of top concrete near the loading assembly shortly after the rupturing of FRP at approximately 1.6% transverse strain. Just before the sudden increase in fibre strains due to rupturing, the strains recorded perpendicular to the direction of loading (end faces) were limited to approximately 8,500 micro strain, as seen in Fig. 3.8(d), whereas those recorded parallel to loading (on side faces) increased up to approximately 10,000 micro strain, as seen in Fig. 3.8(e), confirming the significance of shear in this column. A similar comparison for earlier columns, with flexure dominant response, indicates that maximum strains on side faces were approximately 20% lower than those recorded on the end faces. Additional confirmation of the significance of shear on column RC-4 is the level of transverse strains recorded on side faces at the top, near the zero-moment region. The maximum transverse strain of 1%, recorded immediately preceding the rupturing of FRP near the loading beam, indicates that column RC-4 could have completed additional drift cycles had it not failed prematurely. Table 3.5 summarizes drift ratios recorded at various stages of loading.

Column RC-3 contained mechanically spliced longitudinal reinforcement. The mechanical splices used were for 16.0 mm diameter deformed bars, and were located 500 mm above the footing. Observations during testing indicated that the column longitudinal reinforcement developed its strength, without any slippage at the splice locations. The behaviour of the column

was not affected by mechanical splices, as evidenced by the hystereses loops shown in Fig. 3.7 (c) and the longitudinal bars remained intact till the end of testing.

3.3.3 Contributions of FRP Casings

One of the primary objectives of the current research program was to investigate the effectiveness of FRP casings in confining high-strength concrete. Therefore, the behaviour of FRP was further studied in detail. The casings were well instrumented by a large number of strain gages to monitor the lateral expansion of concrete. Unlike conventional steel reinforcement, which exhibits elasto-plastic stress strain behaviour, FRP material shows linear-elastic stress-strain behaviour. Therefore, the confinement pressure provided by FRP casings is directly related to the amount of transverse strain generated on the material. This underlines the importance of experimental strain data in understanding the mechanism of confinement.

Strain gages were placed on each FRP casing at eight to ten different levels along column height. Typical transverse strain-lateral drift hysteretic relationships are shown in Fig. 3.9. The relationships presented in Fig. 3.9 were selected from 29 such plots for each column, representing strain data at critical locations during each deformation level. The maximum transverse strains recorded on casings were in excess of 1%, and close to the fibre rupture strain reported by the manufacturer. The recorded values were consistently higher than those recommended for design in current design guidelines (Buckle and Friedland 1994; ACI 440 2002; CSA S806 2002).

The plots of maximum transverse strains presented in Fig. 3.8 provide strain data at each level of lateral drift, from which confinement pressure can be calculated. These strain readings reflect combined effects of lateral expansion resulting from concrete confinement and diagonal tension caused by shear. The effects of shear and flexure are expected to be more dominant on column side and end faces, respectively. The strain data obtained from columns with longer shear spans confirmed that transverse strains due to confinement were higher on faces perpendicular to the direction of loading. Therefore, the maximum transverse strains plotted for these columns in Fig. 3.8 are almost always the strain data recorded on end faces. To further demonstrate this point, two separate plots are provided for column RC-4 with a short shear-span; i) Fig. 3.8(d) showing maximum strains on the end faces and ii) Fig. 3.8(e) showing those recorded on the side faces. The maximum strains on long columns occurred at a distance approximately equal to the column cross sectional dimension measured from the base. The short column developed its maximum transverse stain at approximately half the cross-sectional dimension above the footing until the stress concentration effect near the applied load, discussed earlier, caused a sudden increase in transverse strains on the side faces. It is important to recognize that the short column developed a relatively uniform distribution of transverse strains above the plastic hinge region, until shortly before the failure at the top, signifying the influence of shear stresses, whereas a linear variation of strains was observed above the plastic hinge region in all other columns due to the linear reduction of flexure and associated confinement action. Furthermore, it is instructive to examine the strain readings away from the high flexure region where shear stresses dominate the behaviour. The readings taken at 4% drift ratio, when column capacities reached their peak resistance, the strains in upper regions of long columns were limited to approximately 1000 micro strain, whereas column RC-4, with a short shear-span, developed in excess of 4000 micro

strains in the same low moment region illustrating the effect of shear on the column casing (Fig. 3.8).

The significance of shear on column behaviour was investigated further with due considerations given to concrete shear resistance and the load at which initial diagonal tension cracks are expected. Shear capacities of test columns, as dictated by shear resistance provided by concrete alone (V_c), are tabulated in Table 3.4. These capacities were calculated on the basis of the ACI 318 (2005) shear expression. Table 3.4 illustrates that all columns, except column RC-4, had higher concrete shear capacities (V_c) than the maximum shear force applied during testing (V_{max}), implying that long columns are not expected to have developed diagonal tension cracks under shear prior to the formation of plastic hinging, beyond which a decay in concrete shear resistance (V_c) is anticipated. Therefore, the FRP casings for these columns are not expected to provide any appreciable resistance to shear while they confine concrete against flexural compression. However, (V_{max}) was computed to be higher than (V_c) for the short column (RC-4), indicating that column concrete may have developed diagonal tension cracks and the FRP casing is strained to provide additional shear resistance until failure. This point can be illustrated by comparing the strain data for column RC-4 with a short shear span and a companion column RC-2 with a long shear span. Accordingly, the short column reached the same transverse strain level at a much lower drift ratio than the long column (Fig. 3.8). An important conclusion that can be drawn from the strain data is that the casings are effective as confinement reinforcement in long columns and shear/confinement reinforcement in short columns.

Another important observation that can be made on the strain data presented in Fig. 3.8 is the location of the critical zone for transverse strains under flexural bending. The maximum strain location was consistently observed to be approximately cross-sectional dimension above the footing for columns that behaved entirely in the flexure mode, though the maximum flexural stress location coincided with the column-footing interface. This may be explained by the confining effect of the footing, which provides a further lateral restraint against the expansion of concrete, thereby limiting damage on concrete near the immediate vicinity of the footing. The strain profiles presented in Fig. 3.8 further demonstrate the progression of hinging and associated damage to concrete.

Closer examination of maximum strains in Fig. 3.8 indicates that the FRP casing was fully effective for columns RC-2 and RC-3, both of which strained sufficiently to rupture the FRP casings, resulting in sudden column failures. Both of these columns developed slightly above 1.5% transverse strain. Column RC-1, with 4 plies of FRP sheets developed a maximum of about 1.1% transverse strain and the test was aborted prior to column failure as the actuator stroke capacity was exceeded due to excessive inelastic deformability prior to full utilization of the FRP material. Unlike the results of experimental observations on lightly loaded bridge columns, the columns maintained their integrity until the FRP tensile capacity was attained in the circumferential direction. This full effectiveness of FRP is attributed to the effect of higher axial compression applied on the columns, which increased the contribution of confined concrete to overall column behaviour and eliminated premature failure due to the tensile rupturing of longitudinal reinforcement.

3.4 COMPARISONS WITH COLUMNS CONFINED BY STEEL REINFORCEMENT

The seismic performance of FRP confined columns were compared with companion HSC columns confined with conventional steel reinforcement, tested by Saatcioglu and Baingo [1999]. Three specimens were adopted from earlier research, with columns SRC-2 and SRC-3 confined by steel spirals and column SRC-8 confined by individual circular hoops. These columns had similar material and geometric properties as the columns tested in the current investigation. Table 3.6 provides a summary of column properties. These columns had higher concrete shear capacities than shear forces applied during testing. This is shown in Table 3.4, implying flexure dominant behaviour. Therefore, the comparison was made for flexure dominant columns, i.e., RC-1, RC-2 and RC-3. Hysteretic moment-drift relationships of conventionally reinforced columns are presented in Fig. 3.10.

It is important to express the amount of confinement reinforcement using a common term to enable proper comparison. The volumetric ratio of transverse reinforcement, commonly used for this purpose, was deemed inappropriate because of the substantial difference in material properties. Therefore, uniform confinement pressure (f_l), as defined in Eq. 2, was used. The lateral pressure provided by closely spaced circular transverse reinforcement in conventional columns was considered to be uniform around the perimeter of the core, as often done by researchers (Sheikh and Uzumeri 1980; Mander et al. 1988; Saatcioglu and Razvi 1992).

$$f_l = \frac{2A_s \cdot f_{yt}}{D_c \cdot s} \tag{2}$$

where (A_s) is the cross-section area, (f_{yt}) is the yield strength, and (s) is the spacing of transverse reinforcement; (D_c) is the core dimension measured center- to-center of perimeter hoops. Eq. 2 translates into Eq. 3 for FRP confinement with fibres covering the entire column surface

$$f_l = \frac{2 f_{fc} \cdot t}{D} \tag{3}$$

where (f_{fc}) is the average maximum tensile stress due to confinement (excluding stress caused by shear) within the critical region of column at failure, (t) is the thickness of fibre material; and (D) is the cross-section dimension of the concrete section. The maximum tensile stress is computed from recorded strains and depends on the stress-strain relationship. This relationship could be for the FRP composite or the fibres alone, with due considerations given to the material thickness. Because the contribution of the epoxy resin to FRP strength is negligibly small, the thickness (t) and (f_{fc}) can either be determined from the properties of FRP composite material or from that of the fibre material alone. Data obtained from FRP coupon tests confirm that either the strength of FRP composite or the fibres can be used provided the corresponding material thicknesses are accounted for. In applications where variations in FRP thickness are anticipated due to the on-site manual application of the material, it may be more convenient to use fibre properties specified by the manufacturer. In this thesis, the properties of FRP confinement are characterized in terms of strength (f_{fc}) and elastic modulus (E_f) of the fibre material, as specified by the manufacturer.

The use of maximum recorded strain value provides a challenge in establishing the maximum stress in transverse FRP reinforcement. Strain values obtained from strain gages reflect localized effects. Furthermore, there are variations in strains within the confinement region of compression concrete, reaching the maximum value near the extreme concrete compression fibre, and

showing somewhat reduced values circumferentially away from the maximum point. Because this was anticipated earlier, a large number of strain gages were used in column tests to assess the distribution of transverse strains as accurately as possible. Typically, the circumferential strains reduce by about 20% going from the extreme compression fibre to the neutral axis. Therefore, the maximum recorded strain (ε_{fm}) was multiplied by 0.9 to obtain the average maximum tensile strain in the FRP casing within the compression zone. It is noteworthy that the maximum recorded tensile strain of 1.5% at FRP rupture is somewhat lower than the rupturing strain obtained from coupon tests, as well as that reported by the manufacturer. This can be attributed to differences in fibre alignment and the level of perfection achieved in the casing, as compared to coupons.

Transverse stress corresponding to 90% of recorded maximum strain (ε_{fm}) gives an average value under combined shear and confinement, as further elaborated in the next section, where the contribution of shear was computed to be approximately 10% in columns with long shear spans. Therefore, an estimate of lateral stress in transverse reinforcement associated with confinement (ε_{fc}) was computed by deducting the effect of shear (ε_{fs}) from recorded maximum strain (ε_{fm}), and finding the average within the concrete compression zone, as previously explained. The use of transverse FRP stress caused by confinement alone resulted in lateral pressure of 6.60 MPa for columns RC-2 and RC-3. Similarly, the value of uniform confining pressure for column RC-1 was computed to be 9.88 MPa. For steel confined columns, the uniform confining pressure was calculated from Eq.(2) as 7.95 MPa for columns SRC-3 and SRC-8, and as 7.68 MPa for column SRC-2. These values indicate that the confinement pressures of FRP-confined and steel-confined columns are close enough to allow a meaningful comparison of specimens with similar material

and sectional properties under similar loading conditions. However, the level of axial compression and concrete strength are close but not equal in most companion columns, permitting only an approximate comparison of overall drift capacities.

Table 3.5 provides the details of columns that are compared. Hysteretic relationships of steel reinforced concrete columns are shown in Fig. 3.10 and are to be compared with those of FRP confined columns given in Fig. 3.7. The results indicate that FRP confined columns show superior performance, with drift capacities approaching twice the values attained in steel reinforced columns. These findings are in line with those reported by other researches (Iacobucci et al. 2002) and can be explained with the continuous coverage of entire concrete surface with FRP casing and associated improvements in confinement efficiency, in contrast with hoop and spiral reinforcement that is placed at a specific spacing along the height of the column. The improvement in deformability is also affected by the significant increase in plastic hinge length and associated increase in plastic deformations, as well as the confinement of the entire column concrete, including what would otherwise become the cover. Similar observations were made by other researchers for concentrically loaded columns (Demers and Neale 1999).

3.5 DESIGN INFORMATION

Designing FRP stay-in-place formwork requires the determination of strength and deformation capacity of columns. The deformation capacity is especially important for HSC columns in seismically active regions. One of the assets of FRP stay-in-place formwork is its ability to confine HSC which would otherwise exhibit brittle behaviour, posing challenges in earthquake

resistant construction. Therefore, strength and inelastic deformability of HSC columns, confined by FRP casings are addressed in detail in this section for use in practice.

3.5.1 Strength of HSC Columns Confined by FRP Casings

An important component of FRP casing design for columns is the computation of its strength under flexure and axial load in presence of shear. This requires sectional and member analyses under combined stresses.

The current methods of analysis used for conventional reinforced concrete column design have been verified to assess their applicability to FRP encased HSC columns. Flexural capacities of test columns were computed by plane-section analyses of critical sections, with due considerations given to the stress-strain relationships of HSC and FRP materials. Nominal moment capacities were computed using, i) the stress-strain relationship proposed by Popovic (1973) for unconfined HSC, ii) the stress-strain relationship proposed by Saafi et al. (1999) for FRP confined concrete and iii) the stress-strain relationship proposed by Razvi and Saatcioglu (1999) for HSC confined by steel reinforcement. The rectangular stress block simplification was not considered because of the circular geometry of columns. The FRP confined concrete model by Saafi et al. (1999) was selected among many considered (Miyauchi et al. 1997; Samaan et al. 1998; Spoelstra and Monti 1999; Saafi et al. 1999; Moran and Pantelides 2002; Lam and Teng 2002) because it was developed for FRP casings, as opposed to FRP wrapped columns, and provided fairly accurate flexural capacities of test columns. In all cases the in-place strength of concrete was taken as 0.9 times the strength determined by standard cylinder tests (Ozbakkaloglu and Saatcioglu 2004). The stress-strain relationship used for longitudinal steel reinforcement was

obtained from coupon tests. The stress-strain characteristics of FRP casings were established on the basis of fibre properties obtained from manufacturer's data. This was done by determining the effective tensile stress in FRP at critical column section, on the compression side where it provided confinement. This value was based on experimentally recorded strains after allowing for contributions of shear and the variation of strains circumferentially within the compression zone, as previously explained. Column flexural capacity was established through moment-curvature analysis, which was conducted by employing a computer program, and taking peak moment resistance as the flexural capacity. Table 3.4 summarizes the results for all test columns.

The results indicate that nominal flexural capacities (M_n) computed by Popovics' unconfined concrete model (1973) produced lower strength values than those observed experimentally (M_{max}). This was attributed to the significance of confinement provided by the FRP casings. The flexural capacities computed by the steel confined concrete model (Razvi and Saatcioglu 1999) ($M_{R\&S}$) showed higher values relative to those recorded in tests. Similar observations were made by other researchers (Mirmiran and Shahawy 1997) who concluded that models developed for conventional steel confined concrete are not applicable to FRP confined concrete elements. Flexural capacities based on the confinement model proposed by Saafi et al. (1999) for FRP casings (M_S) showed reasonable correlation with test data. However, this model was developed from concentrically tested small-scale specimens, and may have to be improved for application to columns under seismic loading.

All the columns tested in the current investigation had higher shear capacities than those corresponding to flexural capacities. While the columns with a long shear span of 2.0 m behaved

predominantly in the flexure mode, with little or no contributions from shear, Column RC-4 had a shorter shear span of 1.2 m and showed significant contributions from shear, although it did not experience shear failure because of the excessive shear reinforcement provided by the FRP casing. The contribution of concrete to shear resistance (V_c) as per ACI 318-05 and the contribution of FRP (V_f) as the difference between experimentally recorded shear resistance and (V_c) are tabulated in Table 3.4. It should be noted however, that these design expressions are intended to reflect the contribution of each material prior to any degradation in concrete shear resistance caused by the deterioration of concrete at high inelastic deformations. The maximum applied shear for long columns often occurred at high lateral drift, though this value was observed to remain within 5% of the applied shear shortly after initial flexural yielding prior to significant damage to concrete. Therefore, the experimental shear force values indicated in Table 3.4 can be viewed as representatives of shear applied during the entire inelastic range. According to Table 3.4, the concrete in long columns was sufficient to resist the applied shear. Column RC-4, however, developed transverse strains in FRP near the zero-moment region, due to shear. These strains were recorded at early stages of inelasticity when the column developed its peak resistance at about 1.5% drift ratio, prior to experiencing sufficient damage to cause degradation in shear resistance mechanism of concrete.

Previous research indicated that concrete shear resistance decays with inelastic deformations of the plastic hinge region, where the damage imparted on concrete could reduce its shear resistance significantly (Priestley and Paulay 1992, Priestley et al. 1994). Table 3.7 provides concrete resistance to shear beyond a displacement ductility ratio of eight (V_c^*) as suggested by Priestley et al. (1994) which indicates a substantial reduction in (V_c) and a significant participation of FRP

(V_f^*). Computed contribution of FRP, included in the same table, indicates that approximately 10% of FRP strains in long columns provide resistance to shear, while the remaining strain capacity is utilized for concrete confinement. The percentage contribution of FRP strains to shear is computed to be approximately 30% in the short column (RC-4).

3.5.2 Deformability of HSC Columns Confined by FRP Casings

Because of the brittle behaviour of HSC, especially in the presence of axial compression, the deformability of HSC columns becomes an important design consideration for earthquake resistant construction. A convenient approach to improving column inelastic deformability is to provide sufficient confinement. FRP casing provides an ideal alternative to conventional reinforcement for confinement of HSC.

The challenge in design for inelastic deformability is to establish a relationship between the parameters of confinement, applied loading and lateral deformations. A displacement based design procedure was developed for conventional steel reinforced concrete columns by Saatcioglu and Razvi (2002), which was subsequently modified for FRP wrapped columns and adopted by the Canadian Standard CSA S806 (2002). Accordingly, the required FRP jacket thickness is a function of column axial load, the level of effectiveness of FRP in terms of maximum useable tensile strength and as dictated by column geometry, concrete strength and lateral drift ratio. The CSA S806-02 expression is reproduced below.

$$t_j = 2D\frac{f'_c}{f_{Fj}}\frac{P_f}{P_{ro}}\frac{\delta}{\sqrt{k_c}} \tag{4}$$

Where, (f_{Fj}) and (t_j) are the maximum stress in the FRP jacket that can be mobilized and thickness, respectively and (f'_c) is the cylinder strength of column concrete. The level of axial

compression is expressed as the ratio of maximum expected axial compression to column concentric capacity (P_f/P_{ro}). The confinement efficiency, as governed by the geometry of FRP jacket, is expressed through coefficient (k_c), where $k_c = 1.0$ for the most efficient confinement geometry of circular FRP jacket, where confinement is provided by hoop tension. Drift ratio (δ) was used as a measure of lateral deformability.

The maximum tensile stress allowed in CSA S806 (2002) is limited by the stress corresponding to 0.4% strain. This value was suggested as a conservative limit for the useful limit of FRP jacket as obtained from bridge column tests under a low level of axial compression, equal to 15% of P_o. The current experimental program indicates that the effectiveness of FRP casings improve with the level of axial compression, which increases the contribution of compression concrete to the overall behaviour of column. Indeed, strains as high as rupturing strains, reaching 1.5% were recorded during testing. Therefore, a higher limit on the FRP stress may be in order for FRP encased concrete columns. Furthermore, the casings resulted in significantly higher redistribution of stresses in concrete within the plastic range of deformations, extending the plastic hinge region beyond lengths that are typically assumed for columns with conventional reinforcement. This improved inelastic deformability significantly.

Eq. 4 was used to compute drift capacities of columns tested in the current research program. The FRP stress near column failure was computed from recorded strains, having deducted strains due to shear (ε_{fs}), as indicated in Table 3.8. The drift capacity for column RC-2, with a transverse strain of 1.2% was calculated to be 6.5%. However, this column completed 11% lateral drift cycles and could sustain one cycle at 12% drift ratio before it failed. Similarly, the computed

drift capacities based on Eq. 4 were consistently lower than those observed during actual column tests, as shown in Table 3.8. It should be noted that the drift capacities discussed in this section refer to those obtained from moment-displacement relationships, and do not include the strength decay due to P-Δ effect. The comparisons indicate that the CSA S806-02 expression provides a conservative estimate of drift capacities. FRP encased concrete columns can develop higher drift ratios when subjected to high axial compression that increases the effectiveness of FRP reinforcement while changing the failure mode from longitudinal bar rupturing to concrete crushing followed by FRP rupturing. The apparent effectiveness of FRP confinement under high axial compression results in the extension of the plastic hinge region, which results in increased drift ratios. The extended plastic hinge length was particularly noticeable in flexure dominant long columns. Therefore, the discrepancy was higher in columns with a longer shear span than the column with a short shear span. Further research is needed to model the formation and extension of the plastic hinge in FRP encased concrete columns.

3.6 CONCLUSIONS

The following conclusions can be drawn from the experimental study reported in this thesis:

- Circular high-strength concrete columns confined with carbon FRP stay-in-place formwork can develop extremely ductile behaviour under simulated seismic loading. Column tests reported in this thesis indicate that inelastic deformability of 90 MPa concrete columns can be increased up to 12% lateral drift ratio with FRP stay-in-place formwork.
- The increased confinement required for HSC columns can be provided with FRP stay-in-place formwork. Unlike conventional steel reinforcement that confines the core concrete FRP stay-in-place formwork provides effective confinement to the entire column section.

Furthermore, the FRP casings cover the entire column surface, unlike conventional steel ties placed at certain spacing, thereby enabling full utilization of higher material strength of FRP reinforcement.

- The strain data recorded during column tests reported in this thesis indicates that the strain limit of 0.4% often used in the current design practice for jacketing bridge columns under low levels of axial compression can be relaxed for columns under high axial compression. Rupturing strain of approximately 1.5% was consistently attained during tests at column failure.
- The seismic performance of FRP encased circular columns is superior to that of columns confined by conventional spiral/hoop reinforcement. This can be attributed to increased effectiveness of FRP casings as confinement reinforcement, as well as the characteristics of plastic hinging, which exhibits significantly more plastification and progression towards the elastic region in FRP encased columns, leading to increased hinging length.
- Column deformability decreases with increasing axial load relative to column concentric capacity (P/P_o) and concrete compressive strength (f'_c). It was experimentally observed that under the same level of applied axial load (P), HSC column developed higher lateral drift capacity than a companion NSC column with the same confinement characteristics.
- Confinement models developed for steel confined concrete may result in the overestimation of flexural strength and underestimation of inelastic deformability of FRP confined columns.
- FRP casings develop transverse tensile stresses caused by the combined action of shear and flexure. The contribution of shear increases under high levels of shear stress reversals, as well as following concrete deterioration in plastic hinge regions. The concrete shear

resistance may diminish very significantly in the latter case, increasing the strain demand on FRP casing.

- Additional confinement provided by a footing appears to strengthen the column critical section at the column-footing interface, shifting the failure away from the interface. This shift was observed to range approximately between one half and full cross-sectional dimension for the columns tested and axial loads applied in the current investigation.

3.7 REFERENCES

American Concrete Institute (ACI) Committee 318. (2005). "Building Code Requirements for Structural Concrete (ACI 318-05) and Commentary (318R-05)." Farmington Hills, Mich., 430pp.

American Concrete Institute (ACI) Committee 440 (2002). "Design and Construction of Externally Bonded FRP Systems for Strengthening Concrete Structures (440.2R-02)." Detroit, 45 pp

Buckle, I. G., and Friedland, I. M. (1994). "Seismic Retrofitting Manual for Highway Bridges." Report No. FHWA-94-052, U.S. Department of Transportation.

Canadian Standards Association (CSA) Committee S806 (2002). "Design and construction of building components with fibre-reinforced polymers (S806-02)." Rexdale Ontario, 177 pp.

Demers, M., and Neale, K.W. (1999). "Confinement of reinforced concrete columns with fibre-reinforced composite sheets-an experimental study." Canadian Journal of Civil Engineering, V. 26, pp. 226-241.

Iacobucci, R. D., Sheikh, S. A., and Bayrak, O. (2002) "Retrofit of Square Concrete Columns with Carbon Fibre-Reinforced Polymer for Seismic Resistance." ACI Structural Journal, V. 100, No. 6, pp. 785-794.

Lam, L., and Teng J. (2002). "Strength models for fibre-reinforced plastic-confined concrete." *Journal of Structural Engineering*, 128(5), 612-623.

Mander, J. B., Priestley, M. J. N., and Park, R. (1988). "Theoretical Stress-Strain Model for Confined Concrete." *Journal of Structural Engineering*, ASCE, V. 114, No. 8, pp. 1804-1826.

Mirmiran, A., and Shahawy, M. (1997). "Behaviour of Concrete Columns Confined by Fibre Composites." *Journal of Structural Engineering*, ASCE, V. 123, No. 5, pp. 583-590.

Miyauchi, K., Nishibayashi, S., and Inoue, S. (1997). "Estimation of Strengthening Effects with Carbon Fibre Sheet for Concrete Column." Proceeding of Nonmetallic (FRP) Reinforcement for Concrete Structures, Sapporo, Japan, V. 1, pp. 217-223.

Moran, A. M., and Pantelides C. P. (2002). "Stress-strain model for fibre-reinforced polymer-confined concrete." *Journal of Composites for Construction*, V.6, No.4, pp. 233-240

Ozbakkaloglu, T., and Saatcioglu., M. (2004). "Rectangular Stress Block for High-Strength Concrete." ACI Structural Journal, V. 101, No. 4, pp. 475-483.

Park, R., and Paulay, T. (1975). "Reinforced Concrete Structures." Wiley, New York, 769 pp.

Popovics, S. (1973). ''Analytical approach to complete stress-strain curves.'' *Cement and Concrete Res.*, 3(5), pp. 583–599.

Priestley, M.J.N., and Paulay, T. (1992). "Seismic Design of Reinforced Concrete and Masonry Buildings." John Wiley&Sons Inc., New York, 744 pp.

Priestley, M. N., Verma, R., and Xiao, Y. (1994). "Seismic Shear Strength of Reinforced Concrete Columns," *ASCE Journal of Structural Engineering*, V.120,No.8, pp 2310-2329,

Razvi, S. R., and Saatcioglu, M. (1999). ''Confinement model for high-strength concrete.'' *J. Struct. Engrg.*, ASCE, 125(3), 281–289.

Saafi, M., Toutanji H.A., Li, Z. (1999). "Behaviour of Concrete Columns Confined with Fibre Reinforced Polymer Tubes." ACI Structural Journal, V. 96, No. 4, pp. 500-509.

Saatcioglu, M. (1991). "Deformability of Reinforced Concrete Columns." Earthquake Resistant Concrete Structures, Inelastic Response and Design, ACI SP-127-10, American Concrete Institute, Detroit, pp. 421-452.

Saatcioglu, M., and Razvi, S. R. (1992). "Strength and Ductility of Confined Concrete." Journal of Structural Engineering, ASCE, V. 118, No. 6, pp. 1590-1607.

Saatioglu, M., and Baingo, D. (1999). "Circular High-Strength Concrete Columns under Simulated Seismic Loading." *Journal of Structural Engineering*, ASCE, V. 125, No. 3, pp. 272-280.

Saatcioglu, M., Razvi, S. R. (2002). "Displacement-Based Design of Reinforced Concrete Columns for Confinement." ACI Structural Journal, V.99, No.1, pp. 3-11

Samaan, M., Mirmiran, A., and Shahawy, M. (1998). "Model of Concrete Confined by Fibre Composites." *Journal of Structural Engineering*, 124(9), pp. 1025-1032.

Sheikh, S. A., and Uzumeri, S. M. (1980). "Strength and Ductility of Tied Concrete Columns." Journal of Structural Engineering, ASCE, V. 106, No. 5, pp. 1079-1102.

Sheikh, S. A., and Khoury S.S. (1993). "Confined Concrete Columns with Stubs." ACI Structural Journal, V. 90, No. 4, pp. 414-431.

Spoelstra, M. R., and Monti, G. (1999). "FRP-confined Concrete Model." Journal of Composites for Construction, ASCE, V. 3, No. 3, pp. 143-150.

Table 3.1 Properties of Test Specimens

Column	Shear Span (mm)	D (mm)	f'_c (MPa)	Layers of FRP	Longitudinal steel			Axial load	
					Reinforcement Arrangement	f_y (MPa)	ρ_l (%)	P (kN)	P/P_o
RC-1	2000	270	90.1	4	8-no.15	500	2.79	1580	0.31
RC-2	2000	270	75.2	2	8-no.15	500	2.79	1480	0.34
RC-3	2000	270	49.7	2	8-no.15	500	2.79	1480	0.47
RC-4	1200	270	75.3	2	8-no.15	500	2.79	1480	0.34

Table 3.2 Properties* of carbon fibres used in manufacturing FRP casings

Fibres	Nominal Thickness (mm/ply)	Ultimate Tensile Strength (MPa)	Elastic Modulus (GPa)	Ultimate Rupture Strain (%)	Areal Weight (g/m^2)
Carbon	0.165	3800	227	1.67	300

*Reported by the manufacturer.

Table 3.3 Properties of reinforcing steel

Bar size	Stress-strain relationship						
	f_y (MPa)	ε_y	E_s (MPa)	ε_{sh}	f_u (MPa)	ε_u	ε_r
No. 15	500*	0.0024	208,750	0.0062	620	0.120	0.135

*Rounded from 500.9 MPa.

Table 3.4 Experimental values and calculated capacities

Column	Layers of FRP	Moment				Shear Force			Damage zone (mm)
		M_{max} (kNm)	M_n (kNm)	M_S (kNm)	$M_{R\&S}$ (kNm)	V_{max} (kN)	V_c (kN)	V_f (kN)	
RC-1	4	174	138	186	205	87	97.1	0	150-350
RC-2	2	148	126	165	183	74	88.8	0	330
RC-3	2	144	93	134	161	72	72.4	0	150
RC-4	2	141	126	161	167	117.5	88.9	28.5	-
SRC-2	0	112	95	-	112	68.1	71.5	0	-
SRC-3	0	131	113	-	142	79.6	85.2	0	-
SRC-8	0	134	113	-	142	81.5	85.2	0	-

M_{max} and V_{max} represent average of maximum moments recorded in each direction of loading. M_n, M_S, and $M_{R\&S}$ are computed moment capacities based on concrete models proposed by Popovics (1973), Saafi et al.(1999) and Razvi and Saatcioglu (1999).

V_c is the contribution of concrete to shear as per ACI 318-05 and V_f is the contribution of FRP to shear $V_f = V_{max} - V_c$.

Table 3.5 Observed deformabilities of columns

Column	f'_c (MPa)	P/P_o	f_l (MPa)	Drift at Failure (%)	Drift at 80% M_{max} (%)	Drift at 90% M_{max} (%)	Drift at M_{max} (%)
RC-1	90.1	0.31	9.88	12+	12+	12+	11
RC-2	75.2	0.34	6.60	12, cycle 1	12	12	9
RC-3	49.7	0.47	6.60	10, cycle 1	10	9	4
RC-4	75.3	0.34	3.72	4, cycle 3	4	4	3.5
SRC-2	90	0.30	7.68	7+	7+	6.5	3
SRC-3	90	0.43	7.95	6, cycle1	4.9	4.2	1.5
SRC-8	90	0.43	7.95	4.5, cycle 3	4	3.3	2.5

Table 3.6 Properties of Comparison Specimens*

Column	Shear Span (mm)	D (mm)	f'_c (MPa)	Transverse steel				Longitudinal steel			Axial load
				ρ_s (%)	f_{yt} (MPa)	d_b (mm)	s (mm)	Reinforcement Arrangement	f_y (MPa)	ρ_l (%)	P/P_o
SRC-2	1645	250	90	3.67	420	11.3	50	8-no.15	419	3.26	0.30
SRC-3	1645	250	90	1.59	1000	7.5	50	8-no.15	419	3.26	0.43
SRC-8	1645	250	90	1.59	1000	7.5	50	8-no.15	419	3.26	0.43

*From Saatcioglu and Baingo (1999). ρ_s, f_{yt}, d_b, and s are volumetric ratio, yield strength, bar diameter and spacing of transverse reinforcement.

Table 3.7 Transverse Strains due to Shear

Column	f'_c (MPa)	V_{max} (kN)	V_c^* (kN)	V_f^* (kN)	ε_{fs} (%)	ε_{fm} (%)	$\varepsilon_{fs}/\varepsilon_{fm}$ (%)
RC-1	90.1	87	19.45	67.55	0.10	1.1	9.1
RC-2	75.2	74	17.75	56.25	0.16	1.5	10.7
RC-3	49.7	72	14.50	57.50	0.16	1.5	10.7
RC-4	75.3	118.3	17.75	100.55	0.28	1.0	28.3

Table 3.8 Experimental and Analytical Drift Capacities

Column	f'_c (MPa)	D (mm)	P/P_o	E_f (GPa)	t (mm)	ε_{fm} (%)	ε_{fs} (%)	ε_{fc} (%)	δ (%)	
									Analytical	Experimental
RC-1	90.1	270	0.31	227	0.66	1.1	0.10	0.89	8.85	12
RC-2	75.2	270	0.34	227	0.33	1.5	0.16	1.19	6.47	11
RC-3	49.7	270	0.47	227	0.33	1.5	0.16	1.19	7.02	9
RC-4	75.3	270	0.34	227	0.33	1.0	0.28	0.67	3.64	4

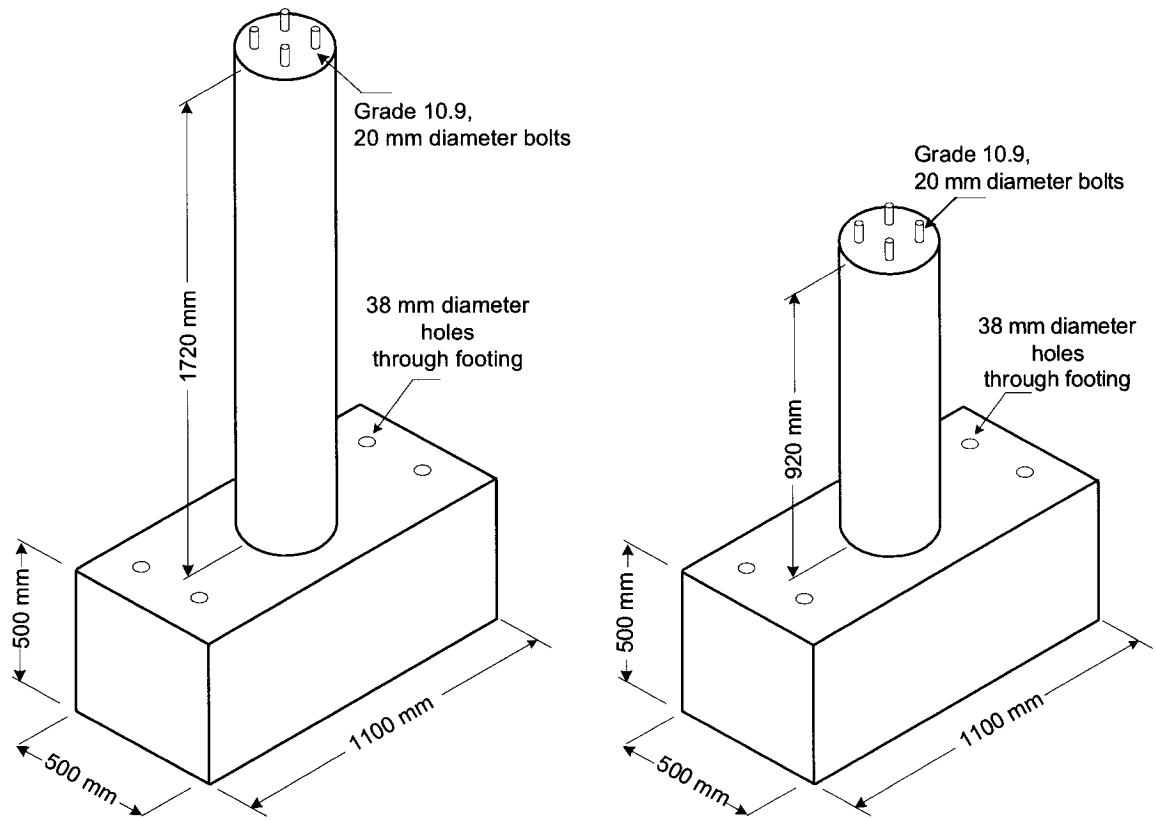

(a) RC-1, RC-2, RC-3 **(b) RC-4**

Fig. 3.1 – Geometry of test specimens

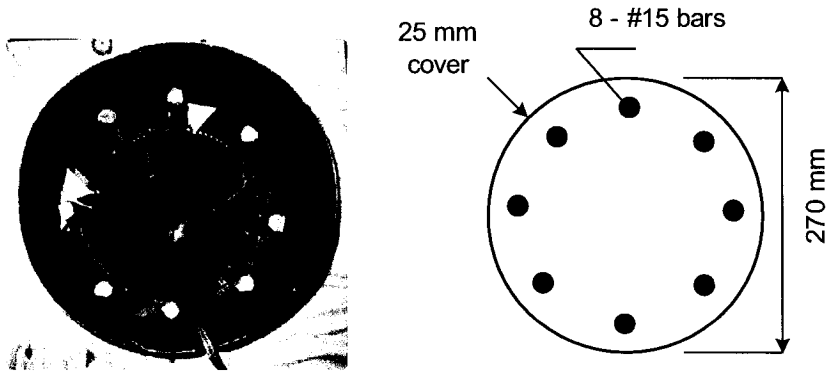

Fig. 3.2 – Column cross-sectional arrangement

Fig. 3.3 – Preparation of FRP casings

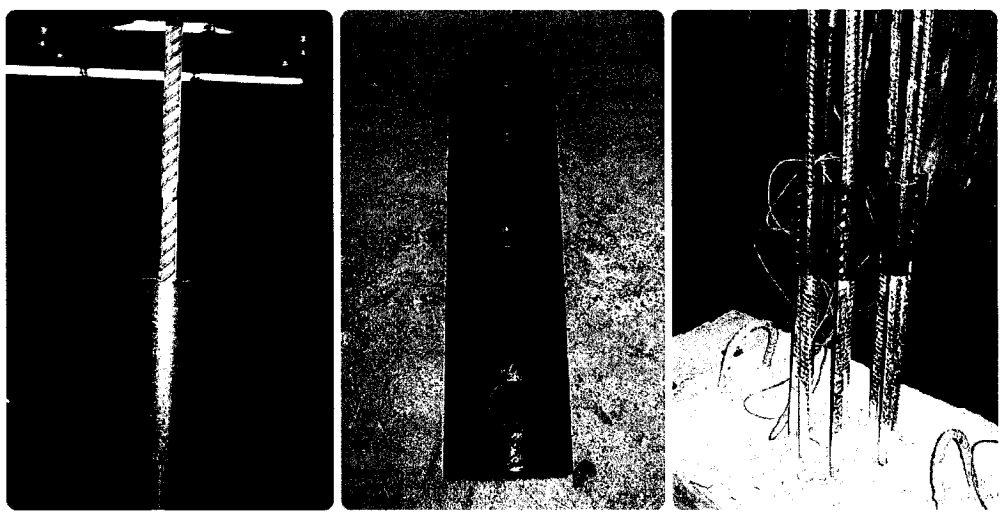

Fig. 3.4 – Mechanical Splices

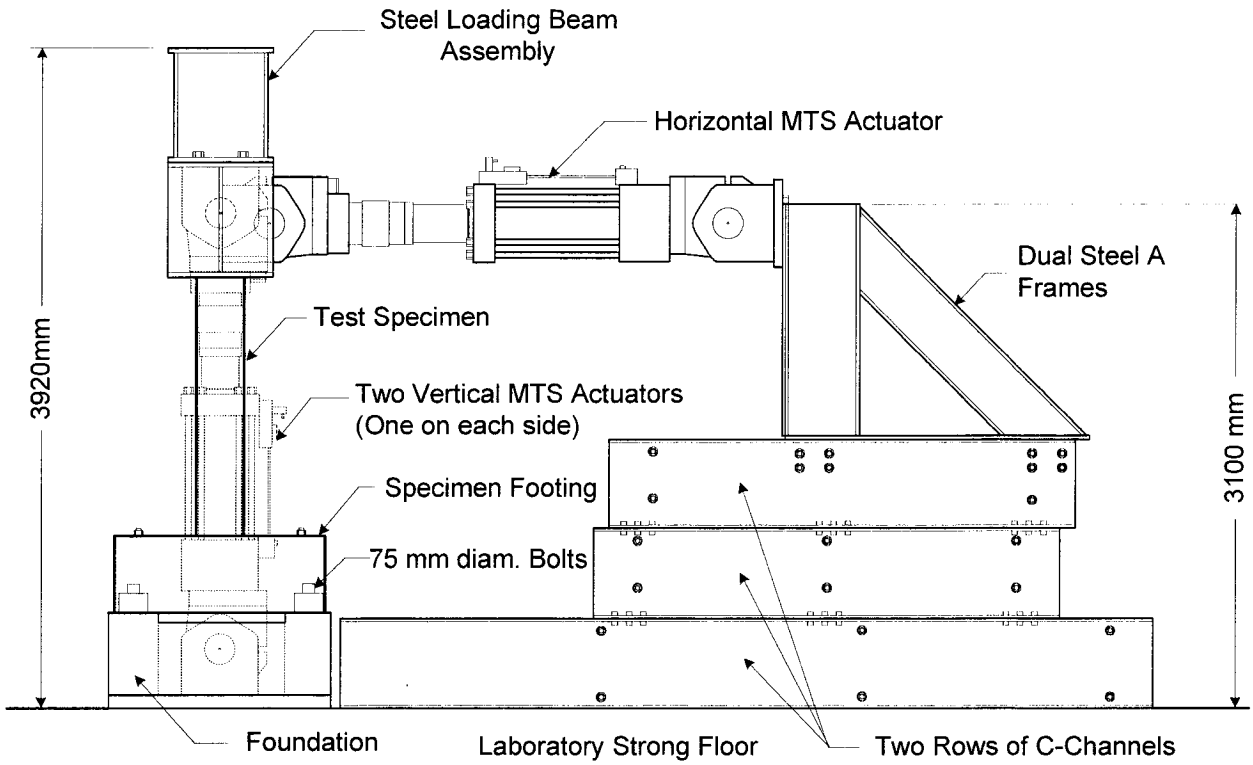

Fig. 3.5 – Test setup

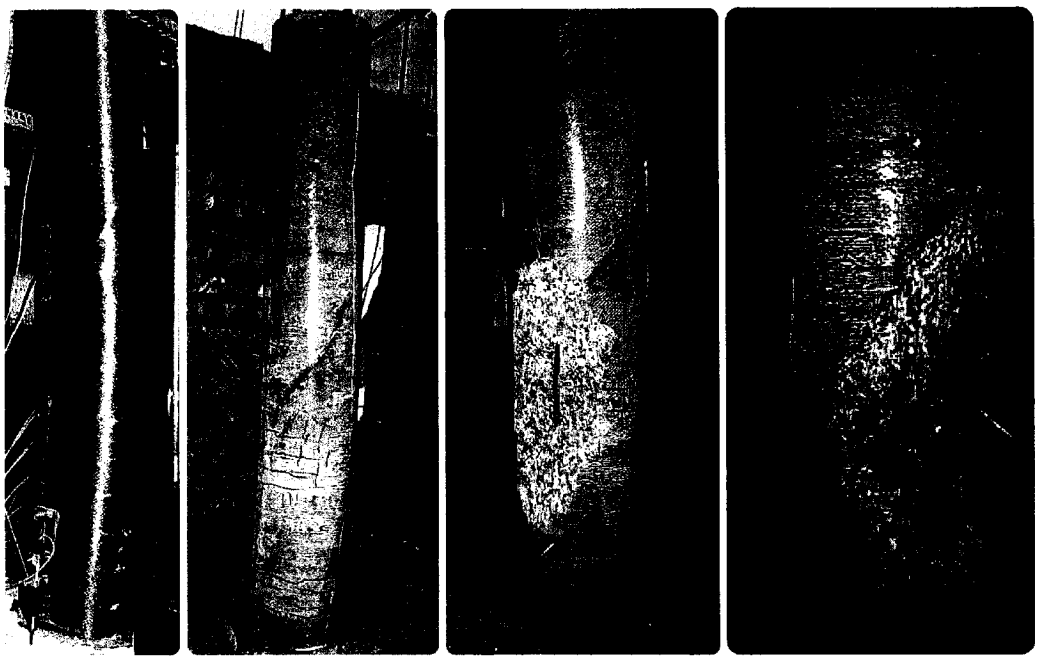

(a) Specimen RC–1

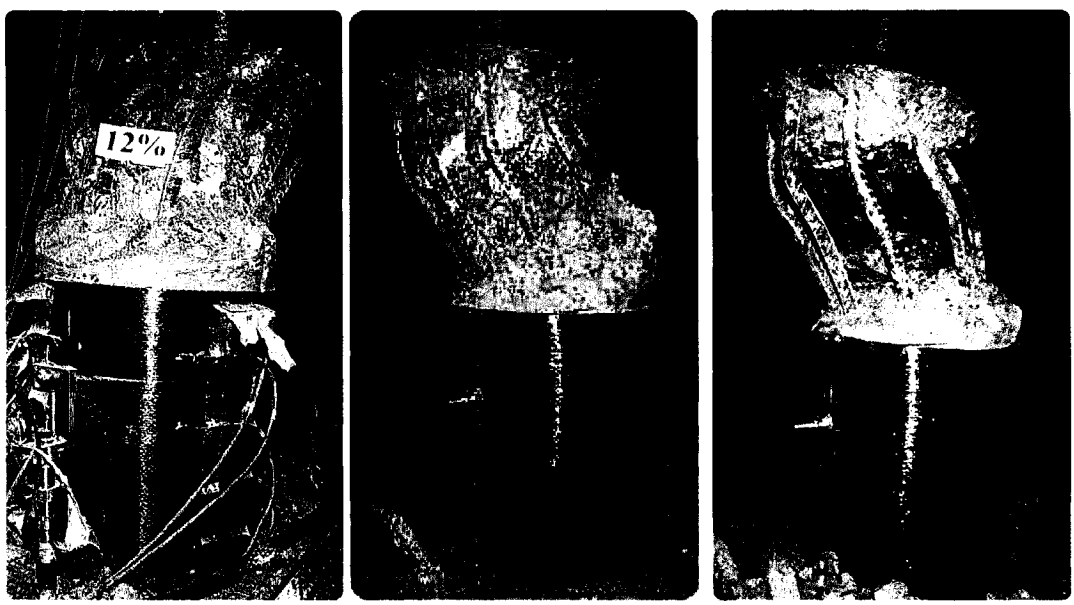

(b) Specimen RC–2

Fig. 3.6 – Specimens at end of testing

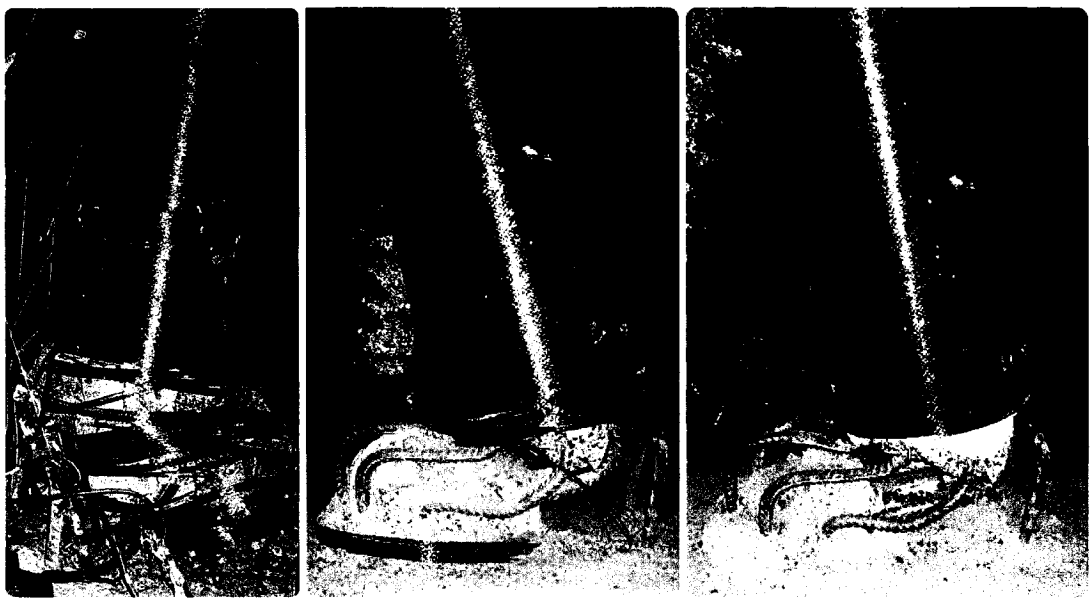

(c) Specimen RC–3

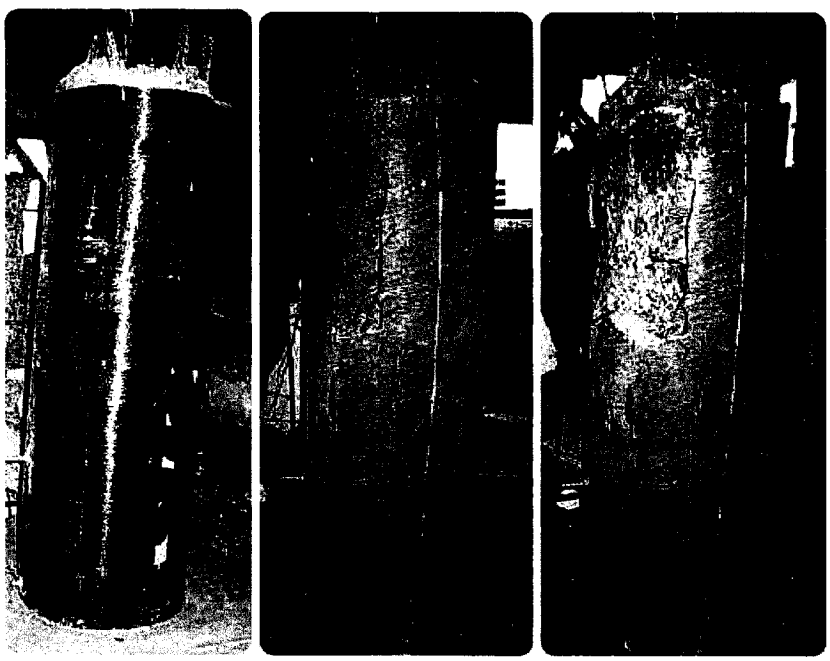

(d) Specimen RC-4

Fig. 3.6 – Cont'd

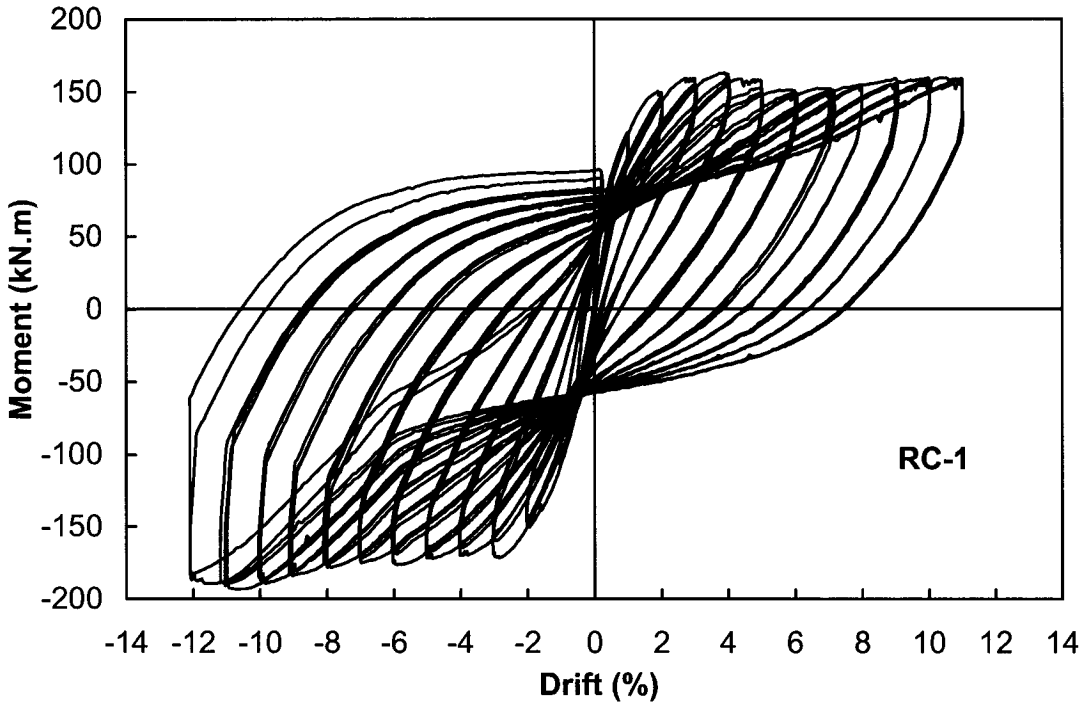

a) Column RC-1

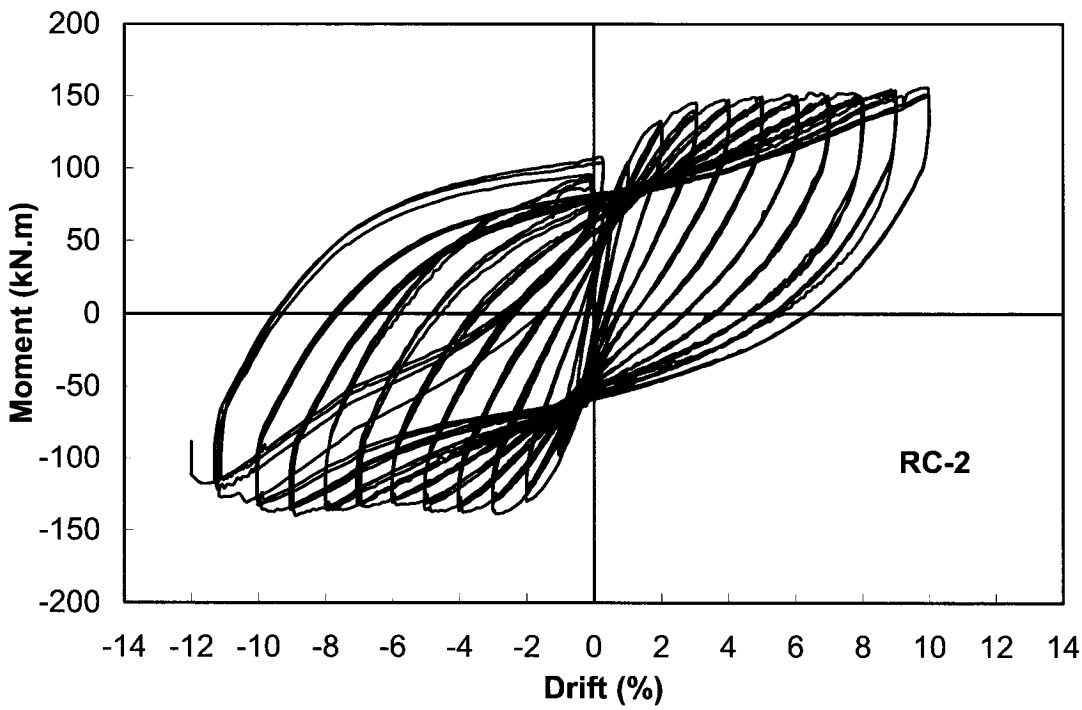

b) Column RC-2

Fig. 3.7 – Experimentally recorded hysteretic moment-lateral drift relationships

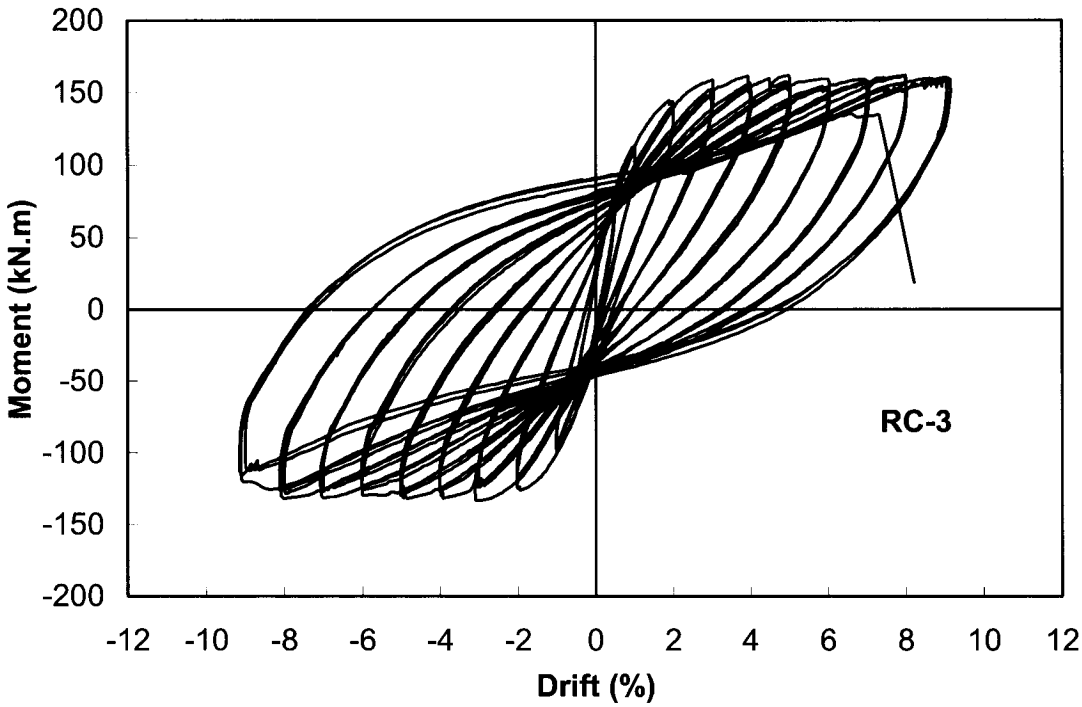

c) Column RC-3

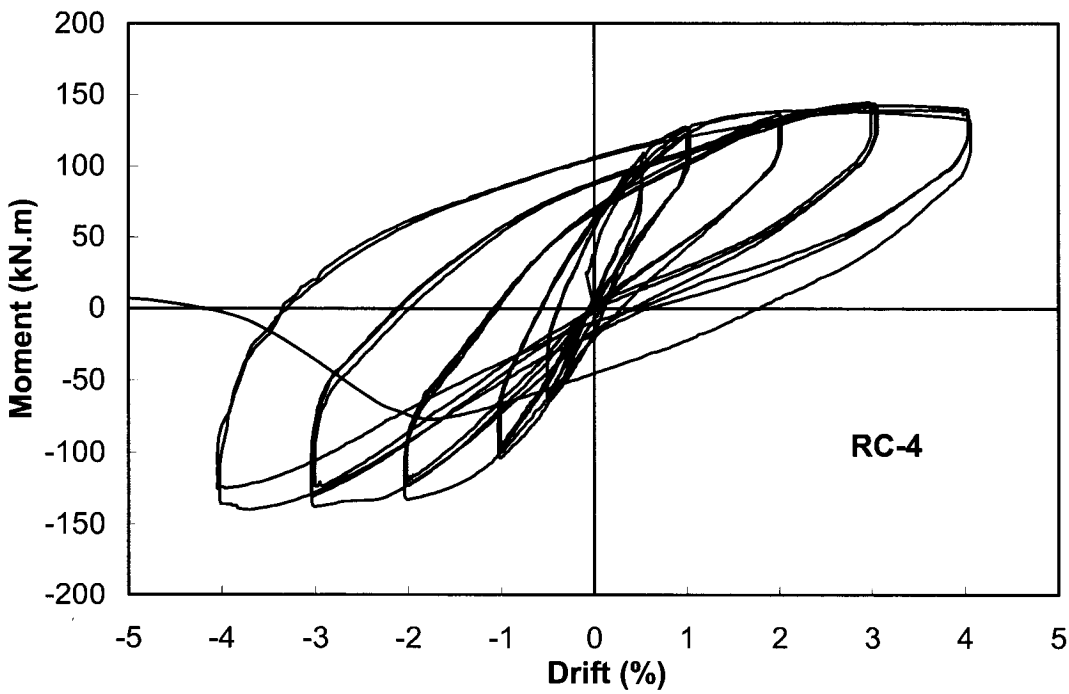

d) Column RC-4

Fig. 3.7 – Cont'd

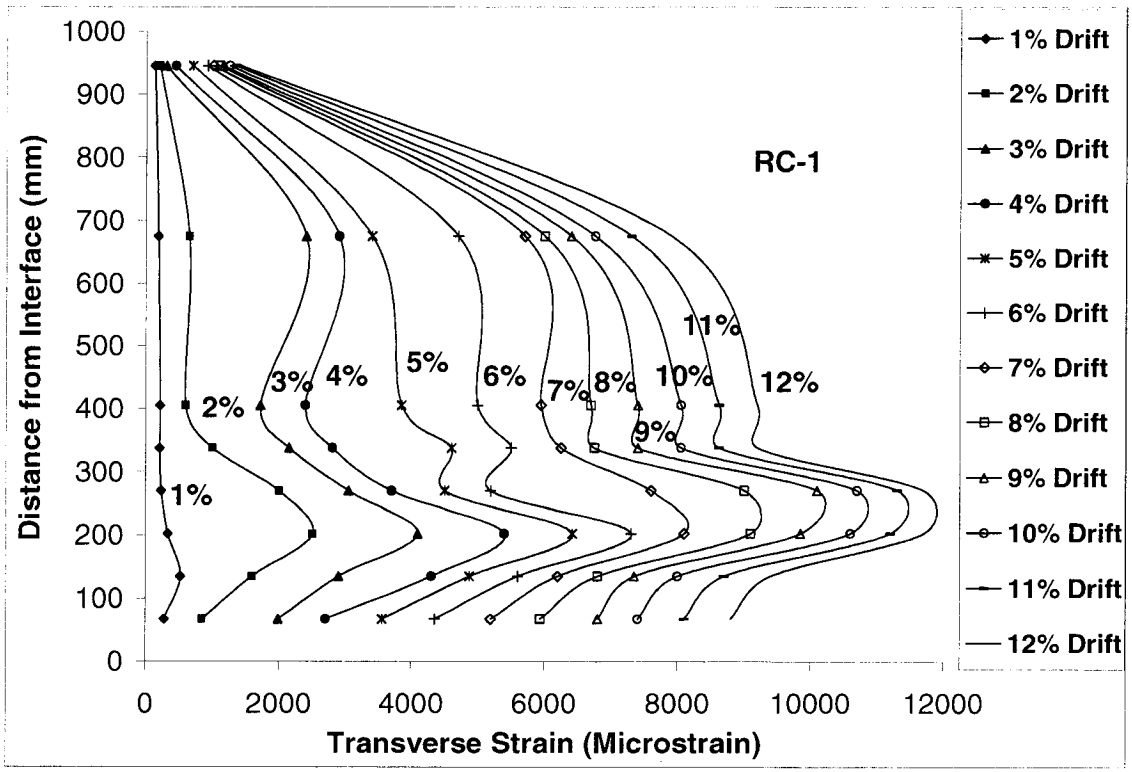

a) Column RC-1

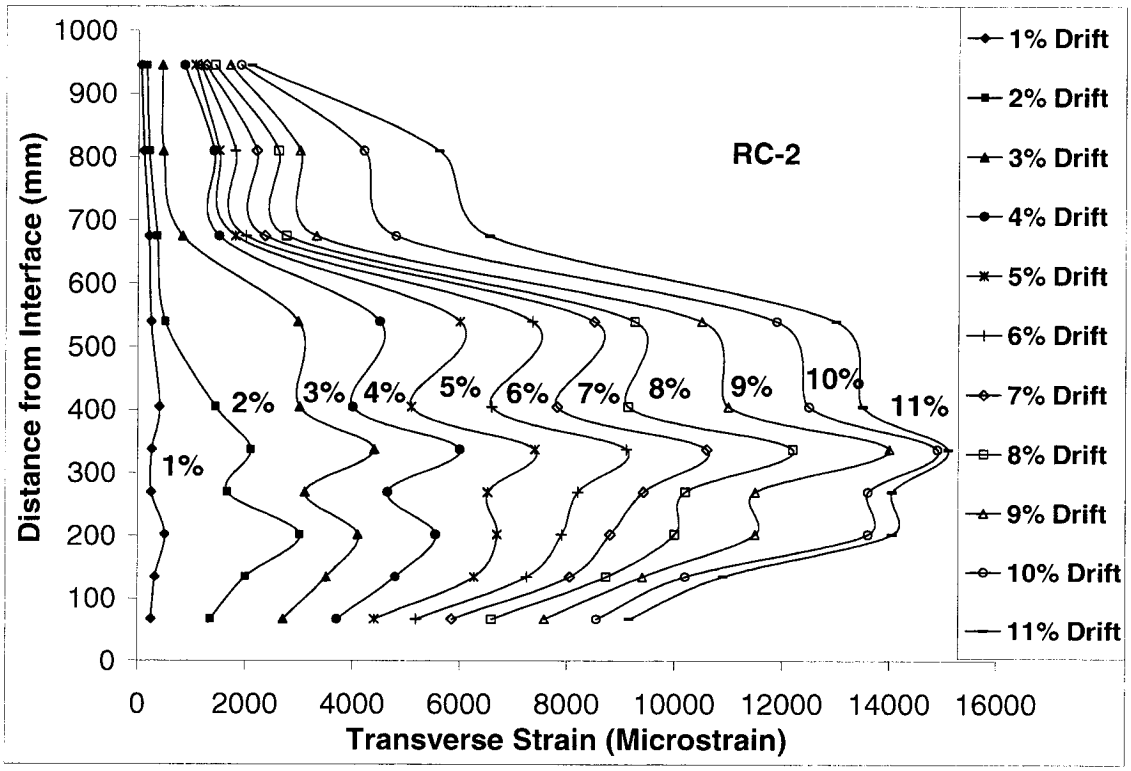

b) Column RC-2

Fig. 3.8 – Variation of transverse strains on FRP casings along column height

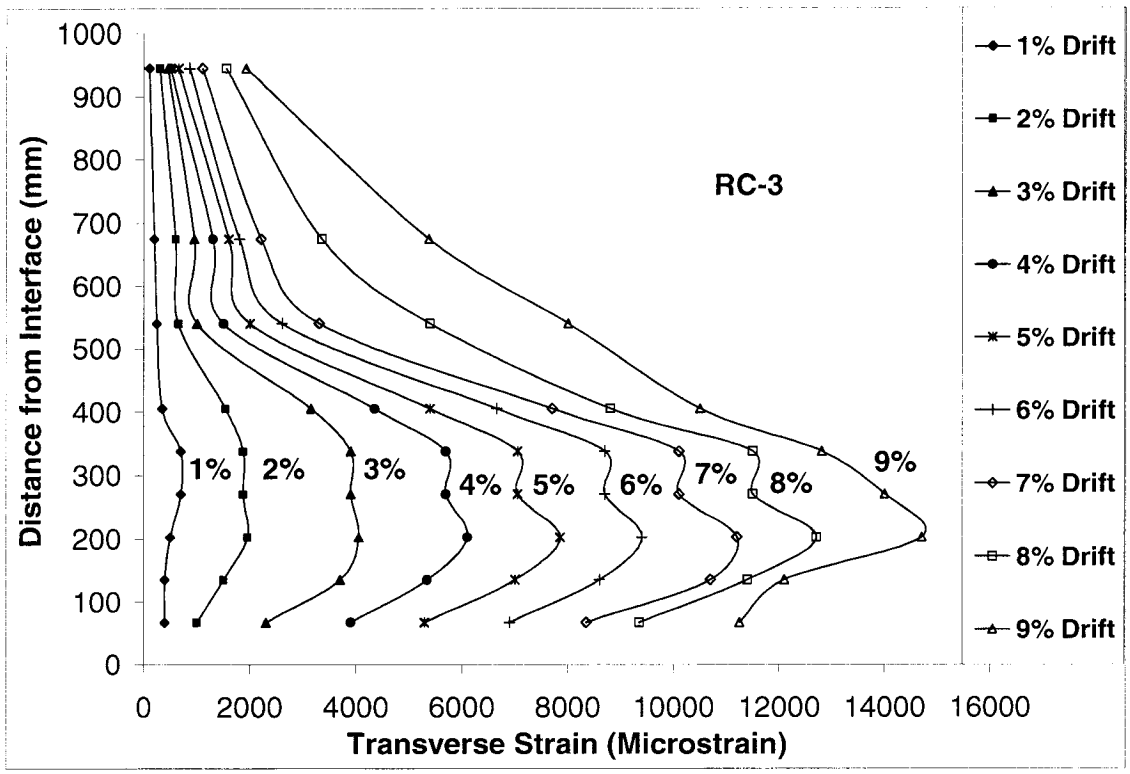

c) Column RC-3

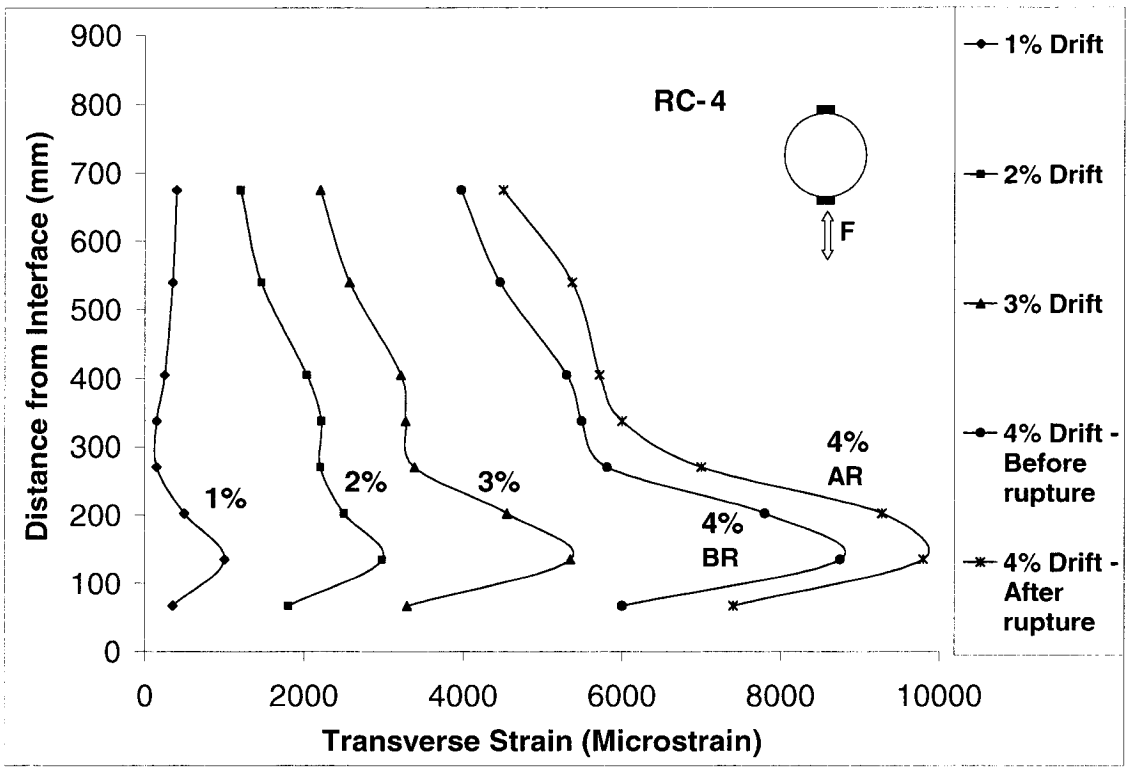

d) Column RC-4, end faces

Fig. 3.8 – Cont'd

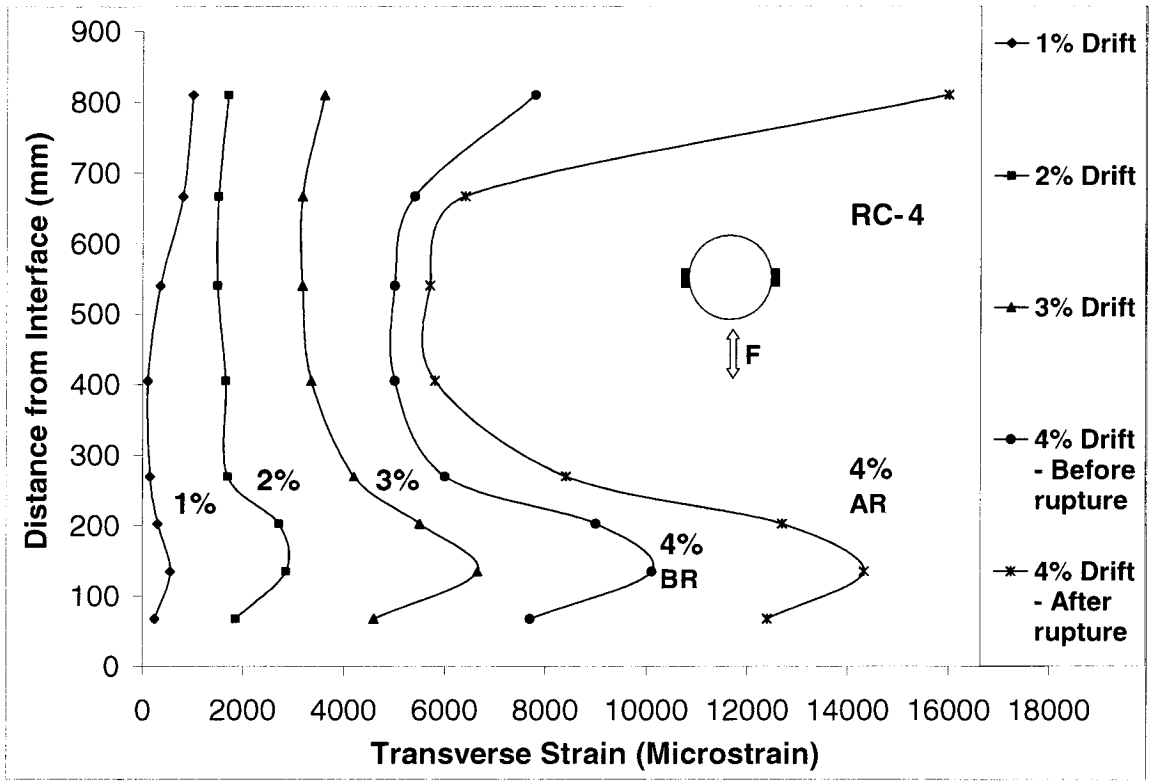

e) Column RC-4, side faces

Fig. 3.8 – Cont'd

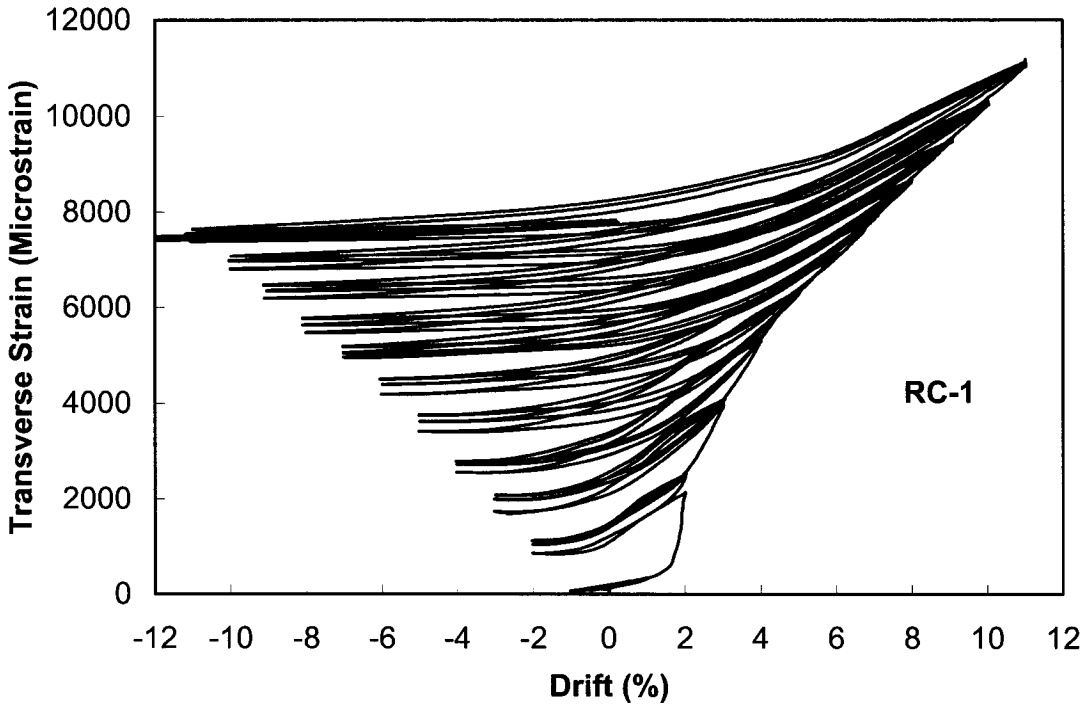

(a) Column RC-1

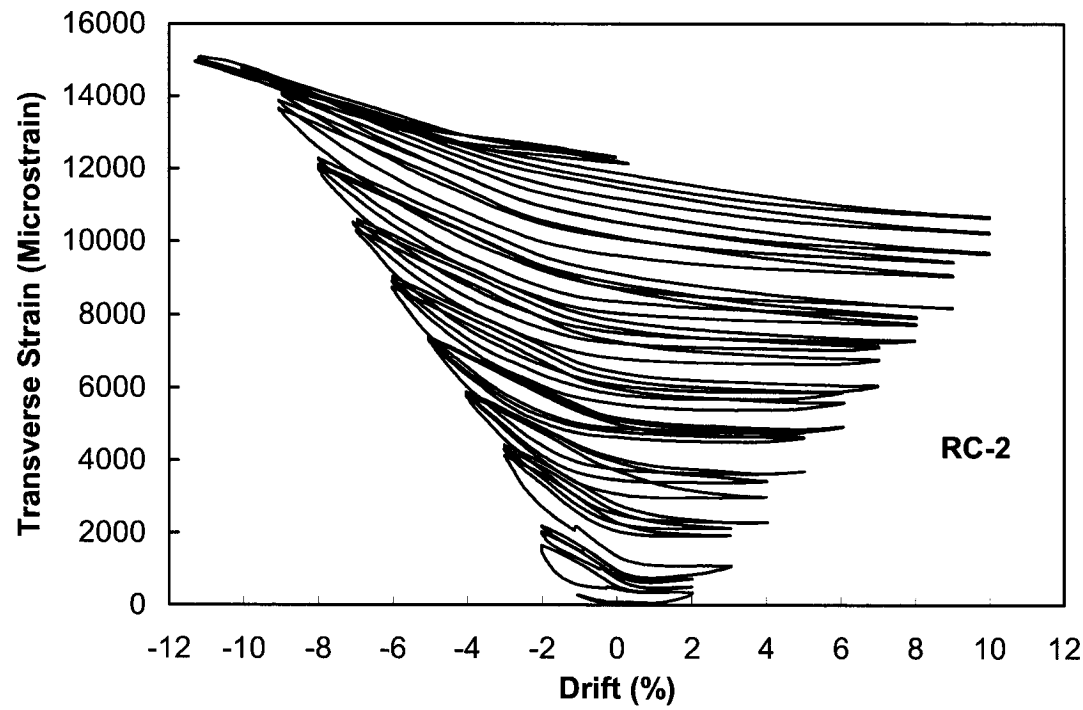

(b) Column RC-2

Fig. 3.9 – Typical hysteretic transverse strain-lateral drift relationships

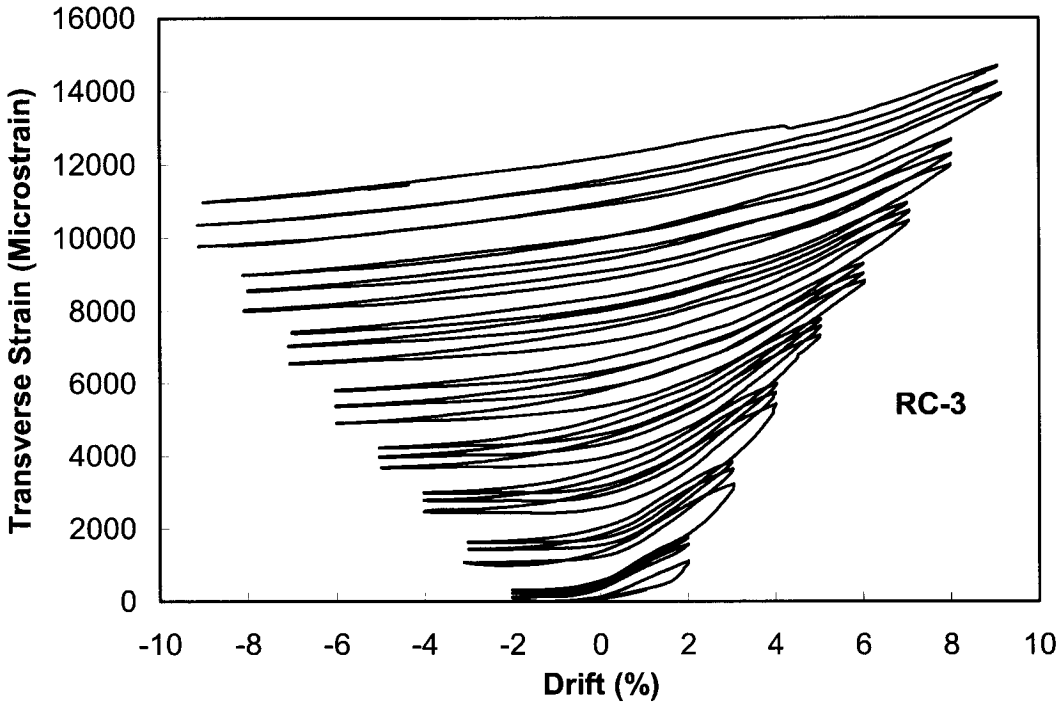

(c) Column RC-3

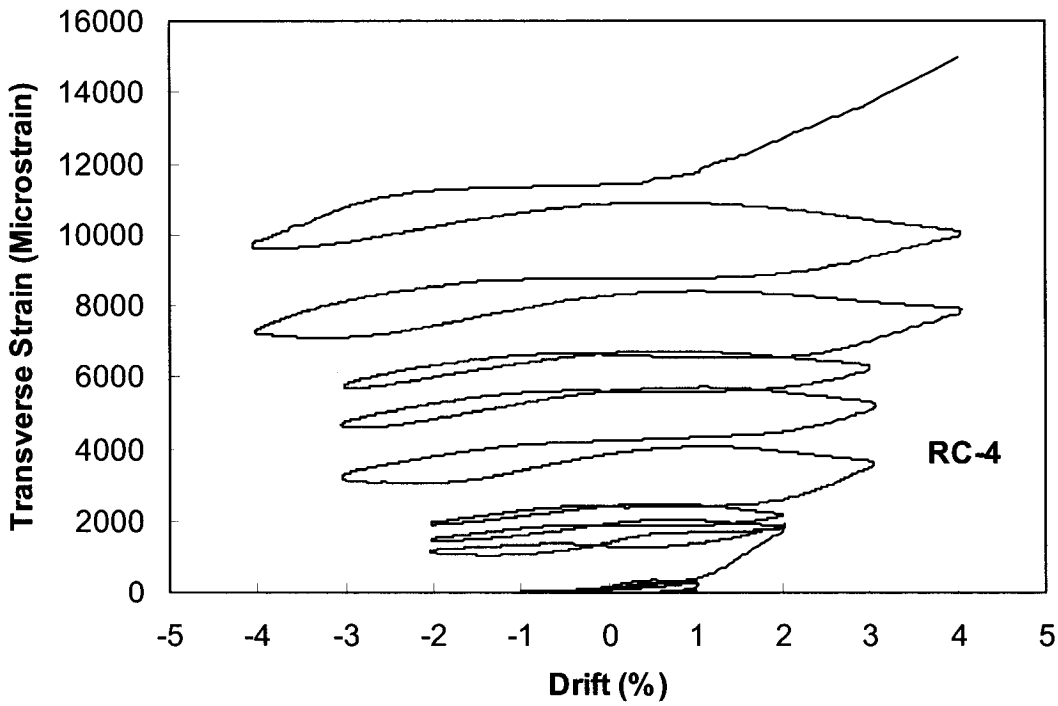

(d) Column RC-4

Fig. 3.9 – Cont'd

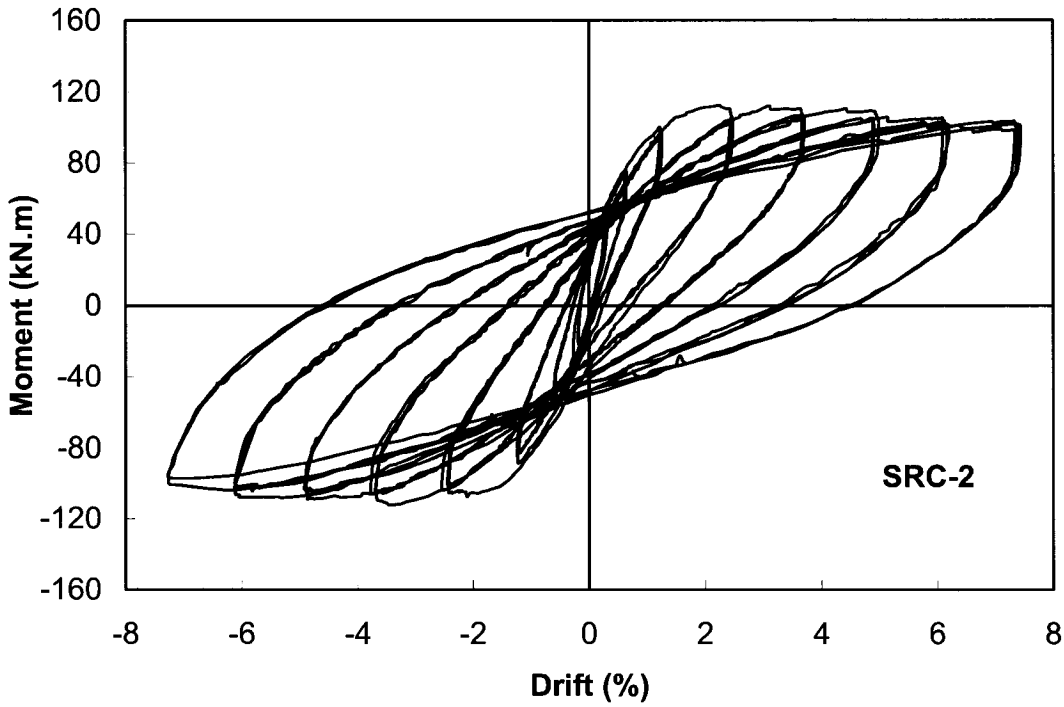

(a) Column SRC-2

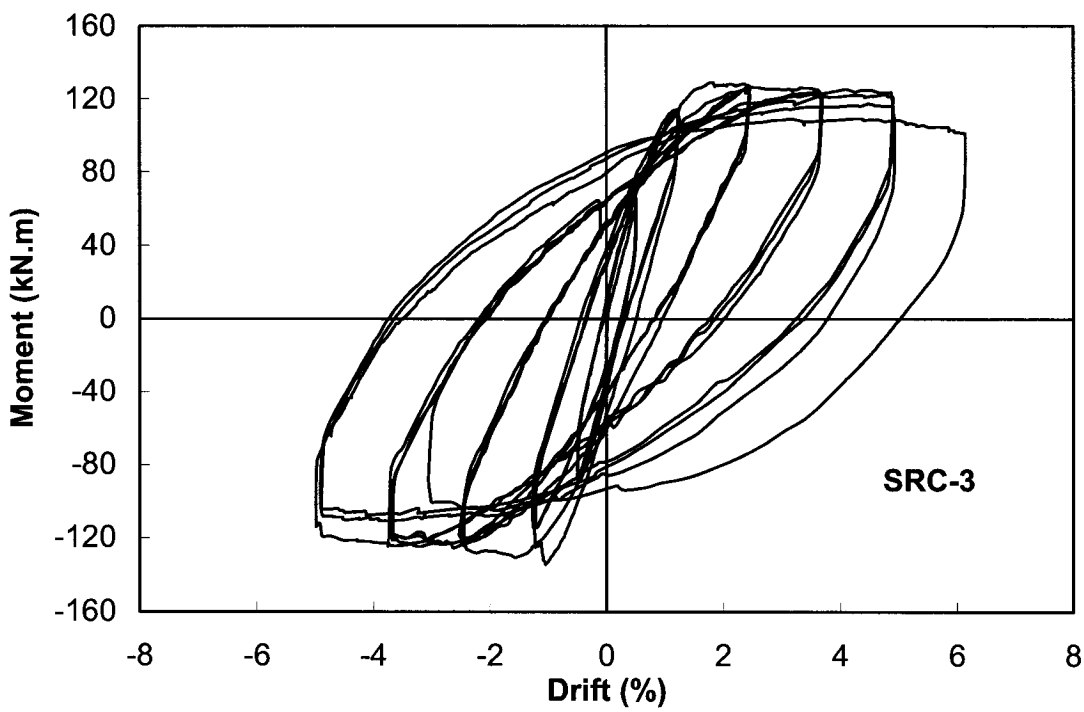

(b) Column SRC-3

Fig. 3.10 – Hysteretic moment-lateral drift relationships of columns confined with conventional steel (Saatcioglu and Baingo 1999)

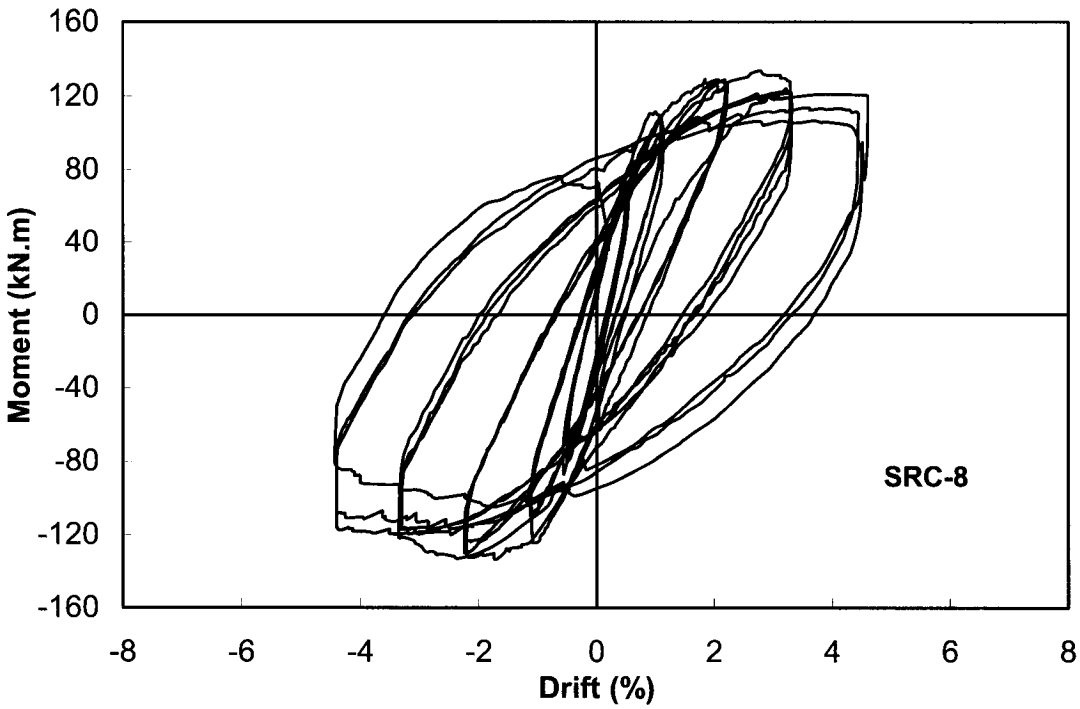

(c) Column SRC-8

Fig. 3.10 – Cont'd

Chapter 4

Seismic Performance of Square High-Strength Concrete Columns in FRP Stay-in-Place Formwork

4.1 INTRODUCTION

The use of high-strength concrete (HSC) in building and bridge construction has increased over the last two decades. HSC offers advantages over normal-strength concrete in terms of increased strength and improved performance. The gain in strength, however, is achieved at the expense of deformability. Indeed, HSC structural elements exhibit brittle behavior at failure, jeopardizing their use in seismically active regions where significant inelastic deformability and energy dissipation are required to resist seismic induced inertia forces. Inelastic deformability of concrete can be improved through confinement. Concrete confined by properly designed transverse reinforcement can develop adequate ductility to allow structures develop sufficient lateral drift without significant strength degradation. However, the confinement requirements become prohibitively stringent for HSC elements when normal-grade conventional steel ties, hoops, overlapping hoops or spirals are used. The excessive amount of conventional confinement reinforcement required for HSC columns leads to the congestion of column cages and resulting concrete placement problems. On the other hand, fiber reinforced polymer (FRP) materials offer

an attractive alternative to confine concrete. FRP pre-formed shapes, in the form of stay-in-place formwork with circular or square cross-sections offer multiple advantages of; i) light and effective formwork with superior handling characteristics, ii) efficient and durable transverse confinement reinforcement with ability to generate high lateral confinement pressures, and iii) protective shell against corrosion, weathering and chemical attacks.

The performance of concrete-filled circular and rectangular FRP casings, under combined bending and axial load, has been studied extensively (Mirmiran et al. 1998a, 1999, 2000; Fam and Rizkalla 2002; and Fam et al. 2003, 2005). Furthermore, FRP wrapping of concrete columns as a seismic retrofit strategy has been studied by researchers in the past (Seible et al. 1997; Sheikh and Yau 2002; and Iacobucci et al. 2003). The use of FRP stay-in-place formwork for improved seismic performance of new columns was investigated by Seible et al. (1996), Shao (2003), Zhu (2004) and Ozbakkaloglu and Saatcioglu (2005a). However, research on seismic performance of concrete filled square/rectangular FRP casings is limited, with the available research focusing on normal strength concrete column behavior. The current thesis has the objective of presenting the results of an experimental investigation on the effectiveness of square stay-in-place FRP formwork for HSC columns, subjected to simulated seismic loading.

4.2 EXPERIMENTAL PROGRAM

HSC columns with square geometry were designed, constructed and tested under simulated seismic loading. The columns were designed with due considerations given to the parameters that affect the efficiency of confinement reinforcement. It has long been established that circular spirals are more effective in confining concrete than rectilinear ties. Similarly, it has been

reported that the effectiveness of FRP jackets is higher in circular columns than square columns (Mirmiran et al. 1998b; Rochette and Labossiere 2000; and Pessiki et al. 2001). This may be explained by hoop tension generated in circular columns, resulting in uniform passive confinement pressure. Square jackets, on the other hand, develop high confining pressures at the corners due to high transverse forces generated in transverse FRP. Confinement diminishes quickly along the sides of a rectilinear section where the restraint is limited to the flexural rigidity of FRP jacket, which is very low. A similar phenomenon was observed in specimens confined with conventional rectilinear steel reinforcement (Saatcioglu and Razvi 1992). Increased corner radius *(R)* promotes hoop tension near the corners, thereby improving the effectiveness of confinement. Furthermore, the cross-sectional size *(D)* influences the flexural rigidity of the FRP casing between the corners, affecting confinement efficiency. These two parameters can be expressed in the form of R/D ratio. The effect of R/D ratio on confinement effectiveness was also reported by other researchers who conducted tests on FRP confined concrete specimens under concentric loading (Mirmiran et al. 1998b; Rochette and Labossiere 2000; and Pessiki et al. 2001). Two diameter-to-depth ratios (R/D) of 1/6 and 1/34 were employed in the current experimental program. These values may be viewed as a lower and a higher R/D ratio of a range that may be employed in practice.

An important parameter of confinement for square and rectangular columns is the use of internal crossties. Crossties are typically required in conventionally reinforced columns and they improve the distribution of lateral restraints against concrete expansion, improving the uniformity of confinement pressure. A similar improvement is anticipated in columns confined with FRP casings if internal crossties can be provided. A new type of stay-in-place formwork was

developed and verified in the experimental program, consisting of exterior FRP casings and internal FRP crossties, as further discussed under "Material Properties." Either one or two crossties in each cross-sectional direction were placed inside the casing, emulating 8-bar and 12-bar arrangements with crossties while providing clamping forces to the exterior shell. This was investigated as part of the test parameters.

4.2.1 Test specimens

A total of six large-scale columns were prepared for testing. Each specimen consisted of a 270 mm square cross-section having a 1,720 mm cantilever height. The shear span for each column was 2,000 mm, measured to the point of application of lateral force which was located on a steel loading beam 280 mm above the column. The specimens represented the lower half of a first-storey building column with an inter-storey height of 4.00 m between fixed ends.

HSC, with cylinder strengths (f'_c) of 75 MPa or 90 MPa, were used to cast the columns. A clear concrete cover of 25 mm was provided as measured to the outside of longitudinal reinforcement. Three different longitudinal reinforcement arrangements were used, consisting of; i) 4-bar, ii) 8-bar and iii)12-bar arrangements. No.15 (16 mm diameter) deformed steel bars, with a yield strength (f_y) of 500 MPa, were used as longitudinal reinforcement for the latter two arrangements, while No.20 bars (19.5 mm diameter), with a yield strength of 476 MPa, were used for the 4-bar arrangement. Three of the columns had FRP formwork with internal FRP crossties, spaced vertically at 68 mm, corresponding to 1/4 of the column dimension. One of the columns had 12 longitudinal bars and two crossties in each cross-sectional direction (RS-3). The other two columns had 8 longitudinal bars and one internal crosstie in each cross-sectional

direction (RS-2 and RS-5). FRP casings were used without any crossties for the remaining columns (RS-1, RS-4, and RS-6).

The specimens were tested in two groups. The columns tested in the first group (RS-1, RS-2, RS-3) had five plies of FRP in their casings, while the specimens in the second group either had two (RS-5) or three plies (RS-4 and RS-6). The number of FRP plies was established based on the behavior of FRP confined (Miyauchi et al. 1997; Samaan et al. 1998; Saafi et al. 1999; Spoelstra and Monti 1999; Lam and Teng 2002, 2003; and Moran and Pantelides 2002) and steel confined (Sheikh and Uzumeri 1980; Mander et al. 1988; and Saatcioglu and Razvi 1992) concrete, while also considering current FRP design guidelines (Buckle and Friedland 1994; ACI 440 2002; and CSA S806 2002). Two important parameters were considered in estimating the required plies of FRP sheets. These were; i) the design transverse strain of FRP material and ii) the effect of corner radius. Because of the linear elastic behavior of FRP, the determination of design transverse strain is critical in establishing the required number of FRP plies. Transverse strains in excess of 1.0% were recorded during the tests of the first group of columns with a corner radius of 45 mm (R/D = 1/6). This indicated that the design fiber strain of 0.4%, recommended by current FRP design guidelines (Buckle and Friedland 1994; ACI 440 2002; and CSA S806 2002) was rather conservative for the columns considered in the first part of the experimental program. Consequently, the number of plies was reduced in the second group.

Column corners were provided with a corner radius of 45 mm, resulting in an R/D ratio of 1/6, except for column RS-6, which had a corner radius of 8 mm, resulting in an R/D ratio of 1/34.

Figures 4.1 and 4.2 illustrate the geometry and reinforcement arrangements. Table 4.1 provides a summary of geometric and material properties.

4.2.2 Material properties

Carbon FRP Composite

A carbon fiber composite system was used to manufacture the stay-in-place formwork manually in the Structures Laboratory of the University of Ottawa. Carbon fiber was selected over glass fiber because of higher elastic modulus and tensile strength of the material, which is believed to be more compatible with high modulus and high strength concretes. The same FRP composite material was used for all casings, with fibers aligned in the circumferential/transverse direction. The nominal thickness of carbon fiber sheet was 0.165 mm/ply, which was increased to 0.8 mm/ply when impregnated with epoxy resin. The stress-strain relationship of composite material was established by coupon tests and showed linear-elastic behavior up to the rupturing strength in tension. The capacity of the composite material was established to be approximately 785 MPa based on the fiber content corresponding to 0.8 mm/ply. This observation was found to be in agreement with the 3800 MPa fiber strength reported by the manufacturer. Table 4.2 provides the properties of carbon fibers as supplied by the manufacturer. The maximum tensile strain of 1.67% specified by the manufacturer was also in agreement with the average ultimate strain recorded in coupon tests. The above values translate into an elastic modulus of 47,000 MPa for the composite material, which is in line with 227,000 MPa reported for the modulus of elasticity of carbon fibers alone.

The manufacturing process involved wrapping impregnated FRP sheets around wooden templates. The templates of columns with 45 mm corner radius had PVC pipes for rounding the corners, while the template for the column with 8 mm corner radius had wood quarter rounds in the corners, as illustrated in Fig. 4.3. The FRP sheets were wrapped one layer at a time with a 100 mm overlap in the direction of fibers to ensure proper bond. Adjacent layers were not overlapped vertically along the column height. While the hand lay-up method used in the laboratory resulted in very good quality casings, an automated technique involving centrifugal (spin) casting, filament winding, or pultrusion may offer better quality control for applications in practice, especially when high volume production is required. FRP crossties were prepared separately by wrapping the same FRP sheets used in manufacturing the casings, around low tensile-strength phenolic bars, prior to securing them to the casings. The phenolic bars were used as templates, without contributing to the strength of the crossties. The fibers protruded loosely (without epoxy impregnation) beyond the ends of the template bars to allow subsequent integration with the casing. This is depicted in Fig. 4.4. Following the installation of the initial plies of impregnated FRP sheets, 8 to 10 mm diameter small holes were drilled to insert the FRP crossties. Upon insertion, the fibers at the ends of crossties were bent and glued to the existing casing by using epoxy resin. A final ply of the composite material was applied to cover the entire casing in RS-5, while two plies were used in RS-2 and RS-3. This is illustrated in Fig. 4.5.

Two different fiber contents were used in FRP crossties, as governed by the width of the fiber sheets cut and rolled to form the crossties. The first width was 40 mm and was used for the columns in the first group (RS-2 and RS-3). They were mainly designed to improve the effectiveness of the casing by providing restraint against expansion, and their contribution to

total fiber area was insignificant. After the encouraging results of the first group of columns, it was decided to replace one ply of FRP from the casing with the same amount of fibers placed in FRP crossties, thereby reducing the number of plies in the casing while increasing the fiber content in the crossties. This resulted in a fiber width of 135 mm, and used for the crossties of RS-5, tested subsequently. The total fiber area of column RS-5, comprised of a two-ply casing and crossties, was equal to the fiber area used in the three-ply casings of RS-4 and RS-6 without the crossties.

Concrete

The columns were cast from two batches of concrete. The mix for HSC was designed and ordered from a ready-mixed company. Both mixes consisted of 10SF cement (8% Silica fume blended Normal Portland Cement) and crushed limestone with 10 mm maximum size. The water cement ratios of 0.22 and 0.26 were used for the first and second batches of concrete to obtain the target strengths of 90MPa and 75MPa, respectively, at the time of testing. The strength and workability were the main criteria in mix designs, which were achieved by selecting a low water-cement ratio and high cement content. It was necessary to use superplasticizers and retarders to achieve and maintain the desired level of workability. An initial concrete slump of 200 mm was achieved and maintained during casting. All specimens were cast vertically and vibrated thoroughly. The strength was monitored through period testing of cylinders. The columns were tested when the average concrete strength reached the target strength.

Steel Reinforcement

Canadian Standard No. 15 and No. 20 deformed steel bars were used as longitudinal reinforcement with nominal diameters of 16 mm and 19.5 mm, and with yield strengths of 500 MPa and 476 MPa, respectively. The stress-strain relationships were established by performing at least three coupon tests for each type of reinforcement. None of the columns had any transverse steel reinforcement, except for the extension of column cage into the footing, where the longitudinal bars were positioned by means of three ties. A single tie was also used at the top to keep the bars in place. Table 4.3 provides average properties for the reinforcement used, with standard notations; (E_s) as the elastic modulus; (f_y) and (f_u) as stresses at yield and ultimate, respectively; (ε_y), (ε_{sh}), (ε_u), and (ε_r) as strains at yield, onset of strain hardening, ultimate, and rupture, respectively.

Mechanical splices were used in columns RS-4 and RS-6 to splice longitudinal bars at 500 mm and 900 mm from column footing interface, respectively as illustrated in Fig. 4.6. High strength reinforcing bar couplers, designed for extreme tension/compression applications, were used to investigate their applicability to columns under seismic loading. The tensile capacity of couplers was specified by the manufacturer to be in excess of 1.6 times the specified yield strength of standard reinforcing bars (60,000 psi or 414 MPa). This corresponds to a capacity of 662 MPa, which is greater than the ultimate tensile capacity (f_u = 620 MPa) of the 16 mm diameter bars used in the current investigation. The tension coupon tests were conducted on mechanically spliced 16 mm bars, and the failure was observed to take place away from the splice region, confirming manufacturer's specification, as shown in Fig. 4.6.

4.2.3 Instrumentation, test setup, and loading program

The columns were instrumented with Linear Variable Displacement Transducers (LVDT) and strain gages to measure horizontal displacements, rotations of the plastic hinge region, anchorage slip, and horizontal and transverse strains. All instrumentation was connected to a data acquisition system and a microcomputer for data recording. The acquisition of strain data on FRP casings was of particular interest to develop a better understanding of the strain profile on the casings. Therefore, a large number of strain gages (26 to 29), were placed on the surface of FRP casings oriented in the direction of carbon fibers, at eight to ten different levels along the height. The first six layers of gages from the base were place at a spacing of one quarter the cross-sectional dimension along column height, followed by either one half or full cross-sectional dimension.

Each column was tested under constant axial compression and incrementally increasing lateral deformation reversals, simulating seismic loading. Two 1000 kN capacity computer servo-controlled MTS hydraulic actuators were positioned vertically, one on each side of the column, to apply constant axial compression. Another 1000 kN capacity MTS actuator was placed horizontally for the application of lateral deformation reversals. Figure 4.7 illustrates the test setup.

The columns represented first story columns of a multistory building and they were tested under 30% or 34% of their concentric capacity, (P_o), computed as indicated below, where (f'_c) is the compressive strength of concrete as established by standard cylinder tests, (A_g) is the gross area of column section and (A_s) is the total area of longitudinal steel:

$$P_o = 0.85 f'_c (A_g - A_s) + A_s f_y \quad (1)$$

The specimens were subjected to lateral displacement excursions, consisting of incrementally increasing deformation reversals. Three full cycles were applied at each deformation level, starting with 0.5% drift ratio and increasing to 1%, 2%, 3% etc., in the deformation control mode of the horizontal actuator. Lateral loading continued until the specimen was unable to maintain a significant fraction of its maximum lateral load resistance. The rate of lateral loading was low and the total duration of a typical test was about four to five hours, depending on the deformability of column.

4.3 TEST RESULTS

4.3.1 Observed Behavior

All columns initially behaved in a similar manner up to 2 % lateral drift ratio, with the exception of the column with small corner radius (RS-6), which started demonstrating signs of distress during the first cycle of 2% lateral drift level. There was no visual sign of damage in the columns with well-rounded corners until the end of this deformation level. At 3% drift, localized changes in FRP color was observed within the plastic hinge region of columns RS-1, RS-4 and RS-5, which had either reduced number of FRP plies and/or no FRP crossties, indicating the separation of FRP material from concrete as the concrete began to crush. A similar discoloration was observed at 4% drift ratio in columns RS-2 and RS-3 with 5 plies of FRP, as well as FRP crossties. The regions of discoloration extended with increasing displacement level, up to about 540 mm from the column-footing interface, which is equal to twice the column cross-sectional dimension. These visual observations were also supported by the strain data recorded on FRP casings, as discussed later in the thesis. Column RS-6 started to expand into a circular shape

beyond 2% lateral drift cycles, due to the increased damage to concrete. Fiber rupturing began to occur at 4% lateral drift level. This phenomenon and associated distortion in FRP was not as prominent in columns with rounded corners; especially the columns with internal crossties maintained their shape until the end of testing. Any increase in deformations beyond 4% lateral drift ratio resulted in a substantial increase in fiber dilatation within the plastic hinge region of columns with well-rounded corners.

Fiber rupture was the failure mode for all but one column, which initiated at or near column corners. The rupturing was accompanied with snapping sound and the release of previously built passive pressure in FRP casings. This occurred during the third cycle of 8% drift in Column RS-1 with 5 plies of FRP without FRP crossties, and the first cycle of 12% drift in Column RS-3 which had the same number of plies in the casing, in addition to double FRP crossties in each direction. Testing of Column RS-2, with 5 plies of FRP and a single crosstie in each direction, was stopped after a complete cycle at 9% drift ratio, due to out of plane deformations. Consequently, fiber rupturing was not observed in this column, though experimental observations and strain readings suggested that the column could sustain up to 10% lateral drift prior to fiber rupturing. Columns RS-4 and RS-5 had the same amount of lateral fibers. RS-4 had three plies of FRP, all placed in the casing whereas RS-5 had two plies in the casing and an additional ply of fibers placed in the form of FRP crossties. The columns demonstrated similar behavior, with RS-4 failing at the first cycle of 7% lateral drift and RS-5 failing at the third cycle of 6% drift, respectively. None of the columns with well-rounded corners developed any appreciable strength decay until after the fibers ruptured. Column RS-6, with small-radius corners, however, developed approximately 20% strength decay immediately after 2% drift ratio

and fiber rupturing at the end of 4% drift cycles. Columns RS-4 and RS-6 were identical in every respect except for the R/D ratio. While RS-4 had an R/D ratio of 1/6, the R/D ratio of RC-6 was 1/34. The most extensive damage occurred at approximately 100 mm to 160 mm above the column-footing interface, which coincided with the location of first fiber rupture in all columns. The shifting of the critical section from the interface was attributed to the confining effect of the footing. Similar observations were previously reported by others (Sheikh and Khoury 1993). Figure 4.8 illustrates hinging regions after the failure of columns. Table 4.4 summarizes the strength values and locations of most damaged sections for all columns.

Displacement components due to flexure and anchorage slip were measured during testing. It was observed that approximately 10% of lateral drifts developed in all columns were caused by the anchorage slip of longitudinal reinforcement, immediately before failure.

4.3.2 Hysteretic Behavior

Experimentally recorded moment-drift hysteretic relationships are shown in Fig. 4.9. They show typical flexure-dominant response, with well-rounded hysteresis loops. The loops did not indicate any sign of shear effect on overall column behavior, as evidenced by the lack of clear pinching of the loops, even after the formation of plastic hinges. No significant strength degradation was observed in any of the columns with well-rounded corners until the end of testing, at which stage local rupturing of FRP occurred. Some strength decay in column resistance can be tolerated in multistory, multi-bay buildings before the column is considered to have failed. If a column maintains at least 80% of its maximum moment resistance for at least three full cycles of deformation, then it may be considered to have maintained its seismic

resistance (Park and Paulay 1975; Saatcioglu 1991). Once the strength decay exceeds 20%, the column is considered to have failed. Displacement ductility factors were computed as the ratio of maximum column displacement prior to 20% strength decay, to displacement at initial yielding of the extreme longitudinal reinforcement. The initial yield of longitudinal reinforcement in all columns was observed to be approximately at 30 mm of lateral displacement. Both drift and ductility ratios are shown in Fig. 4.9 as measures of inelastic column deformability. In columns with well-rounded corners, the 20% decay limit was typically reached just before the complete failure of columns by fiber rupturing. In particular, the moment-drift hysteretic relationship of column RS-3 indicates that the column strength was maintained until 12% lateral drift ratio (Fig. 4.9(c)). On the other hand, the moment resistance of Column RS-6, with small-radius corners, started decaying rapidly after 2% lateral drift, developing 20% strength decay immediately after, but sustaining some resistance until fiber rupturing at 4% lateral drift ratio.

Longitudinal bar buckling was not observed in columns having R/D = 1/6 until after the rupturing of fiber occurred, even though the bars were not stabilized by internal steel ties. This was also true for columns that did not have the FRP crossties. The FRP casing and the concrete cover of 25 mm over the longitudinal reinforcement were sufficient to restrain the bars against instability even at high levels of inelastic drift demands. Column RS-6, however, did not have sufficient confinement due to the smaller corner radius of the FRP casing and therefore was not able to prevent the crushing of concrete beyond 2% lateral drift and subsequent buckling of compression bars, leading to fiber rupturing at 4% drift ratio.

It can be observed in the hysteretic relationship of RS-3, shown in Fig 4.9(c) that the loading was not symmetric beyond 10% lateral drift. This was because the actuator stroke capacity was exceeded at 10% drift ratio in one direction, while deformation cycles were applied in the other direction up to 12% lateral drift. Table 4.5 summarizes inelastic deformabilities recorded for all columns. They consist of drift limits; at the end of testing when fiber rupture was observed, at maximum moment resistance (M_{max}), and at drift ratios at 80% and 90% of maximum moment resistance beyond the peak.

4.3.3 Variation of Transverse FRP Strains with Lateral Drift

Unlike conventional steel reinforcement, which exhibits elasto-plastic stress strain behavior, FRP materials exhibit linear-elastic behavior. Therefore, the confinement pressure of FRP casing is proportional to the amount of strain generated in the casing, underlining the importance of strain measurements.

Strain gages were placed on FRP casings at seven to nine different levels along the column height. The maximum strains recorded on casings having R/D = 1/6 were in excess of 1.0%, which were significantly higher than the recommended design strains of current design guidelines (Buckle and Friedland 1994; ACI 440 2002; and CSA S806 2002) even though, they were lower than those recorded on similar size circular columns tested by the author (Ozbakkaloglu and Saatcioglu 2005a). The initial transverse strain caused by the application of axial load alone was within 0.1%. The maximum strains recorded on FRP casings at the time of fiber rupture, were higher for columns having a higher number of FRP plies. This can be observed by comparing Figs. 4.10(a), 4.10(b) and 4.10(c) with Figs. 4.10(d) and 4.10(e). It was

also observed that, the maximum strains recorded at the time of fiber rupture were considerably lower for the column with small corner radius, as depicted in Fig. 4.10(f).

The variation of maximum transverse strains along the height is shown in Fig. 4.10 for each drift level. The figure provides the maximum transverse strains for each column, from which confinement pressures can be calculated. The strain data further demonstrates the confining effect of the column footing. Accordingly, the strains recorded are consistently higher at 135 mm and 203 mm from the column-footing interface, when compared with those at 68 mm. The strain profiles given in Fig. 4.10 also demonstrate the vertical propagation of plastic hinging towards the tip with increasing inelastic deformations.

Possible contribution of shear to transverse strains was investigated to assess the significance of shear-confinement interaction. The contribution of concrete to shear resistance was computed as per ACI 318 (2005) recommendation. The results are tabulated in Table 4.4, and indicate that shear stresses were not significant enough to result in diagonal tension cracks to further strain the FRP casings. A similar conclusion was arrived in the previous section by examining the hysteretic characteristics of columns under reversed cyclic loading. Lack of clear pinching in hysteresis loops was attributed to little or no effect of shear even after the formation of plastic hinging. Therefore, the effect of shear on transverse FRP strains was neglected in further analysis of test data.

4.4 EFFECT OF TEST PARAMETERS

4.4.1 Ratio of Corner Radius to Column Dimension (R/D)

The effect of R/D ratio was studied by comparing columns RS-4 and RS-6. Column RS-4 had well-rounded corners with a corner radius of 45 mm yielding an R/D ratio of 1/6, while column RS-6 had small-radius corners with a corner radius of 8 mm yielding an R/D ratio of 1/34. The hysteretic moment-lateral drift relationships of these two columns are presented in Figs. 4.9(d) and 4.9(f). The results indicate that Column RS-6 with a lower R/D ratio showed rapid strength decay after 2% lateral drift ratio. On the other hand, Column RS-4 showed little strength degradation until failure at the end of 6% lateral drift cycles. Therefore, the R/D ratio proved to be an important design variable. A similar observation was made by Rochette and Labossiere (2000), who reported that the carbon FRP-wrapped concrete specimens with R/D ratio of 1/6 showed improvements in ductility under concentric loading.

4.4.2 Presence of FRP Crossties

Columns RS-2, RS-3 and RS-5 were provided with internal FRP crossties, spaced at 68 mm, corresponding to 1/4 of the column dimension. Column RS-3 had double crossties in each cross-sectional direction, with 12 longitudinal bars placed along the perimeter. Columns RS-2 and RS-5 were reinforced with 8 longitudinal bars with a single crosstie in each direction. The crossties were manufactured by rolling a selected width of FRP strip of fibers. Hence the strip width directly reflected the fiber content in each crosstie. This width was 40 mm for columns RS-2 and RS-3 and resulted in a small amount of fibers. The ratio of fiber area in crossties to total fiber area in each cross-sectional direction was 5.7% and 11.3% for columns RS-2 and RS-3, respectively. Those crossties were mainly designed to improve the effectiveness of the casing by

providing restraints against lateral expansion, and their contribution to total fiber area was insignificant. The crossties of Column RS-5, however, were designed to have fiber area equal to that in each face of the casing. This resulted in a fiber strip width of 135 mm and 33% of total fiber area in each cross-sectional direction. The casing of Column RS-5 had two plies of FRP. The resulting total fiber area was equal to that used in Columns RS-4 and RS-6, with three plies in the casing without the crossties (Table 4.5).

The improvement in lateral drift capacity, associated with the use of FRP crossties can be observed by comparing the hysteretic moment-lateral drift relationships of Columns RS-1, RS-2 and RS-3 in Figs. 4.9(a), 4.9(b) and 4.9(c). The comparison indicates that Column RS-1, with no crossties, developed a maximum lateral drift ratio of 8%, while Column RS-3 with double crossties developed a maximum lateral drift ratio of 11% and failed during the first cycle at 12% drift ratio. The testing of Column RS-2 with single crossties was halted prior to significant strength decay at 9% drift ratio because of the out of plane deformation of the column. However, the extrapolation of results based on strain data indicated a potential deformability of up to 10% drift ratio. This comparison clearly shows the effectiveness of crossties in terms of improving the distribution of confinement pressure and resulting confinement efficiency.

Furthermore, the moment-lateral drift relationships of column RS-5 having two FRP plies and crossties, and column RS-4 having three FRP plies with no crossties, indicated that both columns failed at approximately the same lateral deformation level. The improvement attained by the use of crossties and resulting efficiency in confinement was offset by the reduction in fiber area in the casing. The maximum strain reading on FRP ties was about 1.0%, which was almost equal to

the maximum casing strain of 1.05% in RS-5. This suggests that while the crossties were not able to develop their full strength, they sustained significantly high tensile strains before they ruptured at their ends where the fibers were bent and adhered to the casing, triggering stress concentration effects. Furthermore, the discrete nature of crossties, as opposed to well distributed fibers in the casing, was also a factor in the effectiveness of fibers in crossties. Hence, the additional fibers provided in the form of crossties barely compensated for the equal amount removed from the casing, though the improvement in confinement efficiency attained by crossties was expected to result in further improvements in column deformability.

The test results were compared with those obtained from tests of concrete columns confined by conventional steel reinforcement. The comparison indicated superior performance of columns cast in FRP stay-in-place formwork, over conventional columns (Ozbakkaloglu and Saatcioglu 2005b).

4.4.3 Existence of Mechanical Splices

Mechanical splices were used to splice longitudinal bars in columns RS-4 and RS-6 at 500 mm and 900 mm above the column footing interface, respectively. Observations during testing indicated that column behavior was not affected by the use of mechanical splices, and the longitudinal bars were able to develop their strengths without any slippage. This is supported by observations made during tension coupon tests of mechanically spliced No. 15 bars, where the failure occurred away from the splice region.

4.5 DESIGN INFORMATION

Designing FRP stay-in-place formwork requires the determination of strength and deformation capacities of columns. The deformation capacity is especially important for HSC columns in seismically active regions. One of the assets of FRP stay-in-place formwork is its ability to confine HSC which would otherwise exhibit brittle behavior, posing challenges in earthquake resistant construction. Therefore, strength and inelastic deformability of HSC columns, confined by FRP casings are addressed in detail in this section for use in practice.

4.5.1 Strength of HSC Columns Confined by FRP Casings

An important component of FRP casing design for columns is the computation of its strength under flexure and axial load in presence of shear. This requires sectional and member analyses under combined stresses.

The current methods of analysis used for conventional reinforced concrete column design have been verified to assess their applicability to FRP encased HSC columns. Flexural capacities of test columns were computed by plane-section analyses of critical sections with due considerations given to the stress-strain relationship of HSC. Nominal moment capacities were computed using stress-strain models for unconfined HSC, including i) the stress-strain relationship proposed by Popovic (1973) (M_P), ii) the rectangular stress block recommended by the author for HSC (Ozbakkaloglu and Saatcioglu 2004) ($M_{O\&S}$), iii) the rectangular stress block recommended by CSA A23.3-04 (M_{CSA}), and iv) the rectangular stress block recommended by ACI 318-05 (M_{ACI}). In addition, the confined concrete model proposed by Lam and Teng (2003) was used to compute the flexural capacities ($M_{L\&T}$). This was the only confinement model

reported in the literature that could trace the entire stress-strain relationship for FRP confined rectangular columns. Since the model did not incorporate the effects of internal FRP crossties, this effect was neglected for columns with crossties. The in-place strength of concrete was taken as 0.9 times the strength determined by standard cylinder tests (Ozbakkaloglu and Saatcioglu 2004). The stress-strain relationship used for longitudinal steel reinforcement was obtained from coupon tests.

Table 4.4 provides the comparison of computed and experimentally recorded flexural capacities (M_{max}). The results indicate that computed capacities based on unconfined HSC models consistently produced lower values than those recorded experimentally. This is attributed to the enhancement of concrete strength due to confinement, which is not considered in the analytical computations, except for the confined concrete model by Lam and Teng (2003). The ACI rectangular stress block intended for normal strength concrete was found to overestimate the strength of HSC columns (Ozbakkaloglu and Saatcioglu 2004). In the same comparison, the expected overestimation was more than offset by significant underestimation associated with neglecting the effects of confinement. However, this should not imply the suitability of ACI rectangular stress block to FRP encased columns.

Table 4.4 indicates that, while none of the unconfined concrete models used above were able to produce good correlations with experimental data, the results did not differ significantly. This was attributed to the level of axial load used in the experimental program, which was close to the balanced section load, and associated role of concrete on strength computations. The difference

is expected to be higher for columns with higher axial compression as concrete contribution to flexural strength becomes more pronounced.

The strength enhancement resulting from concrete confinement is not considered in current practice for reinforced concrete design. If the same practice is followed for FRP encased columns, the sectional analysis procedure used for conventional reinforced concrete columns, i.e., the plane section analysis method, can be employed in designing columns with FRP stay-in-place formwork, provided that an appropriate stress block is used. The analytical predictions computed by the confined concrete model of Lam and Teng (2003) produced good agreements with experimental values, especially for well confined columns. However, as the level of confinement diminished, the analytical results tended to overestimate flexural strengths (Table 4.4).

The test columns were designed to behave predominantly in the flexure mode, and had shear capacities higher than those corresponding to flexural capacities. Therefore, little or no effect of shear was observed during testing. Table 4.4 includes computed concrete contributions to shear (V_c) on the basis of ACI 318-05. Accordingly, the concrete shear resistance alone was sufficient to resist the maximum shear force (V_{max}), observed during testing. Only for Column RS-3, the computed concrete shear resistance was slightly below the maximum shear force.

4.5.2 Deformability of HSC Columns Confined by FRP Casings

The deformability of HSC columns is an important design consideration for earthquake resistant construction because of the brittle nature of HSC, especially in presence of high axial

compression. Therefore, the confinement of concrete by properly designed transverse reinforcement plays an important role in the seismic performance of HSC columns. FRP stay-in-place formwork provides a convenient alternative to conventional confinement reinforcement for improved deformability of earthquake resistant HSC columns.

Inelastic deformability of HSC columns with FRP stay-in-place formwork is a topic which is currently under investigation. Therefore, very little data is available on the topic to suggest a generalized design procedure. CSA Standard S806-02 includes displacement based design recommendations that are essentially intended for fiber wrapping concrete bridge columns for seismic retrofitting. These recommendations are based on experimental data generated on bridge columns with relatively low levels of axial compressions. The columns of the current investigation represent first story columns of a multistory building with axial compression approaching to that of balanced section. This level of axial compression increases the contribution of concrete to overall column behavior, resulting in the change of failure mode from longitudinal bar rupturing to concrete crushing. Increased axial compression also improves the effectiveness of FRP as confinement reinforcement. Furthermore, the current investigation includes the beneficial effects of corner rounding and the use of internal FRP crossties on confinement. Consequently, the experimental results indicate superior inelastic column deformabilities than those suggested by CSA S806-02 expressions.

The hysteretic relationships observed during column tests indicate that the majority of columns showed very favorable deformation characteristics well into the inelastic range. Columns with 5 plies of FRP in the casings developed in excess of 8% drift ratio without significant strength

decay, when the corners were rounded to have an R/D ratio of 1/6. The use of internal FRP crossties further improved column drift capacity, resulting in drift ratios of up to 11% when double crossties were used in each cross-sectional direction. The drift capacity was reduced to 6% in columns with three plies of FRP. However, a severe reduction in drift capacity was observed when the rounding of column corners was kept to a minimum, with R/D = 1/34, developing only 2% lateral drift ratio.

4.6 CONCLUSIONS

The following conclusions can be drawn from the experimental investigation reported in this thesis:

- High-strength concrete columns confined by carbon FRP stay-in-place formwork can develop ductile behavior under simulated seismic loading. The use of FRP formwork as confinement reinforcement substantially increases deformability of square columns. Column tests reported in this thesis indicate that inelastic deformability of 90 MPa concrete square columns can be increased up to 11% lateral drift ratio with FRP stay-in-place formwork.
- The increased confinement requirements for HSC columns can be met by using FRP stay-in-place formwork. Unlike conventional steel reinforcement that only confines the core concrete, FRP stay-in-place formwork confines the entire column. Furthermore, unlike the discrete nature of conventional steel reinforcement, FRP formwork provides continuous confinement, covering the entire column face, resulting in higher confinement efficiency.
- The strain data recorded during column tests indicate that the strength of FRP stay-in-place formwork could be mobilized to a large extent, developing strains of up to 1.5%,

approaching the tensile capacity of material. The observed strains were consistently higher than the 0.4% used in current design recommendations as a safe design limit.

- The ratio of corner radius to column dimension (R/D) has a significant influence on the effectiveness of FRP as confinement reinforcement. Increased corner radius promotes effectiveness of FRP, while preventing premature material failure associated with sharp corners. Columns with three plies of FRP, tested in the experimental program, were able to develop 6% drift ratio prior to significant strength decay when the R/D ratio was 1/6, whereas the column with sharper corners (R/D = 1/34) was able to develop a limited drift ratio of about 2%.
- The use of FRP crossties improves the efficiency of FRP stay-in-place formwork, in much the same manner as overlapping hoops and crossties used in conventional steel confinement reinforcement. Therefore, the concept of integrated crossties in FRP casings, introduced by the author, has proven to be effective.
- Flexural capacity of columns with FRP stay-in-place formwork can be computed using the plane section analysis commonly employed for reinforced concrete members, provided that appropriate material models are incorporated.
- Additional confinement provided by a footing appears to strengthen the column critical section at the column-footing interface, resulting in the shifting of failure zone away from the interface. This shift was observed to be approximately equal to half the column cross-sectional dimension for the level of axial compression considered.

4.7 REFERENCES

American Concrete Institute (ACI) Committee 318. (2005). "Building Code Requirements for Structural Concrete (ACI 318-05) and Commentary (318R-05)." Farmington Hills, Mich., 430 pp.

American Concrete Institute (ACI) Committee 440. (2002). "Design and Construction of Externally Bonded FRP Systems for Strengthening Concrete Structures (440.2R-02)." Detroit, 45 pp.

Buckle, I. G., and Friedland, I. M. (1994). "Seismic Retrofitting Manual for Highway Bridges." Report No. FHWA-94-052, U.S. Department of Transportation.

Canadian Standards Association (CSA) Committee A23.3. (2004). "Design of concrete structures (A23.3-04)." Rexdale, Ontario, 240 pp.

Canadian Standards Association (CSA) Committee S806. (2002). "Design and construction of building components with fibre-reinforced polymers (S806-02)." Rexdale, Ontario, 177 pp.

Fam, A., Flisak, B. and Rizkalla, S. (2003). "Experimental and Analytical Modeling of Concrete-Filled FRP Tubes Subjected to Combined Bending and Axial Loads." ACI Structural Engineering Journal, Vol. 100, No. 4, pp. 499-509.

Fam, A. and Rizkalla, S. (2002). "Flexural Behavior of Concrete-Filled Fiber Reinforced Polymer Circular Tubes." Journal of Composites for Construction, Vol. 6, No. 2, pp. 123-132.

Fam, A., Schnerch, D. and Rizkalla, S. (2005). "Rectangular Filament-Wound GFRP Tubes Filled with Concrete under Flexural and Axial Loading: Experimental Investigation." Journal of Composites for Construction, Vol. 9, No. 1, pp. 25-33.

Iacobucci, R. D., Sheikh, S. A., and Bayrak, O. (2003). "Retrofit of Square Concrete Columns with Carbon Fiber-Reinforced Polymer for Seismic Resistance." ACI Structural Journal, V. 100, No. 6, pp. 785-794.

Lam, L., and Teng J. (2002). "Strength models for fiber-reinforced plastic-confined concrete." *Journal of Structural Engineering*, ASCE , 128(5), pp.612-623.

Lam, L., and Teng, J. G. (2003). "Design-oriented stress-strain model for FRP-confined concrete in rectangular columns." Journal of Reinforced Plastics and Composites, 22(13), pp.1149–1186.

Mander, J. B., Priestley, M. J. N., and Park, R. (1988). "Theoretical Stress-Strain Model for Confined Concrete." *Journal of Structural Engineering*, ASCE, V. 114, No. 8, pp.1804-1826.

Mirmiran, A., Cabrera, S., Samaan, M., and Shahawy, M. (1998a). "Design, Manufacture, and Testing of A New Hybrid Column." *Construction and Building Materials,* Elsevier, 12(1), 39-49.

Mirmiran, A., Shahawy, M., El Khoury, C., and Naguib, W. (2000). "Large Beam-Column Tests on Concrete-Filled Composite Tubes." *ACI Structural Journal*, ACI, 97(2), 268-276.

Mirmiran, A., Shahawy, M., Samaan, M., El Echary, H., Mastrapa, J.C., and Pico, O. (1998b). "Effect of Column Parameters on FRP-confined Concrete." Journal of Composites for Construction, ASCE, V.2, No. 4, pp.175-185.

Mirmiran, A., Shahawy, M., and Samaan, M. (1999). "Strength and Ductility of Hybrid FRP-Concrete Beam-Columns." *Journal of Structural Engineering*, ASCE, 125(10), 1085-1093.

Miyauchi, K., Nishibayashi, S., and Inoue, S. (1997). "Estimation of Strengthening Effects with Carbon Fiber Sheet for Concrete Column." Proceedings of Nonmetallic (FRP) Reinforcement for Concrete Structures, Japan Concrete Institute, Sapporo, Japan, V. 1, pp. 217-223.

Moran, A. M., and Pantelides C. P. (2002). "Stress-strain model for fiber-reinforced polymer-confined concrete." *Journal of Composites for Construction*, ASCE, V.6, No.4, pp. 233-240.

Ozbakkaloglu, T., and Saatcioglu., M. (2004). "Rectangular Stress Block for High-Strength Concrete." ACI Structural Journal, V. 101, No. 4, pp. 475-483.

Ozbakkaloglu, T., and Saatcioglu, M. (2005a). "Seismic performance of circular high-strength concrete columns in stay-in-place FRP formwork." Submitted to Journal of Composites for Construction, ASCE.

Ozbakkaloglu, T., and Saatcioglu, M. (2005b). "Comparisons of Seismic Performance of HSC Square Columns Confined by FRP Casings and Conventional Steel Reinforcement." 33rd CSCE Annual Conference, Toronto, Ontario, June 2-4, 2005.

Park, R., and Paulay, T. (1975). "Reinforced Concrete Structures." Wiley, New York, 769 pp.

Pessiki, S., Harries, K.A., Kestner, J.T., Sause R., and Ricles, J.M. (2001). "Axial Behavior of Reinforced Concrete Columns Confined with FRP Jackets." Journal of Composites for Construction, ASCE, V. 5, No. 4, pp. 237-245.

Popovics, S. (1973). ''Analytical approach to complete stress-strain curves.'' *Cement and Concrete Res.*, 3(5), pp. 583–599.

Rochette, P., and Labossiere, P. (2000). "Axial Testing of Rectangular Column Models Confined with Composites." Journal of Composites for Construction, ASCE, V. 4, No. 3, pp. 129-136.

Saafi, M., Toutanji H.A., Li, Z. (1999). "Behavior of Concrete Columns Confined with Fiber Reinforced Polymer Tubes." ACI Structural Journal, V. 96, No. 4, pp. 500-509.

Saatcioglu, M. (1991). "Deformability of Reinforced Concrete Columns." Earthquake Resistant Concrete Structures, Inelastic Response and Design, ACI SP-127-10, American Concrete Institute, Detroit, pp. 421-452.

Saatcioglu, M., and Razvi, S. R. (1992). "Strength and Ductility of Confined Concrete." Journal of Structural Engineering, ASCE, V. 118, No. 6, pp. 1590-1607.

Samaan, M., Mirmiran, A., and Shahawy, M. (1998). "Model of Concrete Confined by Fiber Composites." *Journal of Structural Engineering*, ASCE, 124(9), pp. 1025-1032.

Seible, F., Burgueño, R., Abdallah, M. G., and Nuismer, R. (1996). "Development of advanced composite carbon shell systems for concrete columns in seismic zones." *Proc., 11th World Conf. Earthquake Engineering*, Pergamon, Elsevier Science, Oxford, Paper No. 1375.

Seible, F., Priestley, M.J.N., and Hegemier, G.A. and Innamorato, D. (1997). "Seismic Retrofit of RC Columns with Continuous Carbon Fiber Jackets." *Journal of Composites for Construction*, ASCE, Vol.1, No.2, pp.52-62.

Shao, Y. (2003). "Behavior of FRP–concrete beam columns under cyclic loading." PhD thesis, North Carolina State Univ., Raleigh, N.C.

Sheikh, S. A., and Khoury S.S. (1993). "Confined Concrete Columns with Stubs." ACI Structural Journal, V. 90, No. 4, pp. 414-431.

Sheikh, S. A., and Uzumeri, S. M. (1980). "Strength and Ductility of Tied Concrete Columns." Journal of Structural Engineering, ASCE, V. 106, No. 5, pp. 1079-1102.

Sheikh, S. A., and Yau, G. (2002). "Seismic Behaviour of Concrete Columns Confined with Steel and Fiber-Reinforced Polymers." *ACI Structural Journal*, V. 99, No. 1, pp. 72-80.

Spoelstra, M. R., and Monti, G. (1999). "FRP-confined Concrete Model." Journal of Composites for Construction, ASCE, V. 3, No. 3, pp. 143-150.

Zhu, Z. (2004). "Joint Construction and Seismic Performance of Concrete-Filled Fiber Reinforced Polymer Tubes." PhD thesis, North Carolina State Univ., Raleigh, N.C.

Table 4.1 Properties of Test Specimens

Column	Shear Span (mm)	f'_c (MPa)	FRP Casing			Longitudinal steel			Axial load	
			Number of plies	R/D	Crosstie A_F (mm^2)	Reinforcement Arrangement	f_y (MPa)	ρ_l (%)	P (kN)	P/P_o
RS-1	2000	90.1	5	1/6	0	4-no.20	476	1.68	1880	0.32
RS-2	2000	90.1	5	1/6	6.6	8-no.15	500	2.24	1880	0.31
RS-3	2000	90.1	5	1/6	2x6.6	12-no.15	500	3.36	1920	0.30
RS-4	2000	75.2	3	1/6	0	8-no.15	500	2.24	1760	0.34
RS-5	2000	75.2	2	1/6	22.3	8-no.15	500	2.24	1760	0.34
RS-6	2000	75.2	3	1/34	0	8-no.15	500	2.20	1800	0.34

ρ_l: Longitudinal reinforcement ratio.

A_F: Cross-sectional area of fibres in a single crosstie.

Table 4.2 Properties* of carbon fibres used in manufacturing FRP casings

Fibres	Nominal Thickness (mm/ply)	Ultimate Tensile Strength (MPa)	Elastic Modulus (GPa)	Ultimate Rupture Strain (%)	Areal Weight (g/m^2)
Carbon	0.165	3800	227	1.67	300

*Reported by the manufacturer.

Table 4.3 Properties of reinforcing steel

Bar size	Stress-strain relationships						
	f_y (MPa)	ε_y	E_s (MPa)	ε_{sh}	f_u (MPa)	ε_u	ε_r
No. 15	500*	0.0024	208,750	0.0062	620	0.120	0.135
No. 20	476	0.0026	182,840	0.0070	570	0.125	0.144

*Rounded from 500.9 MPa.

Table 4.4 Experimental values and calculated capacities

Column	Layers of FRP	Moment						Shear Force		Damage zone (mm)
		M_{max} (kN.m)	$\frac{M_{max}}{M_{O\&S}}$	$\frac{M_{max}}{M_P}$	$\frac{M_{max}}{M_{ACI}}$	$\frac{M_{max}}{M_{CSA}}$	$\frac{M_{max}}{M_{L\&T}}$	V_{max} (kN)	V_c (kN)	
RS-1	5	220	1.12	1.10	1.07	1.13	0.98	110	123	140
RS-2	5	232	1.14	1.12	1.09	1.16	1.00	116	123	100-150
RS-3	5	258	1.16	1.14	1.12	1.17	0.99	129	123	110
RS-4	3	197	1.07	1.06	1.04	1.09	0.95	98.5	112	140
RS-5	2	198	1.07	1.06	1.05	1.09	0.96	99	112	140
RS-6	3	194	1.02	1.01	0.99	1.04	0.93	97	112	160

(M_{max}) represents the average of maximum moments in each direction of loading.

(V_{max}) represents the average of maximum shear forces in each direction of loading.

Table 4.5 Observed deformabilities of columns

Column	f'_c (MPa)	P/P_o	R/D	Casing A_F/s (mm^2)	Crosstie A_F (mm^2)	Drift at Fibre Rupture	Displacement ductility (μ_Δ)	Drift at M_{max} (%)	Drift at 90% M_{max} (%)	Drift at 80% M_{max} (%)
RS-1	90.1	0.32	1/6	55.7	0	8%, cycle 3	5.3	2.8	4	8
RS-2	90.1	0.31	1/6	55.7	6.6	9+%	6+	3	5	9+
RS-3	90.1	0.30	1/6	55.7	2x6.6	12%, cycle 1	7.3	4	8	11
RS-4	75.2	0.34	1/6	33.4	0	7%,cycle 1	4	2.5	4	6
RS-5	75.2	0.34	1/6	22.3	22.3	6%, cycle 3	4	3	4	6
RS-6	75.2	0.34	1/34	33.4	0	4%, cycle 3	1.5	1.6	2	2.3

A_F: Total cross-sectional area of fibres in a single crosstie or one face of casing.

s: Spacing of FRP crossties in longitudinal direction.

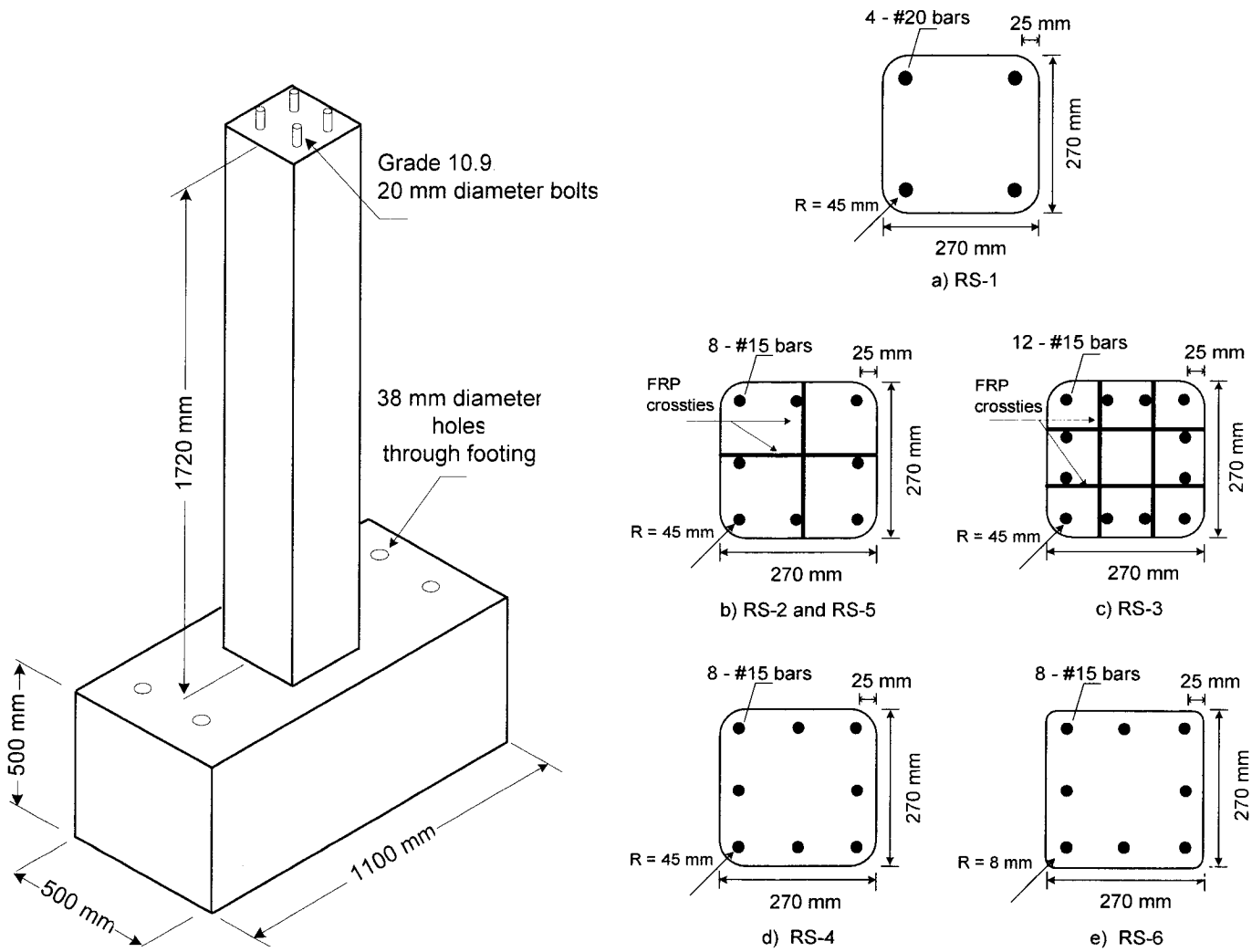

Fig. 4.1 – Geometry and reinforcement arrangements used in column tests

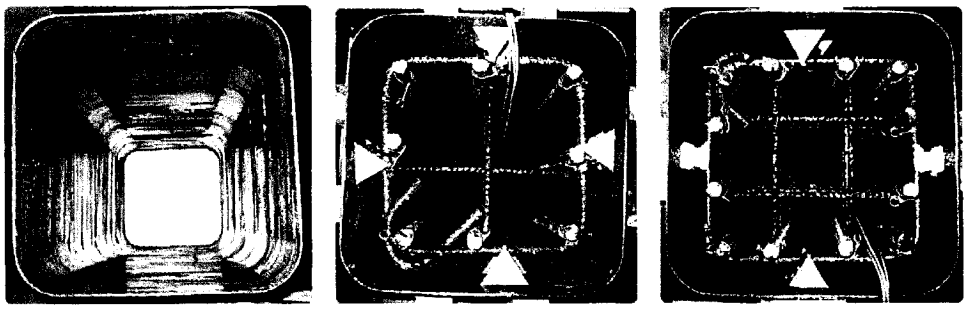

a) RS-1 b) RS-2 and RS-5 c) RS-3

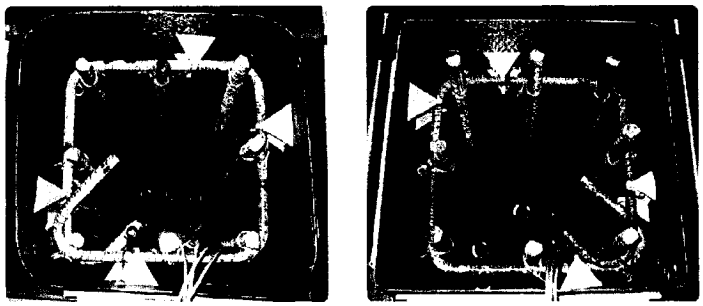

d) RS-4 e) RS-6

Fig. 4.2 – Column cross-sectional arrangements

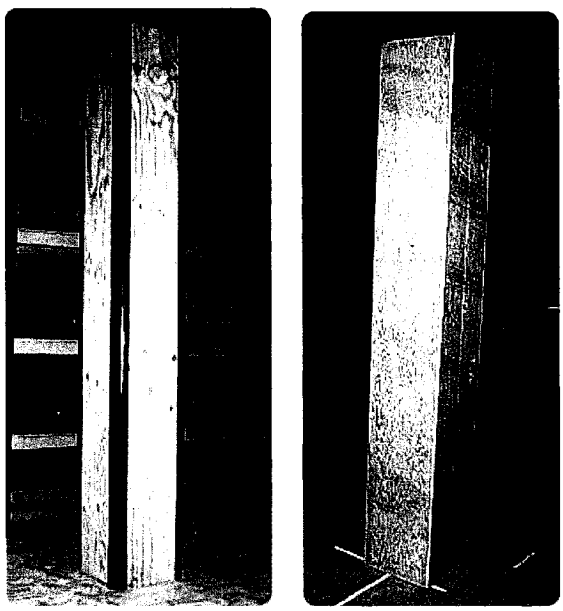

Fig. 4.3 – Templates used to manufacture FRP casings

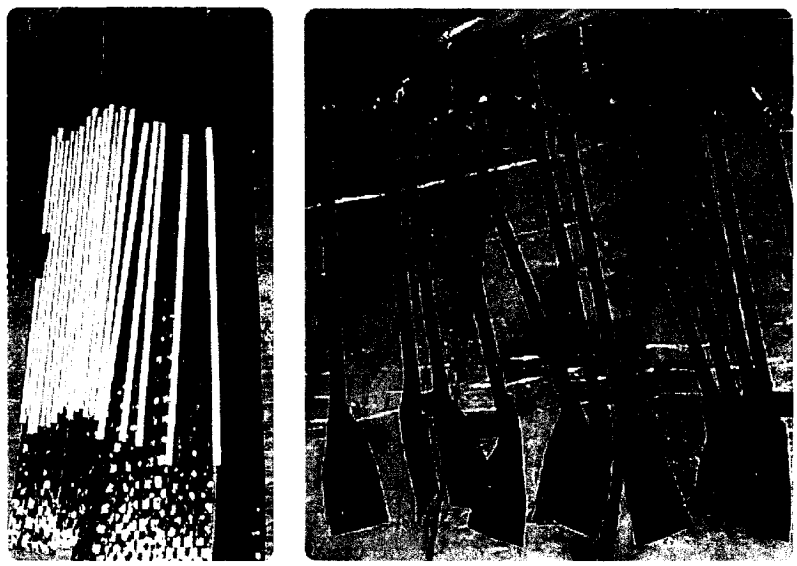

Fig. 4.4 – FRP crossties

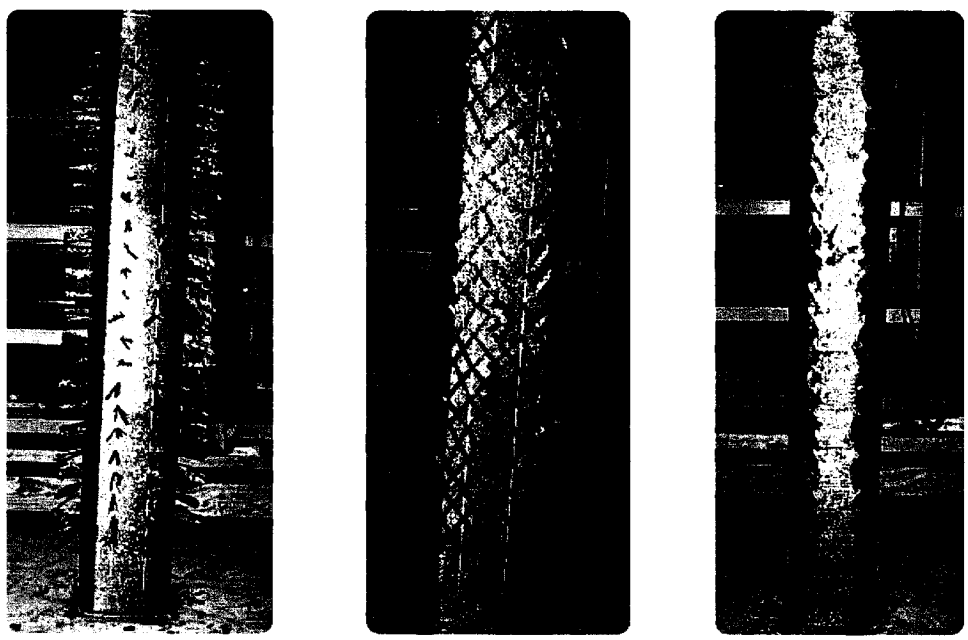

(a) Crossties inserted **(b) End fibres glued on** **(c) Final layer of FRP sheet**

Fig. 4.5 – Placement of crossties in square columns

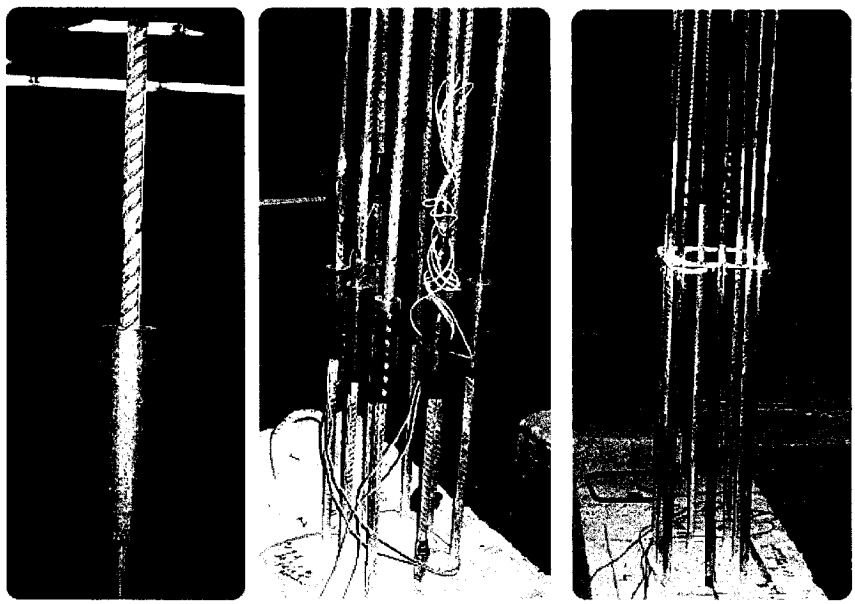

Fig. 4.6 – Mechanical Splices

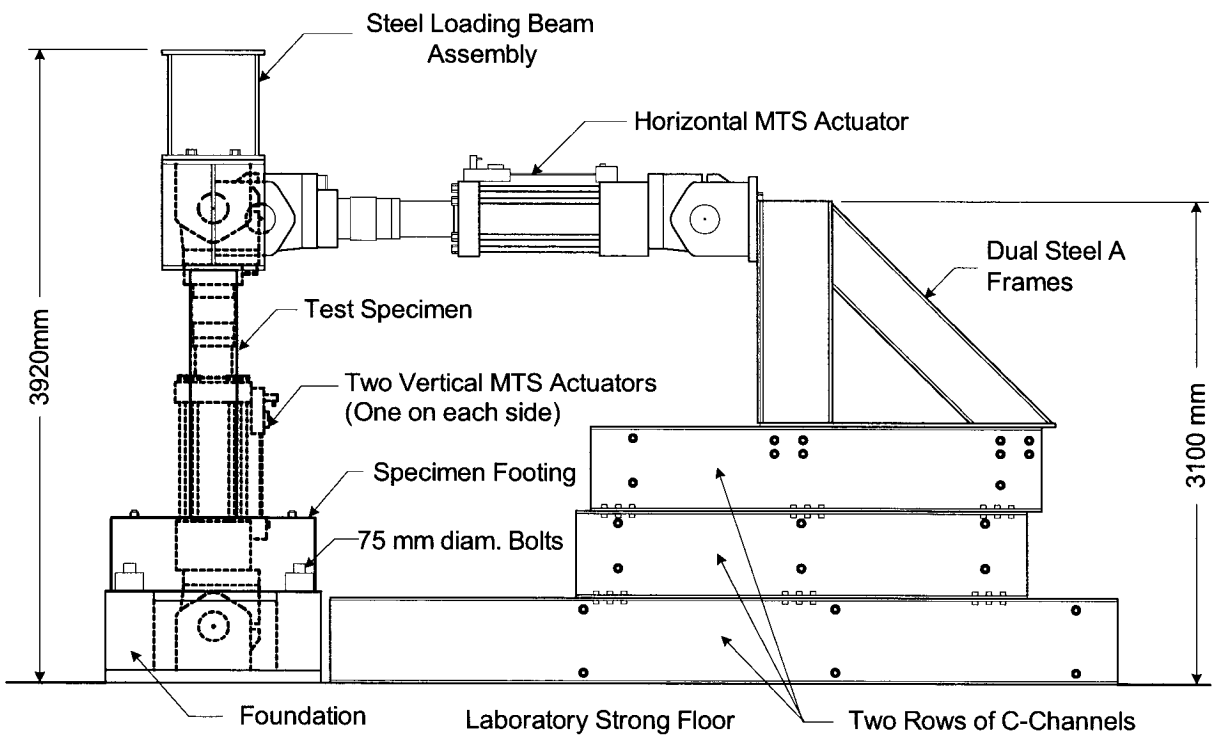

Fig. 4.7 – Test setup

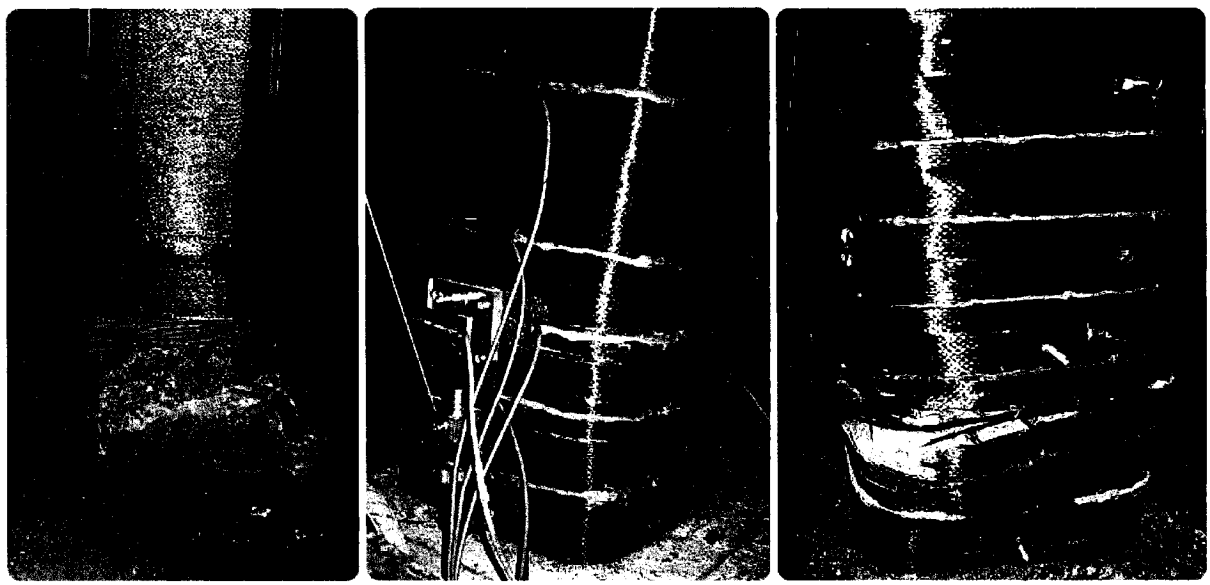

(a) Column RS–1 (b) Column RS–2 (c) Column RS–3

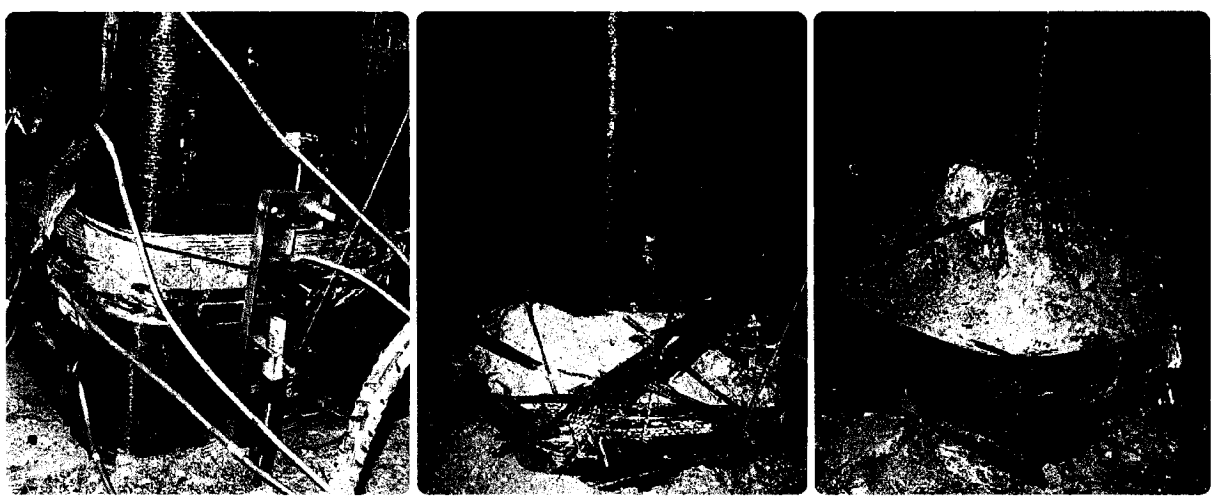

(d) Specimen RS-4 (e) Column RS-5 (f) Column RS-6

Fig. 4.8 – Specimens at end of testing

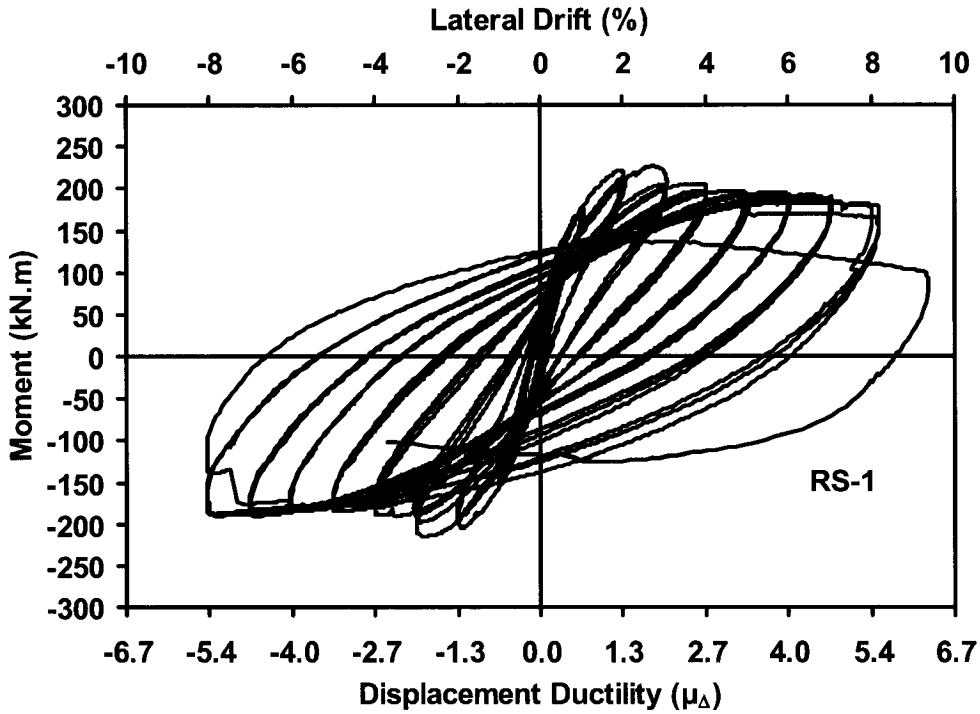

(a) Column RS-1

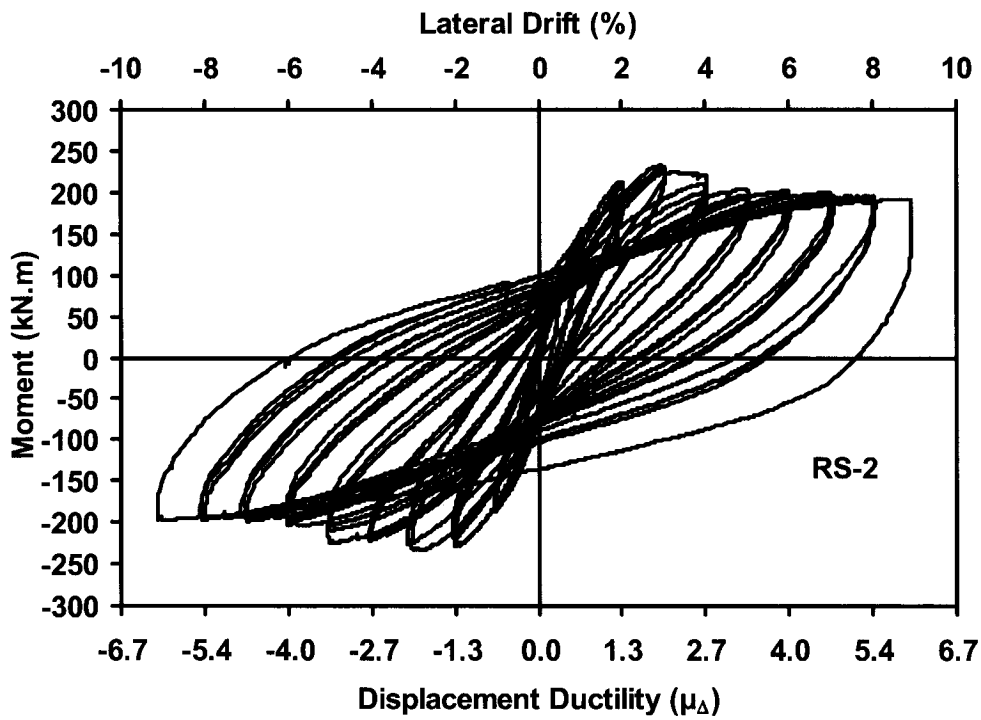

(b) Column RS-2

Fig. 4.9 – Experimentally recorded hysteretic moment-lateral drift relationships

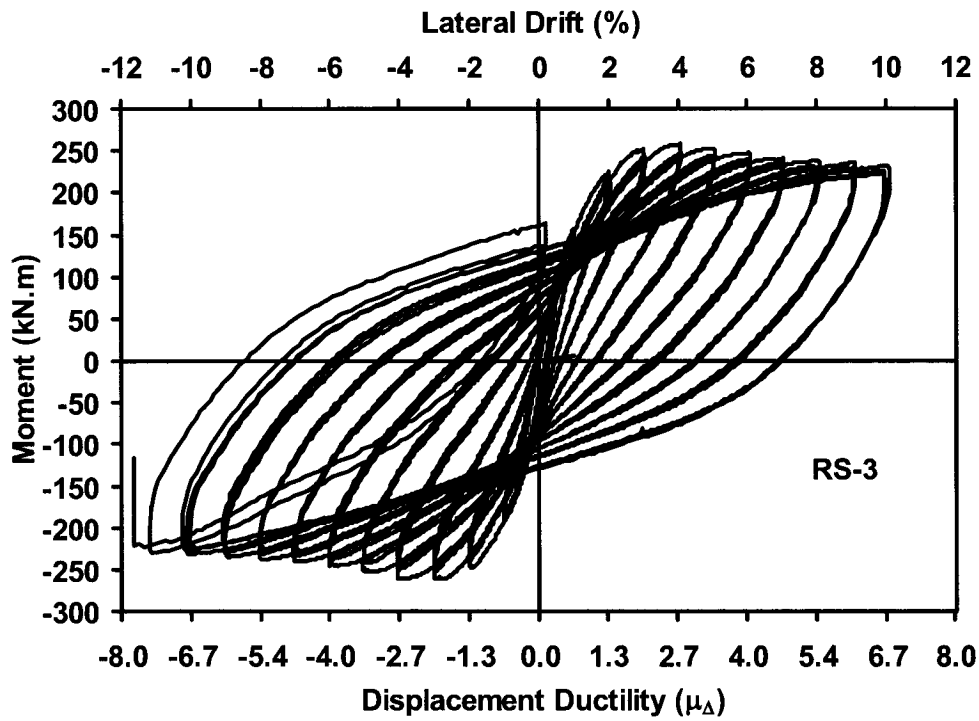

(c) Column RS-3

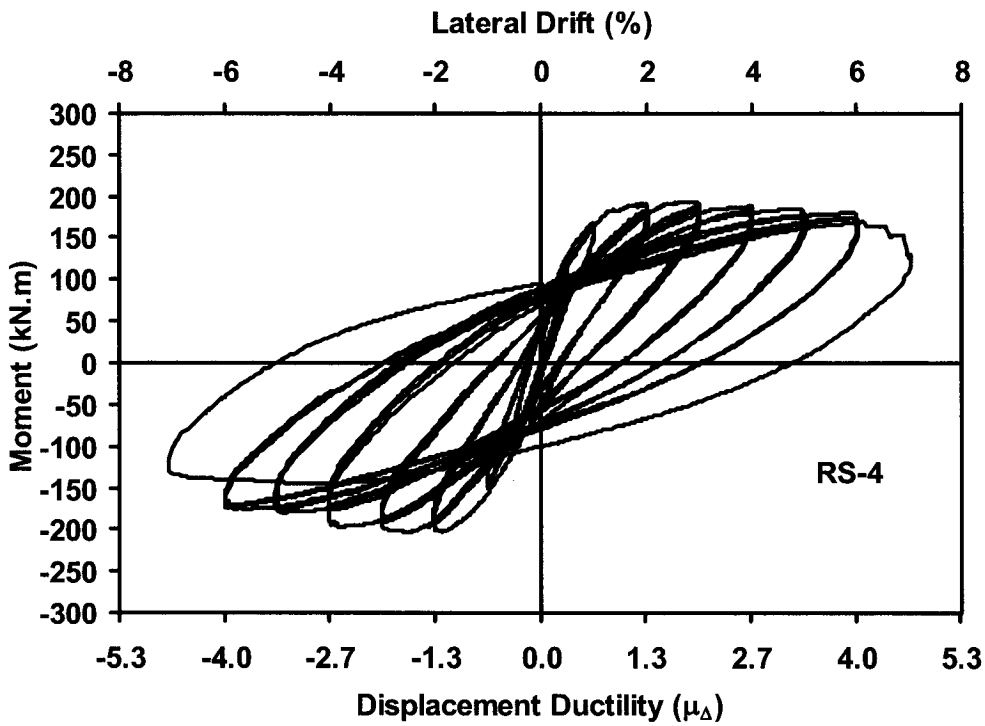

(d) Column RS-4

Fig. 4.9 – Cont'd

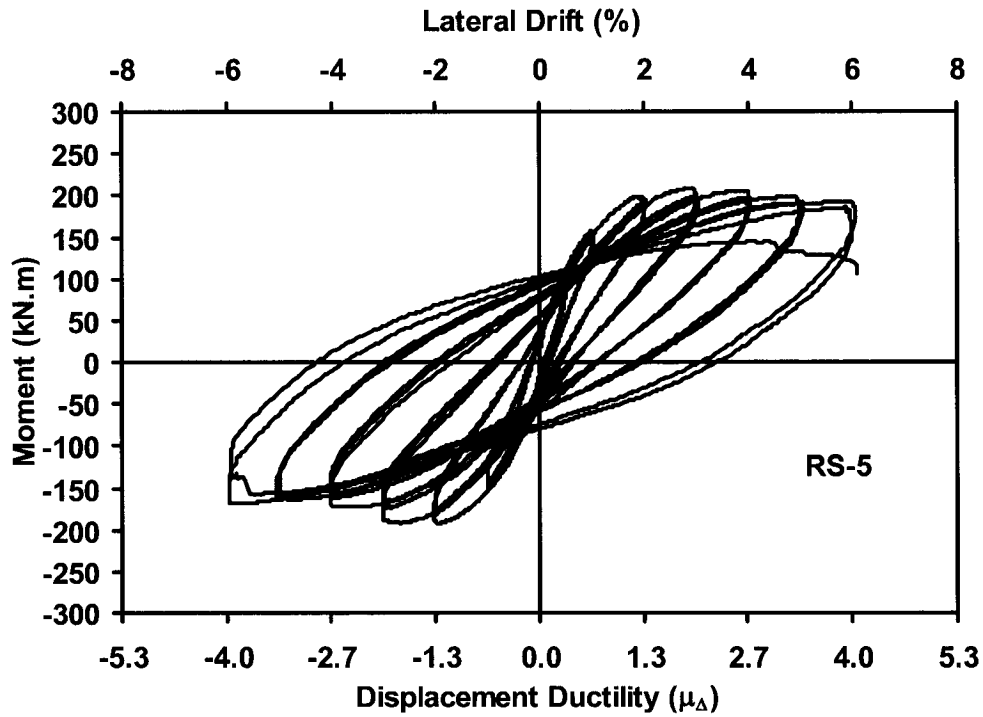

(e) Column RS-5

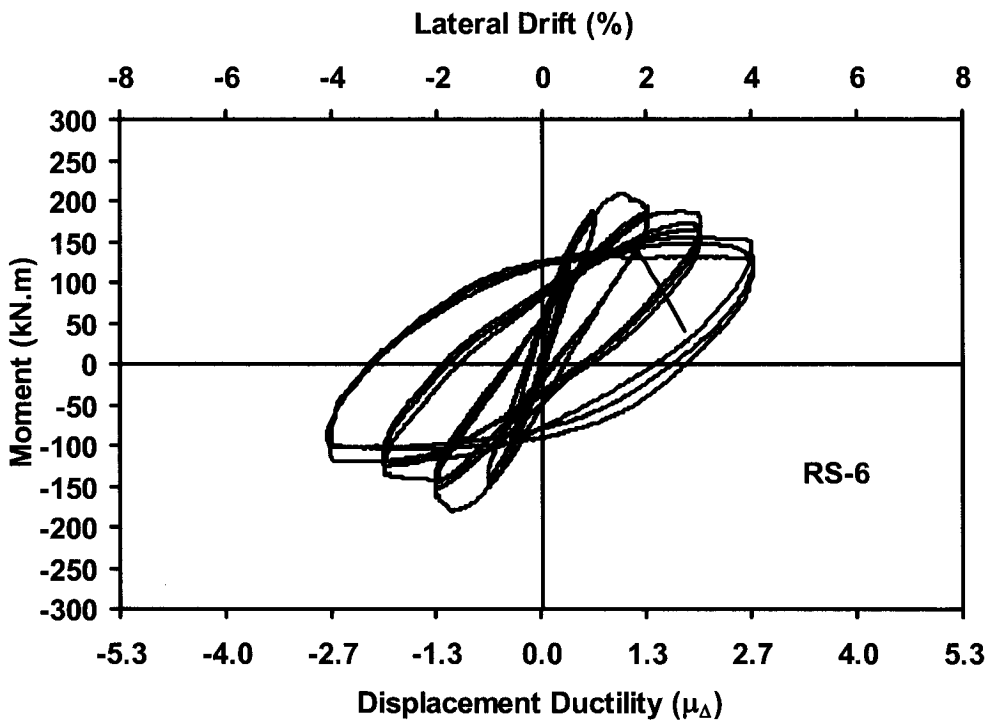

(f) Column RS-6

Fig. 4.9 – Cont'd

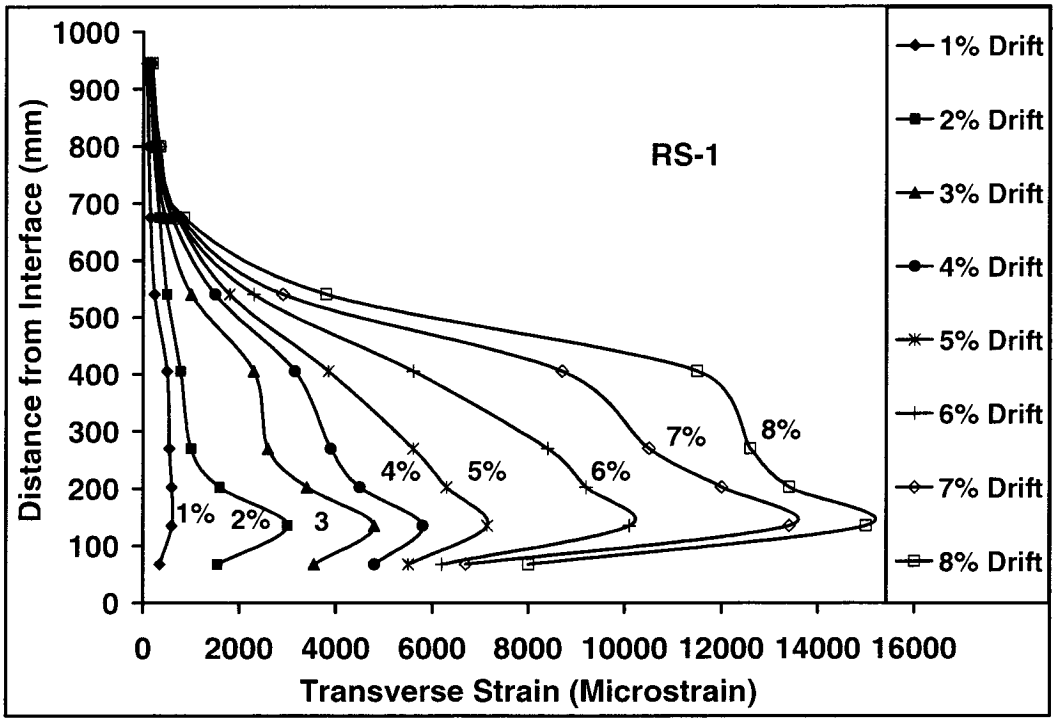

(a) Column RS-1

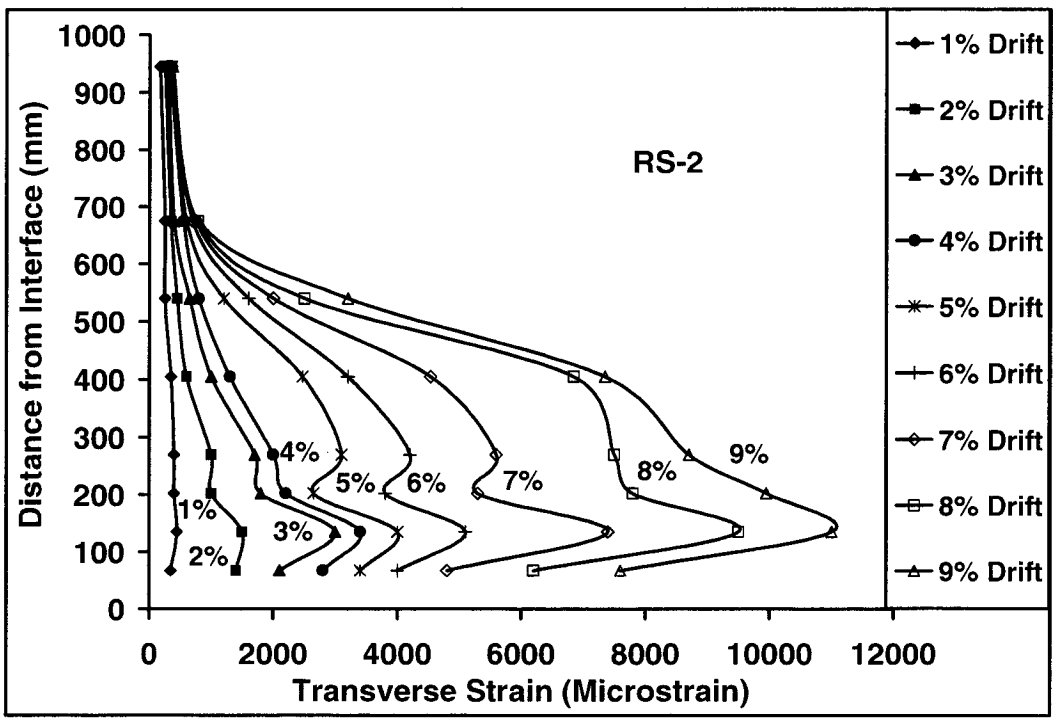

(b) Column RS-2

Fig. 4.10 – Variation of transverse strains on FRP casings along column height

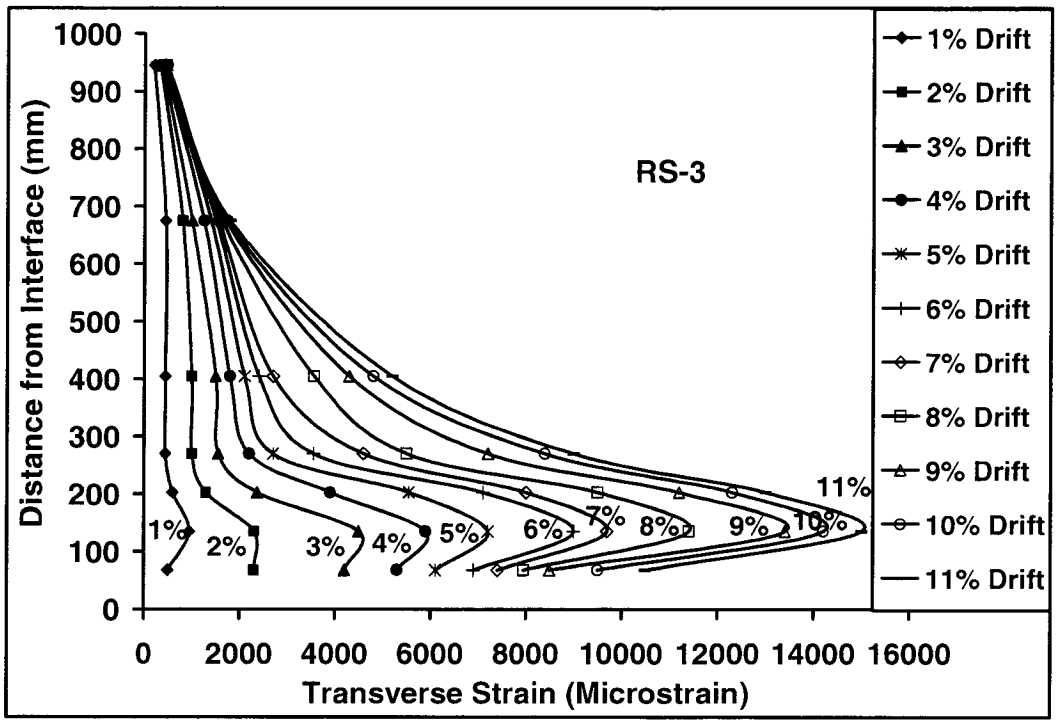

(c) Column RS-3

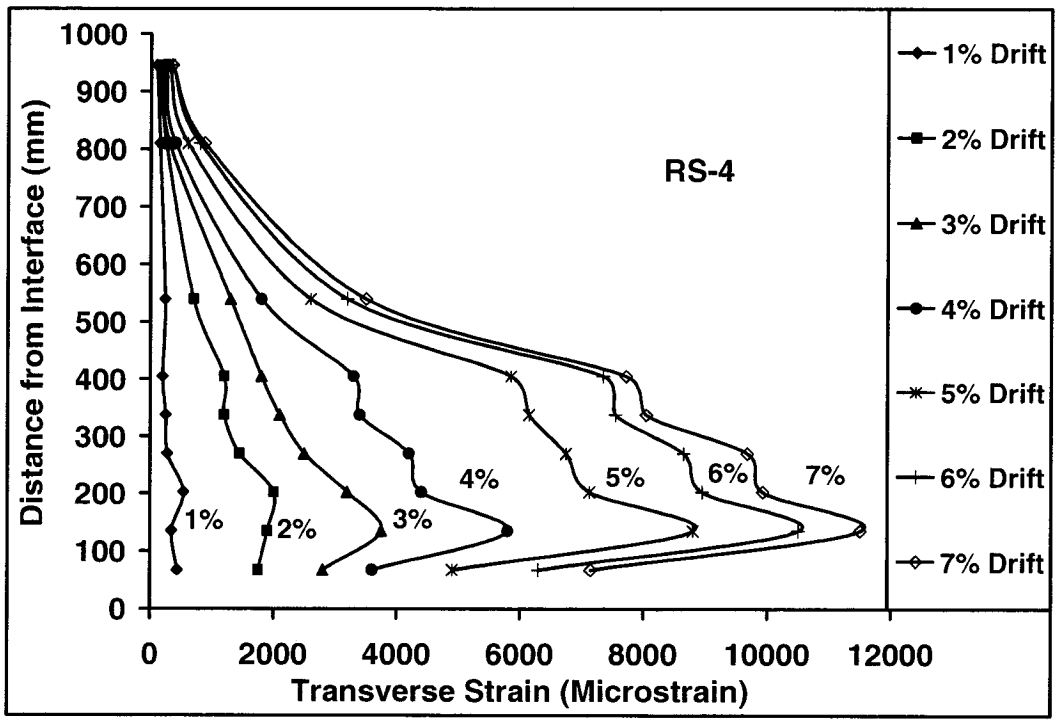

(d) Column RS-4

Fig. 4.10 – Cont'd

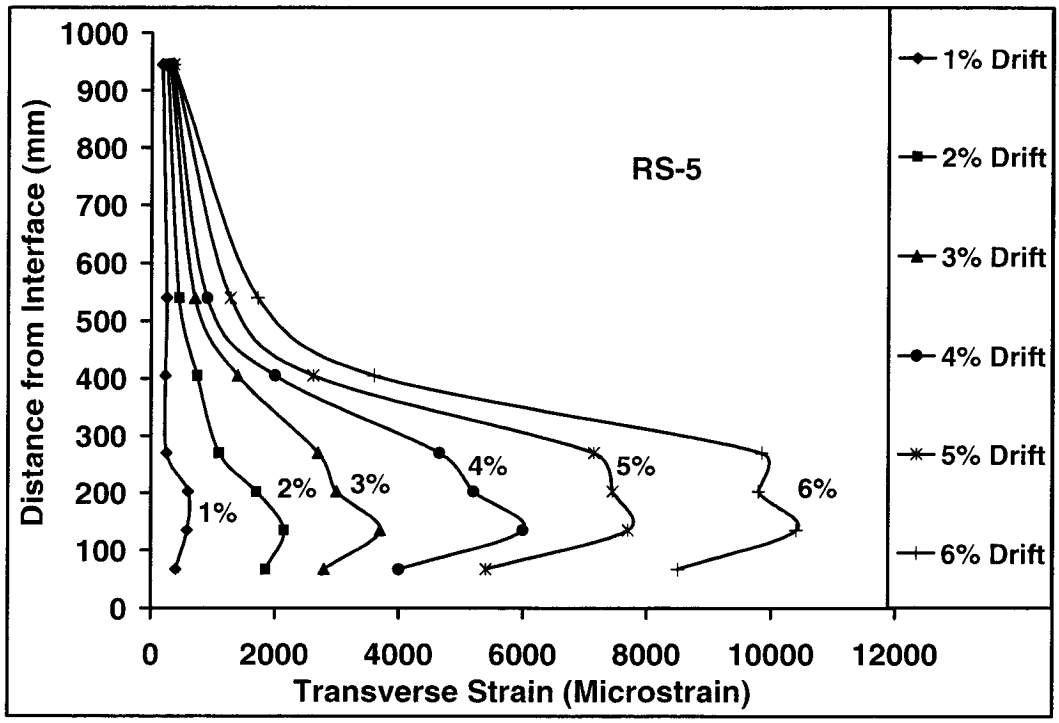

(e) Column RS-5

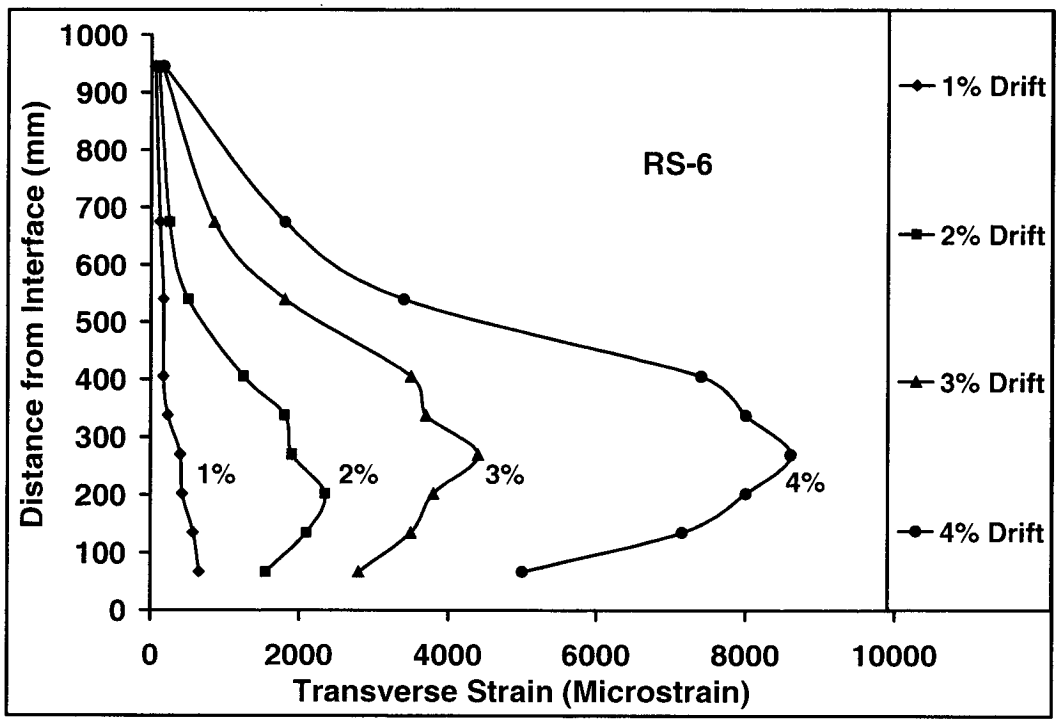

(f) Column RS-6

Fig. 4.10 – Cont'd

Chapter 5

Rectangular Stress Block for High-Strength Concrete

5.1 INTRODUCTION

Stress-strain relationship of concrete varies with strength. The ascending branch of the relationship becomes steeper with increasing strength, indicating higher elastic modulus. The shape of this segment changes from approximately a second order parabola for normal-strength concretes to almost a linear variation for high-strength concretes. The strain at peak stress (ε_o) increases with strength, varying approximately between 0.0015 for 20 MPa concrete and 0.0025 for 100 MPa concrete. Failure becomes more sudden and brittle as the concrete strength increases, and unloading beyond the peak stress becomes more rapid. In summary, concrete becomes more rigid and more brittle with increasing strength.

The stress-strain relationship of concrete plays an important role on structural design. Members subjected to uniform compression attain concentric capacity when concrete reaches a strain level corresponding to peak stress (i.e., ε_o). Under strain gradient, the failure occurs at an extreme compressive fibre strain higher than that at peak stress (i.e., ε_u). This value changes with the geometric shape of compression zone, and may also vary significantly with concrete strength and confinement. Once the limiting strain is established, the sectional capacity can be computed by

evaluating internal forces, including the compressive force in concrete. Concrete compressive force can be established by computing the area under compressive stress distribution up to the ultimate strain. Because it is cumbersome to compute the area under a non-linear stress-strain relationship, building codes provide equivalent stress blocks for ease in design calculations. These stress blocks are derived such that both the area under the actual non-linear stress distribution (force) and the centroid of this area (point of application of force) correspond to those of the stress block, as closely as possible.

The background information for current rectangular stress block in ACI 318-05 (1) dates back to 1930 when an extensive column investigation was conducted jointly by the University of Illinois, Lehigh University and the American Concrete Institute. The initial results of the study were published in 1931 (2) with a more comprehensive follow-up report in 1934 (3). As a result, an expression was proposed for column concentric capacity, consisting of concrete and steel contributions. The concrete contribution was based on total concrete area in the section, including cover concrete. It was possible to express the column concentric capacity in this simple form because both the concrete and steel reached their plastic states at approximately the same strain level. For the material strengths used at the time, this strain level varied between 0.0015 and 0.002. The ability of the longitudinal steel to maintain its compressive yield strength up to strains well above the crushing strain of concrete was another reason for being able to combine the two contributions in this simple form. The ratio of concrete strength in a column to that of a standard cylinder was taken as 0.85.

Another expression was developed in the same investigation for spirally reinforced columns. It was suggested that these columns could develop a second peak resistance beyond the spalling of cover concrete, which could be expressed on the basis of core concrete area. The expression consisted of three components; i) concrete core contribution, ii) longitudinal steel contribution, and iii) a term reflecting the increase in concrete contribution due to the confining effect of spiral reinforcement. Additional column test data were provided subsequently by Richart et al. (4) in 1947, while also providing a discussion on the behaviour of cover concrete under concentric loading.

The behaviour of columns under eccentric loading was studies extensively by Hognestad (5) as part of his doctorate dissertation. He tested a large number of "C" shaped columns to establish the flexural strength of reinforced concrete columns under combined bending and axial compression. A stress-strain model and a rectangular stress block were proposed for use in flexural analysis and design of reinforced concrete sections (6,7,8). The rectangular stress block was defined by three parameters; k_1, k_2, and k_3, as shown in Fig. 5.1. His recommendations were adopted by ACI 318, as presented later under "Stress Blocks in Building Codes," and continue to be used for design of structures. However, the applicability of this stress block, which was derived using normal-strength concrete test data, to HSC raises questions and safety concerns. This is especially true for columns where the behaviour of section is often dominated by concrete. Previous researchers emphasized features of HSC that may be significantly different than those of normal-strength concrete (9,10,11,12), and some proposed new rectangular stress blocks for HSC. These stress blocks were adopted by the Canadian (13), New Zealand (14) and Norwegian (15) codes and standards as discussed below.

5.2 STRESS BLOCKS IN BUILDING CODES

American Concrete Institute: ACI 318-2005 (1)

ACI 318-05 (1) building code recommends a rectangular stress block with a width of $\alpha_1 f'_c$ and a height of $\beta_1 c$. The parameter α_1 has a constant value of 0.85. The parameter β_1 has a constant value of 0.85 for concrete strengths of up to 30 MPa, and is reduced by 0.08 for each 10 MPa-strength above 30 MPa, but limited by 0.65. The ultimate compressive strain at extreme fibre is defined as $\varepsilon_u = 0.003$. ACI 318-05 (1) does not specify an upper limit of concrete strength for its rectangular stress block.

Canadian Standards Association: CSA A23.3-04 (13)

The rectangular stress block defined in CSA A23.3-04 (13) is applicable to HSC. It is defined using α_1 and β_1 parameters, as in the case of ACI 318-05 (1), but with different values as specified below.

$$\alpha_1 = 0.85 - 0.0015 f'_c \geq 0.67 \quad (1)$$

$$\beta_1 = 0.97 - 0.0025 f'_c \geq 0.67 \quad (2)$$

The range of concrete strengths for the Standard is specified in the Explanatory Notes of the Standard as 20 MPA to 80 MPa, though the above limits of 0.67 governs at 125 MPa. The limiting strain at ultimate is defined as $\varepsilon_u = 0.0035$.

New Zealand Code: NZS 3101-1995 (14)

The New Zealand Code permits the use of HSC with strength limits of 70 MPa and 100 MPa for ductile seismic resisting members and other members, respectively. The following define the rectangular stress block parameters in NZS3101-1995(14).

$$\alpha_1 = 0.85 \quad for\, f'_c \leq 55 MPa \tag{3}$$

$$\alpha_1 = 0.85 - 0.004(f'_c - 55) \geq 0.75 \quad for\, f'_c > 55 MPa \tag{4}$$

$$\beta_1 = 0.85 \quad for\, f'_c \leq 30 MPa \tag{5}$$

$$\beta_1 = 0.85 - 0.008(f'_c - 30) \geq 0.65 \quad for\, f'_c > 30 MPa \tag{6}$$

Norwegian Code: NS 3473-1989 (15)

The Norwegian Code permits the use HSC up to 105 MPa established by 100 mm by 100 mm by 100 mm cube tests. The conversion factor suggested for finding cylinder strength is 0.8 up to 55 MPa and cube strength minus 11 MPa for higher strength concretes. This implies that the strength limit in the Norwegian Code is 94 MPa based on standard cylinder tests. A nonlinear stress-strain model is suggested in the code, with changing strain values at peak stress and extreme fibre strain at ultimate. The strain at peak stress (ε_o) is specified to very between 0.00197 for 20 MPa and 0.00215 for 94 MPa. Similarly, the extreme fibre strain at ultimate (ε_u) is specified to vary between 0.00384 for 20 MPa and 0.00268 for 94 MPa. Linear interpolation is permitted for in-between values of strains.

5.3 PROPOSED RECTANGULAR STRESS BLOCK

5.3.1 HSC Columns under Concentric Compression

Concentric capacity of a normal-strength concrete column can be computed using Eq. 7 (1, 13).

$$P_0 = 0.85 f'_c (A_g - A_{st}) + A_{st} f_y \tag{7}$$

The above equation includes contributions from concrete and longitudinal steel, where the former is based on the in-place strength and net area of concrete, including the cover. The in-place strength of concrete is assumed to be 85% of cylinder strength. This is attributed to the

differences in size, shape and concrete casting practice between a standard cylinder and an actual column member.

Experimental data are available for in-place strength of HSC in columns, obtained from tests of plain concrete columns, and show a scatter of values between 0.87 f'_c and 1.0 f'_c. Tests of 250 mm square columns with 124 MPa and 81 MPa cylinder strengths, conducted by Saatcioglu and Razvi (16) indicate in-place strengths of $0.89f'_c$ and $0.92f'_c$, respectively. The average value reported by Cusson et al. (17) from tests of 235 mm square columns with 100 MPa concrete is $0.88f'_c$. Tests conducted by Yong et al. (18) on small-scale specimens with a 152 mm square cross-section indicate $0.87f'_c$ to $0.97f'_c$ for concretes with 84 MPa to 94 MPa cylinder strengths. Tests by Sun and Sakino (19) with 52 MPa and 132 MPa concrete columns indicate $0.93f'_c$ and $0.91f'_c$, respectively. The Canadian Standard CSA A23.3-04 (13) recommends values of up to $0.90f'_c$ to be used as in-place strength of concrete for columns under concentric compression. These values suggest that an average value of $0.9f'_c$ may be used for HSC columns. This value is also shown to be valid for columns under eccentric loading (9,20). Tests by Ibrahim and MacGregor (9) indicate an average value of $0.91f'_c$ for columns with 59 MPa to 126 MPa concretes. Tests by Kaar (20) on columns with 95 MPa to 102 MPa indicate an average value of $0.99f'_c$.

In spite of the favorable in-place strength of HSC, experimentally recorded column capacities are consistently overestimated by Eq. 7 unless the columns are confined by properly designed transverse reinforcement. The strain data recorded by Saatcioglu and Razvi (16, 21) during their tests of HSC columns with 250 mm cross-sectional dimension indicated that premature spalling

of cover concrete occurred in most columns prior to the development of strains associated with concrete crushing. This observation, combined with visual observations of cover spalling during tests suggests that the cover concrete in HSC columns suffers stability failure rather than crushing. Figure 5.2 illustrates the spalling of cover concrete typically observed during tests. It was hypothesized (16, 21) that the presence of closely spaced longitudinal and transverse steel, forming a mesh of reinforcement produced a natural plane of separation between the cover and the core. The separation of this plane was triggered by high compressive stresses associated with HSC as well as the differences in mechanical properties of core and cover concretes. Early spalling of cover concrete resulted in lower capacities than those computed using Eq. 7 when the strength enhancement in core was not sufficient to make-up for the loss of cover. The beginning of cover spalling was visually observed and marked during tests. Accordingly, the initial signs of cover spalling, usually in the form of vertical cracks, began at approximately 0.15 % to 0.30 % strain for 124 MPa, 0.17 % to 0.25 % strain for 92 MPa, and 0.20 % to 0.41 % strain for 60 MPa concretes. It should be emphasized, however, that these strain ranges indicate the initial signs of cover spalling and are not accurate representations of strains at complete spalling.

The test data was further analysed with those reported by other researchers on square columns. Columns tested by Rangan et al. (22), and some of the columns tested by Yong et al. (18) contained widely spaced low volumetric ratio transverse reinforcement. These columns were able to develop unconfined column capacities (P_0) as specified in Eq. 7. Columns tested by Itakura and Yagenji (23) without any cover, consistently showed higher capacities than those computed based on gross cross-sectional area and unconfined concrete since they did not suffer strength loss due to cover spalling. Those that were sufficiently confined to offset the effects of

cover spalling consistently developed higher strengths than P_0. However, the group that contained insufficient volumetric ratio of closely spaced transverse reinforcement could not sustain capacities computed on the basis of total cross-sectional area and unconfined concrete strength. This observation suggests that, given the right conditions, the premature spalling of cover concrete could lead to reduced concentric capacities in HSC columns relative to those predicted by Eq. 7.

Figure 5.3 shows the variation of in-place-strength of concrete, expressed as f'_{co}/f'_c, with concrete cylinder strength. The in-place strength values were obtained from experimental data by deducting the contribution of longitudinal reinforcement from recorded column capacities. It should be noted that the data plotted in this figure also include confined columns. Therefore, some values of in-place strength are higher than those established by standard cylinder tests. However, the figure clearly shows the trend in strength reduction with increasing concrete cylinder strength.

The strength loss associated with cover spalling is naturally a function of the amount of cover concrete to be lost prematurely. This effect can be introduced by core-area to gross-area ratio (A_c/A_g). As this ratio decreases (cover thickness increases), the strength loss increases. Figure 5.4 illustrates the variation of in-place strength of concrete with (A_c/A_g) ratio. It becomes clear that the degree of premature strength loss in HSC is a function of concrete strength as well as the (A_c/A_g) ratio. The test data plotted in Figs. 5.3 and 5.4 are further examined by removing those that have significant confinement, and by grouping them on the basis of concrete strength. These

test data points are plotted in Fig. 5.5. Regression analysis of data indicates that the effect of cover spalling can be introduced through a multiplier; k_4.

$$f'_{co} = k_3 k_4 f'_c \tag{8}$$

Where;

$$k_3 = 0.90 \tag{9}$$

$$k_4 = \gamma + (1-\gamma)\frac{A_c}{A_g} \leq 0.95 \tag{10}$$

$$\gamma = 1.1 - 0.007 f'_c \leq 0.8 \tag{11}$$

The cylinder strength in Eq. 11 is in MPa. The same equation can be re-written as shown below for f'_c in psi.

$$\gamma = 1.1 - \frac{f'_c}{20{,}000} \leq 0.8 \tag{12}$$

The product k_3k_4 in Eq. 8 introduces the effects of differences in size, shape and concrete casting practice between a standard cylinder and an actual column member through k_3; and the effect of cover spalling through k_4. This product reaches a value that can be as low as 0.63 for 120 MPa concrete and $A_c/A_g = 0.6$, which is 26% below the value computed by Eq. 7, i.e. 0.85.

The onset of cover spalling under concentric compression is not only a function of concrete strength, but also a function of cover stability as governed by cover thickness. Clearly, as the cover thickness increases the stability improves. This is one reason why the spalling effect reaches alarming magnitudes in small-scale test columns with thin covers. Because it is difficult to test large size columns with ultra high-strength concrete under concentric compression, currently no test data is available on large size HSC columns with thick concrete covers. Columns with thick covers are not likely to experience premature spalling as severely as those

with thin covers. For such columns, Eq. 10 would result in conservative values. Until further data become available, Eq. 10 can be used, but the A_c/A_g need not be taken less than 0.6.

The following expression can be used for concentric capacity of columns in compression, which is applicable to both normal-strength and high-strength concrete columns.

$$P_0 = k_3 k_4 f'_c (A_g - A_{st}) + A_{st} f_y \qquad (13)$$

In lieu of detailed computation of coefficient k_4 as outlined above, a conservative but a simple approach may be taken for convenience in design. Accordingly, the product k_3k_4 can be taken as 0.85 for f'_c of up to 40 MPa (or 6000 psi) and reduced by 0.05 for every 20 MPa increase over 40 MPa up to 120 MPa (reduced by 0.017 for every 1000 psi increase over 6000 psi, up to 18000 psi).

5.3.2 HSC Columns under Eccentric Compression

Columns under combined bending and axial compression bend in double curvature in most practical applications. Rarely, they also develop single curvature. In either case, the deflected shape of a column is such that the compression side is always on the concave side of the column, which is the side that is susceptible to cover buckling. The cover on this side has a tendency to buckle towards the core concrete and therefore is constrained against buckling. Consequently, cover buckling is not likely to occur in columns under bending. Observations during tests conducted under bending reversals did not indicate premature spalling of cover concrete (31). Therefore, the modifier k_4 specified in Eq. 10, and used in Eq. 13 becomes 1.0 for eccentrically loaded columns.

Another significant difference in strength calculations between concentrically and eccentrically loaded columns is the presence of strain gradient, which allows redistribution of stresses near the extreme compression fibre. This permits the member to develop compressive strains higher than that corresponds to peak stress (ε_o) prior to strength decay. Therefore, the ultimate compressive strain (ε_u) attained at peak moment resistance is higher than that attained during a standard cylinder test. This value is taken in ACI 318-05 (1) as 0.0030, though the Canadian Standard CSA A23.3-04 (13) recommends a value of 0.0035. The applicability of these strain values to HSC elements raises questions. Therefore, an analytical parametric investigation was conducted by the author to establish the strain at flexural failure as affected by concrete strength. Moment-curvature analyses of a square column section were conducted for this purpose with different concrete strengths, different percentages of reinforcement and different axial load levels. The concrete stress-strain relationship proposed by Popovic (32) and modified by Razvi and Saatcioglu (33) was used for the entire strength range, varying between 30 MPa and 120 MPa. The maximum moment resistance and the corresponding maximum compressive fibre strain were recorded for each case. Regression analysis of results is plotted in Fig. 5.6 and suggests that the following expression may be used to compute ultimate compressive fibre strain at failure when f'_c is expressed in MPa.

$$0.0036 \leq \varepsilon_u = 0.0036 - (f'_c - 30)x10^{-5} \leq 0.0027 \qquad (14)$$

The same expression can be re-written as shown in Eq. 15 when the concrete strength is expressed in psi.

$$0.0036 \leq \varepsilon_u = 0.0036 - 0.65(f'_c - 4000)x10^{-7} \leq 0.0027 \qquad (15)$$

Eq. 14 recognizes the brittle nature of HSC beyond the peak stress, with ε_{cu} changing between 0.0036 for 30 MPa concrete and 0.0027 for 120 MPa concrete. However, the sensitivity of Eq.

14 to flexural strength calculations was found to be small when rectangular stress block was employed for strength calculations. Therefore, when a rectangular stress block is employed, an average value of ε_u= 0.003 may be used for the entire range of concrete strengths considered in this thesis.

Once the strain profile for ultimate is established, the computation of column strength can be carried out by plane-section analysis. This can be done by using appropriate material stress-strain models and integrating the concrete stress distribution to obtain internal compressive force, which can then be used to compute moment resistance at ultimate. Alternatively, a rectangular stress block can be employed for ease in calculations.

5.3.3 Rectangular Stress Block for HSC

A rectangular stress block was developed for a wide range of concrete strengths, including HSC up to 130 MPa. The principles used by Hognestad (5) were employed in developing the stress block with coefficients k_1, k_2 and k_3, as illustrated in Fig. 5.1. Coefficient k_3 had already been established experimentally as discussed earlier to be 0.9. This helped define the peak stress of in-place stress-strain relationship of concrete in columns. The stress-stress relationship proposed by Popovic (32) was selected to derive coefficients k_1 and k_2 since it was applicable to high-strength, as well as normal-strength concretes. The descending portion of the curve was simplified as suggested by Razvi and Saatcioglu (33) to be linear. The curve was integrated numerically up to the ultimate compressive strain defined in Eq. 14 to find the area and the centroid of area for different concrete strengths. The centroid of area relative to the extreme fibre strain gave coefficient k_2. Coefficient k_1 was found such that the area of the stress-strain

relationship was equal to an equivalent rectangular stress distribution over the entire compression zone. Regression analysis of the results is shown in Figs. 5.7 and 5.8. Also shown in the figure are those suggested by Ibrahim and MacGregor (9), experimentally obtained values, and those specified by ACI318 (1) and CSA A23.3 (13).

The proposed rectangular stress block was defined to have $\alpha_1 f'_c$ width and $\beta_1 c$ depth as typically done in building codes and standards (1,13). This is illustrated in Fig. 5.1.

$$\alpha_1 \beta_1 = k_1 k_3 \tag{16}$$

$$\beta_1 = 2k_2 \tag{17}$$

Parameters α_1 and β_1 were computed using coefficients k_1, k_2, and k_3, as a function of concrete strength. The proposed expressions, also shown in Fig. 5.9, are shown below.

For $f'_c \leq 30$ MPa:

$$\alpha_1 = 0.85 \tag{18}$$

$$\beta_1 = 0.85 \tag{19}$$

For $f'_c > 30$ MPa:

$$\alpha_1 = 0.85 - 0.0014(f'_c - 30) \geq 0.72 \tag{20}$$

$$\beta_1 = 0.85 - 0.0020(f'_c - 30) \geq 0.67 \tag{21}$$

The above expressions can be re-written for (f'_c) in psi, as indicated below.

For $f'_c \leq 4000$ psi:

$$\alpha_1 = 0.85 \tag{22}$$

$$\beta_1 = 0.85 \tag{23}$$

For $f'_c > 4000$ psi:

$$\alpha_1 = 0.85 - (f'_c - 4000)x10^{-5} \geq 0.72 \quad (24)$$

$$\beta_1 = 0.85 - 1.4(f'_c - 4000)x10^{-5} \geq 0.67 \quad (25)$$

Equations 18 to 21 indicate that (α_1) and (β_1) are equal to 0.85 for concrete strengths of up to 30 MPa and reduce by 0.014 and 0.020 respectively, for every 10 MPa increase in concrete strength such that $\alpha_1 \geq 0.72$, and $\beta_1 \geq 0.67$. Similarly, (α_1) and (β_1) are equal to 0.85 for concrete strengths of up to 4,000 psi and reduce by 0.010 and 0.014 respectively, for every 1000 psi increase in concrete strength such that $\alpha_1 \geq 0.72$, and $\beta_1 \geq 0.67$.

5.4 EXPERIMENTAL VERIFICATIONS

Column capacities computed on the basis of proposed rectangular stress block are compared with those recorded experimentally. The comparison is made separately for columns under concentric and eccentric loadings. Figure 5.5 shows the comparison of the product of proposed coefficients k_3 and k_4 with those computed from experimental column capacities. The comparison indicates very good correlation for all levels of concrete strength. The ACI 318-05 (1) coefficient is also plotted on the same figure. The results indicate that column concentric capacities based on ACI 318-05 (1) overestimate experimental capacities of HSC columns, especially when the A_c/A_g ratio is low. The same code equation provides reasonably good agreement with experimental strength values for normal-strength concrete columns.

Comparisons of column capacities under combined bending and axial compression are made by means of column interaction diagrams. Axial force-bending moment interaction diagrams for a 300 mm square column section are plotted first, as shown in Fig. 5.10, based on different rectangular stress blocks and concrete strengths. The diagrams are computed using the proposed rectangular

stress block, as well as those recommended by ACI 318-05 (1), CSA A23.3-04 (13), and NZS 3101-1995 (14). Figure 5.10 indicates that all four stress blocks result in very similar interaction diagrams for normal-strength concrete columns. As concrete strength increases, the ACI 318 stress block overestimates the strength envelope significantly, while the other three results in similar interaction diagrams, with the CSA A23.3 curve showing the lowest strength envelops.

Of the 145 test data found in the literature for eccentrically tested HSC columns, some were selected for comparison with analytically generated interaction diagrams. Figure 5.11 includes columns tested by Ibrahim and MacGregor (9,37), Rangan (10) and Foster (11), and interaction diagrams computed with proposed and ACI 318 rectangular stress blocks. The results clearly show that the ACI 318 rectangular stress block is not applicable to HSC columns and it consistently overestimates column capacities, especially when the level of axial compression is higher than that at balanced point. The proposed stress block provides reasonably good envelopes for most cases. Figure 5.12 shows the comparison of moment capacities based on proposed rectangular stress block with those recorded experimentally for all 145 HSC columns under different levels of axial compression. The data points are grouped based on concrete strength. The results indicate very good correlation between computed and recorded values, with the proposed rectangular stress block providing lower bound solutions for most cases, suitable for use in design.

5.5 SUMMARY AND CONCLUSIONS

A rectangular stress block was developed for HSC, based on an analytical model for concrete stress-strain relationship and a large volume of column test data. The stress block was verified

extensively against column tests conducted under concentric and eccentric loadings. The results indicate very good correlations of computed and measured strength values. The proposed stress block resembles to that currently used in the ACI 318 code (1) and applies to both normal-strength and high-strength concrete elements. It incorporates prevalent features of HSC in columns that consist of premature spalling of cover under concentric loading, nearly triangular variation of the stress-strain relationship and the brittle nature of failure. The proposed stress block is also shown to produce equally good estimates of column strengths for normal-strength concrete.

Based on the rectangular stress block introduced in this thesis, the following code provisions are proposed for the ACI 318 Building Code:

i. For concrete strengths of up to 120 MPa (18,000 psi), the concentric capacity of columns can be computed by:

$$P_0 = 0.9\, k_4 f'_c (A_g - A_{st}) + A_{st} f_y \tag{26}$$

$$k_4 = \gamma + (1-\gamma)\frac{A_c}{A_g} \le 0.95 \tag{27}$$

$$\gamma = 1.1 - 0.007 f'_c \le 0.8 \text{ where } f'_c \text{ is in MPa} \tag{28}$$

$$\gamma = 1.1 - \frac{f'_c}{20{,}000} \le 0.8 \text{ where } f'_c \text{ is in psi} \tag{29}$$

The ratio A_c/A_g in Eq. (27) need not be taken less than 0.6.

ii. Alternatively, for simplicity, the concentric capacity of columns can be computed by Eq. 26 with a modified coefficient. For concrete strengths of up to 40 MPa (6000 psi), 0.9 k_4 in Eq. 26 is replaced with coefficient 0.85. For concrete strengths greater than

40 MPa (6000 psi), the coefficient 0.85 is reduced by 0.025 for every 10 MPa increase (0.017 for every 1000 psi increase) in strength over 40 MPa (6000 psi).

iii. Under combined bending and axial compression, concrete stress of $\alpha_1 f'_c$ is assumed uniformly distributed over an equivalent compression zone bounded by edges of the cross section and a straight line located parallel to the neutral axis at a distance a = $\beta_1 c$ from the fibre of maximum compressive strain.

iv. Factor α_1 shall be taken as 0.85 for concrete strengths f'_c up to and including 30 MPa (4000 psi). For strengths above 30 MPa (4000 psi), α_1 shall be reduced continuously at a rate of 0.014 for each 10 MPa (0.010 for each 1000 psi) of strength in excess of 30 MPa (4000 psi), but α_1 shall not be taken less than 0.72.

v. Factor β_1 shall be taken as 0.85 for concrete strengths f'_c up to and including 30 MPa (4000 psi). For strengths above 30 MPa (4000 psi), β_1 shall be reduced continuously at a rate of 0.020 for each 10 MPa (0.014 for each 1000 psi) of strength in excess of 30 MPa 4000 psi, but β_1 shall not be taken less than 0.67.

5.6 NOTATION

A_c : Area of core concrete within perimeter tie (centre-to-centre).

A_g : Gross area of column concrete section.

A_{st} : Total area of longitudinal reinforcement.

c : Depth of neutral axis, measured from extreme compression fibre.

f'_c : Concrete cylinder strength.

f'_{co} : In-place strength of concrete in member.

f_y : Yield strength of longitudinal reinforcement.

k_1 : Coefficient defined in Fig. 5.1.

k_2 : Coefficient defined in Fig. 5.1.

k_3 : Coefficient that relates in-place and cylinder strengths of concrete, specified in Eq. (9).

k_4 : Coefficient that accounts for strength loss due to cover spalling, defined in Eq. (10).

P_o : Nominal concentric compressive capacity of column.

α_1 : Coefficient that defines width of rectangular stress block, specified in Eqs. (18) and (20) for f'_c in MPa and Eqs. (22) and (24) for f'_c in psi.

β_1 : Coefficient that defines height of rectangular stress block, specified in Eqs. (19) and (21) for f'_c in MPa and Eqs. (23) and (25) for f'_c in psi.

ε_u : Extreme compression fibre strain in concrete at ultimate moment resistance.

ε_o : Strain in concrete corresponding to peak strength, f'_c.

γ : Coefficient defined in Eq. (11) for f'_c in MPa and Eq. (12) for f'_c in psi.

ρ : Column reinforcement ratio, $\rho = A_{st}/A_g$

5.7 REFERENCES

1. American Concrete Institute (ACI) Committee 318, "Building Code Requirements for Structural Concrete (ACI 318-05) and Commentary (318R-05)," Farmington Hills, Mich., 2005, 430 pp.

2. Slater, W. A. and Lyse, I, "First Progress Report on Column Tests at Lehigh University," Journal of the American Concrete Institute, Vol. 27, February, 1931, p. 766- 864.

3. Richart, F. E. and Brown, R. L., "An Investigation of Reinforced Concrete Columns," University of Illinois Engineering Experimental Station, Bulletin Series No. 267, University of Illinois, Urbana, 1934, 91 pp.

4. Richart, F. E., Draffin, J., Olson, T. A., and Heitman, R. "The Effect of Eccentric Loading, Protective Shells, Slenderness Ratios, and Other Variables in Reinforced Concrete Columns," University of Illinois Engineering Experimental Station, Bulletin Series No. 368, University of Illinois, Urbana, 1947, 130 pp.

5. Hognestad, E., "A Study of Combined Bending and Axial Load in Reinforced Concrete Members," University of Illinois Engineering Experimental Station, Bulletin Series No. 399, University of Illinois, Urbana, 1951, 128 pp.

6. Hognestad, E., "Ultimate Strength of Reinforced Concrete in American Design Practice," Bulletin D12, Portland Cement Association, Research and Development Laboratories, Chicago, 1961, 19 pp.

7. Mattock, A., H., Kriz, L. B., Hognestad, E., "Rectangular Stress Distribution in Ultimate Strength Design," Journal of The American Concrete Institute, No. 57, February, 1961, p. 875-928.

8. Mattock, Kriz, "Ultimate Strength of Non-rectangular Structural Members," Journal of The American Concrete Institute, No. 57, January, 1961, p. 737-766.

9. Ibrahim H., and MacGregor J.G. , "Flexural Behaviour of High-Strength Concrete Columns", Report No. 196, Department of Civil Eng., University of Alberta, Edmenton, Alberta, Canada , March 1994, pp.197.

10. Lloyd N.A., and Rangan B.V., "Studies on High-Strength Concrete Columns under Eccentric Compression", ACI Structural Journal, Vol.93, No.6 , 1996, pp. 631-638.

11. Foster S.J., and Attard M.M., "Experimental Tests on Eccentrically Loaded High-Strength Concrete Columns", ACI Structural Journal, Vol.94, No.3, 1997, pp. 295-303.

12. Lee J.L. and Son H., "Failure and Strength of High-strength Concrete Columns Subjected to Eccentric Loads", ACI Structural Journal, Vol.97, No1, 2000, pp 75-85.

13. Canadian Standards Association (CSA) Committee A23.3 (2004). "Design of concrete structures (A23.3-04)." Rexdale, Ontario, 240 pp.

14. NZS 3101-1995, "The Design of Concrete Structures," Standards New Zealand, Wellington, New Zealand, 1995, 520 pp.

15. NS 3473 (1989), "Norwegian Standard for Design of Concrete Structures," The Norwegian Council for Building Standardisation, N.B.R., Oslo, Norway.

16. Saatcioglu, M. and Razvi, S.R., "High-Strength Concrete Columns with Square Sections," *ASCE Journal of Structural Engineering*, Vol. 124, No. 12, pp. 1438-1447, 1998.

17. Cusson, D., and Paultre, P., " High-Strength Concrete Columns Confined by Rectangular Ties," *ASCE Journal of Structural Engineering*, Vol. 120, No.3, March 1994, pp.783-804.

18. Yong, Y.K., Nour, M.G., and Nawy, E.G., "Behaviour of Laterally Confined High-Strength Concrete Under Axial Loads," *ASCE Journal of Structural Engineering,* Vol.114, No.2,1988, pp. 332-351.

19. Sun, Y. P., and Sakino, K., "Ductility improvement of reinforced concrete columns with high-strength materials," Transaction of the Japan Concrete Institute (JCI), Vol.15, 1993, pp.455-462

20. Kaar, P. H., Hanson, N. W., and Capell, H. T., "Stress-Strain Characteristics of High-Strength Concrete," ACI SP 55-7, Douglas McHenry International Symposium on Concrete and Concrete Structures, ACI Detroit, pp. 161-185.

21. Razvi, S.R., and Saatcioglu, M., "Strength and Deformability of Confined High-Strength Concrete Columns," *ACI Structural Journal*, Vol. 91, No. 6, 1994, pp. 678-687

22. Rangan, B.V., Saunders, P., and Seng, E.J., "Design of High-Strength Concrete Columns." Evaluation and rehabilitation of concrete structures and innovations in design, *ACI SP 128-52*, American Concrete Institute, 1991, pp. 851-862.

23. Itakura, Y., and Yagenji, A., "Compressive Test on High-Strength R/C Columns and Their Analysis Based on Energy Concept." *Proceedings of 10th World Conference on Earthquake Engineering*, Madrid, 1992, pp. 2599-2602.

24. Watanabe, F., and Mugumura, H., "Toward the Ductility Design of Concrete Members (Overview of Researches in Kyoto University)," *Proceedings of Pacific Concrete Conference*, New Zealand, 1988, pp. 89-100.

25. Nagashima, T.; Sugano, S.; Kimura, H.; and Ichikawa, A., "Monotonic Axial Compression Test on Ultra High-Strength Concrete Tied Columns," *Proceedings of 10th World Conference on Earthquake Engineering*, Madrid, 1992, pp. 2983-2988.

26. Nishiyama, M.; Fukushima, I.; Watanabe, F.; and Muguruma, H.,1993, "Axial Loading Tests on High-Strength Concrete Prisms Confined by Ordinary and High-Strength Steel," *Proceedings of the Symposium on High-Strength Concrete*, Norway, pp. 322-329.

27. Sun, Y. P., and Sakino, K. et al., "Effect of Confinement of Transverse Reinforcement on the Axial Behaviour of Concrete," *Proceedings of Japan Concrete Institute (JCI)*, V. 16, No. 2, 1994, pp. 449-454.

28. Sakai, Y.; Hibi, J.; Otani, S.; and Aoyama, H., "Experimental Study of Flexural Behaviour of Reinforced Concrete Columns Using High Strength Concrete," *Transactions of the Japan Concrete Institute*, V. 12, 1990, pp. 323-330.

29. Kato, D., and Wakatsuki, K., "Effects of Hoop Ties on the Stress-Strain Relation of Square Confined R/C Columns," *Summaries of Technical Papers of Annual Meeting*, Architectural Institute of Japan, 1992, pp. 645-646.

30. Kato, D., "Stress-Strain Behaviours of Square Confined Reinforced Concrete Columns," *Journal of Structural and Construction Engineering* No. 422, 1991, Apr., pp. 65-74.

31. Saatcioglu, M., and Baingo, D., "Circular High-Strength Concrete Columns under Simulated Seismic Loading," *ASCE Journal of Structural Engineering*, Vol 125, No.3, 1999, pp. 272-280.

32. Popovics, S., "Analytical Approach to Complete Stress-Strain Curves," *Cement and Concrete Research*, Vol.3, No.5, Sept. 1973, pp. 583-599.

33. Razvi, S. R. and Saatcioglu, M., "Stress-Strain Relationship for Confined High-Strength Concrete," ASCE Journal of Structural Engineering, Vol 125, No.3, pp. 281-289,1999.

34. Nedderman, H., "Flexural Stress Distribution in Very High Strength Concrete," MASc thesis, Dept. of Civil Engineering, University of Texas, Arlington, Tex., 1973.

35. Swartz, S. E.; Nikaeen, A.; Narayan Babu, H. D.; Periyakaruppan, N.; and Rfai, T. M. E., "Structural Bending Properties of Higher Strength Concrete," *High-Strength Concrete*, SP-87, H. G. Russell, ed., American Concrete Institute, Farmington Hills, Mich., 1985, pp. 147-178.

36. Ozden, S., "Behaviour of High-Strength Concrete under Strain Gradient," MA thesis, University of Toronto, Toronto, Ontario, Canada, 1992, pp. 112-113.

37. Ibrahim, H., and MacGregor, J. G., "Modification of the ACI Rectangular Stress Block for High-Strength Concrete," *ACI Structural Journal*, V. 94, No. 1, Jan.-Feb. 1997, pp. 40-48.

38. Schade, J. E., "Flexural Concrete Stress in High Strength Concrete Columns," MASc thesis, Department of Civil Engineering, University of Calgary, Calgary, Alberta, Canada, Sept. 1992, 156 pp.

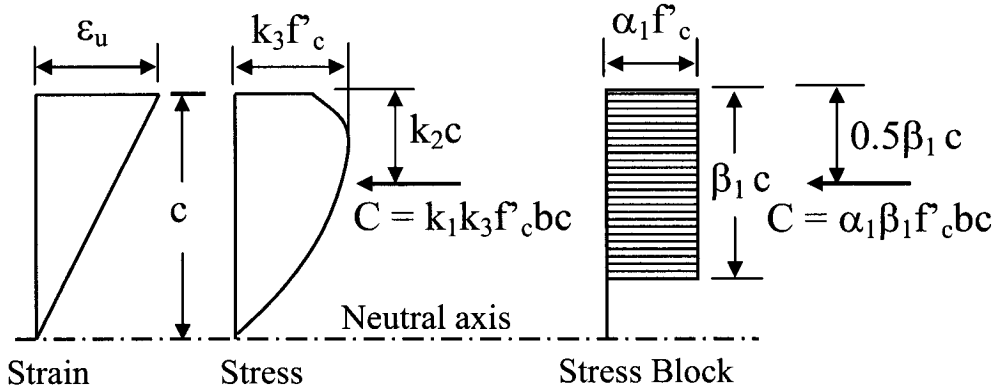

$$f'_{co} = k_3 f'_c \qquad \beta_1 = 2k_2 \qquad \alpha_1\beta_1 = k_1k_3$$

Fig. 5.1 – Rectangular stress block

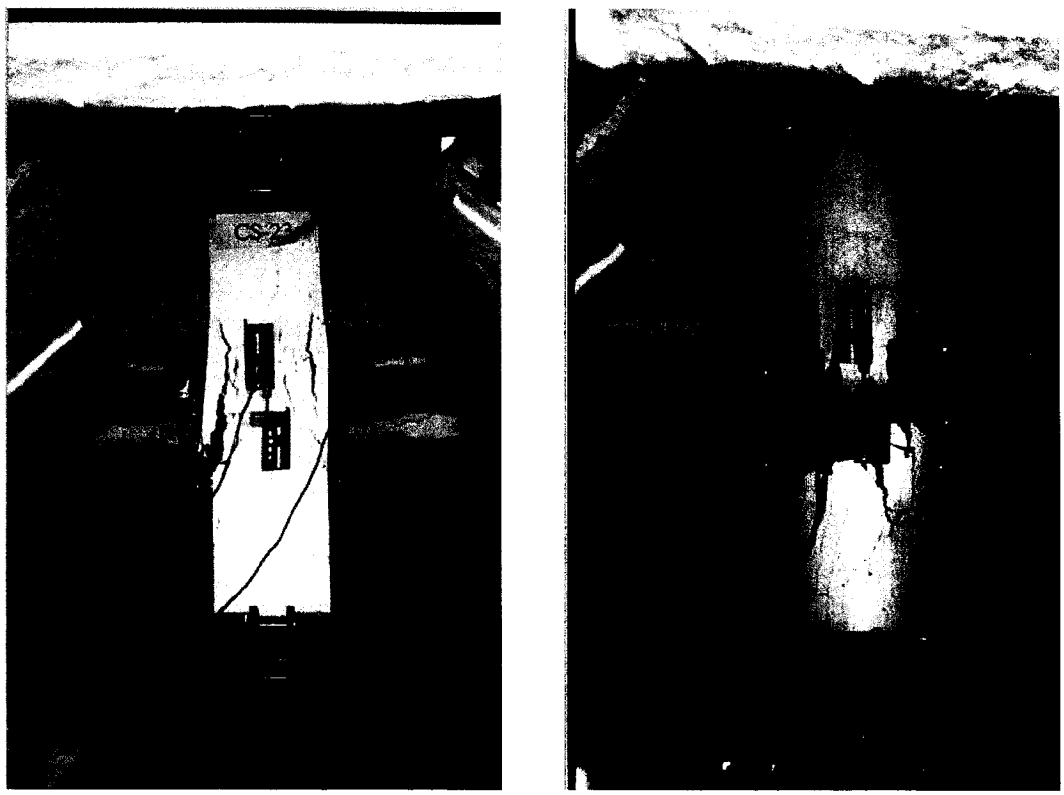

(a) **(b)**

Fig. 5.2 – Instability of cover in HSC columns under concentric compression

(c)

Fig. 5.2 – Cont'd

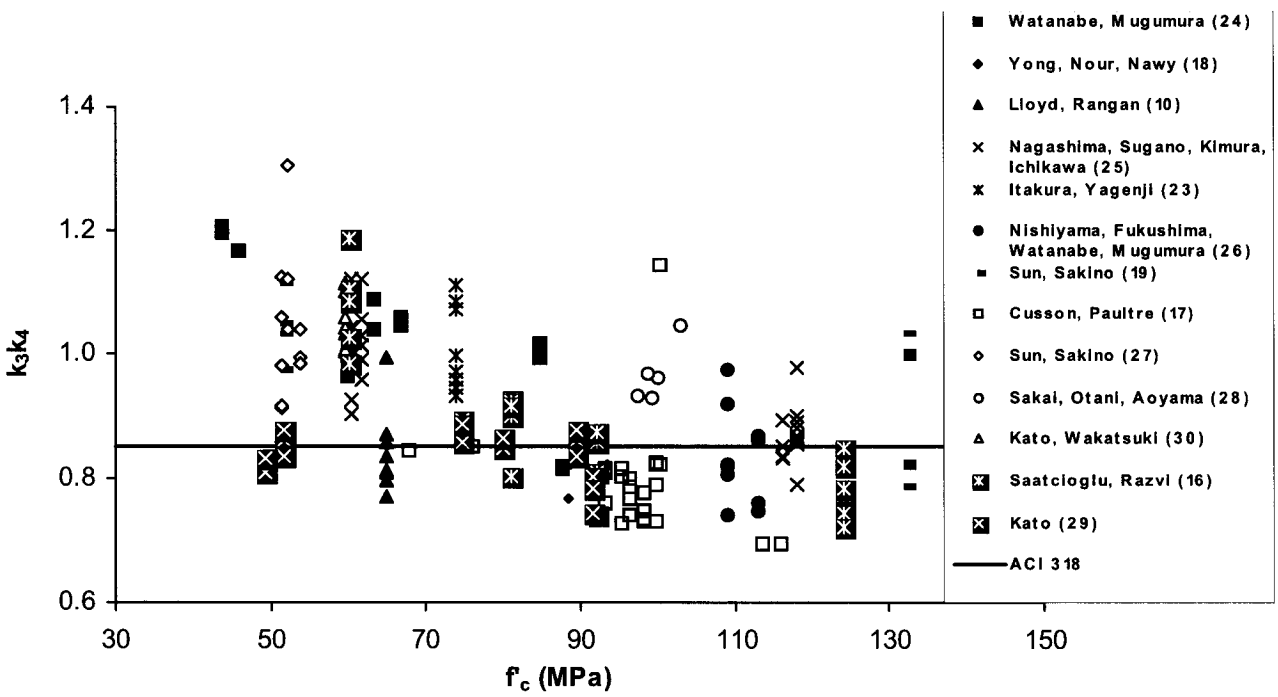

Fig. 5.3 – In-place strength of concrete as affected by cylinder strength

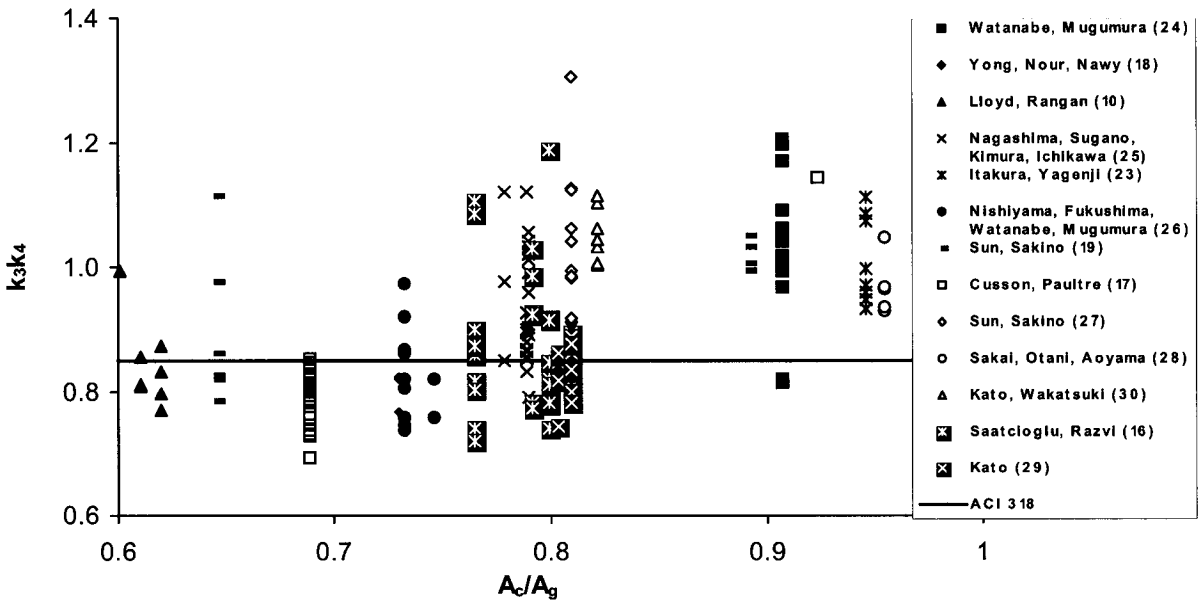

Fig. 5.4 – In-place strength of concrete as affected by core-to-gross-area ratio (A_c/A_g)

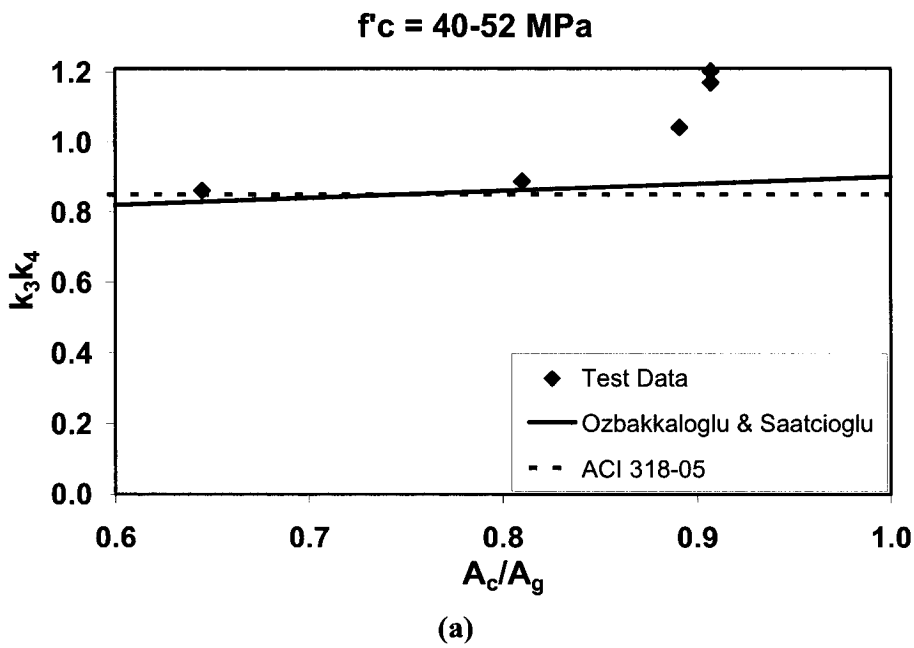

(a)

Fig. 5.5 – Variation of in-place concrete strength with (A_c/A_g) ratio, for different levels of concrete strength

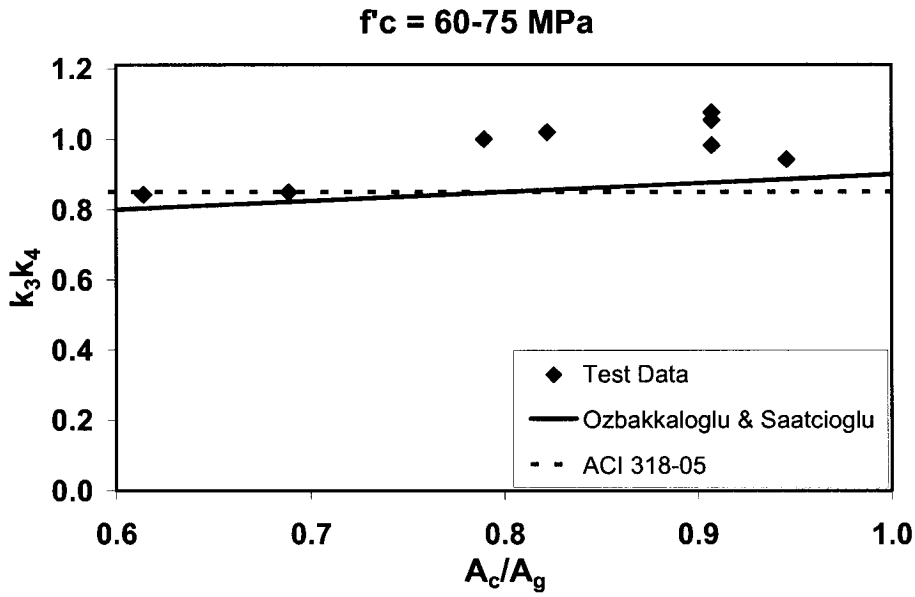

(b)

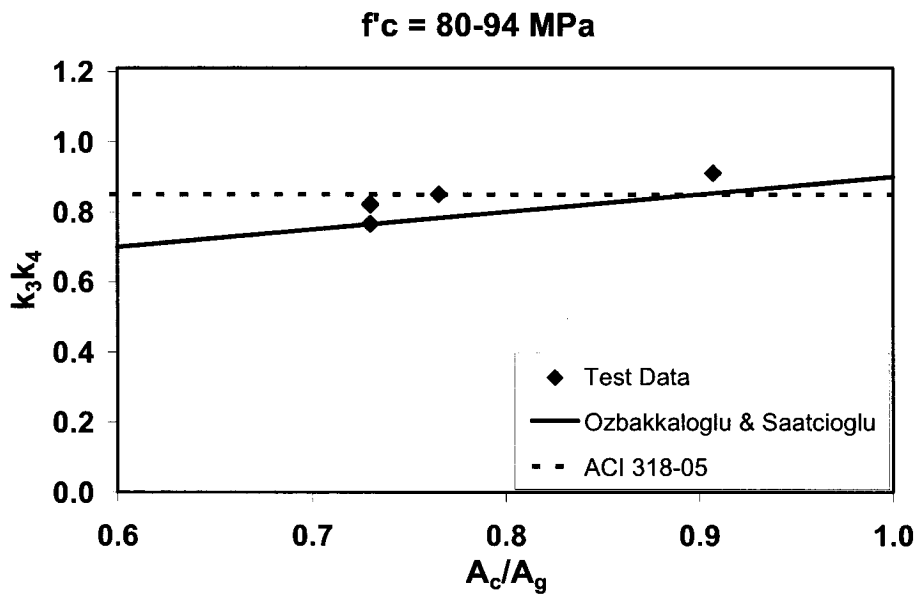

(c)

Fig. 5.5 – Cont'd

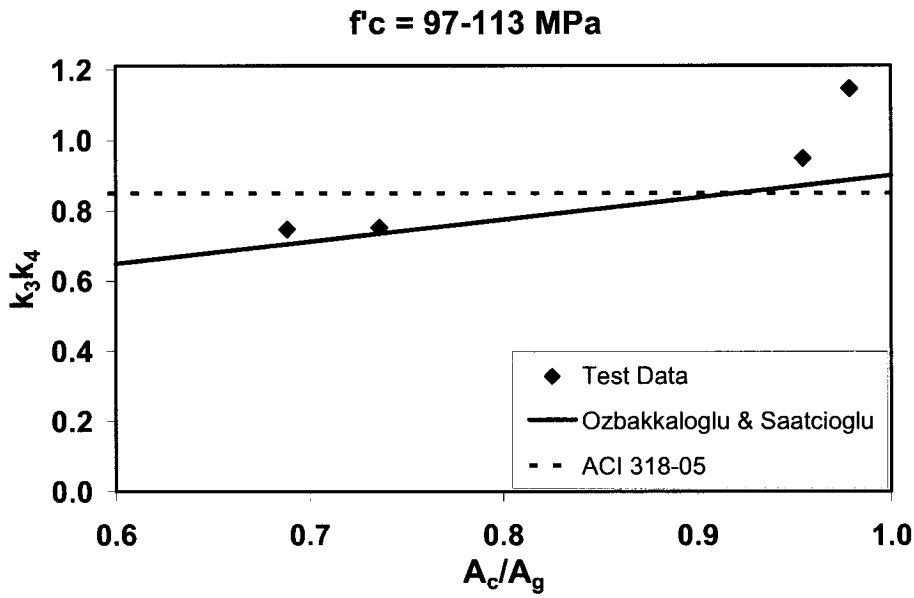

(d)

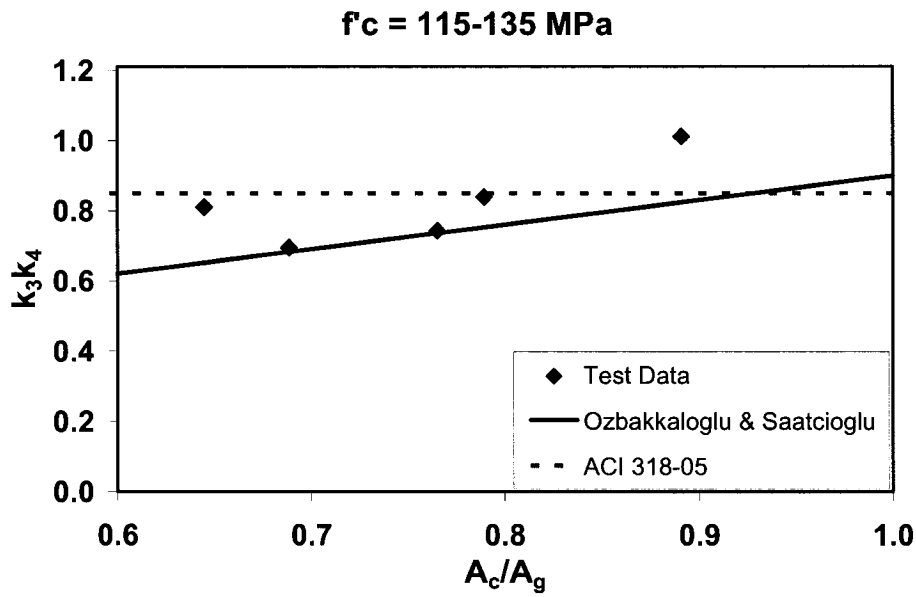

(e)

Fig. 5.5 – Cont'd

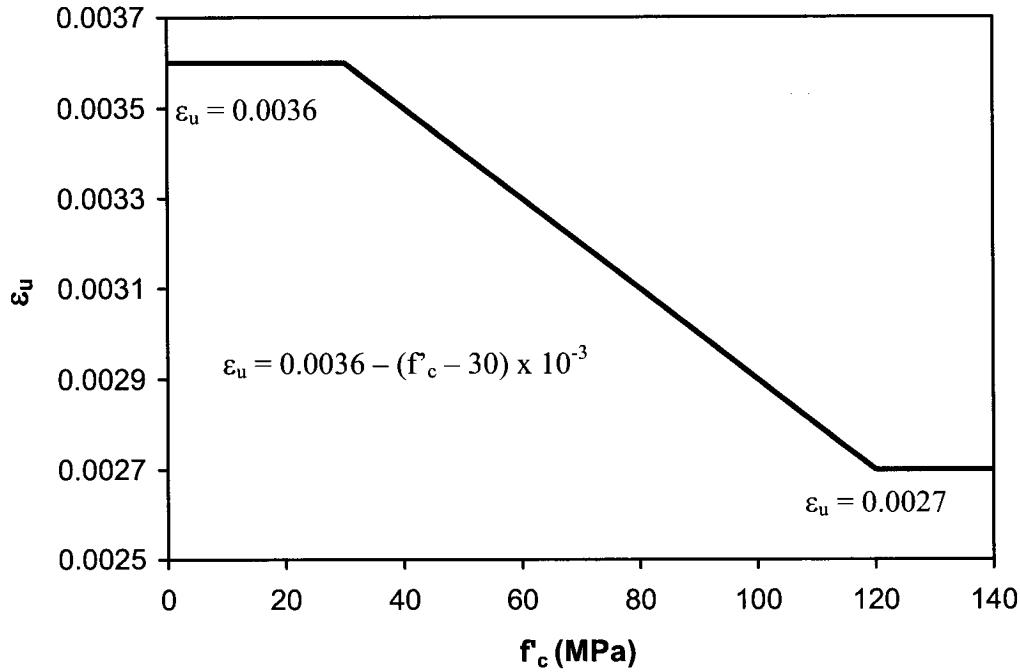

Fig. 5.6 – Ultimate flexural strain ε_u, as affected by concrete strength

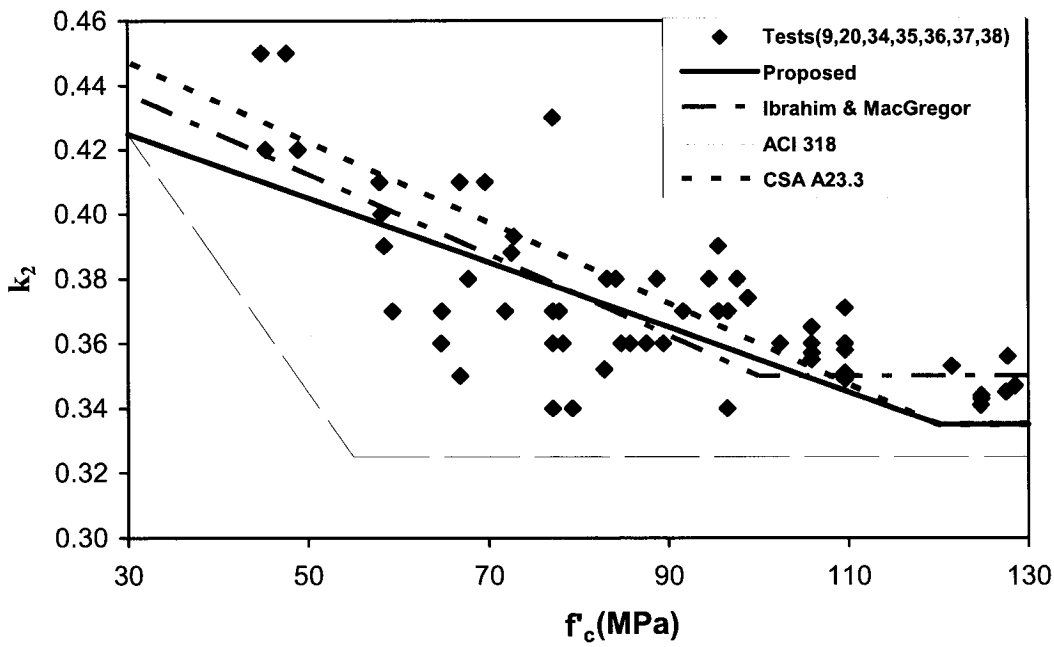

Fig. 5.7 – Variation of coefficient k_2 with concrete strength

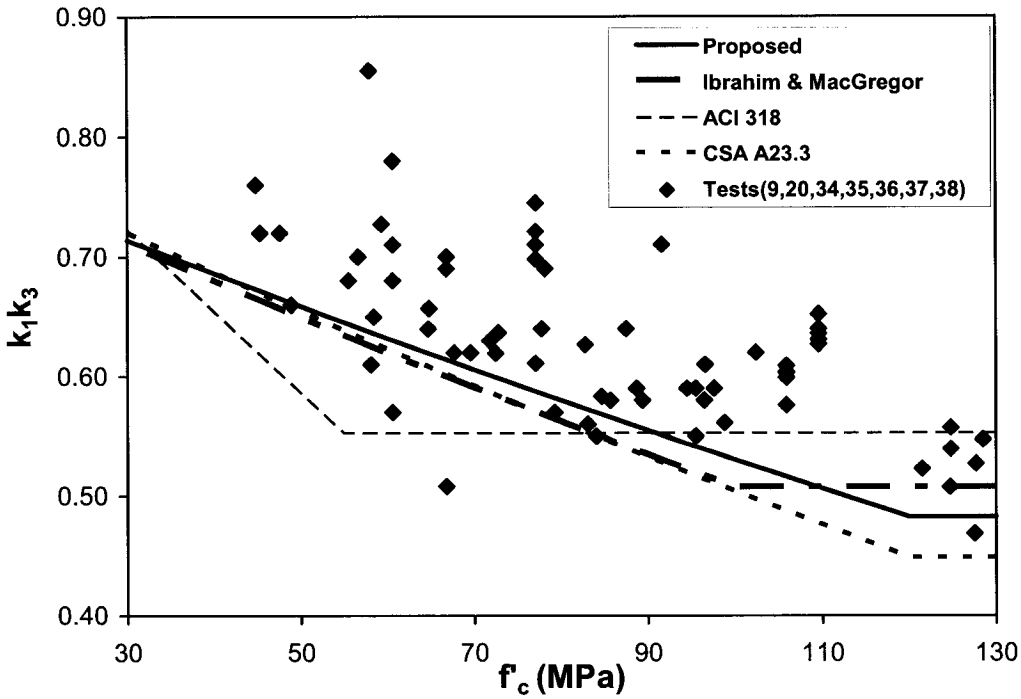

Fig. 5.8 – Variation of the product of coefficients k_1k_3, with concrete strength

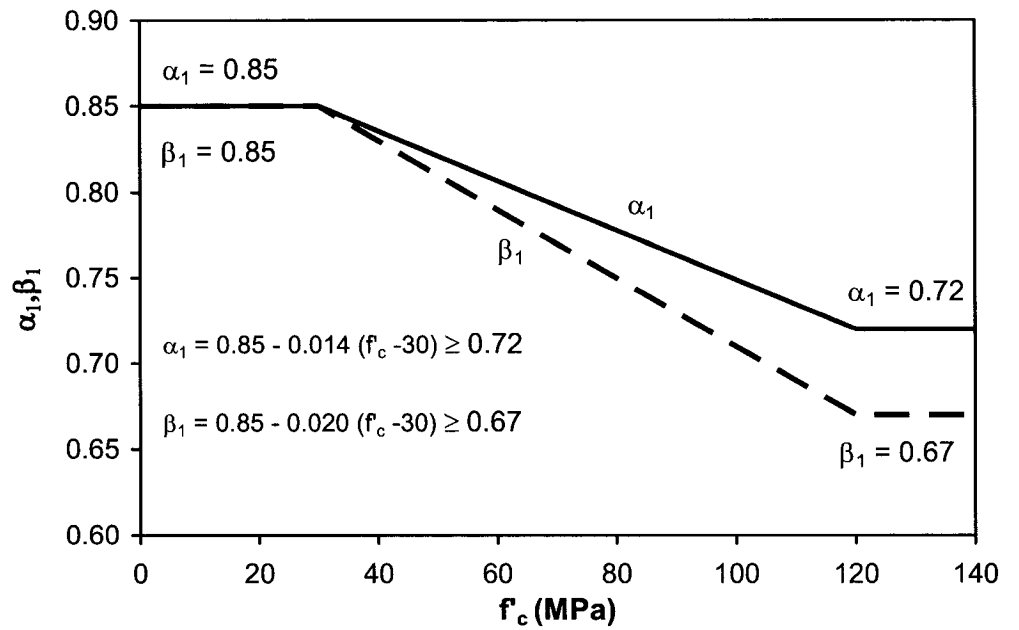

Fig. 5.9 – Variation of α_1 and β_1 with concrete strength

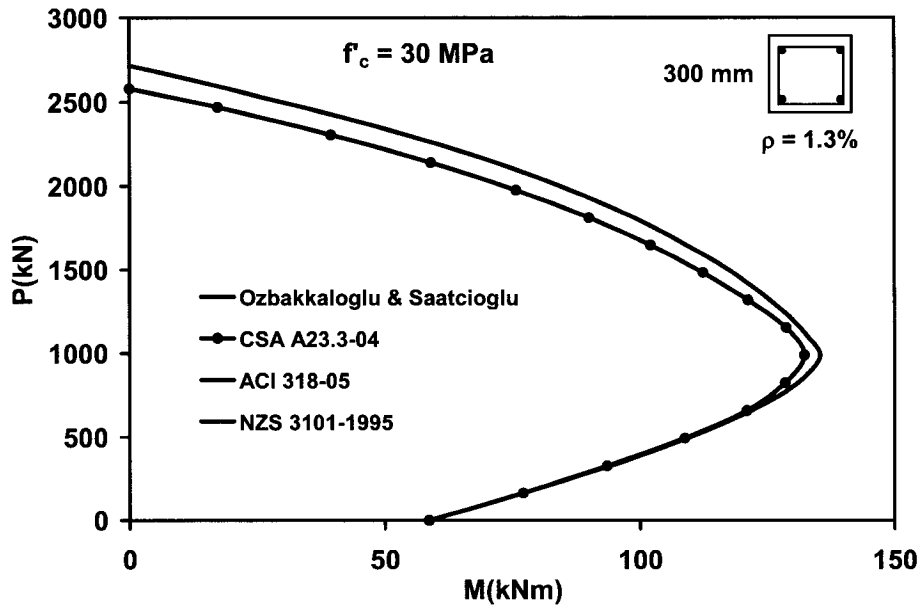

(a)

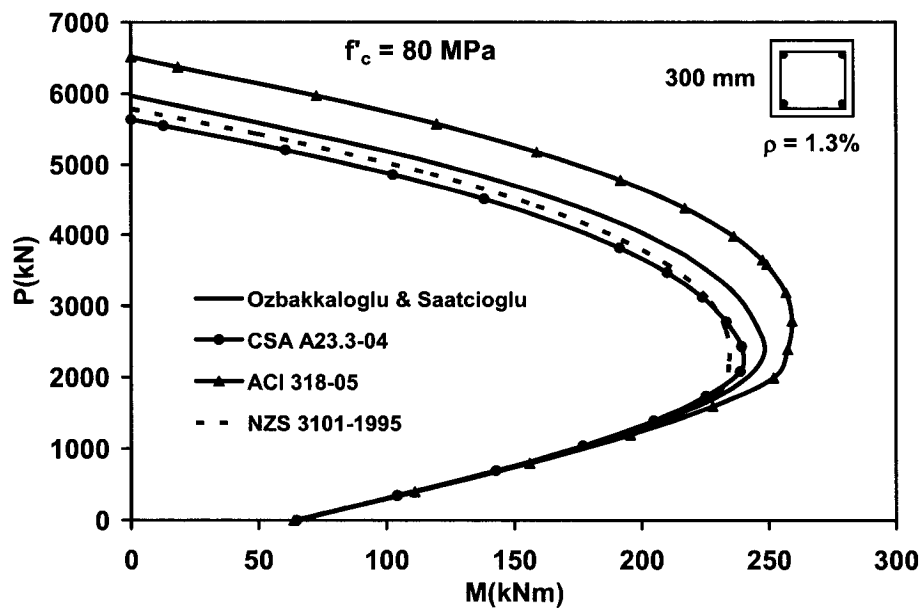

(b)

Fig. 5.10 – Comparisons of column interaction diagrams obtained by selected rectangular stress blocks, for different levels of concrete strength

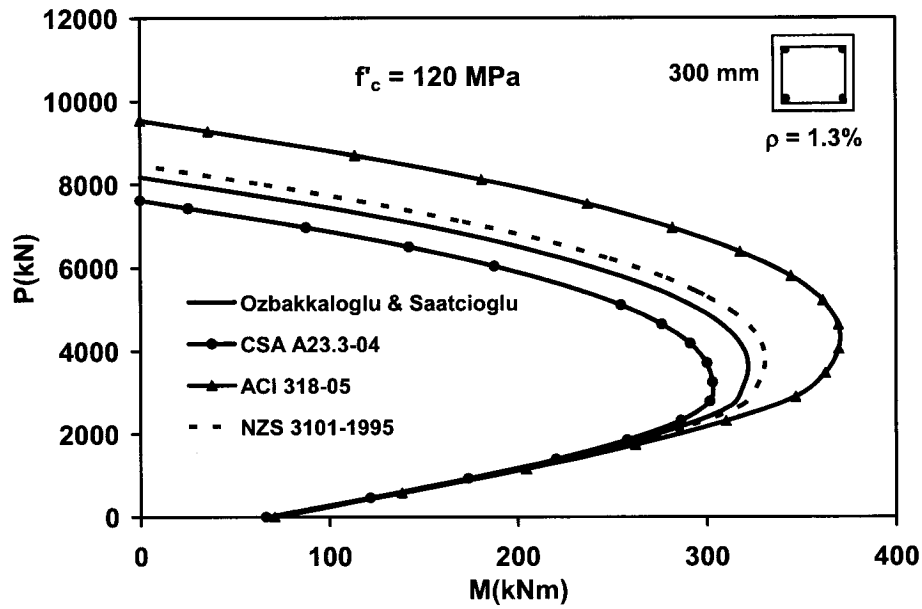

(c)

Fig. 5.10 – Cont'd

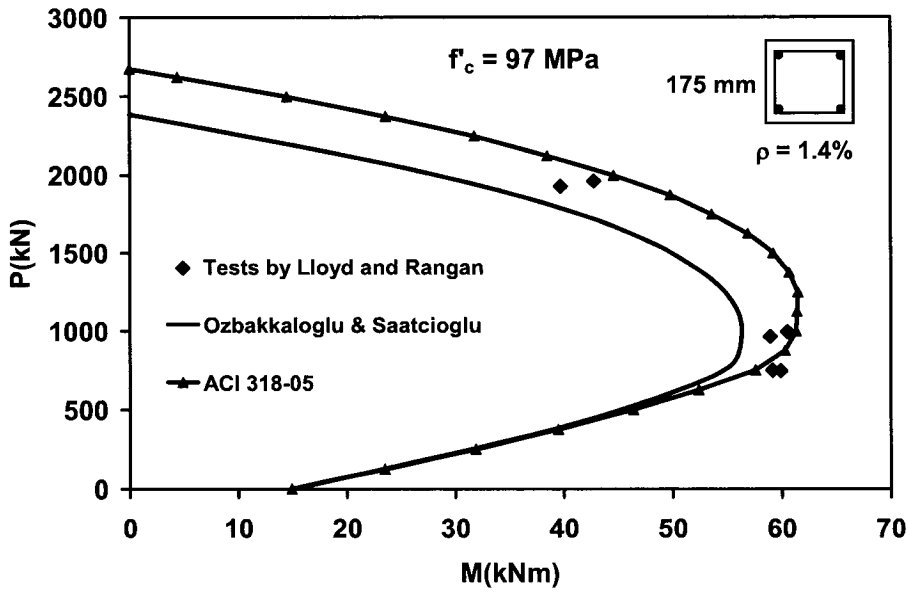

(a)

Fig. 5.11 – Comparisons of experimentally obtained column capacities with those computed by the proposed and ACI 318-05 rectangular stress blocks

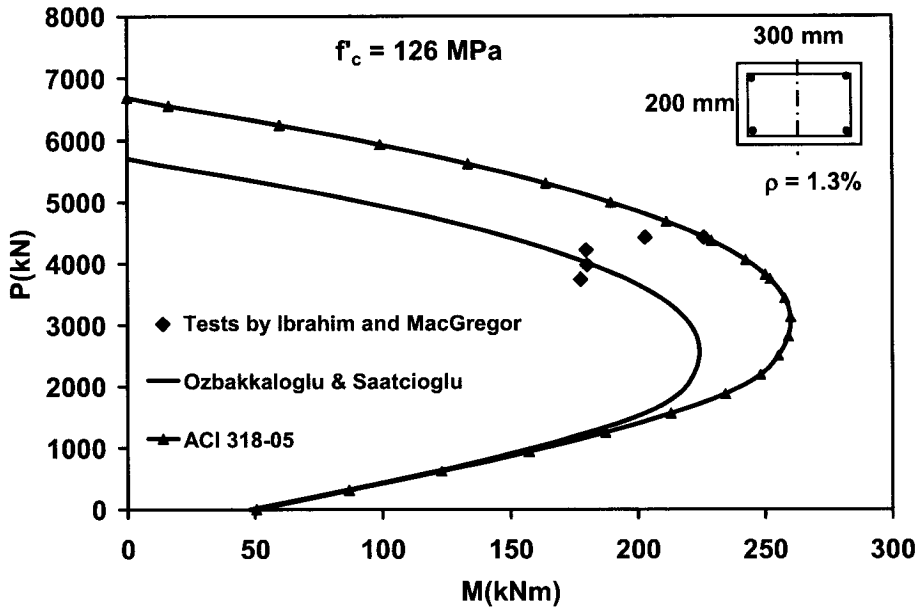

(b)

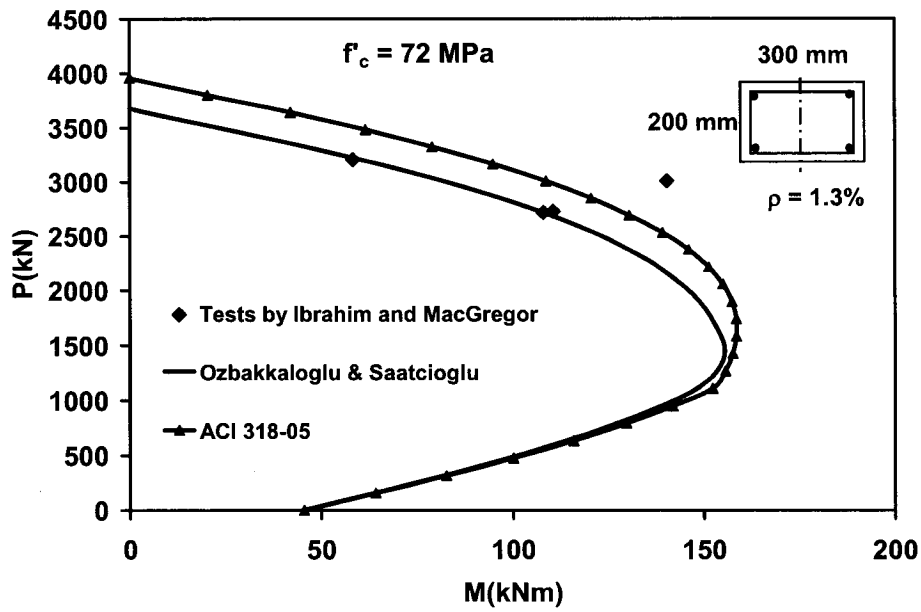

(c)

Fig. 5.11 – Cont'd

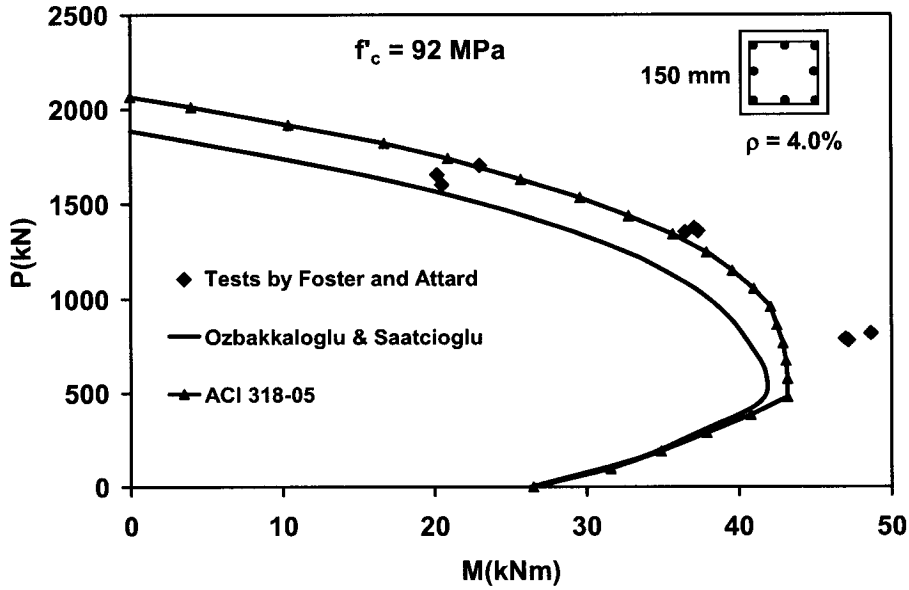

(d)

Fig. 5.11 – Cont'd

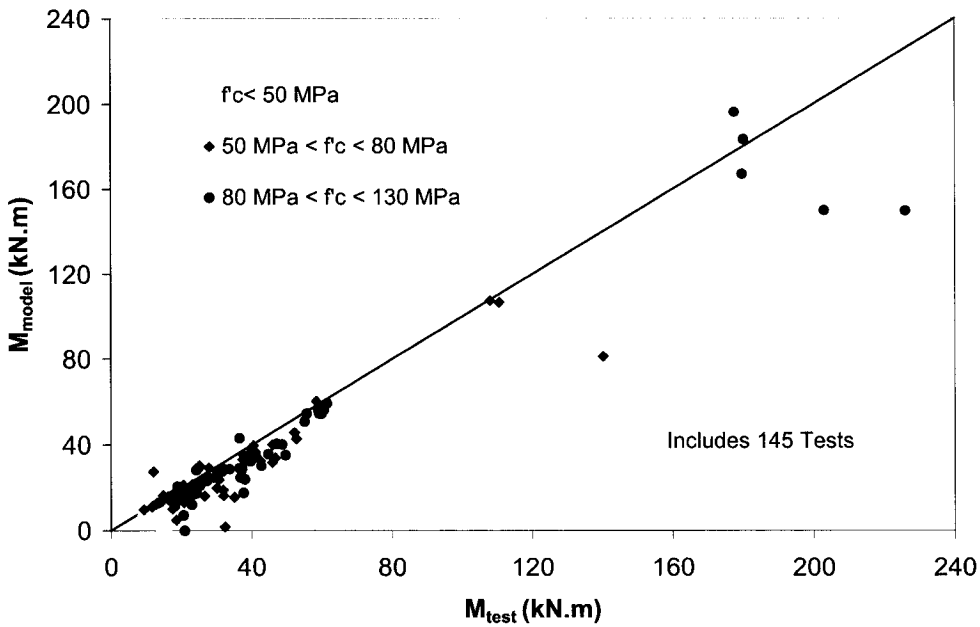

Fig. 5.12 – Comparison of experimentally recorded column moment capacities with those computed on the basis of the proposed rectangular stress block

Chapter 6

Drift Capacities of Concrete Columns Confined with FRP Stay-in-Place Formwork

6.1 INTRODUCTION

The use of FRP sheets for seismic retrofitting and rehabilitation of existing concrete columns has gained acceptance in recent years. Fibre reinforced composites (FRP) offer an attractive alternative to conventional reinforcement for confining concrete. An extensive experimental and analytical research has been underway at the Structures Laboratory of the University of Ottawa to extend the technology developed for FRP jackets to new concrete columns, in the form of FRP stay-in-place formwork (Ozbakkaloglu and Saatcioglu 2005a, 2005b). The performance of large-scale normal and high-strength concrete columns, confined with FRP casings, showed superior inelastic deformability when subjected to simulated seismic loading, developing up to 12% lateral drift. FRP pre-formed shapes offer multiple advantages of; i) light and effective formwork with superior handling characteristics, ii) efficient and durable transverse confinement reinforcement with ability to generate high lateral confinement pressures, and iii) protective shell against corrosion, weathering and chemical attacks.

It has long been established that circular spirals are more effective in confining concrete than rectilinear ties. Similarly, it has been reported that the effectiveness of FRP jackets was higher in

circular columns than square columns (Mirmiran et al. 1998; Rochette and Labossiere 2000; Pessiki et al. 2001; Elnabelsy and Saatcioglu 2004). This may be explained by hoop tension generated in circular columns, resulting in uniform passive confinement pressure. Square jackets, on the other hand, develop high confining pressures at the corners due to high transverse forces generated in transverse FRP elements, which diminish quickly between the edges where the restraint is limited to the flexural rigidity of FRP jacket, which is very low. Increased corner radius *(R)* promotes hoop tension near the corners, thereby improving the effectiveness of confinement. Furthermore, the cross-sectional size *(D)* influences the flexural rigidity of FRP casing between the corners, affecting confinement efficiency. These two parameters can be expressed in the form of R/D ratio, which is considered as an important design variable in this research program. Furthermore, the effectiveness of square sections may be increased by the use of FRP crossties (Ozbakkaloglu and Saatcioglu, 2005b). A new design approach was developed for displacement based design of FRP stay-in-place formwork, with due considerations given to all relevant parameters, including those that affect confinement efficiency. The approach developed is also applicable to FRP jacketed existing concrete columns. This thesis presents the details of the procedure, which include an analytical expression that can predict lateral drift capacities of FRP confined square and circular columns.

6.2 RESEARCH SIGNIFICANCE

Reinforced concrete columns are responsible for overall strength and stability of the entire structure. Deformability of these columns is an essential requirement for earthquake resistant construction. This is especially true for high-strength concrete columns since concrete strength is inversely proportional to inelastic column deformability. The research project reported in the

thesis includes the development of a displacement based design approach for normal and high-strength concrete columns encased in FRP stay-in-place formwork, which is a new technique suggested to improve column deformability. Unlike the current building code approach, the lateral drift capacity is used as a design parameter in the proposed approach for improved response of reinforced concrete columns during strong earthquakes. As such, the research work presented has significant practical implications.

6.3 PROPOSED DESIGN APPROACH

A displacement based design approach was developed for column confinement, incorporating the relationship between confinement parameters and column drift capacity, while also considering a wide range of concrete strength and axial load level. The parameters of confinement that pertain to FRP casings included; i) the amount of fibres, ii) fibre strength and modulus, and iii) cross-sectional shape. In addition, corner radius and internal FRP crossties were considered as confinement parameters for square columns. The significance of these parameters was assessed on the basis of experimental data and test observations (Seible et al. 1996; Mirmiran et al. 1999, 2000; Fam and Rizkalla 2002, Fam et al. 2003, 2005; Iacobucci et al. 2003; Zhu 2004; Shao and Mirmiran 2005). Column tests conducted by the author (Ozbakkaloglu and Saatcioglu 2005a, 2005b) provide invaluable information to quantify the effects of design parameters, while also explaining the mechanism of concrete confinement.

6.3.1 Mechanism of Confinement with FRP Casings

FRP encased circular columns generate hoop tension resulting in uniform confinement pressure (f_l) in the FRP casing, when subjected to concentric compression. This uniform passive pressure can be computed as illustrated in Fig. 6.1(a) and Eq. (1), where (E_f) is the elastic modulus, (t) is

the of thickness of fibre material; and (ε_{fc}) is the maximum transverse strain associated with confinement;

$$f_l = \frac{2E_f \cdot \varepsilon_{fc} \cdot t}{D} \tag{1}$$

The contribution of epoxy resin to FRP strength is negligibly small. Therefore, the properties of the confining material are characterized in terms of those of the fibre material, rather than the FRP composite material. This approach eliminates potential inaccuracies that may be introduced due to the uneven use of epoxy and resulting variations in casing thickness.

The lateral pressure increases gradually as longitudinal compressive stresses on concrete increases. The rate of increase in lateral confinement pressure is directly related to the transverse strains in the enclosed column. Lateral expansion of concrete within the elastic range of material occurs at a slower rate than that for post elastic behaviour of concrete. The Poisson's ratio of unconfined concrete may be used to characterize the relationship between longitudinal and transverse strains within this initial range of loading. As longitudinal stresses reach the compressive strength of unconfined concrete, the rate of increase in transverse strains becomes faster, making the confinement mechanism more pronounced. The mechanism of confinement in FRP casings and/or FRP jackets is maintained at very high transverse strains, because the damaged concrete is fully contained in the enclosing FRP casing. The built-up of confinement pressure continues until the eventual failure of FRP takes place at the hoop tensile strength of material. In conventional steel reinforced concrete columns, the discrete nature of hoops and ties limit the lateral expansion and ability of high-strength transverse reinforcement to attain very high values, unless the efficiency of confinement reinforcement is very high, as in the case of closely spaced hoops or spirals (Saatcioglu and Razvi 2002). Moreover, unlike the conventional

steel reinforcement, FRP casings cover the entire column concrete, thereby preventing the spalling of damaged concrete, resulting in a significant increase in hoop strains.

Unlike circular sections, square sections are not subjected to uniform confinement pressure associated with hoop tension. Therefore, the determination of confining pressure exerted by a square casing is more complex. Square casings/jackets develop high confining pressures near the corners where high lateral restraint is provided by transverse FRP fibres, which diminish quickly and becomes very low between the edges where the restraint is limited to the flexural rigidity of FRP casing/jacket. Increased corner radius *(R)* promotes hoop tension near the corners, thereby improving the effectiveness of confinement. Furthermore, the cross-sectional size *(D)* influences the flexural rigidity of FRP casing between the corners, affecting confinement efficiency. These two parameters can be expressed in the form of R/D ratio, which is considered an important parameter of confinement. Furthermore, the effectiveness of square sections may be increased by the use of FRP crossties (Ozbakkaloglu and Saatcioglu 2005b). Different distributions of confinement pressures in FRP encased square sections, with different confinement arrangements, are illustrated in Fig. 6.1(b) to Fig. 6.1(e). The figure clearly shows that the uniformity of confinement pressure can be significantly improved by rounding the column corners and providing internal FRP crossties. The efficiency of FRP casing/jacket as confinement material improves with the uniformity of lateral pressure, with circular casings providing the best confinement arrangement for strength and ductility enhancements. Therefore, it is important to quantify the lateral confinement pressure in devising a design methodology. This was done in the following sections on the basis of experimental research.

6.3.2 Experimental Research

Circular and square columns, with concrete strengths ranging between 50 MPa (7250 psi) and 90 MPa (13000 psi), were cast in carbon FRP casings and tested under a constant axial compression and incrementally increasing lateral deformation reversals. The details of the test program and recorded data are presented elsewhere (Ozbakkaloglu and Saatcioglu 2005a, 2005b). The specimens represented part of a first-story building column between the footing and point of inflection. They had a 270 mm (10.5 in.) cross-section and a 2.0 m (6.6 ft) shear span. Table 6.1 provides a summary of geometric and material properties. Cross-sectional details and reinforcement arrangements are presented in Fig. 6.2 and the material properties of reinforcing steel are provided in Table 6.2. A carbon fibre composite system was used to manufacture the stay-in-place formwork manually in the Structures Laboratory of the University of Ottawa. The same FRP composite material was used for all casings, with fibres aligned in the circumferential/transverse direction. The thickness of the carbon fibre sheet was 0.165 mm/ply (0.007 in./ply), which was increased to 0.8 mm/ply (0.03 in./ply) when impregnated with epoxy resin. The stress-strain relationship of the composite material was established by coupon tests and showed linear-elastic behaviour up to the rupturing strength in tension. The capacity of the composite material was established to be approximately 785 MPa (115 ksi) based on a fibre content corresponding to 0.8 mm/ply (0.03 in./ply). This observation was found to be in agreement with the 3800 MPa (550 ksi) fibre strength reported by the manufacturer. Table 6.3 provides the properties of carbon fibres as supplied by the manufacturer. The ultimate rupture strain (ε_{fu}) of 1.67% specified by the manufacturer was also in agreement with the average ultimate strain obtained from coupon tests. The above values translate into the elastic modulus of

47,000 MPa (6800 ksi) for the composite material, which is in line with 227,000 MPa (33000 ksi) reported for the modulus of elasticity of carbon fibres alone.

The casings of circular columns had two plies of carbon FRP sheets, except for column RC-1, which had four plies. Square columns had two (RS-5), three (RS-4 and RS-6), or five plies (RS-1, RS-2, and RS-3) of FRP in their casings. Column corners of square casings were rounded with a corner radius of 45 mm (1.8 in.) , resulting in an R/D ratio of 1/6, except for column RS-6, which had a corner radius of 8 mm (0.3 in.), yielding an R/D ratio of 1/34. Three of the columns had FRP casings with internal FRP crossties, spaced at 68 mm (2.7 in.), corresponding to 1/4 of the column dimension. One of the columns had 12 longitudinal bars and two crossties in each cross-sectional direction (RS-3). The other two columns had 8 longitudinal bars and one internal crosstie in each cross-sectional direction (RS-2 and RS-5). FRP casings were used without crossties for the remaining square columns (RS-1, RS-4, and RS-6). Two different fibre contents were used in the FRP crossties, as governed by the width of fibre sheets cut and rolled to form the crossties. The crossties of Columns RS-2 and RS-3 were formed from a 40 mm (1.6 in.) wide FRP strip, while the strip width used to form the crossties of Column RS-5 was 135 mm (5.3 in.). The total fibre area of column RS-5, comprised of a two-ply casing and crossties, was equal to the fibre area used in the three-ply casings of RS-4 and RS-6 without the crossties.

6.3.3 Recorded Test Data

Unlike structural steel, fibre composites exhibit linear stress/strain behaviour up to failure. Therefore, the design transverse strain plays a crucial role on the accuracy of confinement calculations. While the confinement pressure can be assumed to be uniform for circular columns

subjected to concentric compression, this may change under eccentric loading due to the strain gradient, resulting in maximum and minimum pressures in extreme compression and tension regions, respectively. The ultimate hoop strain (ε_{fm}) was measured in column tests to be approximately 1.5% at fibre rupturing. This value reduced by about 20% between the extreme compression region and the section centroid, which coincided approximately with the neutral axis for the columns tested. Fig. 6.3(a) illustrates the recorded strain profile for a typical circular column tested.

The transverse strain profiles on square casings are shown in Fig. 6.3(b) and Fig. 6.3(c). The ultimate hoop strain (ε_{fm}) in these columns was always recorded at or near the middle of the compression face to be approximately 1.2% and 0.9% for columns with well-rounded and small-radius corners, respectively. The strains decreased towards the corners. As concrete was damaged inside the casing, at high levels of axial strain, it showed a tendency to expand into a circular shape. This was particularly pronounced in the column with small-radius corners, developing high tensile strains in the middle of the compression face, showing a parabolic reduction towards the corners, attaining negative (compressive) strain values at the corners. The maximum strain along side-faces was approximately 90% of ε_{fm}, as indicated in Fig. 6.3(b). In columns with well-rounded corners, the strain profile showed a parabolic variation along the four faces, as indicated in Fig. 6.3(c). The ultimate hoop strain (ε_{fm}), measured in the middle region of compression faces reduced to 70% towards the corners, and to 80% in the middle of side faces.

The strain profile in FRP crossties, parallel to loading, was obtained experimentally as illustrated in Fig. 6.4. The maximum strain recorded was approximately equal to 1.0%, and was measured

near the ends, where the crossties were secured to the casing through bending and epoxy gluing the end fibres. The minimum strains were measured near the central region of crossties with an approximate value of 0.6%.

6.3.4 Design Parameters

6.3.4.1 Ultimate Confinement Strain

The effectiveness of FRP stay-in-place formwork is directly dependent on the level of tensile stress developed in the material prior to significant concrete strength decay. In a linearly elastic FRP material, this information can be obtained from transverse strains. Figures 6.3 and 6.4 illustrate experimentally observed strain profiles, which can be used in the computation of maximum effective FRP forces and resulting confinement pressures. An average transverse strain along column side faces can be used to compute the FRP forces shown in Fig. 6.5 to establish the confinement pressure within the compression zone of concrete. In circular columns, where a variation of 20% was observed between the recorded hoop strains at the end and the side faces, the use of an average value of $0.9\varepsilon_{fm}$ may be in order, as illustrated in Fig. 6.5(a).

In square columns, the average strain along side faces can be computed from Fig. 6.3(b) and (c), depending on the corner radius. The integration of the parabolic strain profiles shown in the same figure yields an average value of $0.75\varepsilon_{fm}$ for columns with well-rounded corners and $0.6\varepsilon_{fm}$ for columns with small radius corners as illustrated in Fig 6.5(b) and (e). Similarly an average value of 0.70% strain may be used for the crossties, as shown in Fig. 6.4.

When failure of FRP-confined concrete is caused by the rupturing of FRP casing, the ultimate condition of the confined concrete is closely related to the ultimate hoop strain of the FRP casing

(ε_{fm}). Experimental results indicate that the hoop strain in the jacket can be considerably smaller than that obtained by a flat coupon test (ε_{fu}), which is referred to hereafter as the material ultimate tensile strain (Shahawy et al. 2000; Xiao and Wu 2000; Pessiki et al. 2001). The ratio of these strains was defined as a confinement parameter by Pessiki et al. (2001). The same ratio was used in the current investigation to represent the in-place strain limit of FRP as; $\varepsilon_{fm} = k_\varepsilon \varepsilon_{fu}$. Lam and Teng (2003) reported an average value of $k_\varepsilon = 0.586$ for carbon FRP circular jackets on the basis of a large experimental database. The specimens considered were tested under concentric loading and k_ε was calculated using the average values of FRP hoop strains. However, hoop strain profile attained under reversed cyclic loading is different than that under concentric compression. Therefore, in the current investigation, the maximum recorded values of FRP hoop strains were used. Accordingly, k_ε was found to be approximately 0.9 for circular columns. The recorded maximum transverse strains in square columns were lower than those recorded on similar size circular columns. This is attributed to reduced uniformity of strain distributions in square columns and the existence of stress concentrations at the corners. The recorded transverse strains on columns with small corner radius were significantly lower than those recorded on columns with well-rounded corners, indicating the importance of corner radius on transverse strains. The in-place-strain factor (k_ε) for square casings with well-rounded corners having 45 mm (1.8 in.) radius was found to be 0.72, which reduced to 0.54 when the corner radius was decreased to 8 mm. These corner radii reflect the limits that may be used in practice.

The transverse strain data indicated that columns with higher number of FRP plies developed higher transverse strains than those with lower number of plies, for otherwise identical columns. In fact, the ultimate strains recorded in square columns with five FRP plies were comparable to

those recorded in circular columns, whereas square columns with two or three FRP plies developed only about 75% of that recorded in circular columns. Further research is needed to establish the relationship between the amount and ultimate strain of FRP when used to form a column jacket. The in-place-strain factor (k_ε) used in the current investigation, for square columns with well rounded corners, was adopted conservatively from columns with low FRP content.

6.3.4.2 Contribution of Shear Strains

Concrete columns are often subjected to shear stresses along with flexure. The contribution of shear to flexure dominant columns is very small, without any substantial influence on flexural strength calculations. Transverse strains associated with the mechanism of concrete confinement may be affected by transverse strains caused by accompanying shear stresses. The contribution of shear to total transverse strain is a function of column loading, as well as column geometry. The columns tested by the author (Ozbakkaloglu and Saatcioglu 2005a, 2005b), also listed in Table 6.1, indicated that approximately 10% of total transverse strains could be attributed to shear. Therefore, the maximum transverse strain associated with confinement (ε_{fc}), is computed by deducting the effect of shear from recorded ultimate hoop strain (ε_{fm}).

6.3.4.3 Confinement Efficiency Parameter

The distribution of confinement pressure is a function of section geometry and confinement arrangement. Figure 6.5 illustrates different distributions of confinement pressures along the compression side of columns with different geometry and confinement arrangement. Hoop tension generated in circular columns that are subjected to concentric compression result in

uniform passive confinement pressure. Square casings, on the other hand, develop high confining pressures at the corners due to the high restraint provided by the side faces of FRP casings against lateral expansion. The restraining action diminishes quickly with distance from the corners along the column face where the mechanism of lateral restraint changes from that caused by the axial rigidity of FRP in the sides to that provided by the flexural rigidity of FRP casing between the corners. While the uniform confinement pressure for circular columns can easily be computed from hoop tension, the computation of non-uniform stress profiles in square sections becomes a challenging task. Figure 6.6 illustrates the distribution of passive confinement pressure in a square column. An average uniform pressure can be calculated by dividing the summation of forces developed in each face of the casing parallel to loading by the unit area of concrete crossed by these FRP forces, bound by column cross-sectional dimension and unit column height. The use of this average pressure as uniform confinement pressure overestimates confinement, as reported by Saatcioglu and Razvi (1992) since a significant portion of compression concrete between the corners is subjected to a lower lateral pressure than the computed average value. Therefore, an equivalent uniform pressure, with the same effect as that of the actual non-uniform pressure needs to be defined. Figure 6.6 illustrates the actual, average, and equivalent lateral pressures for a square column. The equivalent uniform pressure (f_{le}) can be established by reducing the average pressure (f_l) through a coefficient which reflects variations in the geometry of confinement reinforcement and corresponding lateral pressure. Coefficient (β), characterizing the distribution of confinement pressure, is introduced for this purpose and used as follows.

$$f_{le} = \beta . f_l \tag{2}$$

Coefficient (β) has a maximum value of unity for circular columns, where uniform pressure is generated by hoop tension, and a lower value for square and rectangular columns where the pressure becomes non-uniform. It can be quantified for different confinement arrangements having different geometry by evaluating the experimental data. Drift capacities recorded experimentally were used to generate sectional characteristics of columns from which equivalent lateral pressures were computed by relating the enhancement in concrete compressive strain to lateral confining pressure. The uniform confinement pressure at ultimate (at fibre rupture) was assumed to be directly proportional to the maximum concrete compressive strain developed in the column critical section (ε_{cu}). The critical section properties, including sectional curvatures and ultimate compressive strains were computed from lateral drifts for experimentally observed plastic hinge lengths. These values were then used to relate confinement pressures of different sections, allowing the computation of corresponding (β) coefficients.

The distribution of confinement pressure also affects the level of strains that can be developed in the transverse FRP reinforcement, influencing confinement efficiency. Furthermore, the type of loading, concentric versus eccentric, also affects the efficiency of confinement, as previously discussed. These effects were introduced through coefficient (c_{avg}), which is the ratio of average transverse FRP strain on side faces to the experimentally measured maximum FRP strain in columns. Therefore, the (β) coefficient was multiplied by (c_{avg}) to define the "confinement efficiency parameter," (k_e).

$$k_e = c_{avg}\,\beta \tag{3}$$

The coefficient (c_{avg}) was assessed to be 0.9 for circular columns, 0.75 for well rounded square columns and 0.6 for square columns with sharp corners. The regression analysis of test data

indicated that Eq. 4 can be used to define (k_e) for square columns, in terms of column cross sectional dimension along the compression side (D) and (s_l) where, s_l is the unsupported length of FRP casing on column compression face between the perimeter ends and/or cross-ties (if any) in the column cross-sectional plane. This is illustrated in Fig. 6.5.

$$k_e = 0.25\,(3.2 - \frac{\sum s_l^2}{D^2} - \frac{\sqrt{\sum s_l^2}}{D}) \tag{4}$$

The confinement efficiency coefficient (k_e) is equal to 0.9 for circular columns, because of the strain gradient under bending and resulting variation in transverse strain (effect of c_{avg}), as indicated in Fig. 6.3(a).

The change in (k_e) with different arrangements of confinement reinforcement is illustrated in Table 6.1. The computed values of (k_e) for square columns range from 0.34 for a column with small-radius corners (RS-6) to 0.67 for a column with well-rounded corners and two FRP crossties in each direction (RS-3). Table 6.1 clearly indicates that (k_e) can be significantly increased by increasing corner rounding and/or providing additional lateral restraints though the use of FRP crossties. Furthermore, the distribution factors (β) tabulated in the same table indicate the effectiveness of FRP crossties in increasing the uniformity of confinement pressure.

6.3.4.4 FRP Crossties

FRP crossties have a pronounced effect on confinement efficiency, as described earlier. The area of a crosstie can be computed to be equivalent to the total area of carbon fibres, since neither the epoxy nor the internal phenolic bars used for the purpose of manufacturing have any appreciable strength to contribute.

An important distinction between the lateral restraint provided by continuous FRP casing and that provided by a discrete crosstie is the distribution of confinement pressure along the column height and resulting effect on confinement efficiency. The comparison of two columns having the same total transverse fibre area, one with the other without FRP crossties revealed that the discrete nature of crossties, placed at a spacing of ¼ the cross-sectional dimension was about 75%. Therefore, in computing total confinement pressure due to the casing and crossties, the efficiency of crossties was reduced to 75% of equivalent FRP had they been provided in the casing, while recognizing their beneficial effects on improving the uniformity of confinement pressure in the cross-sectional plane. This is introduced by reducing FRP tie forces by 25%, as illustrated in Fig. 6.5.

6.3.4.5 Plastic Hinging and Plastic Hinge Length

Figure 6.7 (a) and (b) illustrate plastic hinges in circular and square columns at end of testing. The figure indicates differences in plastic hinge characteristics of circular and square columns. Transverse strain distribution along the column height was used to determine the plastic hinging of columns. Typical strain profiles for circular and square columns are presented in Fig. 6.8(a) and Fig. 6.8(b), respectively. The idealization of plastic hinges for the computation of sectional properties is illustrated in Fig. 6.9 for square and circular columns. The rotations recorded within the plastic hinge region were used to verify the plastic hinge length. Figure 6.9 shows that the extent of plastification in circular columns was more than that for square columns due to the higher confinement efficiency attained by circular geometry. Accordingly, the plastic hinge length of a circular column was found to be 1.5 times the sectional dimension, whereas for square columns it was found to be approximately equal to the sectional dimension, as reported

earlier for columns confined by conventional steel reinforcement (Sheikh and Khoury 1993, Sheikh et al. 1994, Razvi and Saatcioglu 1999). These hinging lengths were idealized for axial load levels lower than the balanced section load. The circular column tested with an axial load higher than the balanced section load (RC-3) was observed to develop a more localized plastic hinging, similar to that observed in square columns, with slightly more progressed hinging.

The ultimate curvature (ϕ_u) of the plastic hinge, indicated in Fig. 6.9, was computed from the corresponding ultimate column top displacement recorded experimentally. The moment of the area under curvature distribution was set equal to recorded column displacement to solve for the ultimate curvature. The computed ultimate curvatures for different columns were then verified against average curvatures recorded experimentally by means of displacement transducers placed vertically within the plastic hinge region. Ultimate curvatures were then used to compute ultimate axial strains in concrete (ε_{cu}), as indicated in Eq. 5, which were subsequently related to lateral confinement pressure for the computation of k_e.

$$\varepsilon_{cu} = \phi_u \cdot c \tag{5}$$

It has been previously established that the increase in ultimate compressive strain of confined concrete is directly proportional to uniform confinement pressure (Mander et al. 1988, Saatcioglu and Razvi 1992, Saafi et al. 1999, Chaallal et al. 2003, Lam and Teng 2003). The ultimate strain values computed by Eq. 5 for columns with different confinement efficiencies, as dictated by different geometry and reinforcement arrangement, were related to equivalent uniform confinement pressures. Each arrangement produces a different distribution of confinement pressure, as illustrated in Fig. 6.5. A relationship was established between the computed uniform pressures and the reinforcement arrangements for which they were computed. This relationship helped quantify confinement efficiency parameter k_e, as specified in Eq. 4.

The spread of plastification observed experimentally has been quantified by factor (k_p). The nature of plastification affects plastic deformations in columns, which plays an important role on overall column drift capacity. Two aspects of plastic hinge becomes important; i) plastic hinge length and ii) the magnitude of ultimate curvature within the idealized plastic hinge region. The latter is controlled by the amount of confinement, which affects the maximum compressive longitudinal strain within the hinge and the corresponding ultimate curvature. The curvature and the ultimate strain is related through the neutral axis depth *(c)*, as indicated in Eq. 5, which changes with sectional geometry. It has been observed that the effect of *(c)* on curvature (and hence the characteristics of plastic hinge) is such that for the same ultimate compressive strain, circular columns have approximately 10% higher *(c)* to maintain sectional equilibrium. This factor has been accounted for in defining the level of plastification in columns, which is introduced through the plastic hinge factor (k_p). This factor was quantified relative to square columns, which exhibit plastic hinge characteristics similar to those observed in conventionally reinforced columns. Therefore, k_p = 1.0 for square columns and can be taken as k_p = 1.5*0.9 = 1.35 for circular columns, where 1.5 accounts for experimentally observed progression of hinging length relative to square columns, and 0.9 accounts for the approximate difference in neutral axis depth *(c)*. The same coefficient can be conservatively taken as 1.0 for circular columns subjected to high axial compression, typically the levels above balanced point, to reflect more localized hinging observed experimentally in such columns.

6.3.4.6 Lower Limit for Effective Confinement

FRP confinement is dependent on the transverse expansion of concrete, becoming more pronounced beyond transverse strain corresponding to unconfined concrete strength. The ability of FRP to control concrete crushing depends on a number of parameters as discussed previously. However, there exists a limit, below which the strength decay in concrete becomes significant prior to full utilization of the FRP casing. In this low range of confinement the flexural resistance of a column can drop well below 80% of its moment capacity as FRP continues maintaining its integrity without reaching its material limit. This level of minimum confinement is taken as the lower limit for the effectiveness of FRP confinement. Column RS-6, with small-radius corners, experienced a 20% strength decay in moment capacity shortly after developing 2% lateral drift ratio while the FRP material remained well below its rupturing strength. The rupturing of FRP occurred when the column reached 4% lateral drift ratio, after experiencing significant strength decay. It was clear that the amount of lateral pressure generated by the FRP casing was not sufficient to maintain the flexural capacity of column beyond the 2% lateral drift level. In contrast, all other columns, with sufficiently high confinement effectiveness maintained their flexural resistances until after the FRP rupturing was recorded.

A similar limiting condition was also observed by Mirmiran et al. (1998), who defined "modified confinement ratio (*MCR*)" as indicated in Eq. 6, with a limiting value of 15%, below which no strength enhancement was observed in confined concrete and the stress strain relationship exhibited a descending branch beyond the peak concrete stress. This limit was developed based on column tests conducted under concentric loading.

$$MCR = \left(\frac{2R}{D}\right) \cdot \frac{f_l}{f'_{co}} \tag{6}$$

(f'_{co}) in Eq. 6 is the in-place strength of unconfined concrete. This value can be estimated by reducing concrete cylinder strength (f'_c) through coefficient (k_3). Coefficient (k_3) was reported to be approximately equal to 0.9 for normal-strength and high-strength concrete columns (Ozbakkaloglu and Saatcioglu 2004). The average lateral pressure (f_l) in Eq. 6 is obtained by distributing confinement forces over unit column height. The same ratio is adopted in the current research project, with (f_l) replaced by ($k_e.f_l$). However, the limit for this ratio is assessed to be 1.0 % on the basis of test data (Mirmiran et al. 1998; Rochette and Labossiere 2000; Iacobucci et al. 2003; Ozbakkaloglu and Saatcioglu 2005a, 2005b), below which the FRP reinforcement is not expected to develop its rupturing strength prior to significant loss in compression strength of concrete. All the columns tested by the author (Ozbakkaloglu and Saatcioglu 2005a, 2005b), with the exception of RS-6, met this requirement and utilized the full capacity of FRP material by maintaining their strengths until the rupturing of FRP. Column RS-6, with small-radius corners and an MCR of 0.2%, experienced 20% strength decay in moment capacity when the maximum recorded strain in FRP was approximately at 50% of the ultimate hoop strain (ε_{fm}). This implies that the effectiveness of the FRP casing in this column was 50% and that the FRP strain to be used in drift computations should be taken as 50% of the ultimate hoop strain.

6.4 DESIGN EXPRESSION

It is well established that the inelastic deformation capacity of columns are directly proportional to the amount and the effectiveness of confinement (ACI 318-05, CSA A23.3-04, Saatcioglu and Razvi 2002). The design expression for FRP confined columns in CSA S806 (2002) was adopted from a displacement based design approach (Saatcioglu and Razvi 2002) with lateral drift as a

design parameter. This expression was verified against bridge columns tested under low levels of axial compression and was found to be conservative for building columns tested under increased axial compression (Ozbakkaloglu and Saatcioglu, 2005a, 2005b). The failure mode in lightly loaded columns was the rupturing of tension reinforcement in flexure, as opposed to the rupturing of FRP casings in heavily loaded columns. Therefore, the CSA S806-02 expression is modified as shown below, on the basis of test observations.

$$\delta = 1 + \left[\frac{E_f \cdot \varepsilon_{fc} (2t + 0.5 \frac{A_f}{s})}{4D \cdot f'_c} \cdot \frac{k_e \cdot k_p}{P/P_o} \right] \times 100 \tag{7}$$

where (δ) is the lateral drift capacity of column in percent, (P/P_o) is the axial load level, (A_f) is total cross-sectional area of fibres in FRP crossties in each direction, and (s) is the spacing of crossties along the height of column. (E_f) is the elastic modulus of fibres used in casings and/or crossties, and (t) is the total fibre thickness in casing per side. The expression accounts for the effect of axial compression, confinement efficiency of FRP casing, the extent of plastification in FRP confined columns, material strengths as well as the R/D ratio. It is applicable to circular and square building columns with sufficiently high axial compression to preclude rupturing of tension reinforcement as the failure mode, allowing full utilization of FRP. However, the expression may overestimate drift capacities of bridge columns under lower levels of axial compression, which typically ranges between 10 to 15% of column concentric capacity. In these columns the failure occurs because of the rupturing of extreme tension bars in flexure prior to full mobilization of FRP strength. A conservative value for the maximum level of transverse tensile strain in such columns can be taken as $\varepsilon_{fc} = 0.004$, as suggested in the past (Buckle and Friedland 1994, ACI 440 2002, and CSA S806 2002). The drift capacity computed by Eq. 7

corresponds to a post-peak displacement at 20% decay in moment resistance. Hence, it does not account for further degradation in column capacity associated with P-Δ effects.

6.4.1 Verification of the proposed expression against test columns

Results of column tests conducted by the author (Ozbakkaloglu Saatcioglu 2005a, 2005b) were used to verify the proposed expression for column drift capacity. The comparisons between analytical and experimental lateral drift capacities are presented in Table 6.1 and Fig. 6.10 for all the columns tested. The results indicate very good correlation between the analytical and experimental values. The testing of Column RS-2 was terminated at 9% lateral drift ratio, prior to failure. The strain data indicated that the column had the potential to sustain deformation reversals up to about 10% drift, which is inline with the calculated drift capacity of 9.7%. Column RS-3 was subjected to asymmetric loading beyond 10% lateral drift ratio. This was because the actuator stroke capacity was exceeded in one direction and the column was subjected to single cycles of further loading only in one direction, up to 12% drift ratio at which level the failure occurred. This can be observed in Fig. 6.10. Similarly, Column RC-1 was subjected to 11% drift ratio in one direction and 12% drift ratio in the other direction due to the actuator stroke capacity. The analytical drift capacity for this column was computed using the recorded strain at maximum drift ratio. Furthermore, because the plastic hinge could not be developed fully, the plastic hinge factor (k_p) was taken as 1.20, based on the experimentally measured plastic hinge length. Figure 6.10 indicates that Eq. 7 can be used in estimating lateral drift capacities of FRP encased concrete columns.

6.5 SUMMARY AND CONCLUSIONS

The mechanism of concrete confinement in FRP encased concrete columns was modeled on the basis of column tests conducted under constant axial compression and lateral deformation reversals. The variation of confinement pressure with FRP casings of different geometry and configuration was investigated and quantified using the parameters of confinement. Coefficients were developed for confinement efficiency and progression of plastification within the inelastic range of deformations. Experimentally observed strain limits and material properties were selected along with empirically derived coefficients to formulate an expression to predict inelastic drift capacities of normal-strength and high-strength concrete columns confined by FRP casings. The comparison of experimentally recorded and analytically computed drift capacities show good correlations, suggesting that the proposed expression may be used for the design of concrete columns confined with FRP stay-in-place formwork.

6.6 NOTATION

A_f = total cross-sectional area of fibres in FRP crossties in each direction

c = depth of neutral axis, measured from extreme compression fibre

c_{avg} = ratio of average transverse FRP strain on column side faces to ultimate hoop strain

D = column cross-sectional dimension

E_f = modulus of elasticity of fibre material

E_s = modulus of elasticity of steel

f'_c = concrete cylinder strength

f'_{co} = in-place strength of unconfined concrete

f_l = average confinement pressure

f_{le} = equivalent uniform confinement pressure

f_u, f_y = ultimate and yield strength of steel

k_3 = coefficient that relates in-place and cylinder strengths of concrete

k_e = confinement efficiency parameter

k_p = plastic hinge factor

k_ε = in-place strain factor

MCR = modified confinement ratio

P = axial load applied to column sections

P_o = unconfined theoretical concentric capacity of column

R = column corner radius

s = spacing of FRP crossties along column height

s_l = unsupported length of FRP casing on column compression face between the perimeter ends and/or cross-ties (if any) in the column cross-sectional plane

t = thickness of fibre material

β = coefficient characterizing the distribution of confinement pressure

Δ = lateral deflection

δ = lateral drift capacity of column

ε_{avg} = average strain in FRP crossties at column critical section

ε_{cu} = ultimate axial strain in concrete

ε_{fc} = maximum transverse strain associated with confinement

ε_{fm} = ultimate hoop strain

ε_{fu} = ultimate rupture strain of fibre material

ε_r, ε_{sh}, ε_u, ε_y = strains in steel; at rupture, onset of strain hardening, ultimate, and yield

ϕ_u, ϕ_y = ultimate and yield curvatures

6.7 REFERENCES

American Concrete Institute (ACI) Committee 318. (2005). "Building Code Requirements for Structural Concrete (ACI 318-05) and Commentary (318R-05)." Farmington Hills, Mich., 430 pp.

American Concrete Institute (ACI) Committee 440. (2002). "Design and Construction of Externally Bonded FRP Systems for Strengthening Concrete Structures (440.2R-02)." Detroit, 45 pp.

Buckle, I. G., and Friedland, I. M. (1994). "Seismic Retrofitting Manual for Highway Bridges." Report No. FHWA-94-052, U.S. Department of Transportation.

Canadian Standards Association (CSA) Committee A23.3. (2004). "Design of concrete structures (A23.3-04)." Rexdale, Ontario, 240 pp.

Canadian Standards Association (CSA) Committee S806. (2002). "Design and construction of building components with fibre-reinforced polymers (S806-02)." Rexdale, Ontario, 177 pp.

Chaallal, O., Hassan, M., and Shahawy, M. (2003). "Confinement model for axially loaded short rectangular columns strengthened with fibre reinforced polymer wrapping." *ACI Struct. J.*, 100(2), 215–221.

Elnabelsy, G. and Saatcioglu, M. (2004). "Seismic Retrofit of Circular and Square Columns with CFRP Jackets," Proceedings of the Fourth International Conference on Advanced Composite Materials in Bridges and Structures (ACMBS-4), Calgary, Canada.

Fam, A., Flisak, B. and Rizkalla, S. (2003). "Experimental and Analytical Modeling of Concrete-Filled FRP Tubes Subjected to Combined Bending and Axial Loads." ACI Structural Journal, Vol. 100, No. 4, pp. 499-509.

Fam, A., Schnerch, D. and Rizkalla, S. (2005). "Rectangular Filament-Wound GFRP Tubes Filled with Concrete under Flexural and Axial Loading: Experimental Investigation." Journal of Composites for Construction, Vol. 9, No. 1, pp. 25-33.

Fam, A. and Rizkalla, S. (2002). "Flexural Behaviour of Concrete-Filled Fibre Reinforced Polymer Circular Tubes." Journal of Composites for Construction, Vol. 6, No. 2, pp. 123-132.

Iacobucci, R. D., Sheikh, S. A., and Bayrak, O. (2003). "Retrofit of Square Concrete Columns with Carbon Fibre-Reinforced Polymer for Seismic Resistance." ACI Structural Journal, V. 100, No. 6, pp. 785-794.

Lam, L., and Teng, J. G. (2003). "Design-oriented stress-strain model for FRP-confined concrete." *Constr. Build. Mater.*, 17(6&7), 471–489.

Mander, J. B., Priestley, M. J. N., and Park, R. (1988). "Theoretical stress-strain model for confined concrete" *J. Struct. Eng.*, 114(8), pp.1804–1826.

Mirmiran, A., Shahawy, M., El Khoury, C., and Naguib, W. (2000). "Large Beam-Column Tests on Concrete-Filled Composite Tubes." *ACI Structural Journal*, ACI, 97(2), 268-276.

Mirmiran, A., Shahawy, M., and Samaan, M. (1999). "Strength and Ductility of Hybrid FRP-Concrete Beam-Columns." *Journal of Structural Engineering*, ASCE, 125(10), 1085-1093.

Mirmiran, A., Shahawy, M., Samaan, M., El Echary, H., Mastrapa, J.C., and Pico, O. (1998). "Effect of Column Parameters on FRP-confined Concrete." Journal of Composites for Construction, ASCE, V.2, No. 4, pp.175-185.

Ozbakkaloglu, T., and Saatcioglu., M. (2004). "Rectangular Stress Block for High-Strength Concrete." ACI Structural Journal, V. 101, No. 4, pp. 475-483

Ozbakkaloglu, T., and Saatcioglu, M. (2005a). "Seismic performance of circular high-strength concrete columns in stay-in-place FRP formwork." Submitted to Journal of Composites for Construction, ASCE.

Ozbakkaloglu, T., and Saatcioglu, M. (2005b). "Seismic performance of square high-strength concrete columns in stay-in-place FRP formwork." Accepted for publication in Journal of Structural Engineering, ASCE.

Pessiki, S., Harries, K.A., Kestner, J.T., Sause R., and Ricles, J.M. (2001). "Axial Behaviour of Reinforced Concrete Columns Confined with FRP Jackets." Journal of Composites for Construction, ASCE, V. 5, No. 4, pp. 237-245.

Razvi, S. R., and Saatcioglu, M. (1999). "Analysis and Design of Concrete Columns for Confinement," *Earthquake Spectra*, V. 15, No. 4, pp. 791-811.

Rochette, P., and Labossiere, P. (2000). "Axial Testing of Rectangular Column Models Confined with Composites." Journal of Composites for Construction, ASCE, V. 4, No. 3, pp. 129-136.

Saafi, M., Toutanji H.A., Li, Z. (1999). "Behaviour of Concrete Columns Confined with Fibre Reinforced Polymer Tubes." ACI Structural Journal, V. 96, No. 4, pp. 500-509.

Saatcioglu, M. and Razvi, S. R. (2002) "Displacement Based Design of Reinforced Concrete Columns for Confinement." ACI Structural Journal, ACI, Vol. 90, No.1, pp.3-11

Saatcioglu, M., and Razvi, S. R. (1992). "Strength and Ductility of Confined Concrete." Journal of Structural Engineering, ASCE, V. 118, No. 6, pp. 1590-1607.

Seible, F., Burgueño, R., Abdallah, M. G., and Nuismer, R. (1996). "Development of advanced composite carbon shell systems for concrete columns in seismic zones." *Proc., 11th World Conf. Earthquake Engineering*, Pergamon, Elsevier Science, Oxford, Paper No. 1375.

Shahawy, M., Mirmiran, A., and Beitleman, T. (2000). "Tests and Modeling of Carbon-Wrapped Concrete Columns," *Composites Part B: Engineering*, Elsevier, 31B(6-7), 471-480.

Shao, Y., and Mirmiran, A. (2005). "Experimental Investigation of Cyclic Behaviour of Concrete-Filled FRP Tubes," Journal of Composites for Construction, ASCE, 9(3), 263-273.

Sheikh, S. A., and Khoury, S.S. (1994). "Confined Concrete Columns with Stubs." ACI Structural Journal, V. 90, No. 4, pp. 414-431.

Sheikh, S. A., Shah, D. V., and Khoury, S.S. (1993). "Confinement of High-Strength Concrete Columns." ACI Structural Journal, V. 91, No.1, pp. 100-111.

Xiao, Y. and Wu, H. (2000). Compressive Behaviour of Concrete Confined by Carbon Fibre Composite Jackets, Journal of Materials in Civil Engineering, ASCE, 12(2): 139–146.

Zhu, Z. (2004). "Joint Construction and Seismic Performance of Concrete-Filled Fibre Reinforced Polymer Tubes." PhD thesis, North Carolina State Univ., Raleigh, N.C.

Table 6.1 Properties and Capacities of Test Specimens

Column	Shear Span (mm)	f'_c (MPa)	D (mm)	R/D	P/P_o	E_f (GPa)	t (mm)	A_f (mm^2)	s (mm)	ε_{fu} (%)	k_ε	ε_{fm} (%)	ε_{fc} (%)	β	k_e	k_p	δ (%)	
																	Analy.	Exp.
RC-1	2000	90.1	270	1/2	0.31	227	0.660	-	-	1.67	0.90	1.1	0.99	1	0.9	1.20	11.6	12
RC-2	2000	75.2	270	1/2	0.34	227	0.330	-	-	1.67	0.90	1.5	1.35	1	0.9	1.35	9.92	11
RC-3	2000	49.7	270	1/2	0.47	227	0.330	-	-	1.67	0.90	1.5	1.35	1	0.9	1	8.17	9
RS-1	2000	90.1	270	1/6	0.32	227	0.825	-	-	1.67	0.72	1.2	1.08	0.696	0.522	1	7.79	8
RS-2	2000	90.1	270	1/6	0.31	227	0.825	6.6	67.5	1.67	0.72	1.2	1.08	0.835	0.626	1	9.68	9+
RS-3	2000	90.1	270	1/6	0.30	227	0.825	13.2	67.5	1.67	0.72	1.2	1.08	0.889	0.667	1	10.90	11
RS-4	2000	75.2	270	1/6	0.34	227	0.495	-	-	1.67	0.72	1.2	1.08	0.696	0.522	1	5.60	6
RS-5	2000	75.2	270	1/6	0.34	227	0.330	22.3	67.5	1.67	0.72	1.2	1.08	0.835	0.626	1	5.60	6
RS-6	2000	75.2	270	1/34	0.34	227	0.495	-	-	1.67	0.54	0.9	0.81	0.572	0.343	1	2.13	2.3

Table 6.2 Properties of reinforcing steel

Bar size	Stress-strain relationships						
	f_y (MPa)	ε_y	E_s (MPa)	ε_{sh}	f_u (MPa)	ε_u	ε_r
No. 15	500*	0.0024	208,750	0.0062	620	0.120	0.135
No. 20	476	0.0026	182,840	0.0070	570	0.125	0.144

where (E_s) is the elastic modulus; (f_y) and (f_u) are stresses at yield and ultimate, respectively; (ε_y), (ε_{sh}), (ε_u), and (ε_r) are strains at yield, onset of strain hardening, ultimate, and rupture, respectively.

*Rounded from 500.9 MPa.

Table 6.3 Properties* of carbon fibres used in manufacturing FRP casings

Fibres	Nominal Thickness (mm/ply)	Ultimate Tensile Strength (MPa)	Elastic Modulus (GPa)	Ultimate Rupture Strain (%)	Areal Weight (g/m^2)
Carbon	0.165	3800	227	1.67	300

*Reported by the manufacturer.

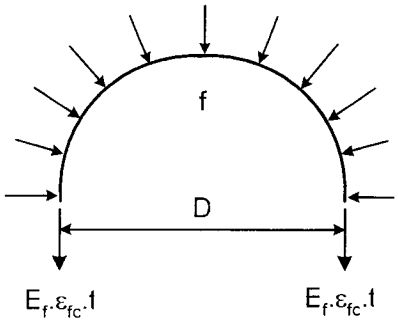

a) Circular section

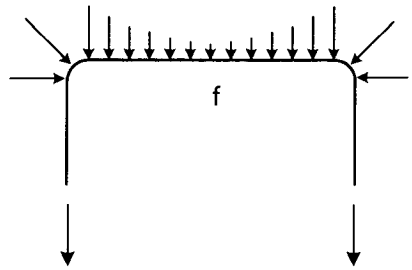

b) Square section with small-radius corners

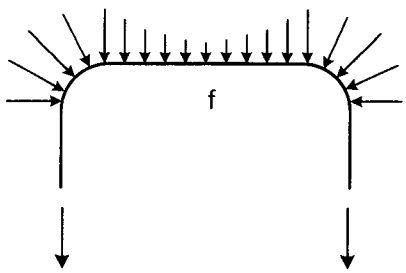

c) Square section with well-rounded corners

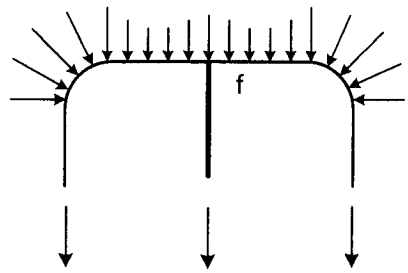

d) Square section with well-rounded corners and a single FRP crosstie in each direction

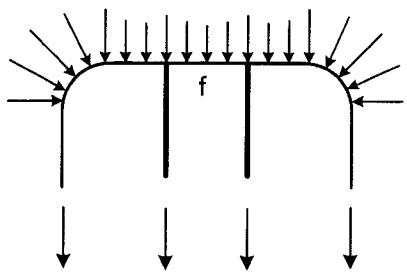

e) Square section with well-rounded corners and double FRP crossties in each direction

Fig. 6.1 – Confinement mechanism

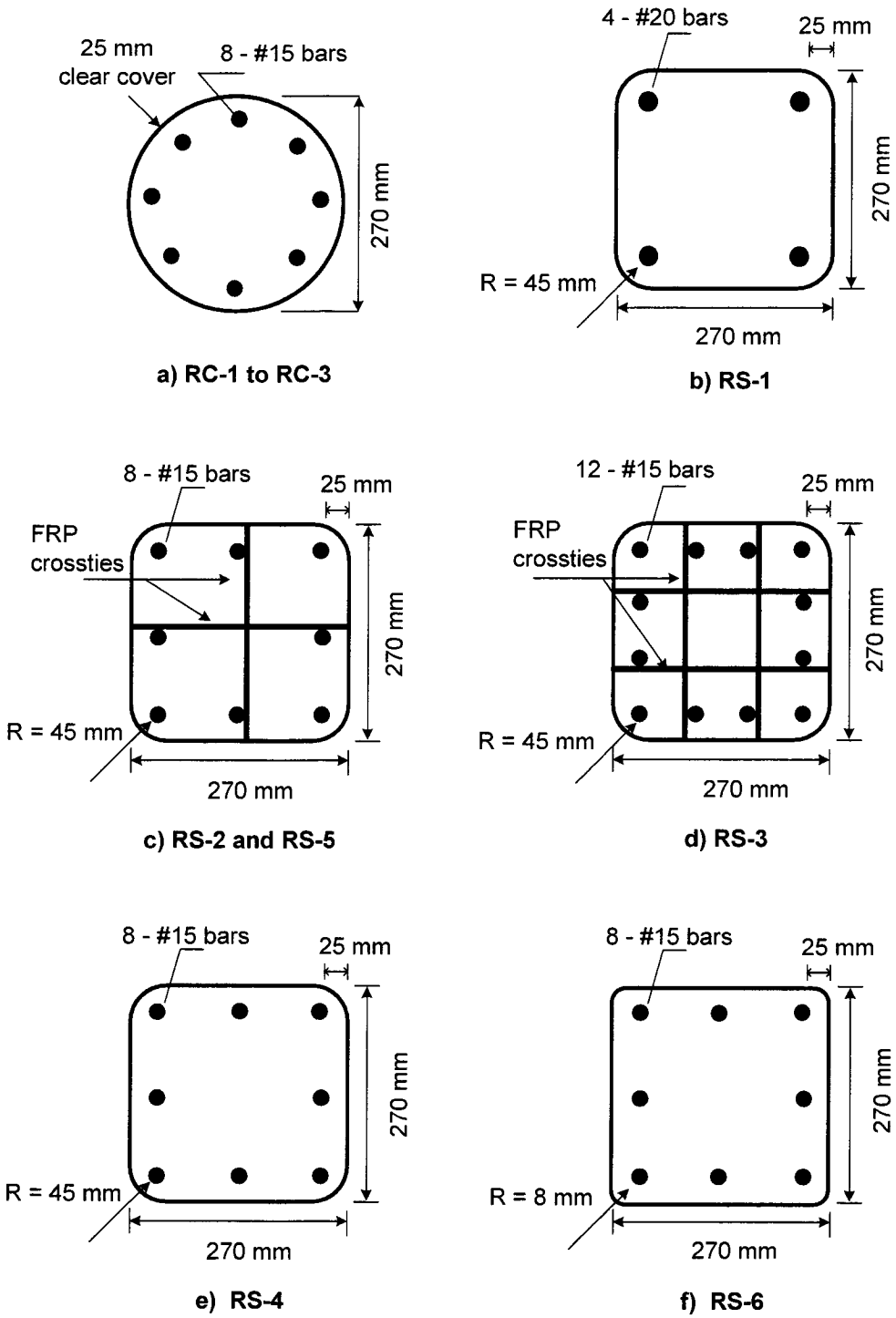

Fig. 6.2 – Reinforcement arrangements used in column tests

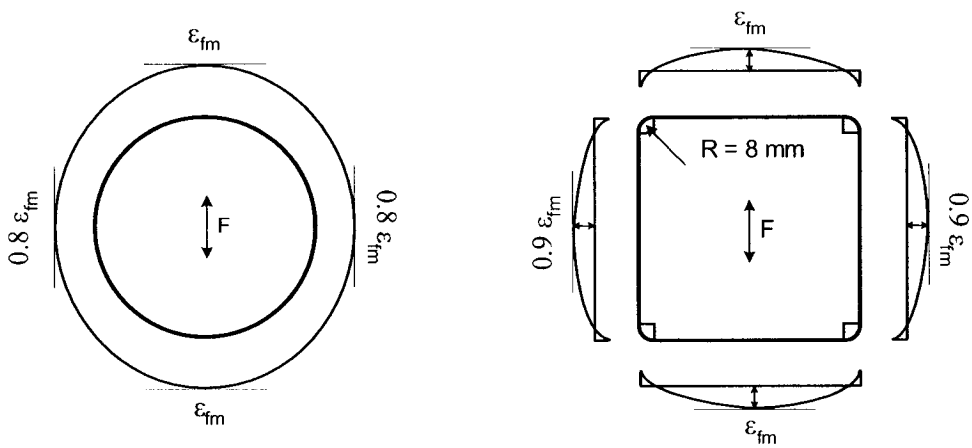

a) RC-1 to RC-3

b) RS-6

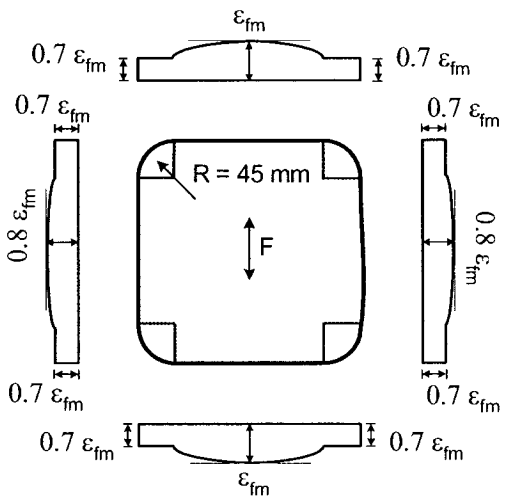

c) RS-1 to RS-5

Fig. 6.3 – Strain distribution in FRP casings

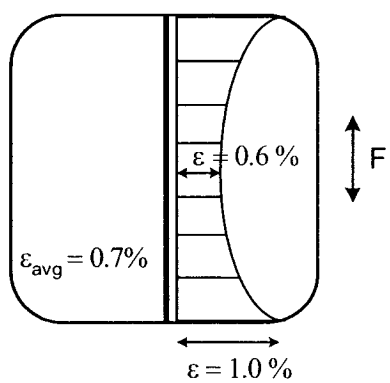

Fig. 6.4 – Strain distribution in FRP crossties

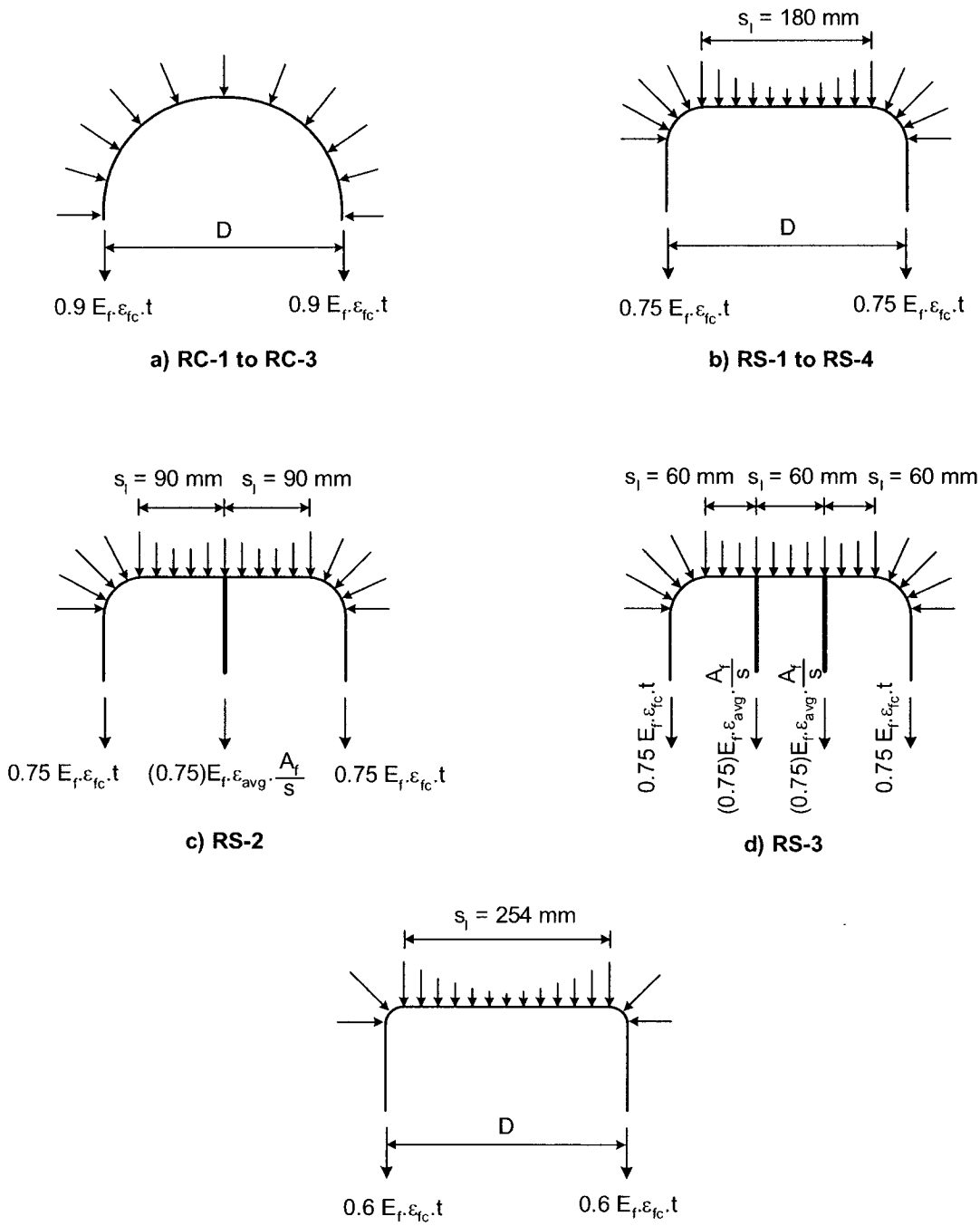

Fig. 6.5 – Confinement forces in test specimens

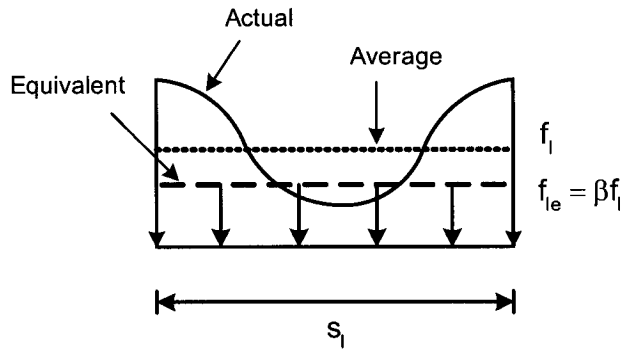

Fig. 6.6 – Equivalent lateral pressure

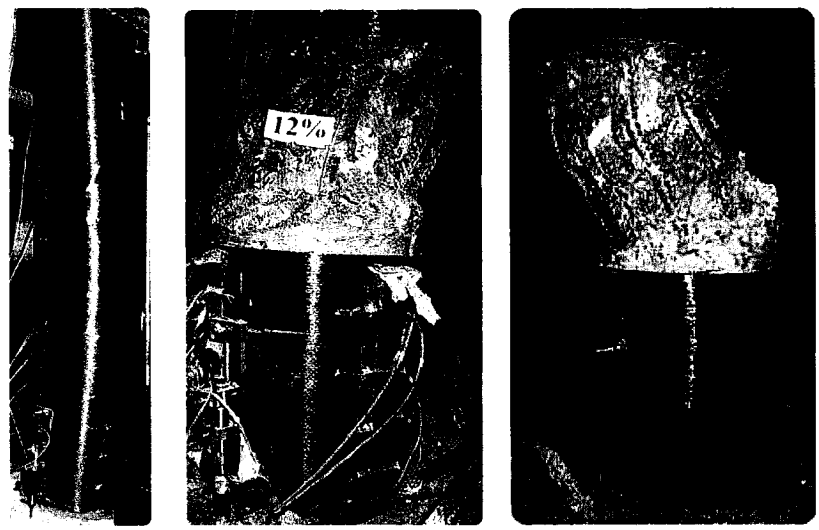

(a) Circular Columns

(b) Square Columns

Fig 6.7 – Specimens at end of testing

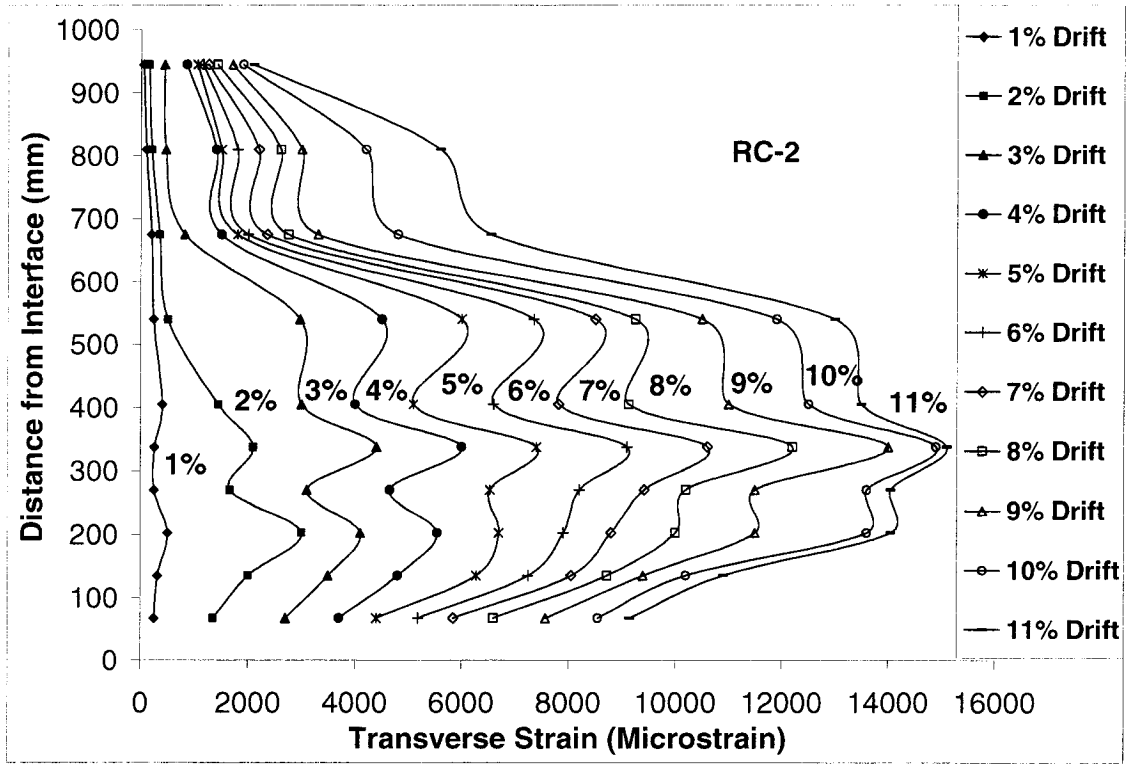

(a) Circular Column

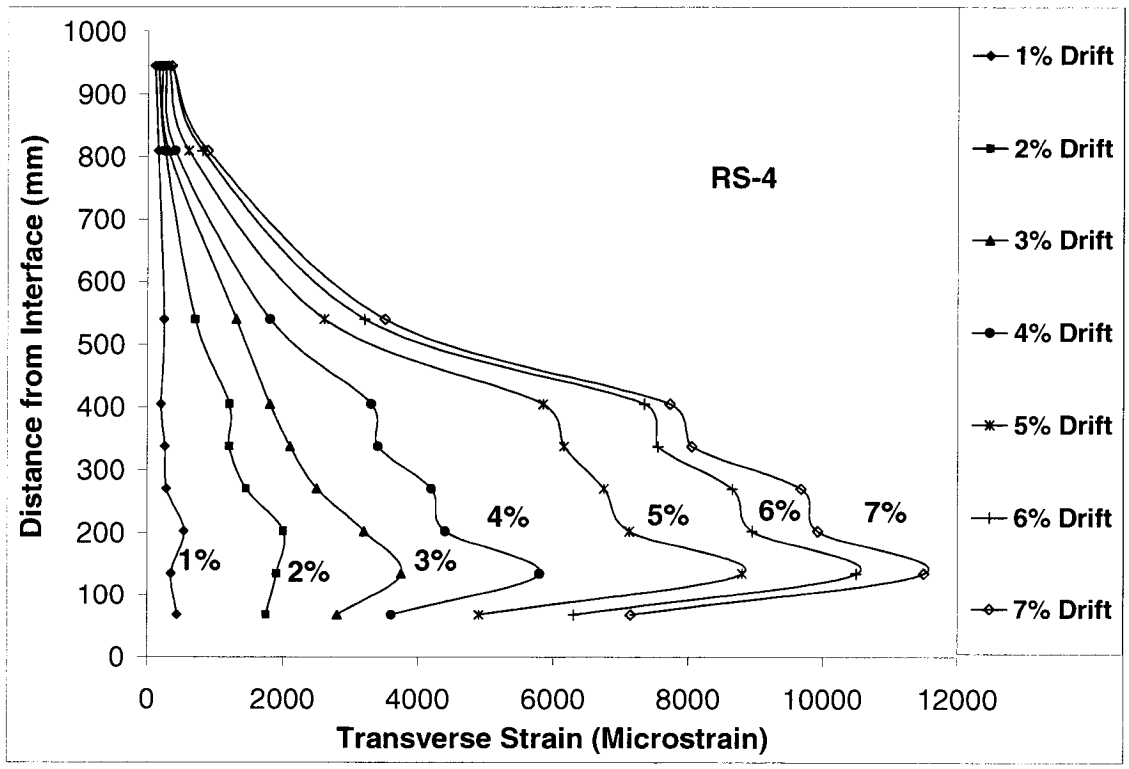

(b) Square Column

Fig. 6.8 – Variation of transverse strains on FRP casings along column height

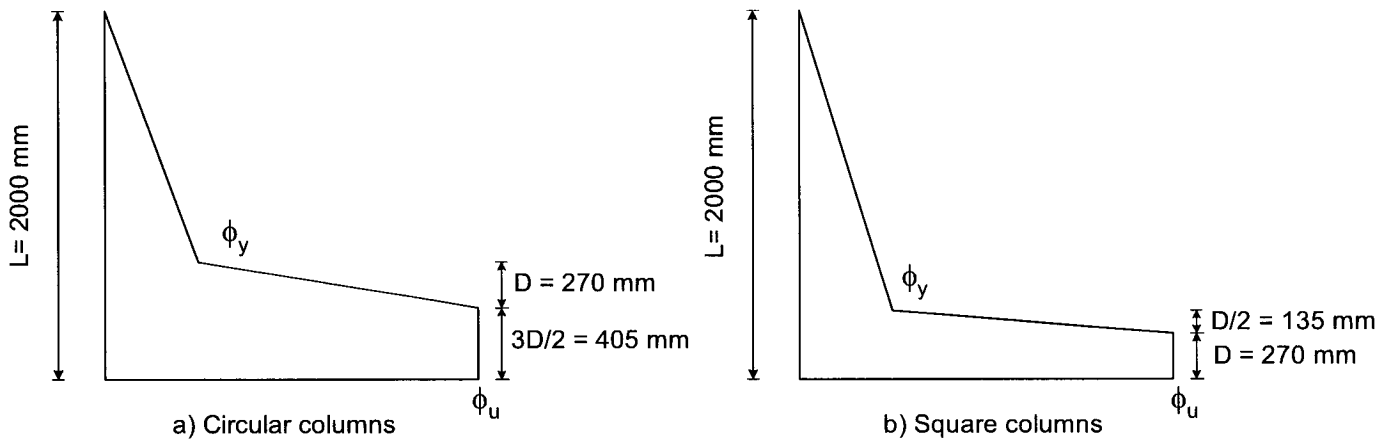

Fig. 6.9 – Plastic hinging of circular and square columns

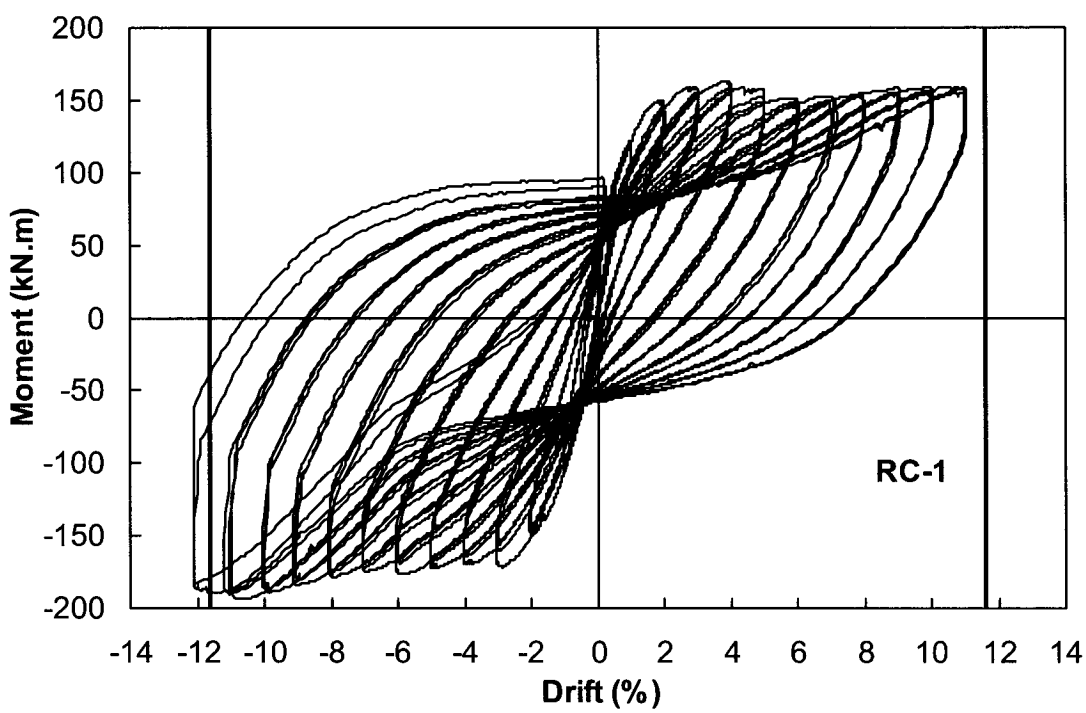

(a) Column RC-1

Fig. 6.10 – Experimentally recorded hysteretic moment-lateral drift relationships and analytically calculated lateral drift capacities

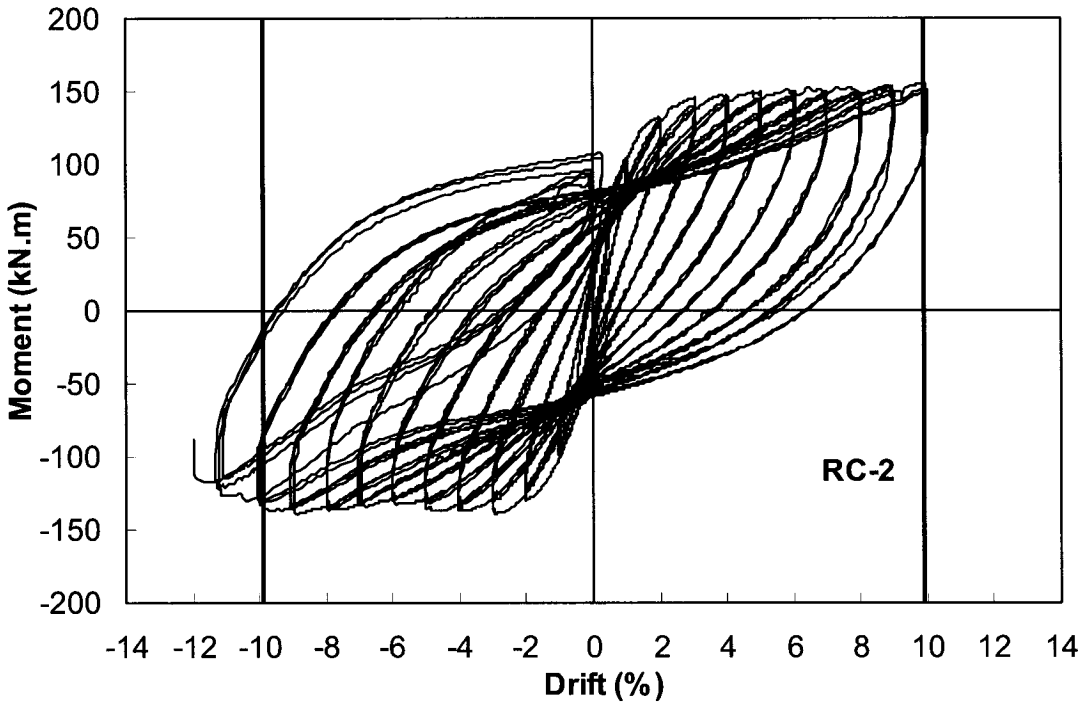

(b) Column RC-2

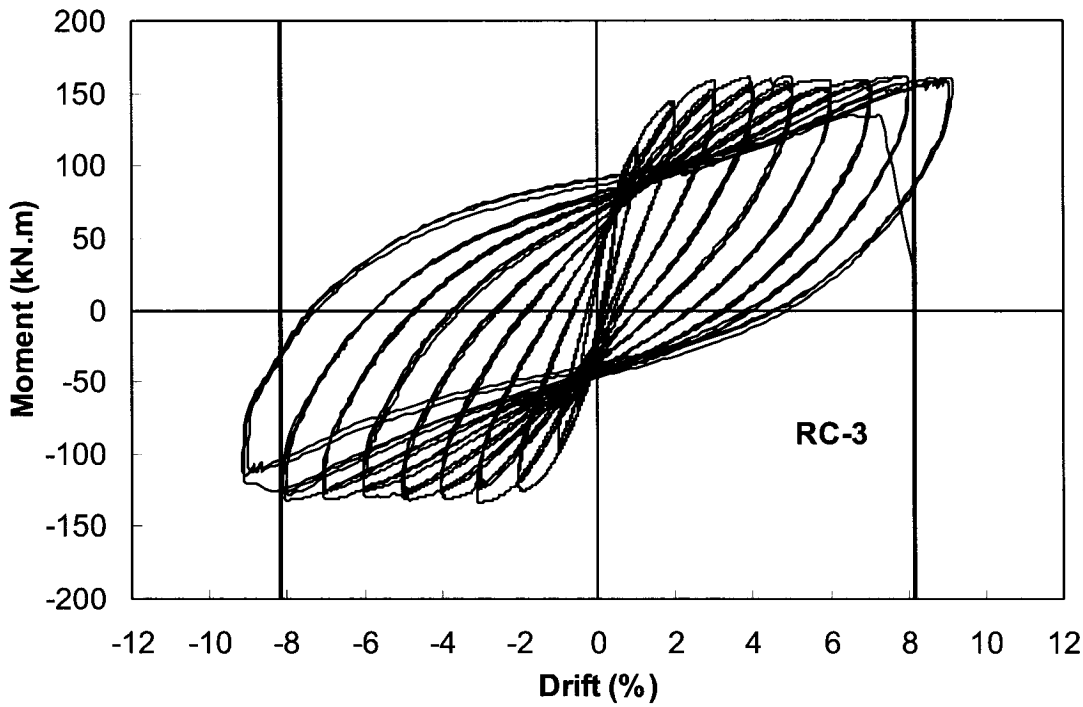

(c) Column RC-3

Fig. 6.10 – Cont'd

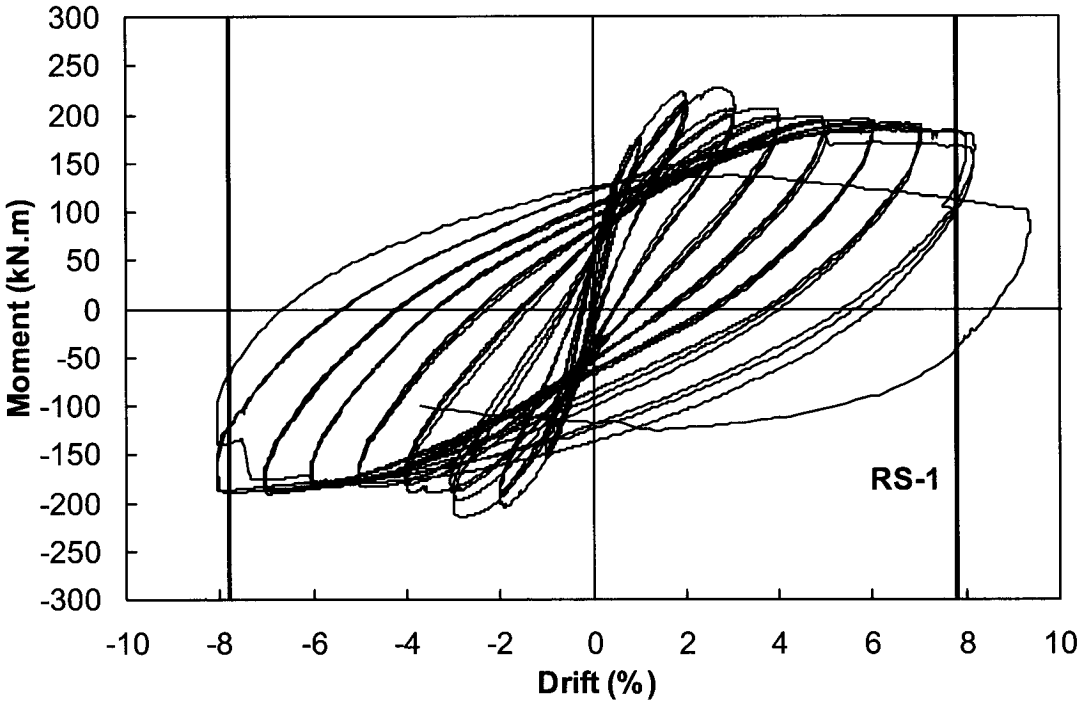

(d) Column RS-1

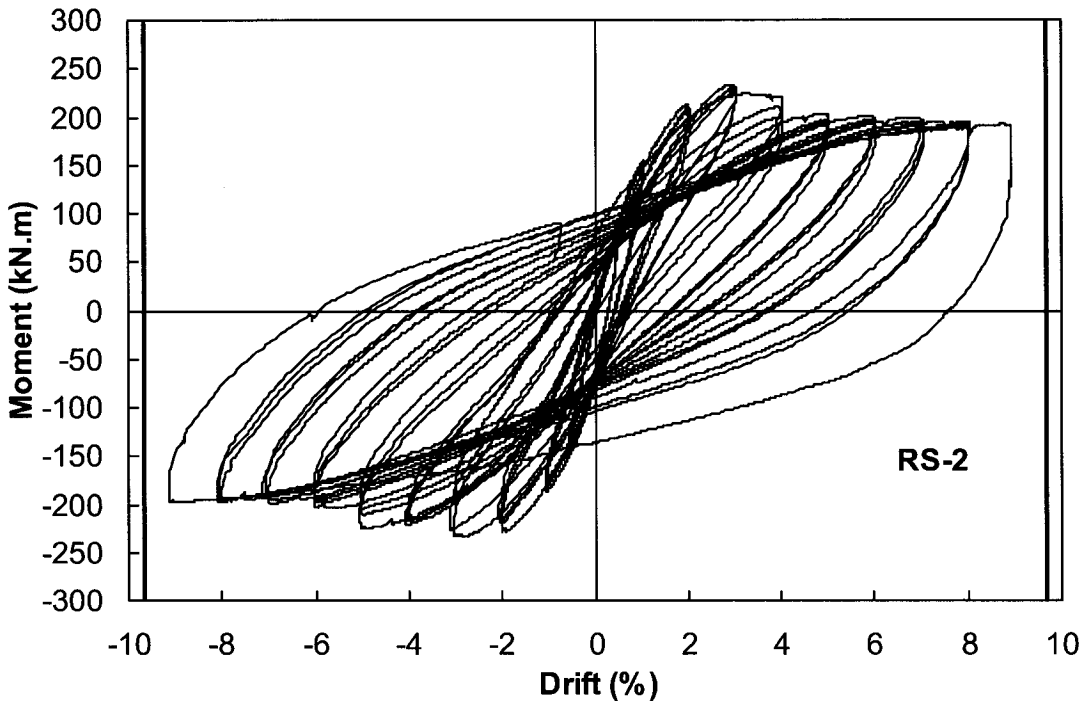

(e) Column RS-2

Fig. 6.10 – Cont'd

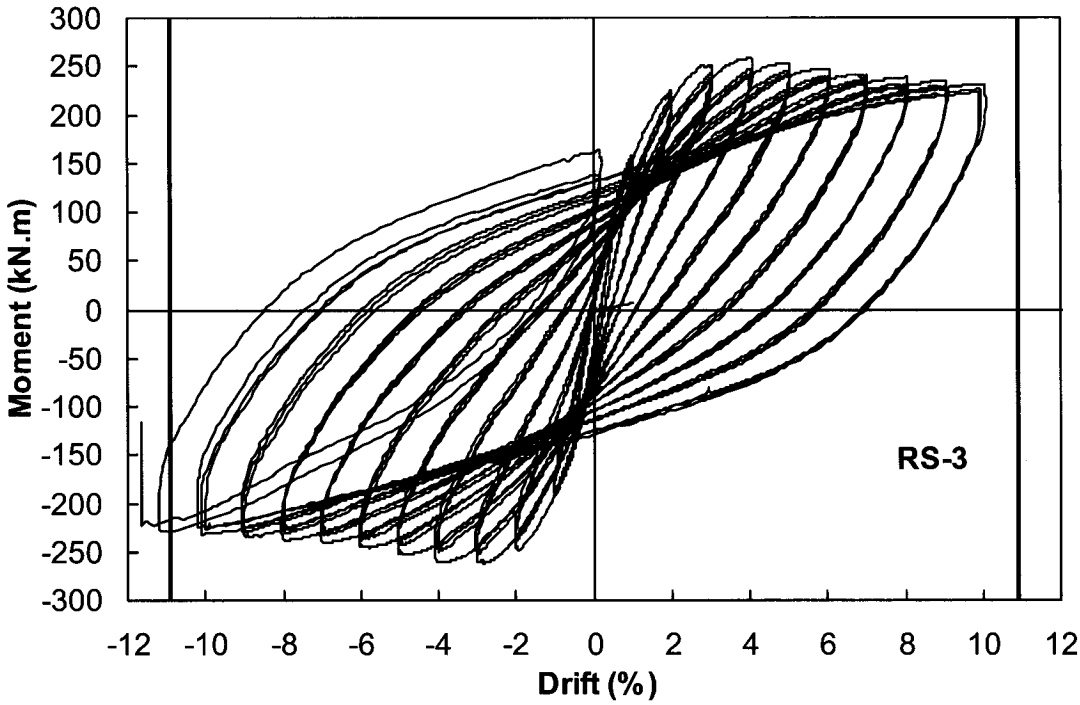

(f) Column RS-3

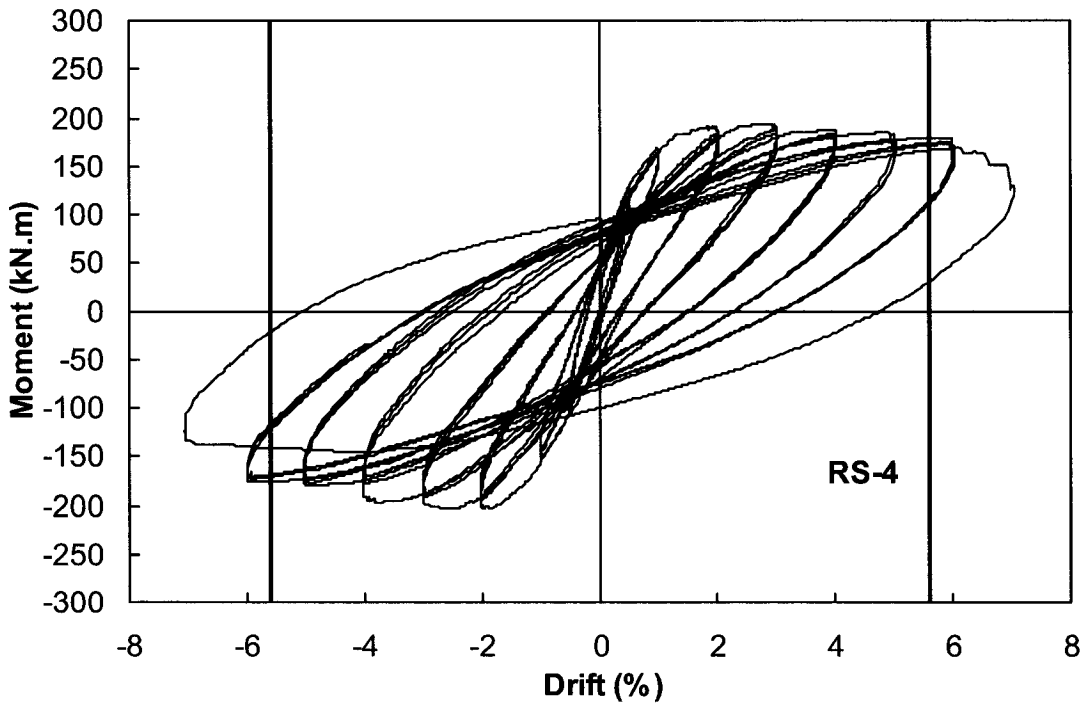

(g) Column RS-4

Fig. 6.10 – Cont'd

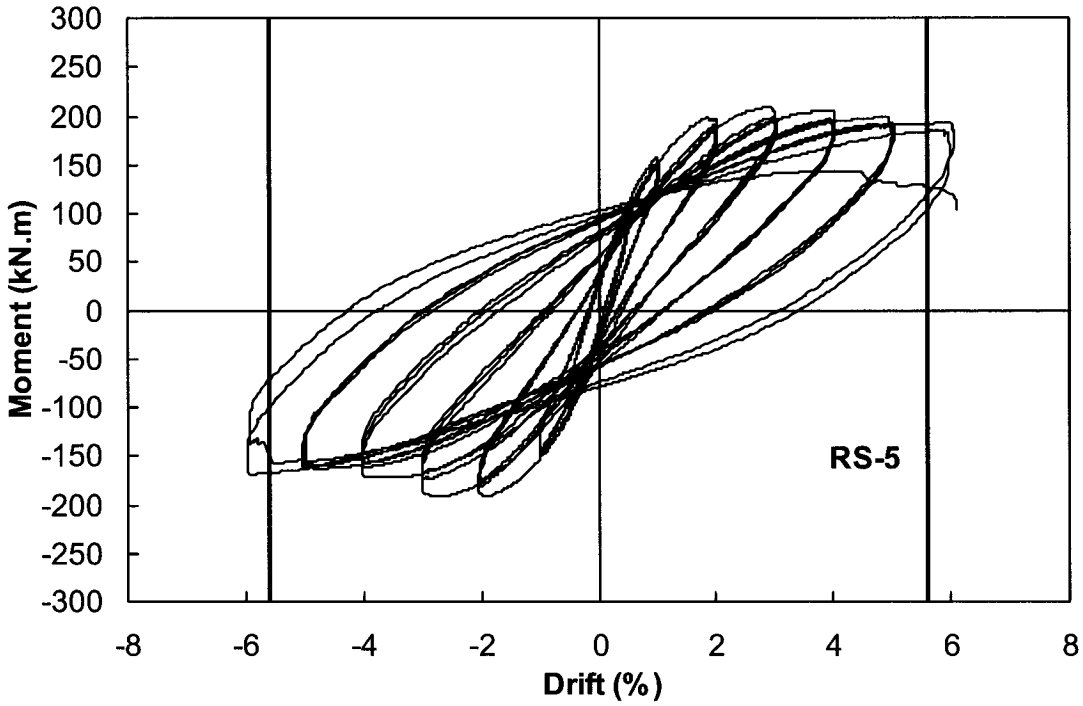

(h) Column RS-5

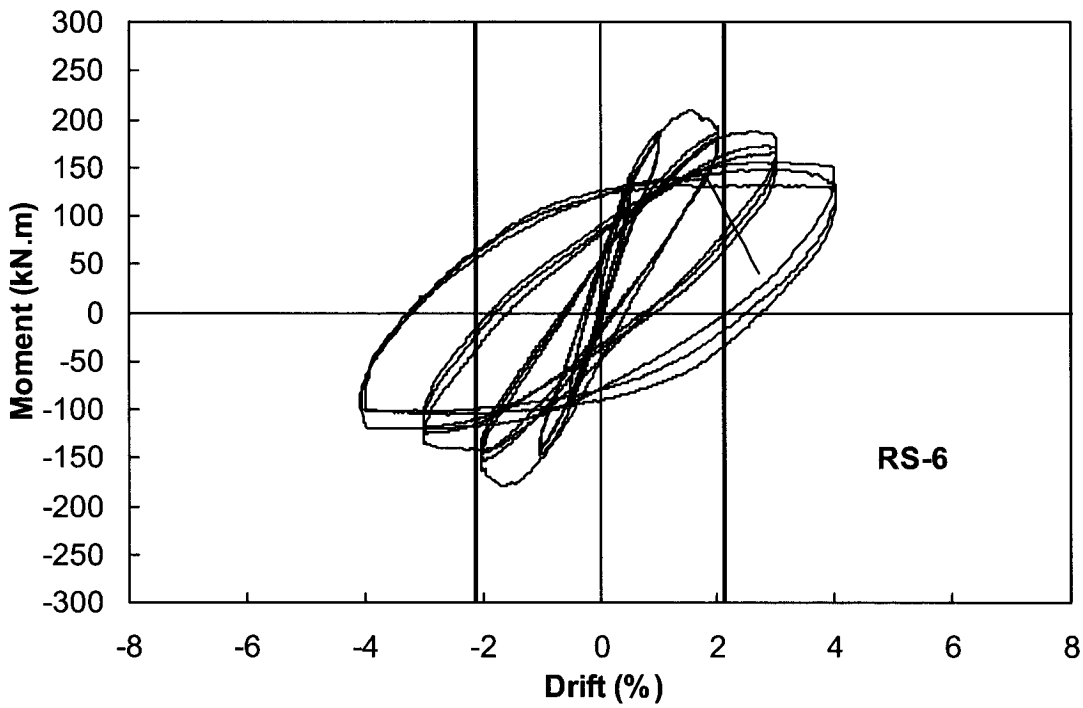

(i) Column RS-6

Fig. 6.10 – Cont'd

Chapter 7

Conclusions

7.1 CONCLUSIONS

The following conclusions can be drawn from the combined experimental and analytical investigation conducted on concrete columns confined by FRP stay-in-place formwork:

- High-strength concrete columns confined with carbon FRP stay-in-place formwork can develop extremely ductile behaviour under simulated seismic loading. The use of FRP formwork as confinement reinforcement substantially increases deformability of circular and square columns. Column tests indicate that inelastic deformability of 90 MPa concrete columns can be increased up to 12% lateral drift ratio with FRP stay-in-place formwork.
- The increased confinement required for HSC columns can be provided with FRP stay-in-place formwork. Unlike conventional steel reinforcement that confines the core concrete, FRP stay-in-place formwork provides effective confinement to the entire column section. Furthermore, the FRP casings cover the entire column surface, unlike conventional steel ties placed at certain spacing, thereby enabling full utilization of higher material strength of FRP reinforcement.
- The strain data recorded during column tests indicate that the strength of FRP stay-in-place formwork could be mobilized to a large extent, developing strains of up to 1.5%,

approaching the tensile capacity of material. The observed strains were consistently higher than the 0.4% used in current design recommendations as a safe design limit.

- The ratio of corner radius to column dimension (R/D) has a significant influence on the effectiveness of FRP as confinement reinforcement. Increased corner radius promotes effectiveness of FRP, while preventing premature material failure associated with sharp corners. Columns with three plies of FRP, tested in the experimental program, were able to develop 6% drift ratio prior to significant strength decay when the R/D ratio was 1/6, whereas the column with sharper corners (R/D = 1/34) was able to develop a limited drift ratio of 2%.
- The use of FRP crossties improves the efficiency of FRP stay-in-place formwork, in much the same manner as overlapping hoops and crossties used in conventional steel confinement reinforcement. Therefore, the concept of integrated crossties in FRP casings, introduced by the author, has proven to be effective.
- The seismic performance of FRP encased circular columns is superior to that of columns confined by conventional spiral/hoop reinforcement. This can be attributed to increased effectiveness of FRP casings as confinement reinforcement, as well as the characteristics of plastic hinging, which exhibits significantly more plastification and progression towards the elastic region in FRP encased columns, leading to increased hinging length.
- Column deformability decreases with increasing axial load relative to column concentric capacity (P/P_o) and concrete compressive strength (f'_c). It was experimentally observed that under the same level of applied axial load (P), HSC column developed higher lateral drift capacity than a companion NSC column with the same confinement characteristics.

- Flexural capacity of columns with FRP stay-in-place formwork can be computed using the plane section analysis commonly employed for reinforced concrete members, provided that appropriate material models are incorporated.
- Confinement models developed for steel confined concrete may result in the overestimation of flexural strength and underestimation of inelastic deformability of FRP confined columns.
- FRP casings develop transverse tensile stresses caused by the combined action of shear and flexure. The contribution of shear increases under high levels of shear stress reversals, as well as following concrete deterioration in plastic hinge regions. The concrete shear resistance may diminish very significantly in the latter case, increasing the strain demand on the FRP casing.
- Additional confinement provided by a footing appears to strengthen the column critical section at the column-footing interface, shifting the failure away from the interface. This shift was observed to range approximately between one half and full cross-sectional dimension for the columns tested and axial loads applied in the current investigation.
- The rectangular stress block developed for HSC provides an accurate analytical tool for flexural strength calculations. The stress block is applicable to a wide range of concrete strengths, including normal-strength and high-strength concretes of up to 130 MPa.
- The analytical expression for the computation of inelastic deformability of reinforced concrete columns confined by FRP casings, developed by modelling experimentally observed behaviour, provide good correlations with test data. Therefore, the expression may be used for the design of concrete columns confined with FRP stay-in-place formwork.

7.2 RECOMMENDATIONS FOR FUTURE RESEARCH

The following recommendations are made for future research;

- More research is needed to investigate the behaviour of FRP confined square and rectangular columns under reversed cyclic loading.
- There is a need for a confinement model that represents the stress-strain behaviour of FRP confined concrete accurately. Although, recently a number of confinement models have been proposed for FRP confined concrete, they are all based on limited number of column tests. In particular, tests on square and rectangular columns are quite limited. It is necessary to expand this ensemble to be able to accurately model the behaviour of FRP confined concrete.
- The effect of corner radius and presence of FRP cross-ties on confinement efficiency of FRP confined square and rectangular columns need to be investigated.
- Further research is needed to model the formation and extension of the plastic hinge in FRP encased concrete columns with different aspect ratios.

Appendix A

Additional Figures of the Test Setup

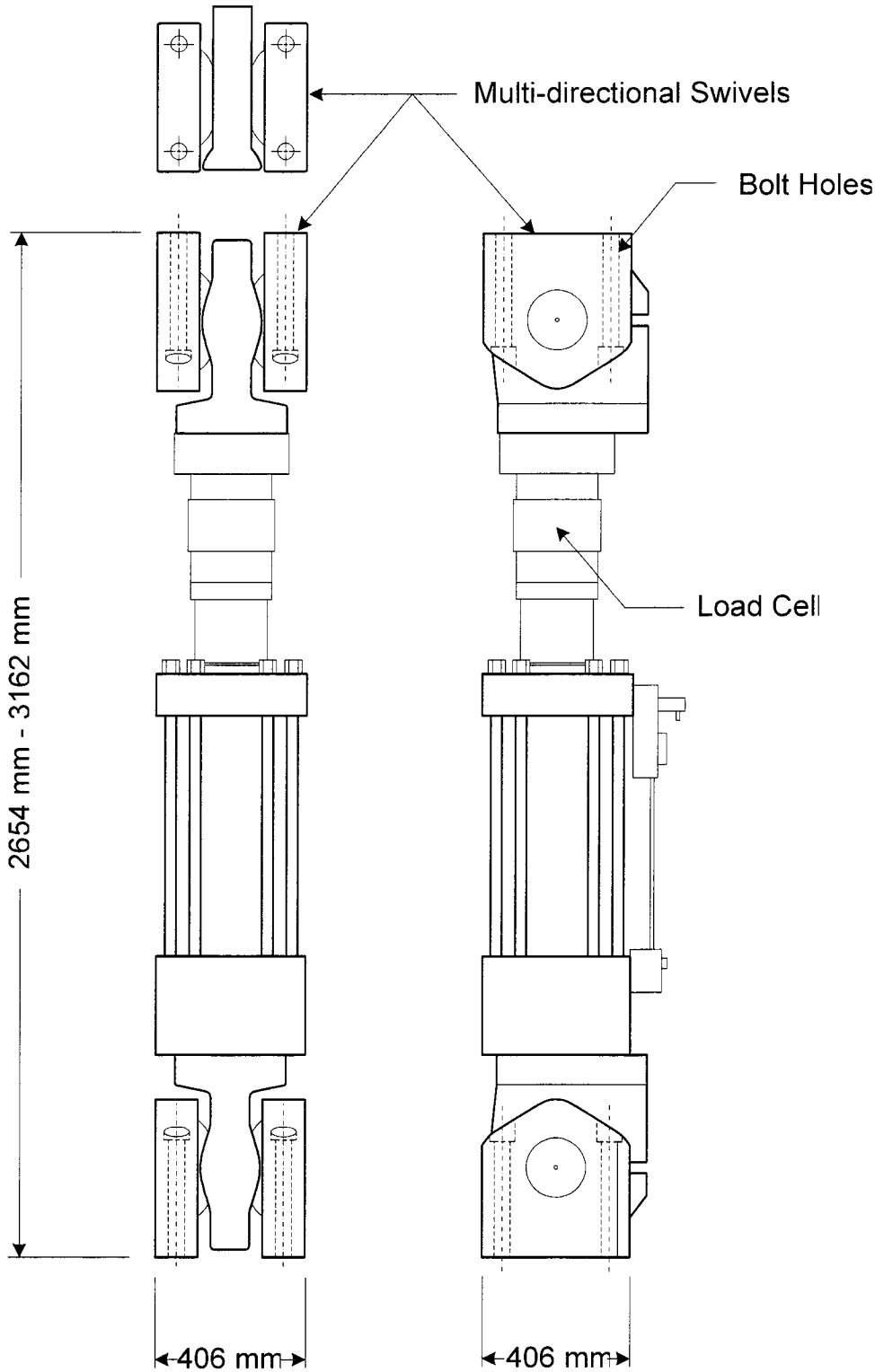

Fig. A.1 – Details of the MTS Actuators

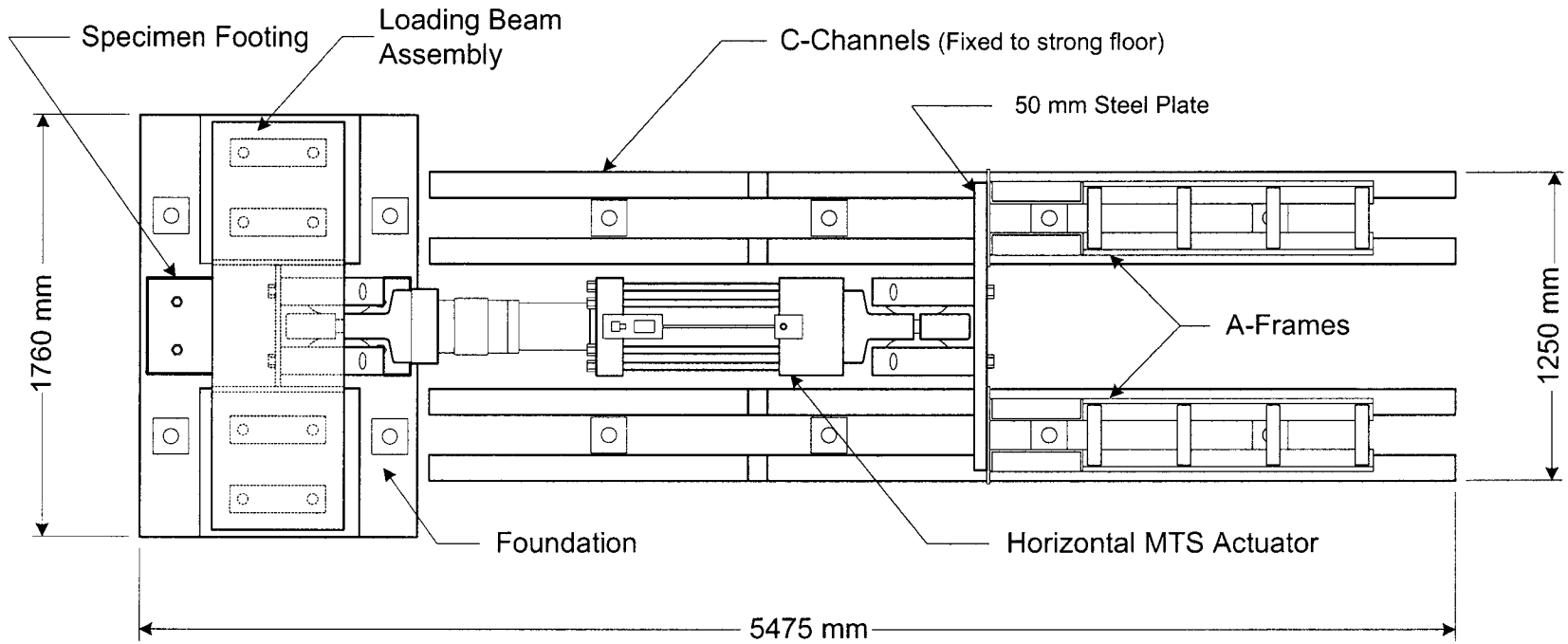

Fig. A.2 – Plan View of the Test Setup

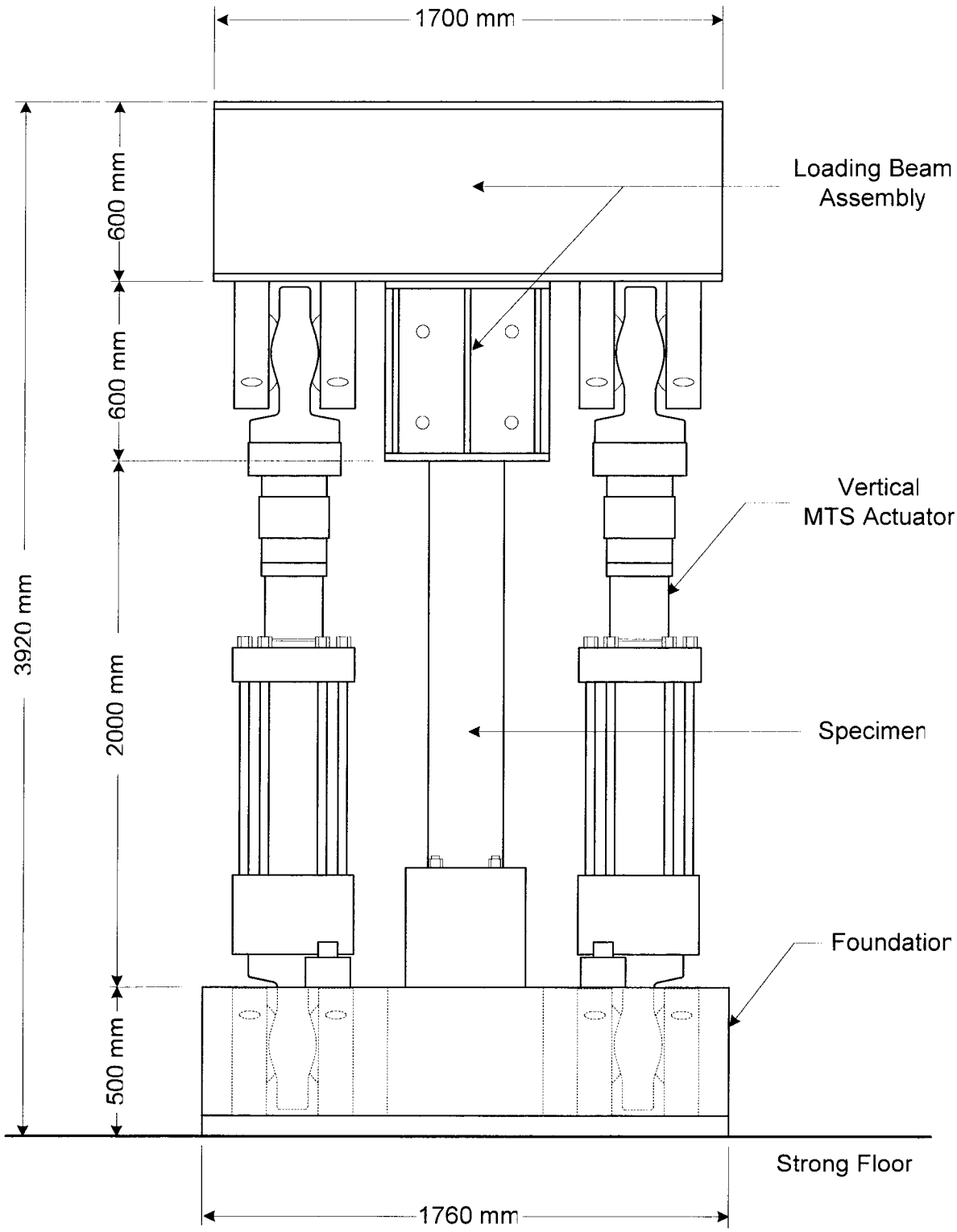

Fig. A.3 – Front Elevation of the Test Setup

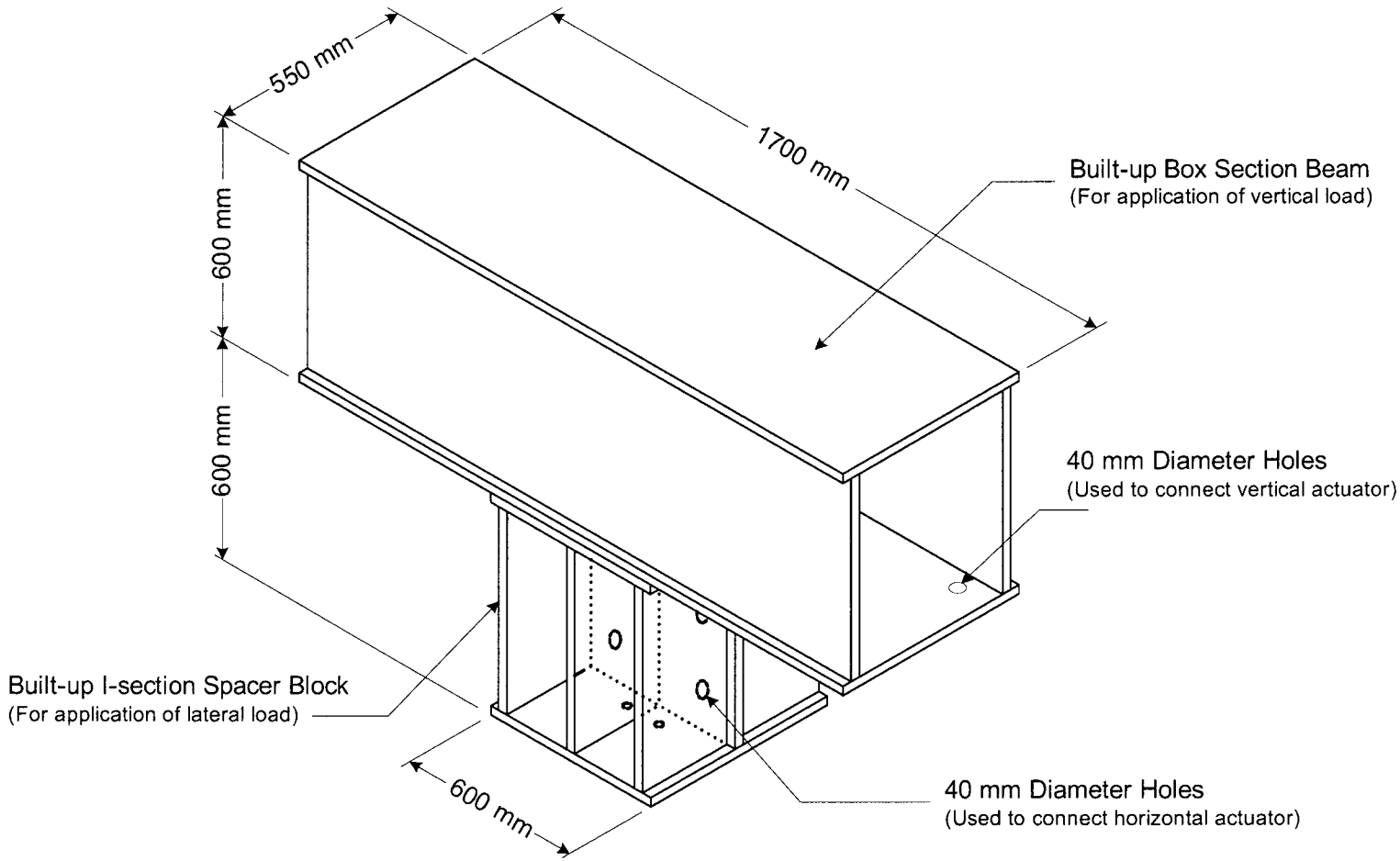

Fig. A.4 – Details of the Loading Beam Assembly

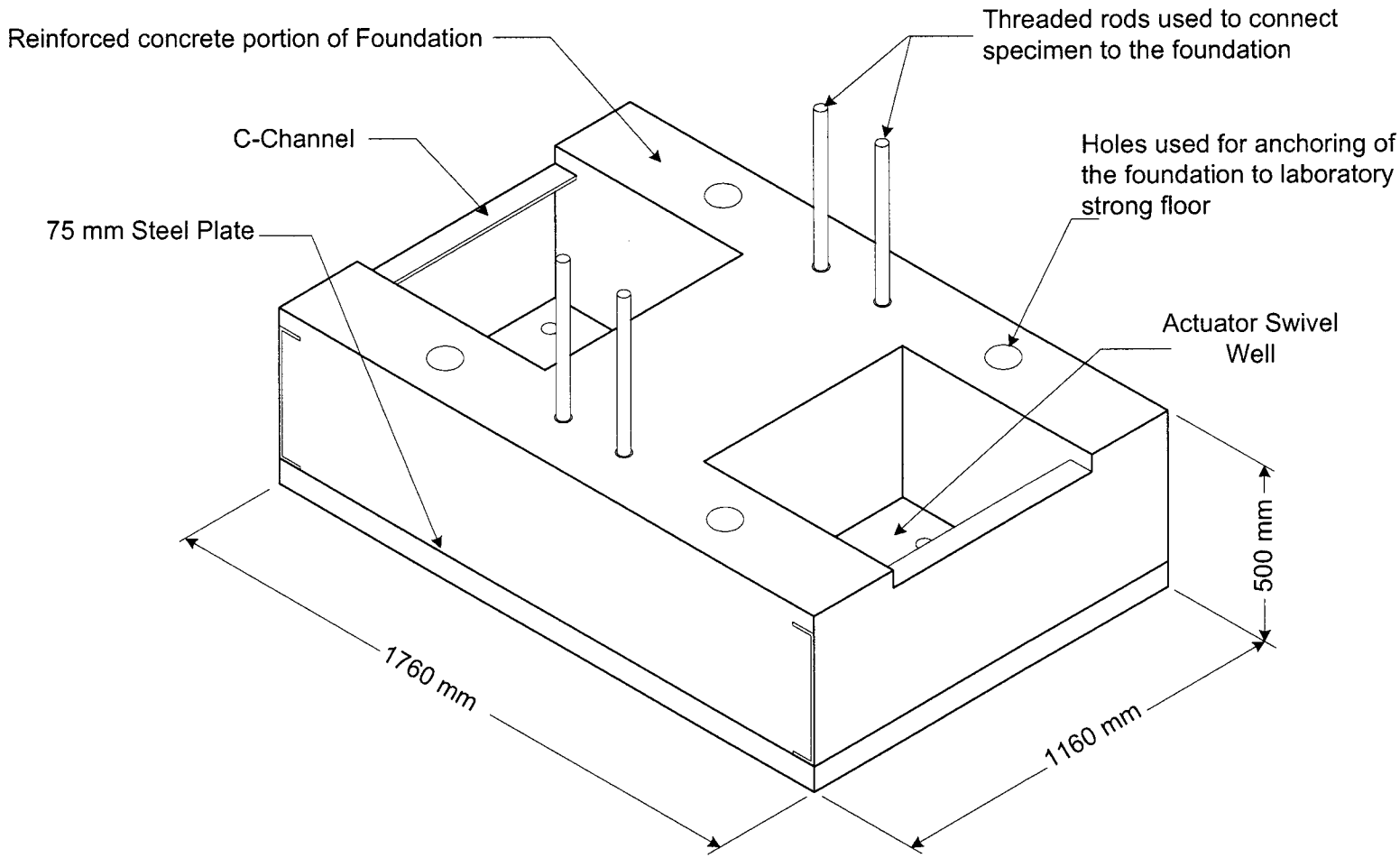

Fig. A.5 – Details of the Composite Foundation

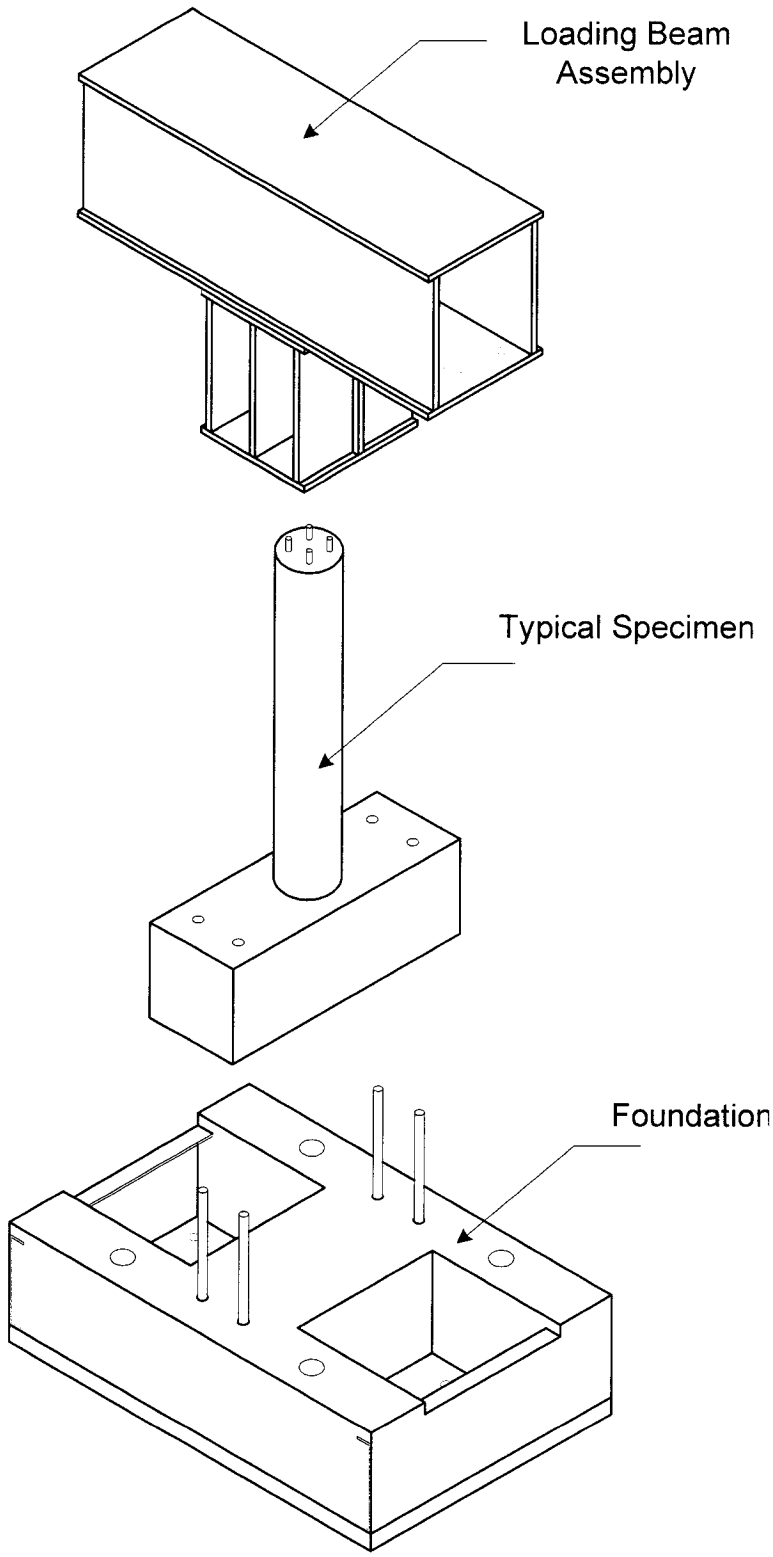

Fig. A.6 – Assembly Drawing of the Vertical Test Setup

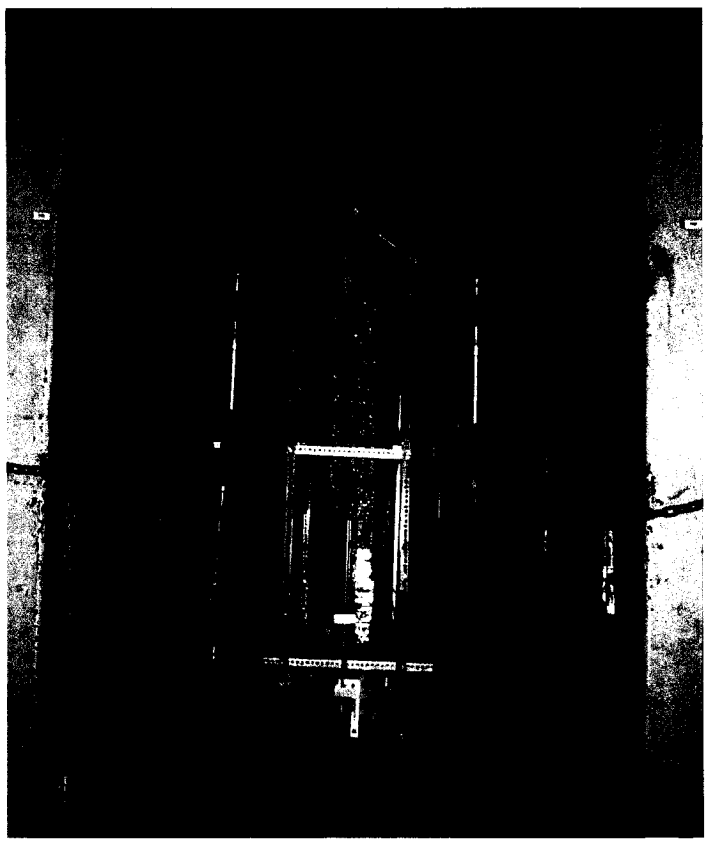

(a) Front Elevation

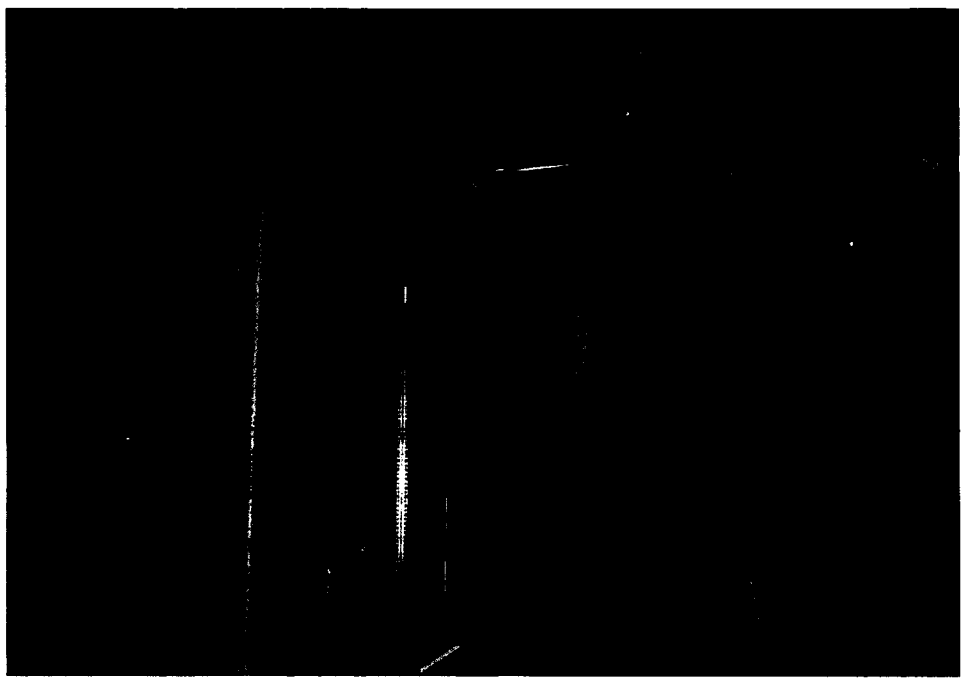

(b) Side Elevation

Fig. A.7 – General Views of the Test Setup

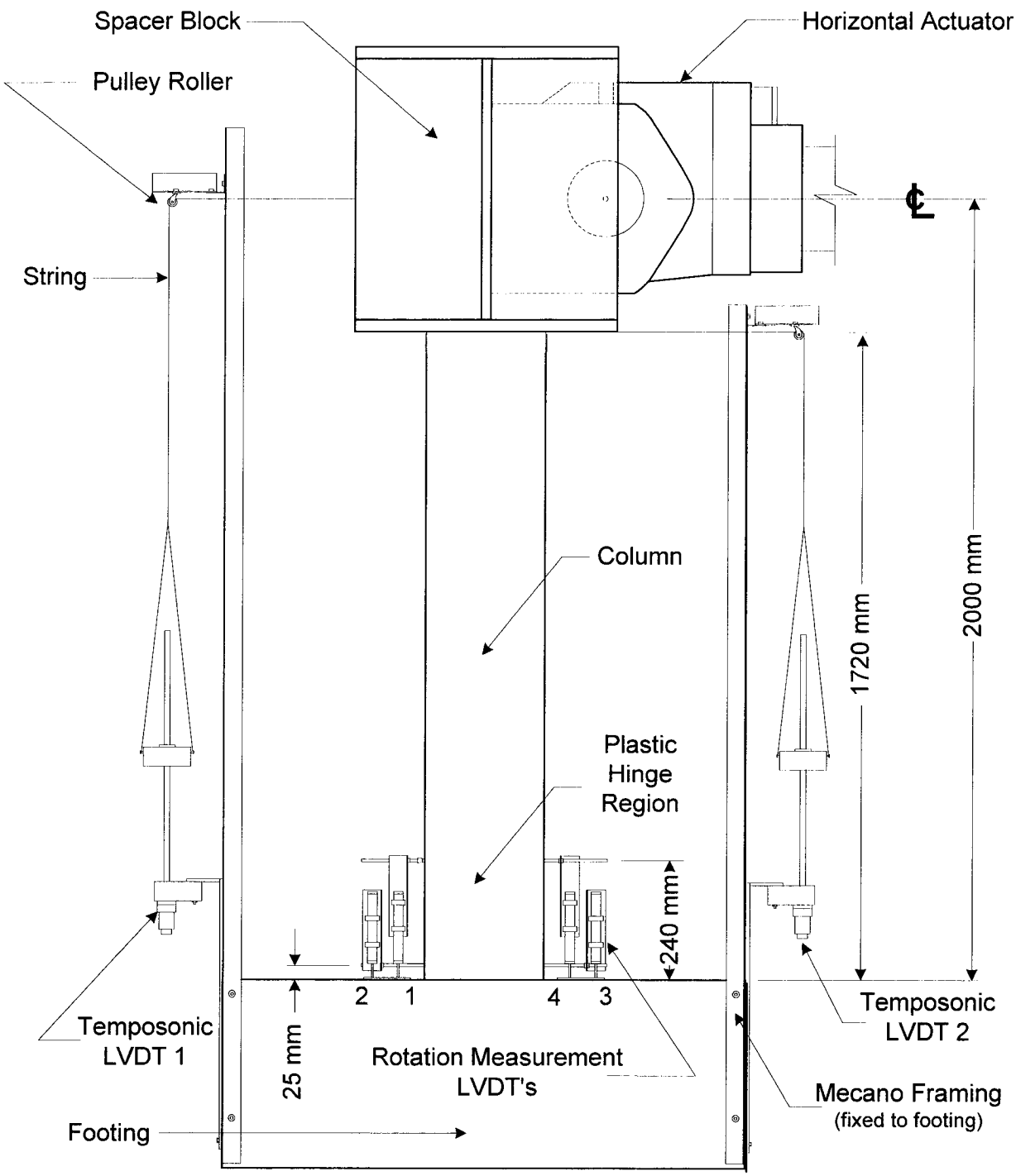

Fig. A.8 – Configuration of LVDT's on a Typical Specimen

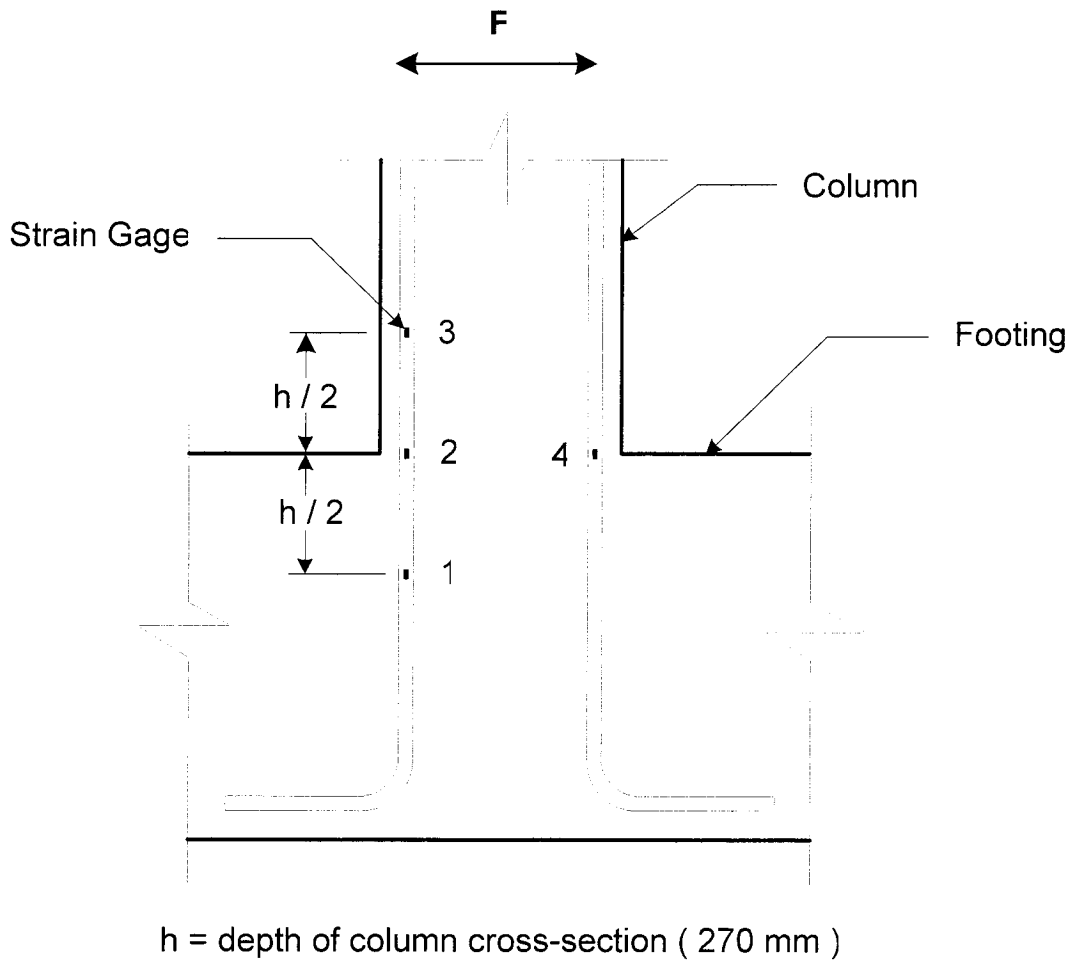

Fig. A.9 – Location of Strain Gages on Longitudinal Bars in All Specimens

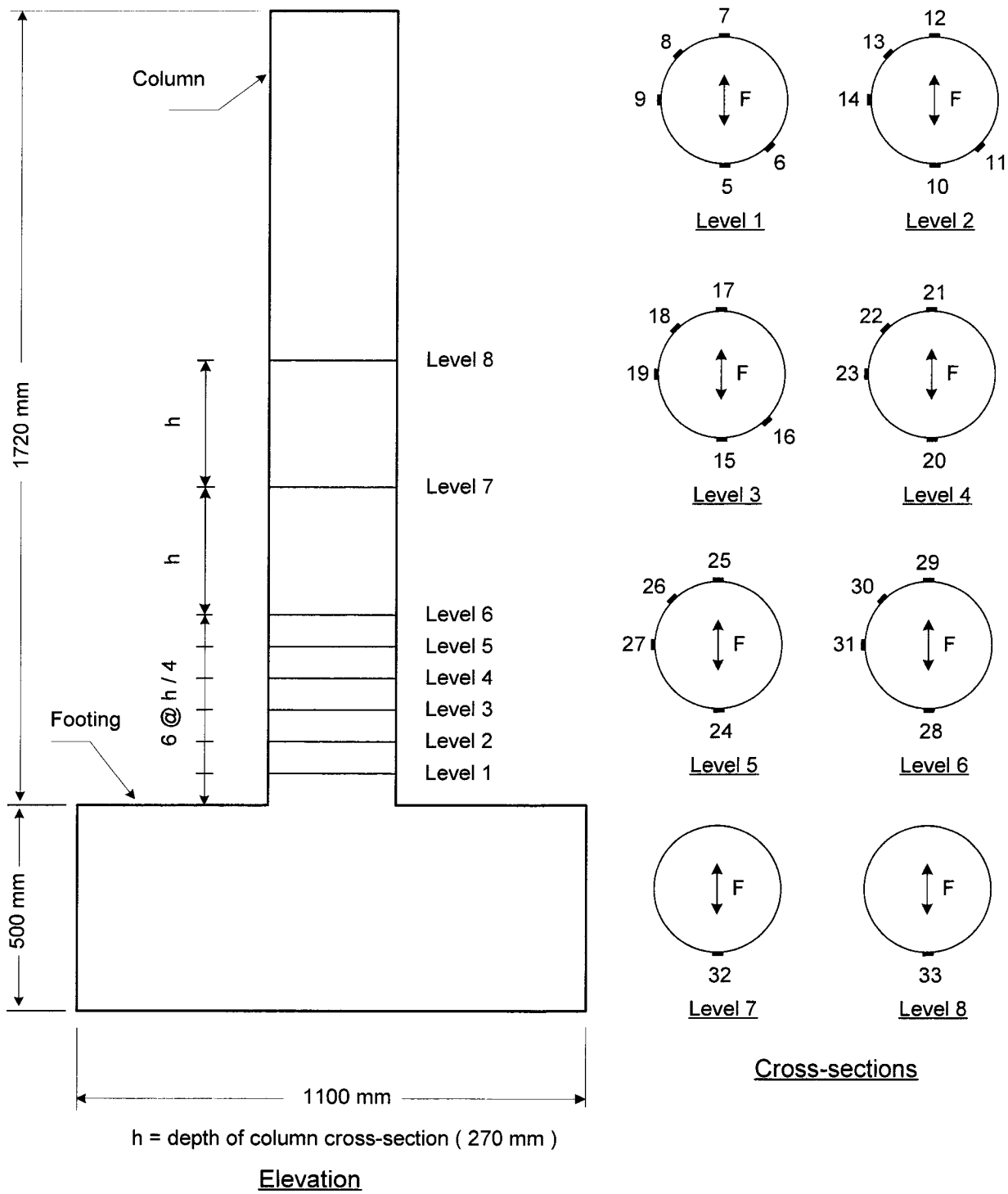

Fig. A.10 – Location of Strain Gages on the FRP Casing of Specimen RC-1

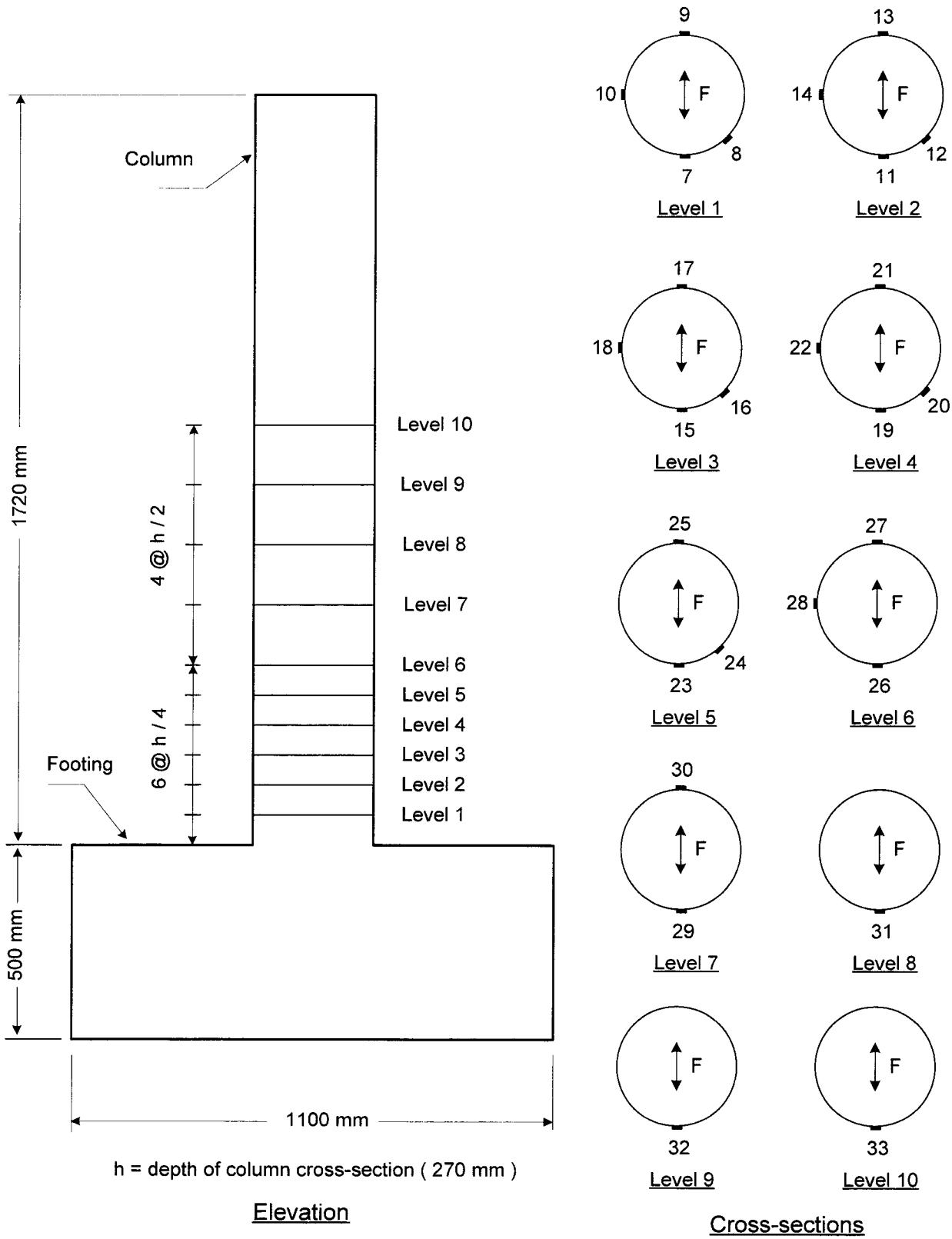

Fig. A.11 – Location of Strain Gages on the FRP Casing of Specimen RC-2

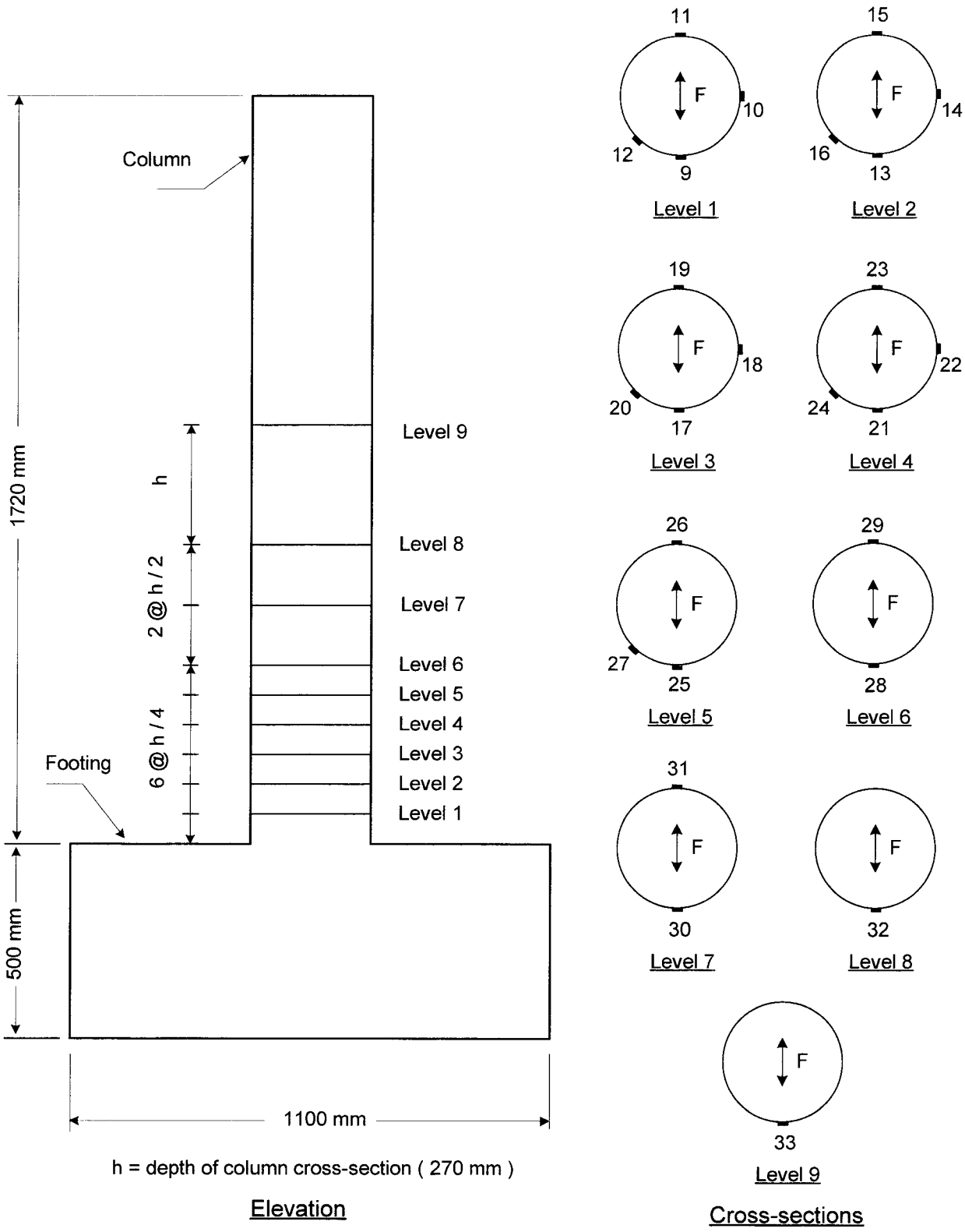

Fig. A.12 – Location of Strain Gages on the FRP Casing of Specimen RC-3

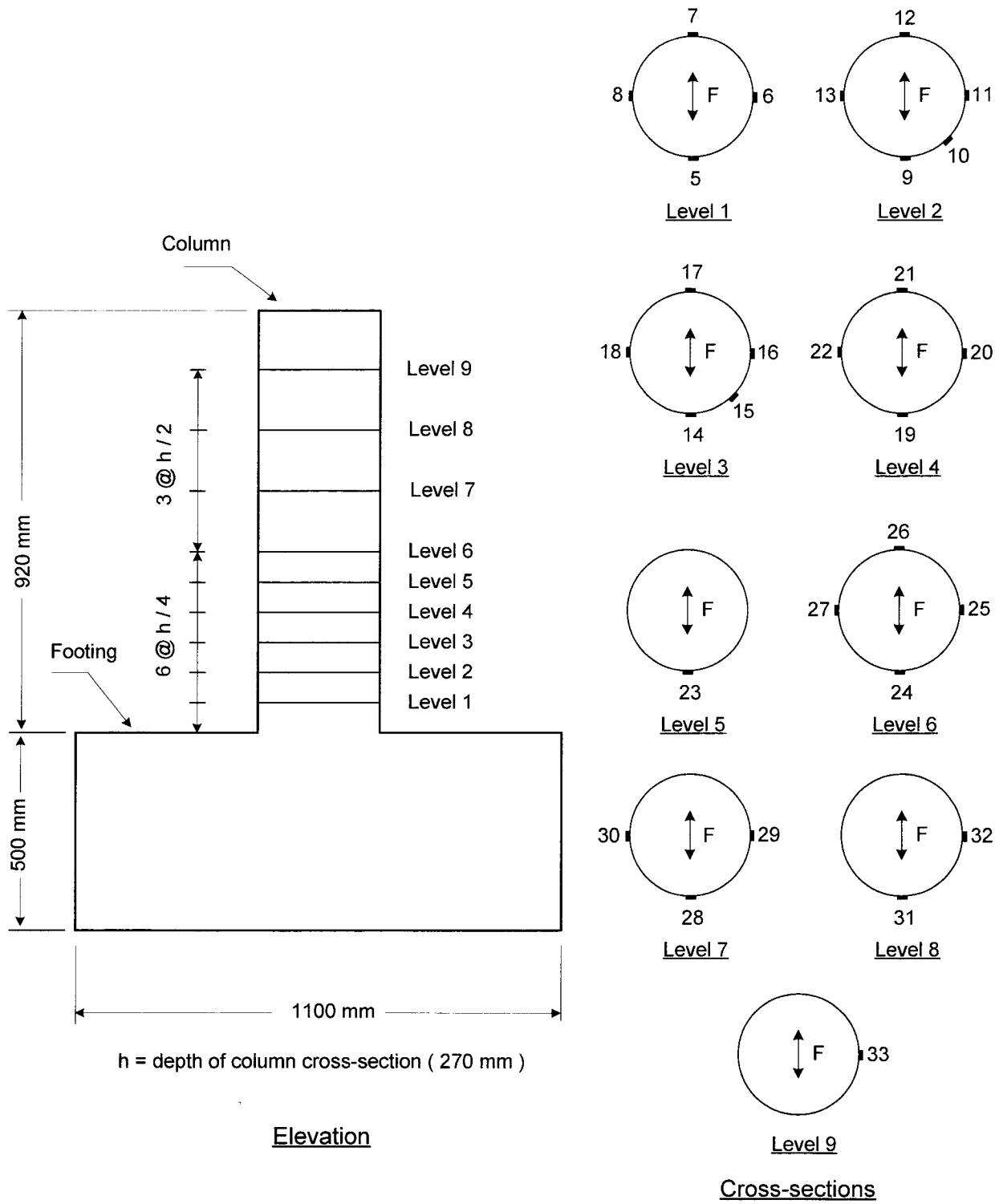

Fig. A.13 – Location of Strain Gages on the FRP Casing of Specimen RC-4

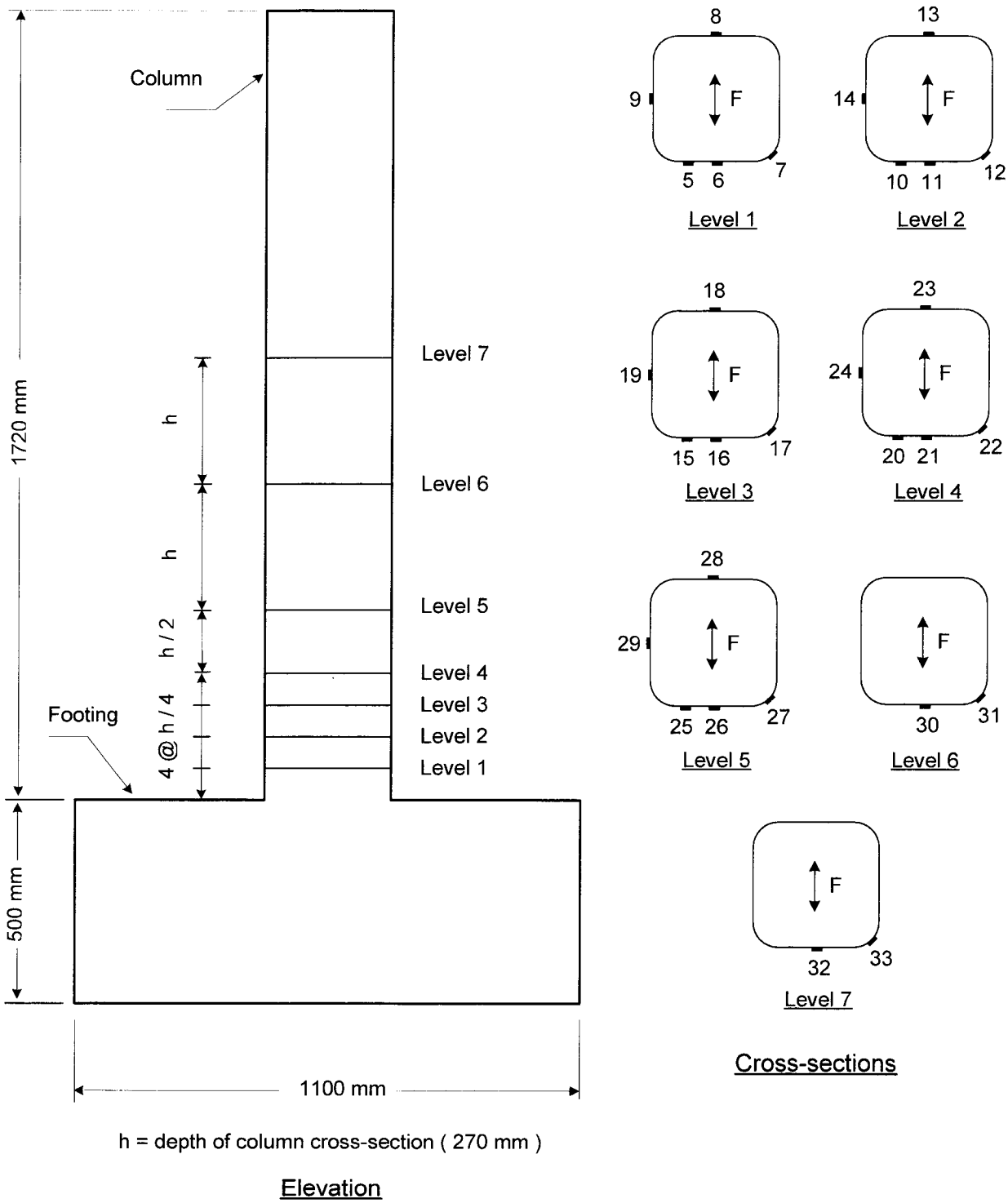

Fig. A.14 – Location of Strain Gages on the FRP Casing of Specimen RS-1

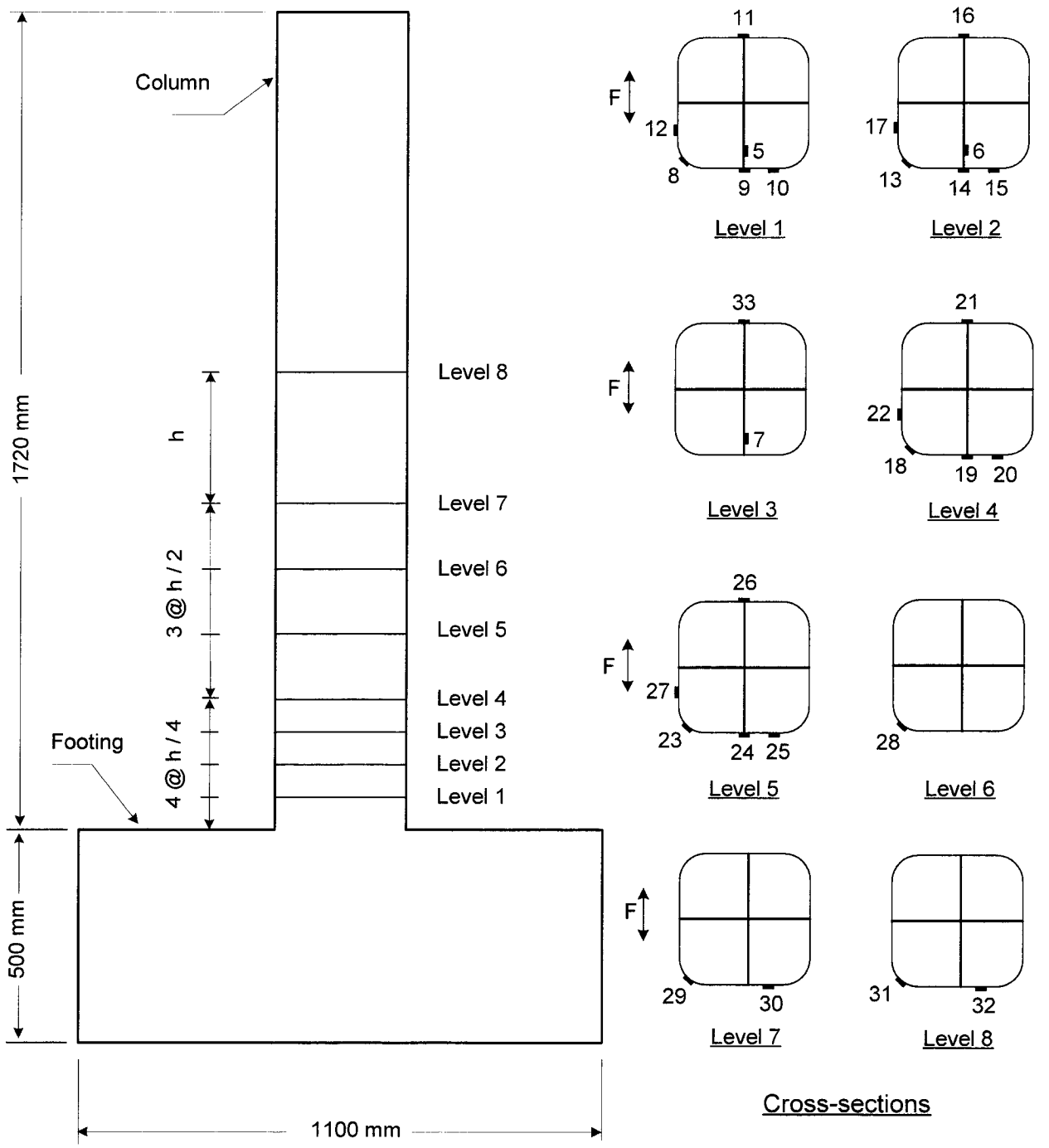

Fig. A.15 – Location of Strain Gages on the FRP Casing of Specimen RS-2

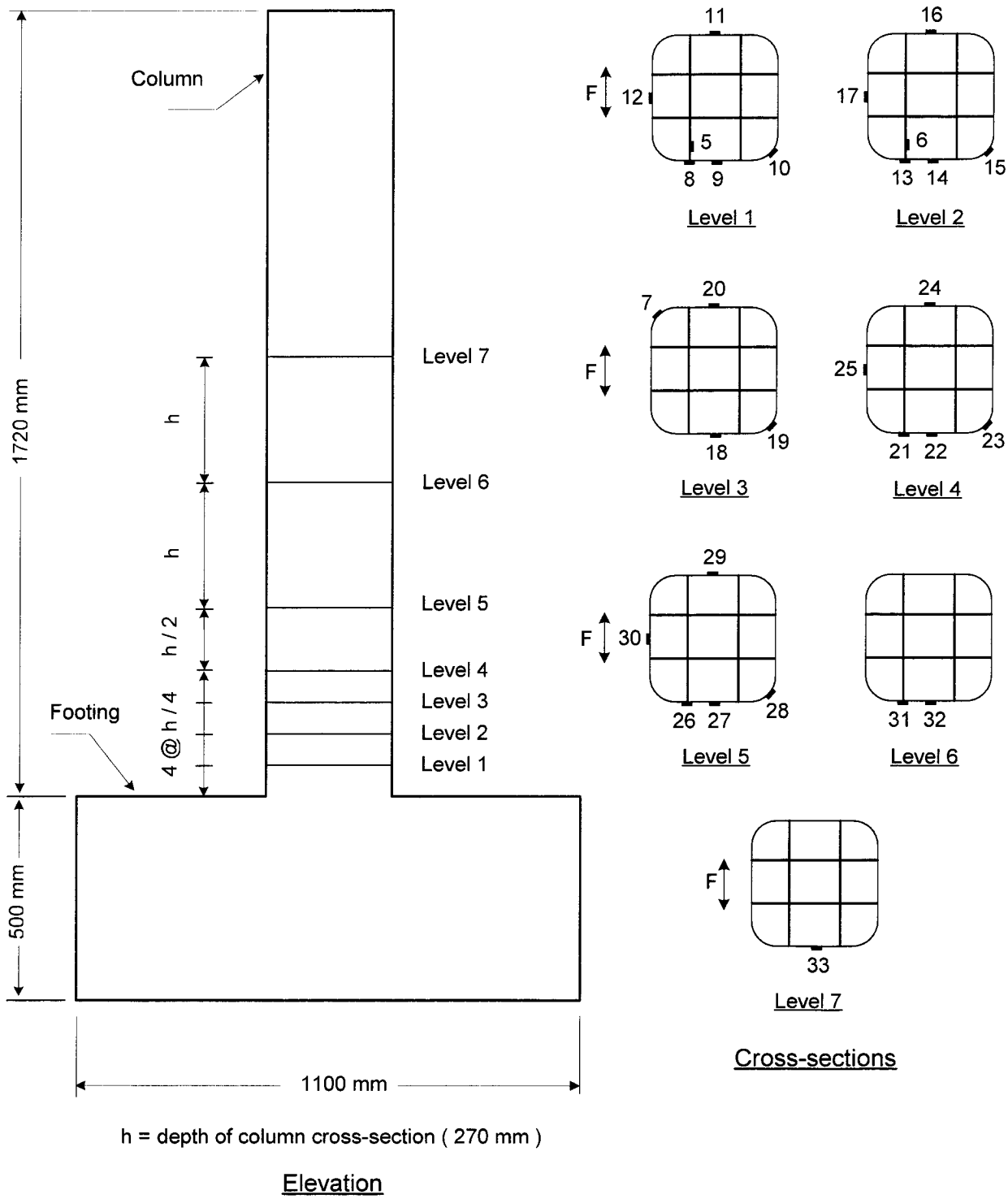

Fig. A.16 – Location of Strain Gages on the FRP Casing of Specimen RS-3

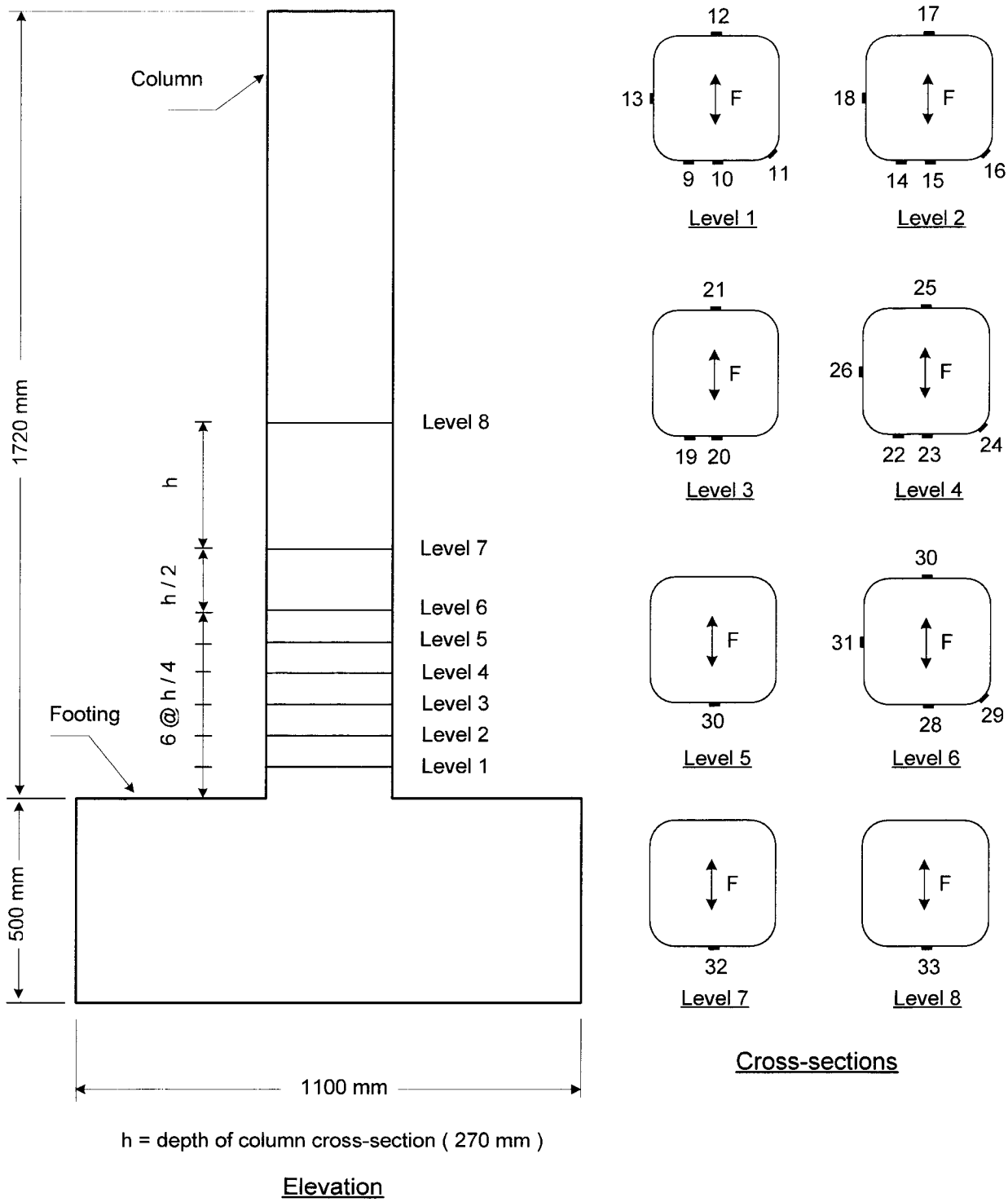

Fig. A.17 – Location of Strain Gages on the FRP Casing of Specimen RS-4

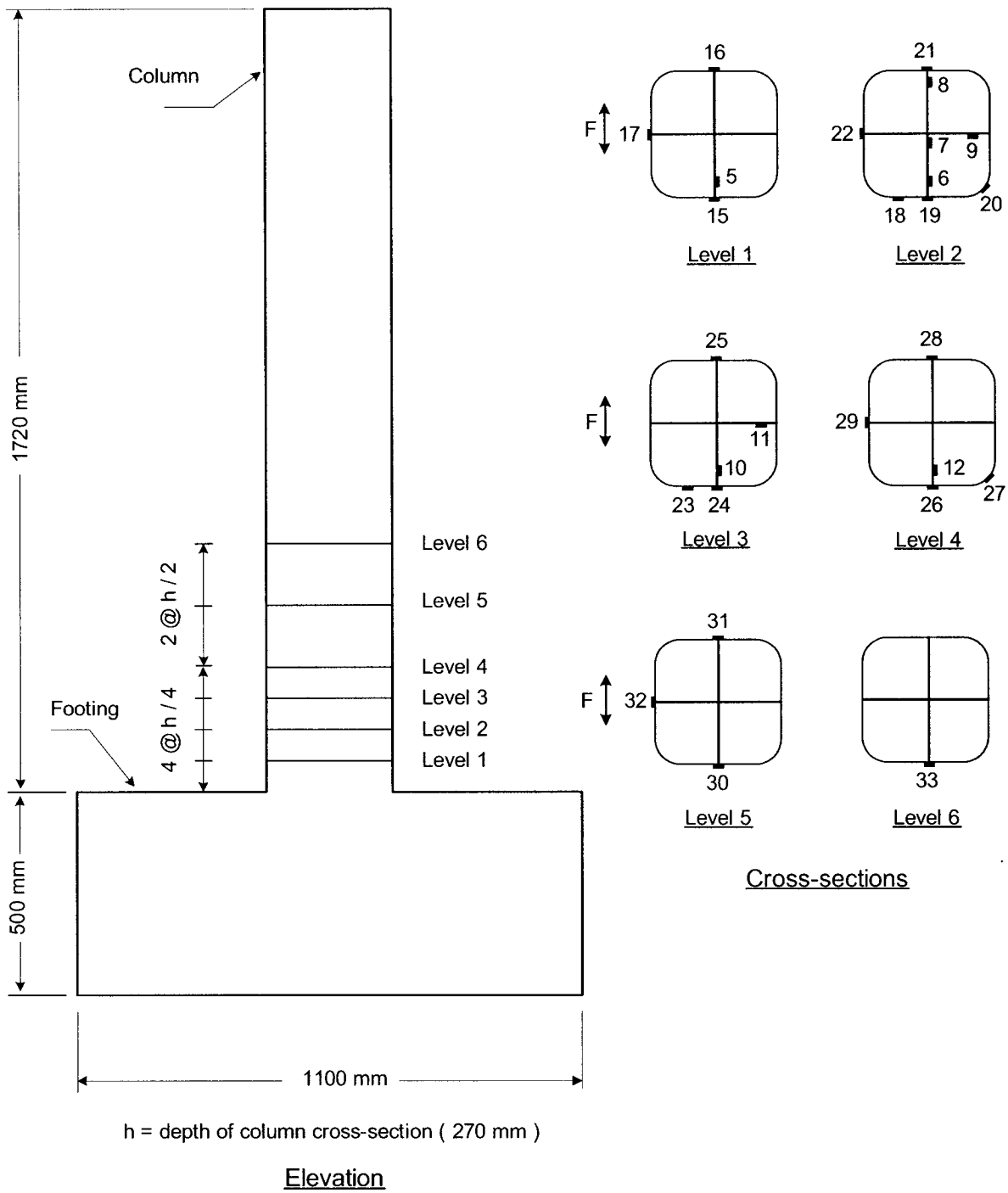

Fig. A.18 – Location of Strain Gages on the FRP Casing of Specimen RS-5

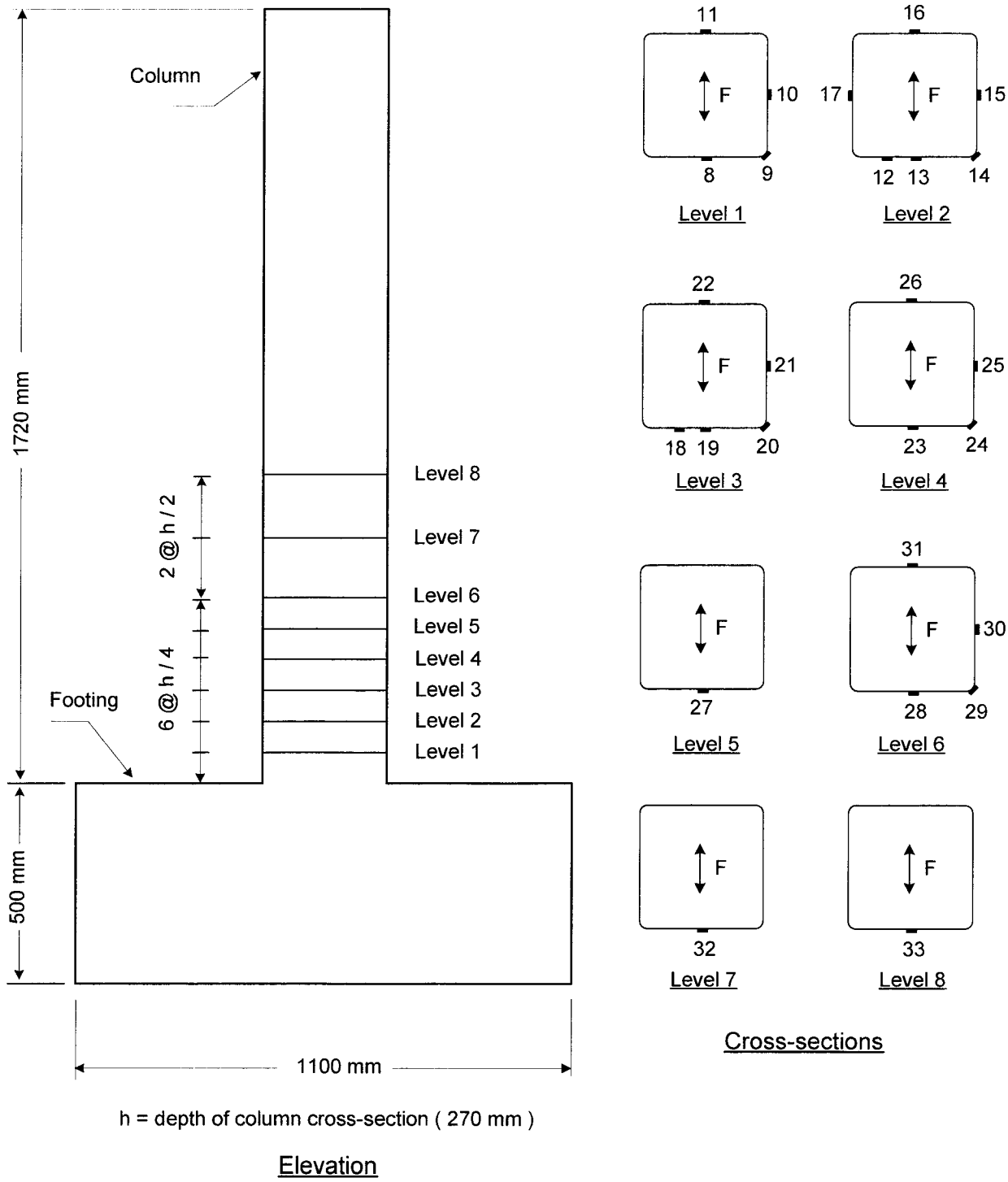

Fig. A.19 – Location of Strain Gages on the FRP Casing of Specimen RS-6

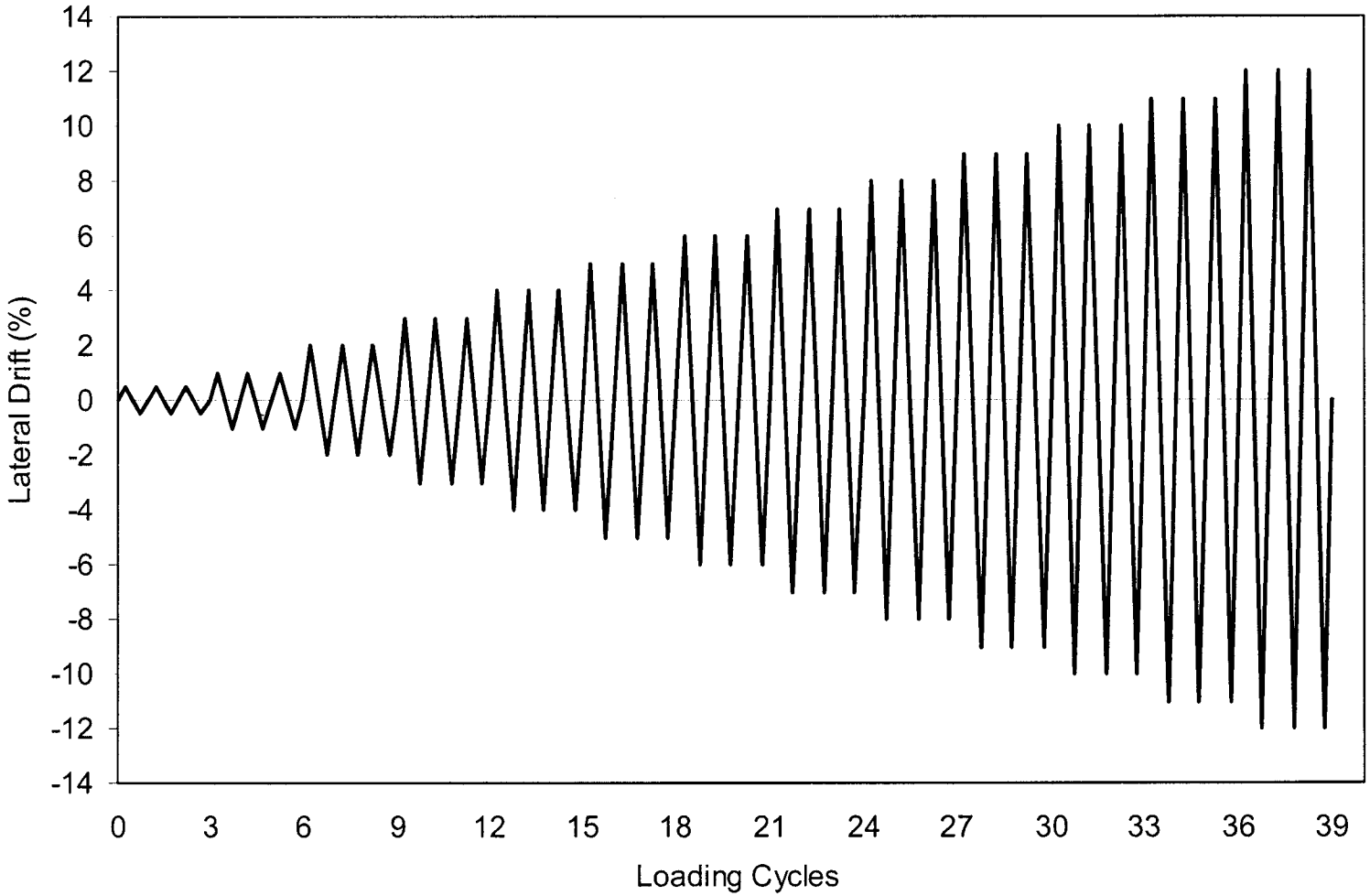

Fig. A.20 – Horizontal Loading Cycles

Appendix B

Preparation of Test Specimens

Table B.1 Concrete mix designs

Batch	Coarse Aggregate (kg)	Fine Aggregate (kg)	Cement (kg)	Total Water (kg)	Superplasticizer (L)	Retarder (L)	Water/ Cement Ratio
HSC-1	1122	726	555	122	20	1.6	0.22
HSC-2	1122	726	555	144	20	1.6	0.26
NSC	1130	740	370	163	4	N/A	0.44

Notes:

1. Coarse aggregate: 10 mm crushed limestone

2. HSC mixes contained Silica Fume Cement SF Type 10 (8% Silica fume blended with ordinary Portland Cement).

3. NSC mix contained ordinary Portland Cement Type 10.

4. Total water includes added water, moisture content of sand and aggregate, and water contents of superplasticizer and retarder.

5. Superplasticizer: Conchem S.P.N. Each liter of superplasticizer contained 0.708 kg water and 0.490 kg solids.

6. Retarder: Conchem Protard. Each liter contained 0.790 kg water and 0.410 kg solids.

Table B.2 Development of concrete compressive strength with time

Age (days)	HSC-1 (MPa)	HSC-2 (MPa)	NSC (MPa)
1	36.8	-	-
3	51.4	36.1	33.7
7	60.9	45.7	38.2
14	69.5	59.1	41.0
21	73.3	66.4	-
28	78.5	70.8	46.5
42	83.0	73.5	-
56	89.1	-	-
Test Period	90.1	75.3	49.7

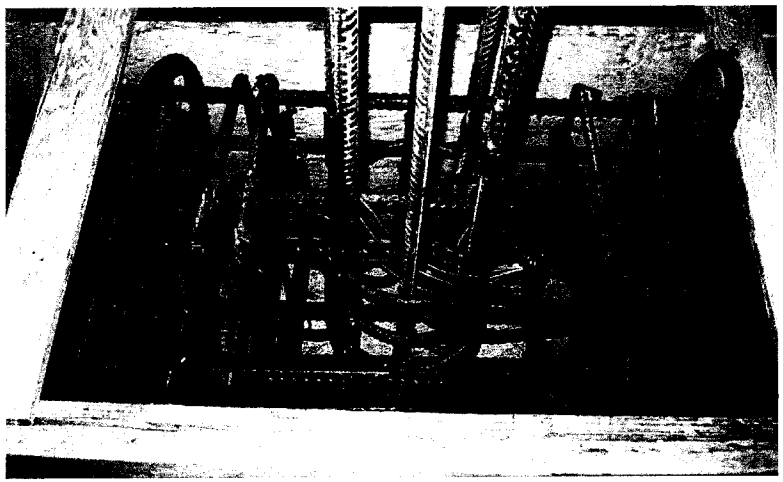

Fig. B.1 – Typical Footing Reinforcement Cage

(a) Before Casting **(b) After Casting**

Fig. B.2 – Casting of Footings

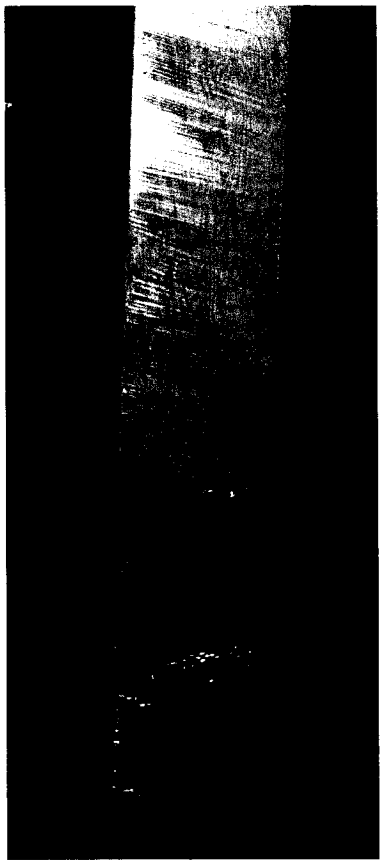

(a) Specimen RS-6

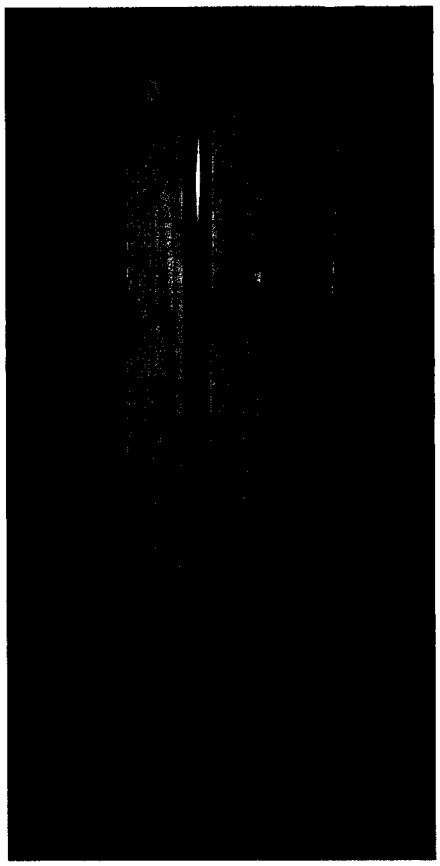

(b) Specimens RS-1 to RS-5

(c) Specimens RS-1 to RS-5

Fig. B.3 – Templates for Square Specimens

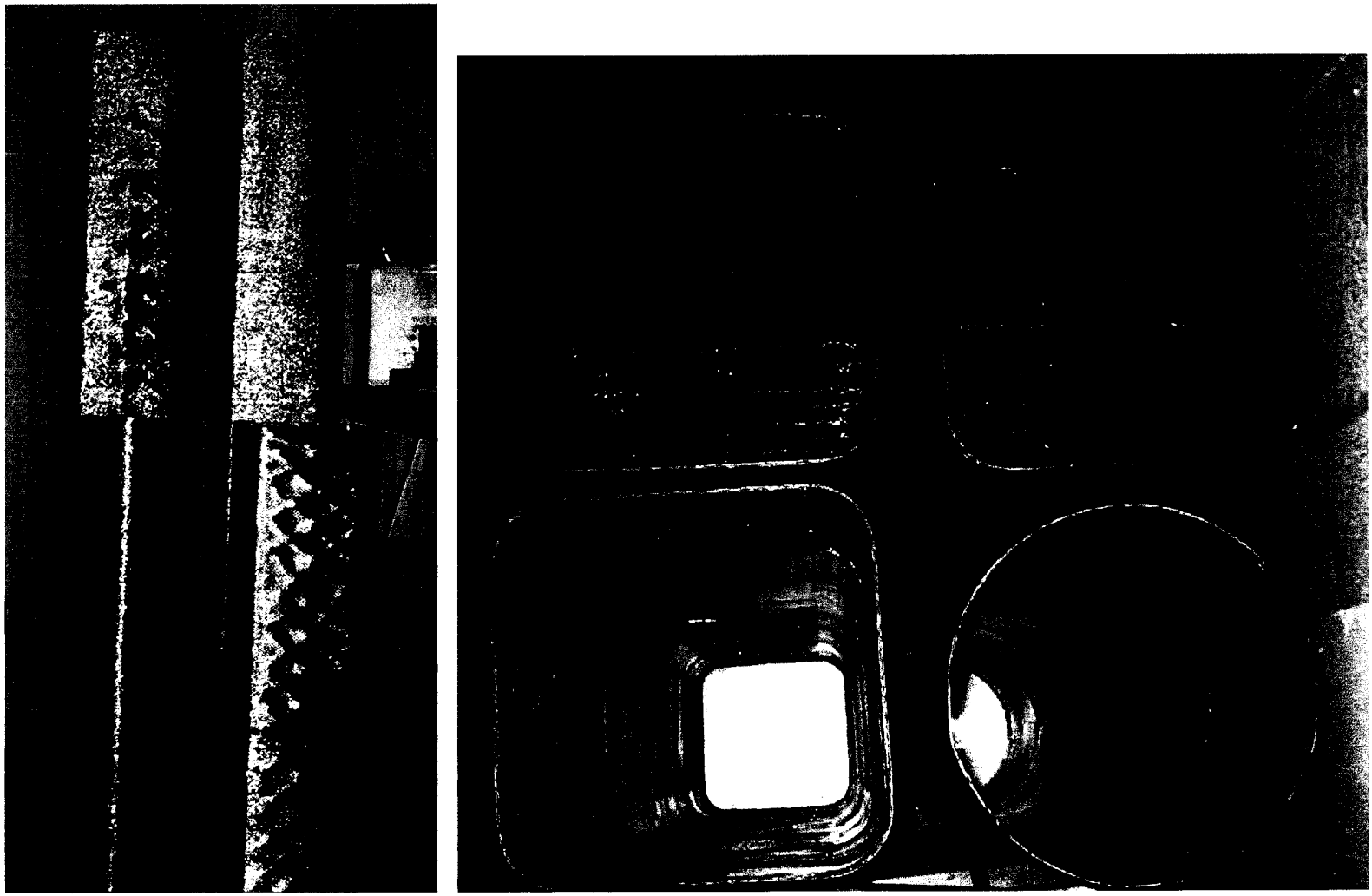

Fig. B.4 – FRP Casings

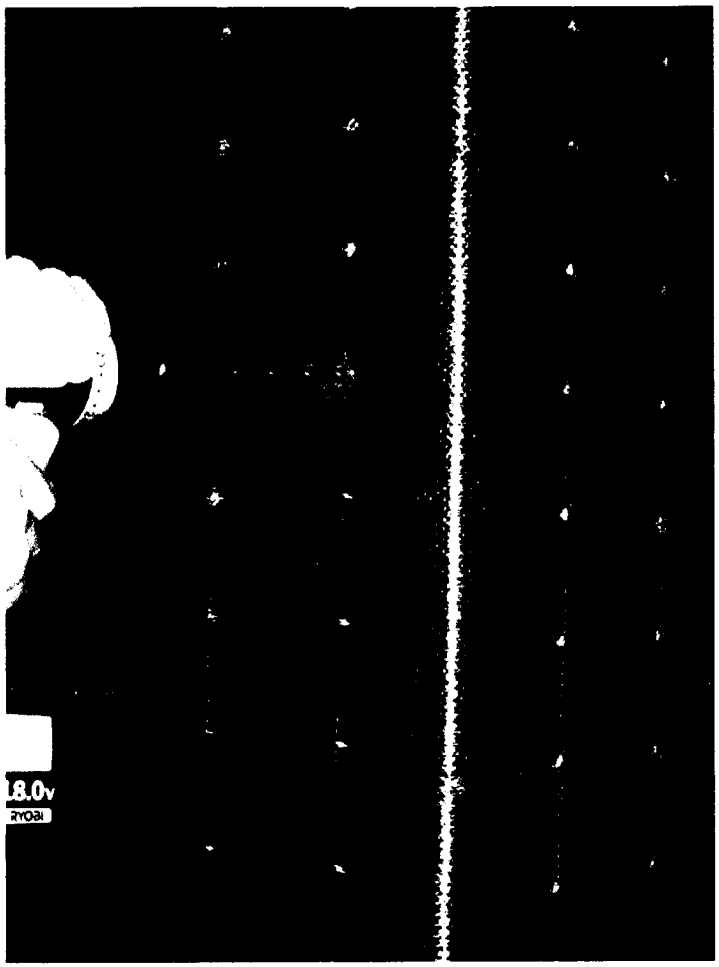

(a) Drilling of FRP Casing

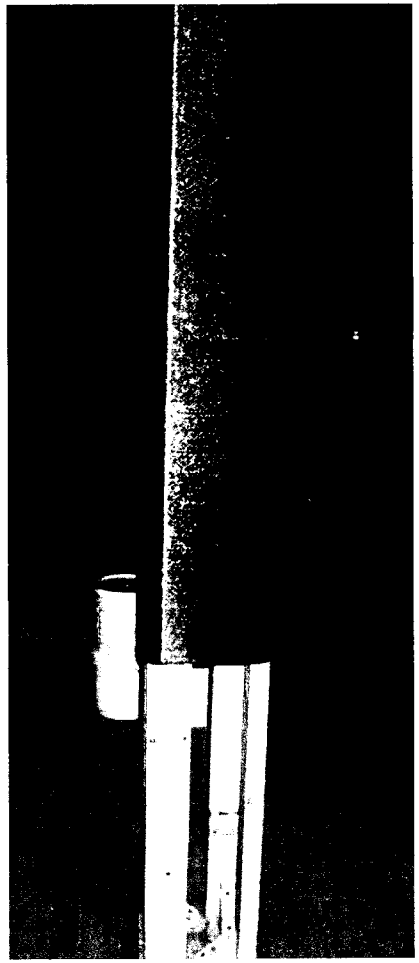

(b) Template for the Insertion of Crossties

Fig. B.5 – Preparation of FRP Casings with Crossties

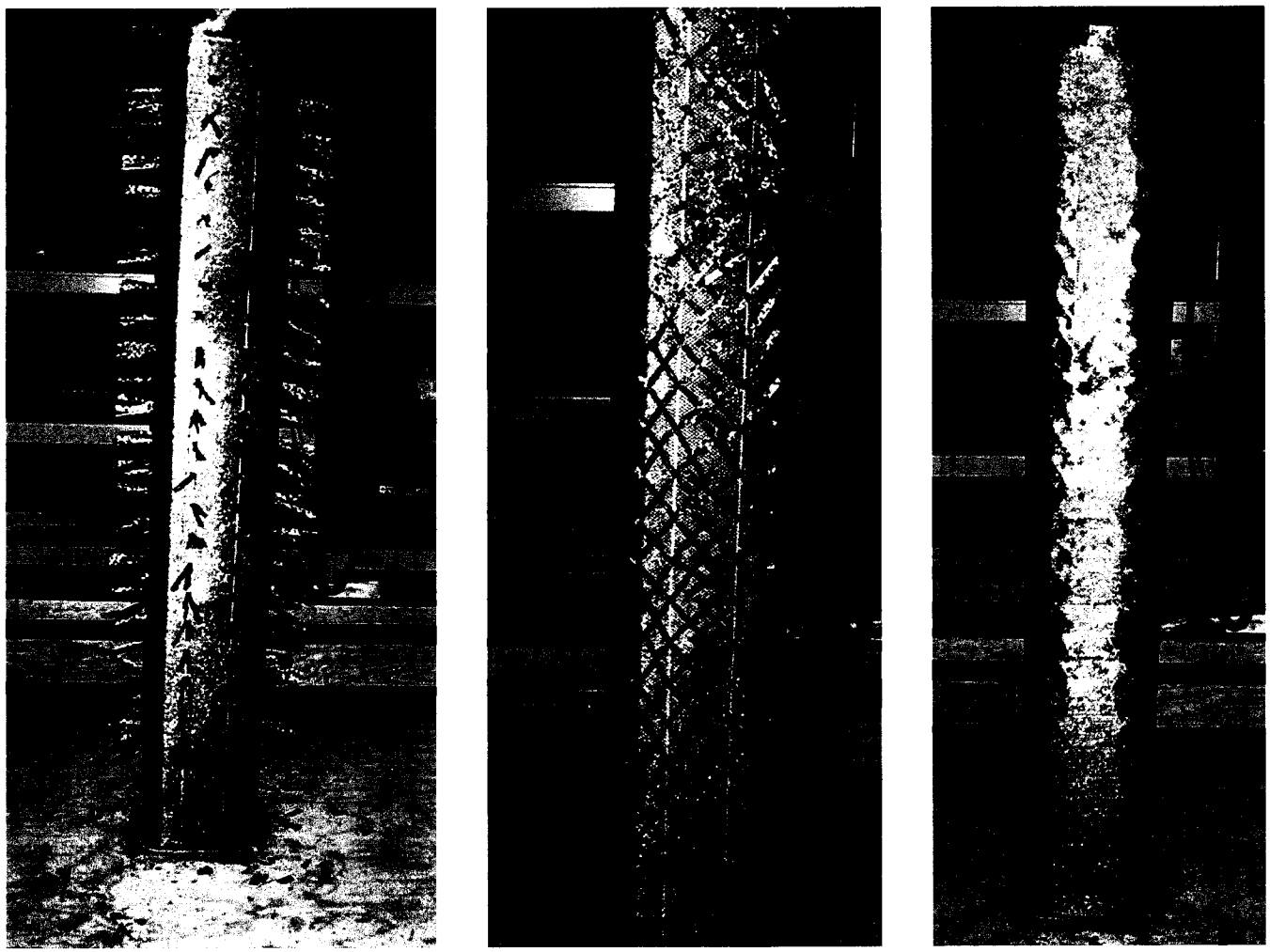

(a) Crossties Inserted (b) End fibres Glued on (c) Final Layer of FRP Sheet

Fig. B.6 – Placement of Crossties in Square Columns

Fig. B.7 – Specimens before Casting

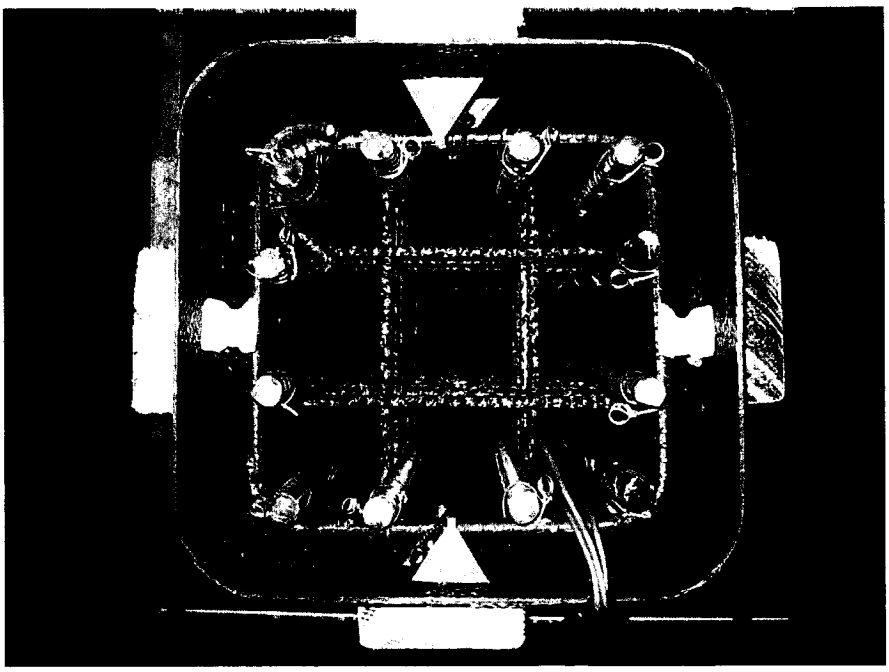

(a) Column RS-3

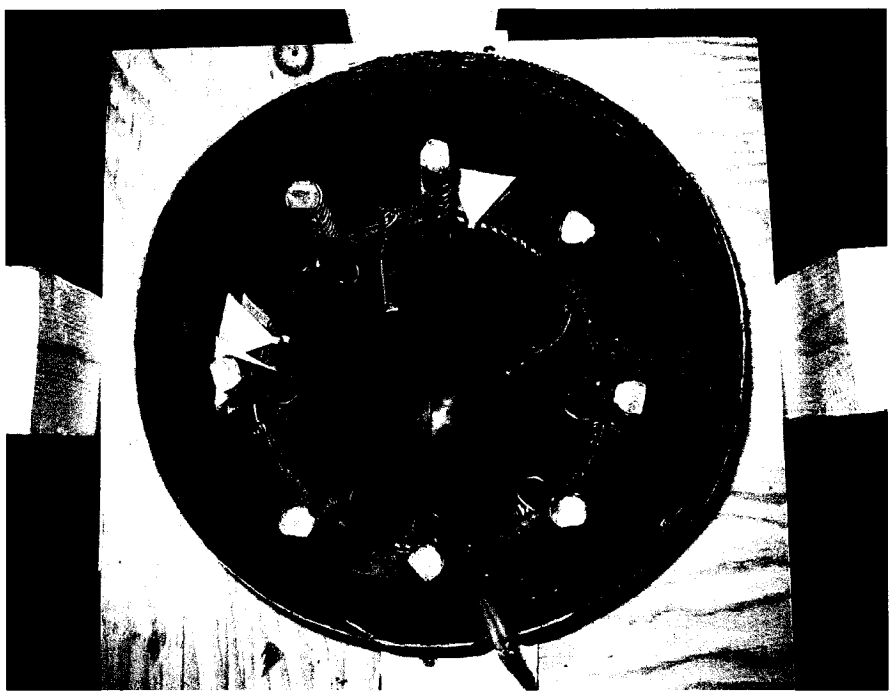

(b) Column RC-2

Fig. B.8 – Typical Column Cross-sections

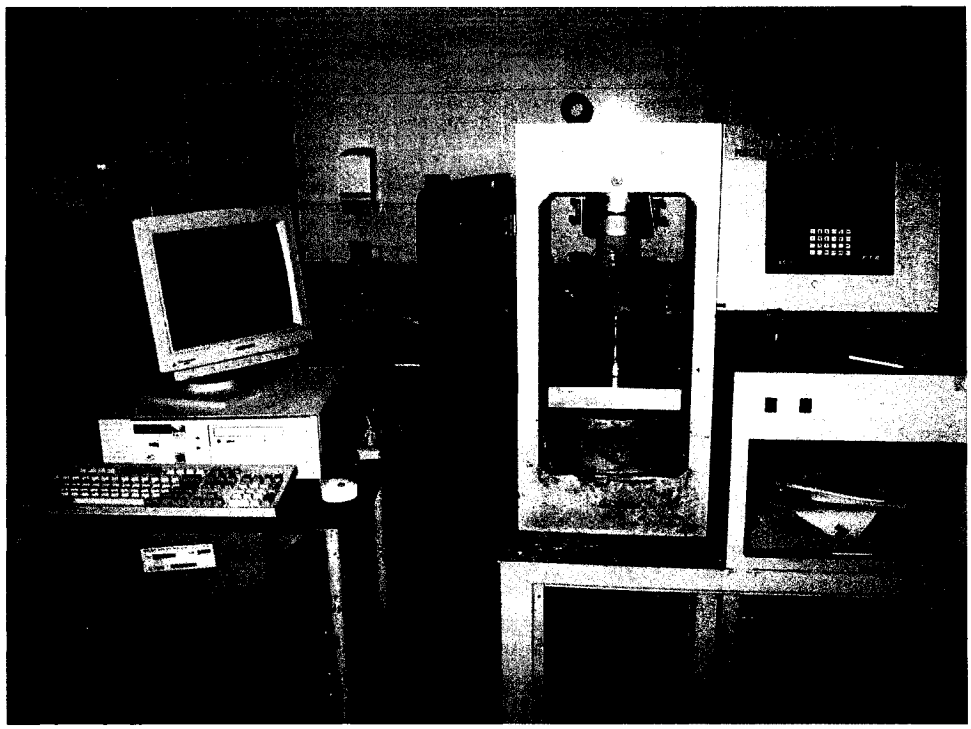

(a) Testing of Concrete Cylinders on a Forney Testing Machine

(b) HSC Specimen at the End of Testing

Fig. B.9 – Testing of Concrete Cylinders

Appendix C

Specimens during Testing

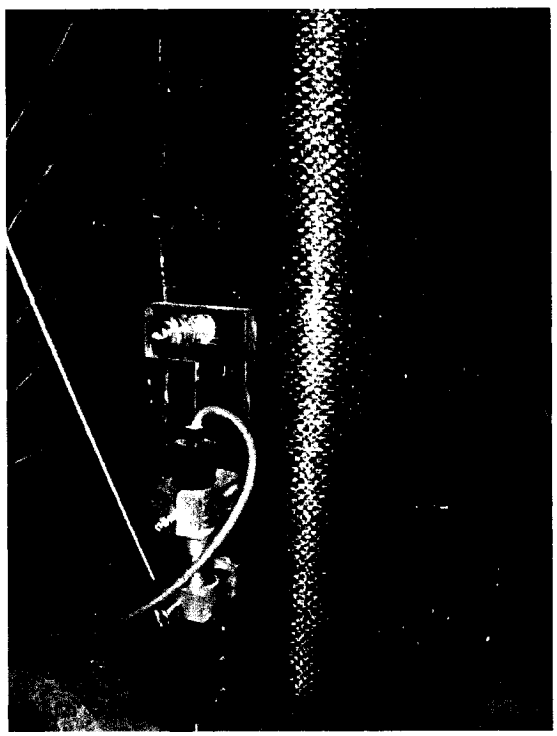

(a) At 4% Drift

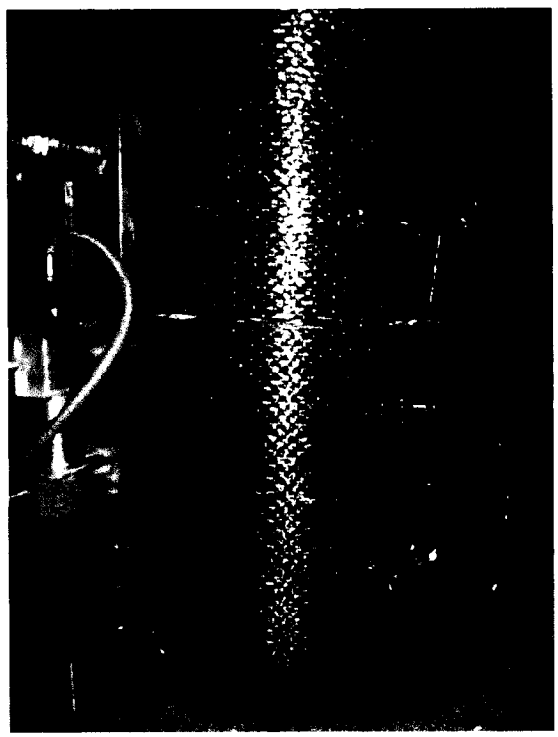

(b) At 7% Drift

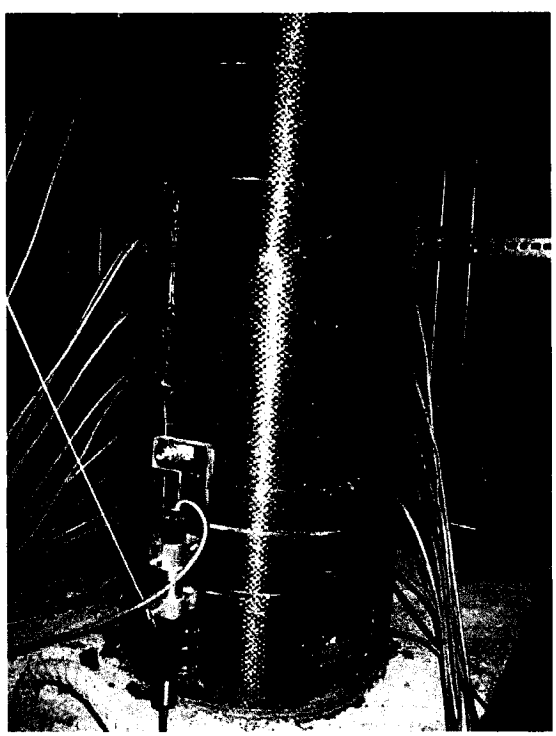

(c) At 10% Drift

(d) At 12% Drift

Fig. C.1 – Extent of Damage for Column RC-1 at Different Stages of Testing

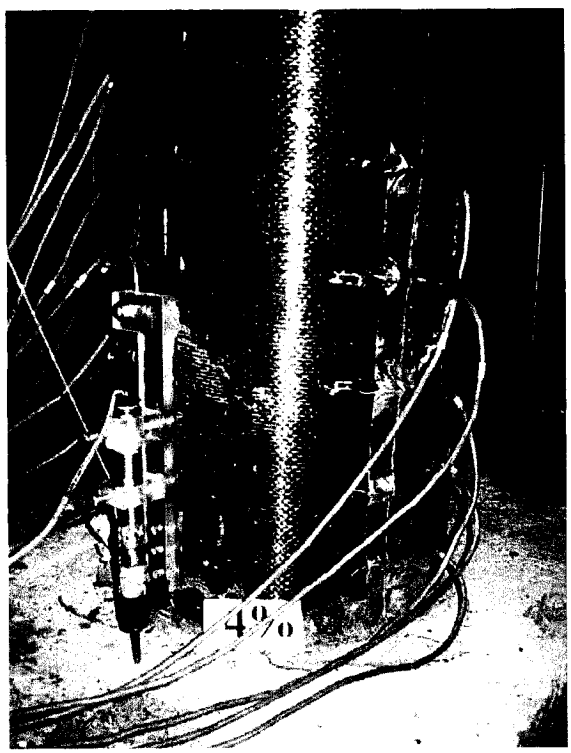

(a) At 4% Drift

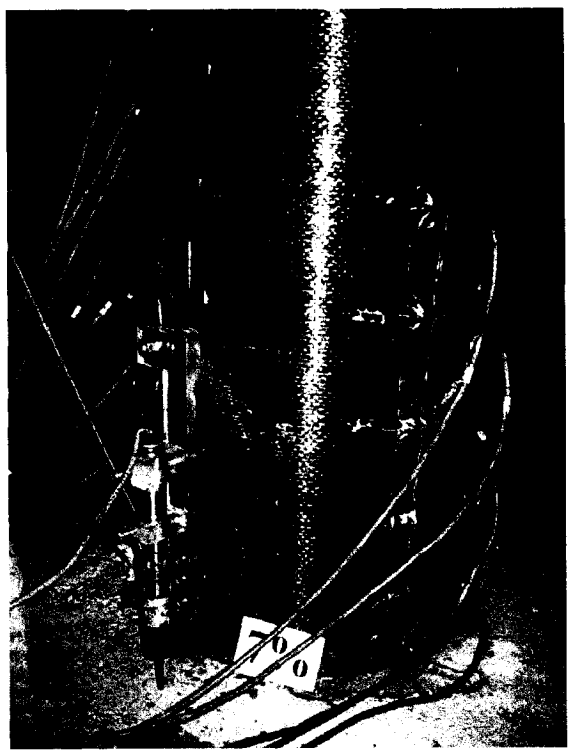

(b) At 7% Drift

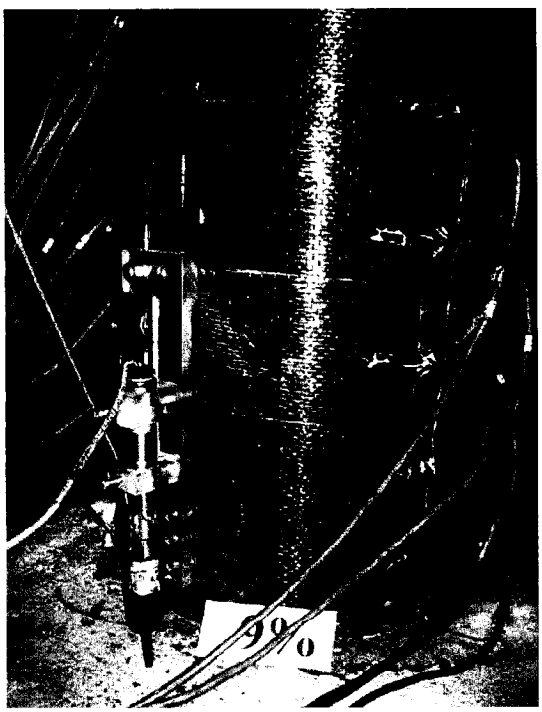

(c) At 9% Drift

(d) At 12% Drift

Fig. C.2 – Extent of Damage for Column RC-2 at Different Stages of Testing

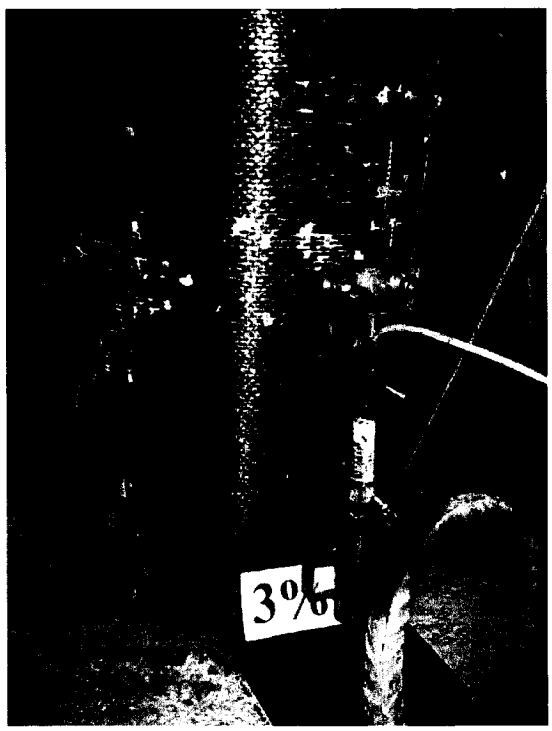

(a) At 3% Drift

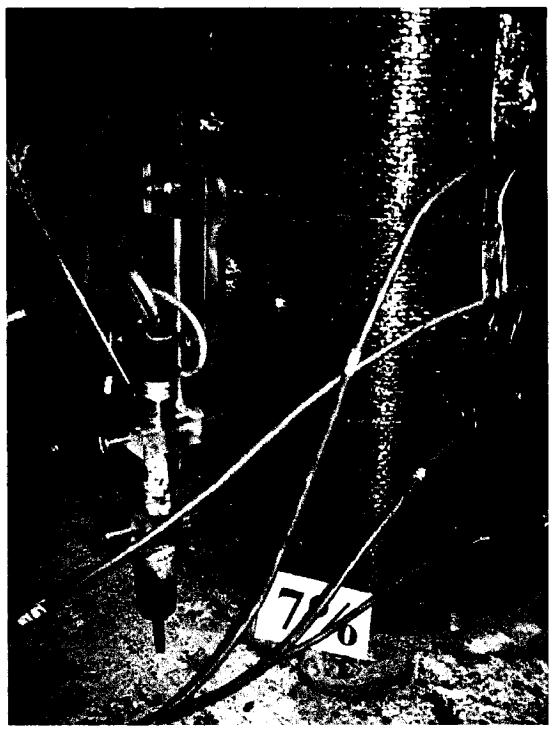

(b) At 7% Drift

(c) At 9% Drift

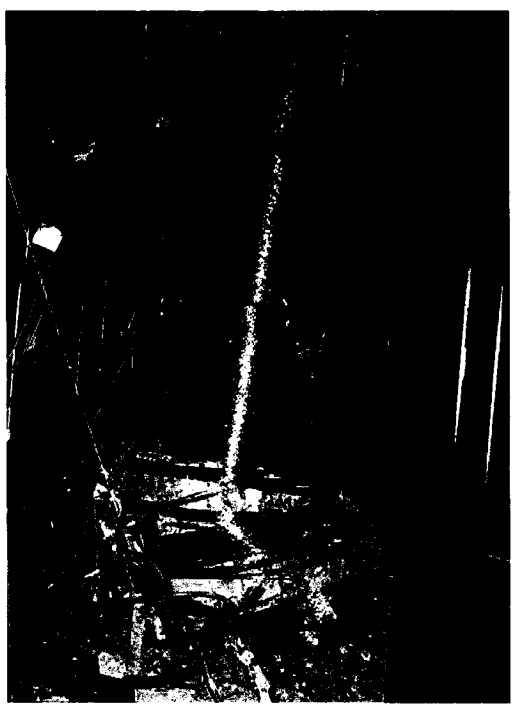

(d) At 10% Drift

Fig. C.3 – Extent of Damage for Column RC-3 at Different Stages of Testing

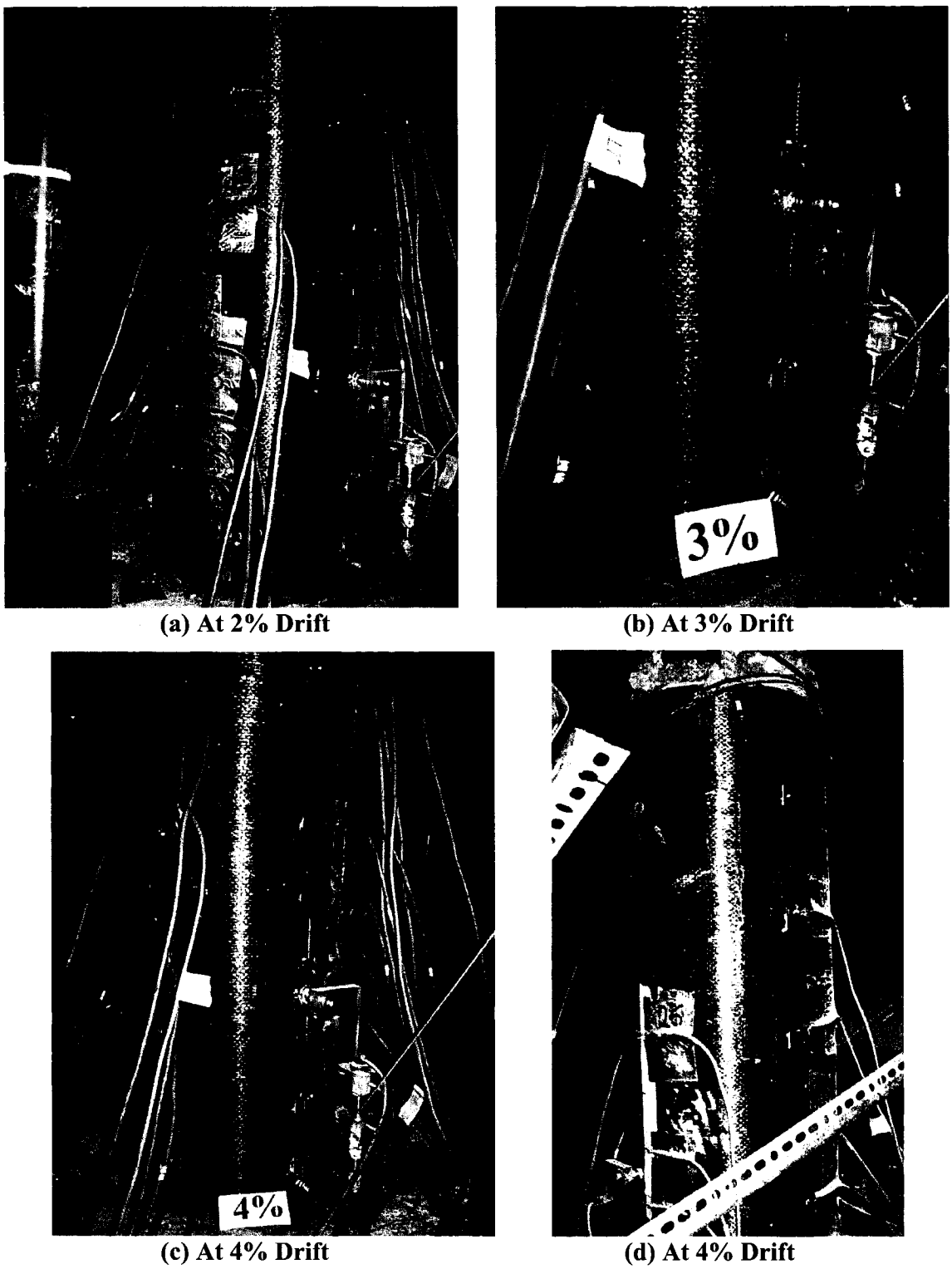

(a) At 2% Drift (b) At 3% Drift

(c) At 4% Drift (d) At 4% Drift

Fig. C.4 – Extent of Damage for Column RC-4 at Different Stages of Testing

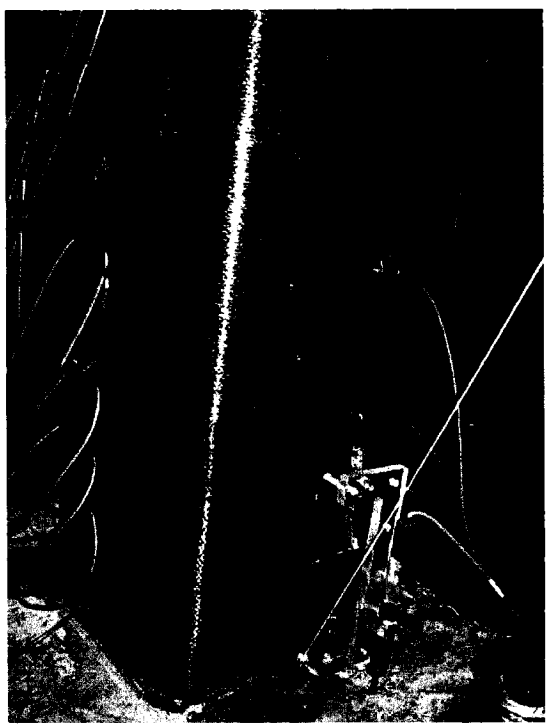

(a) At 3% Drift

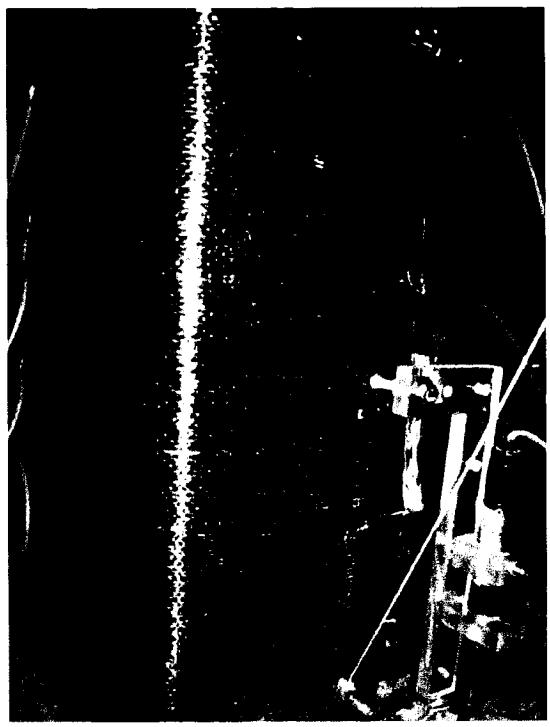

(b) At 7% Drift

(c) At 9% Drift

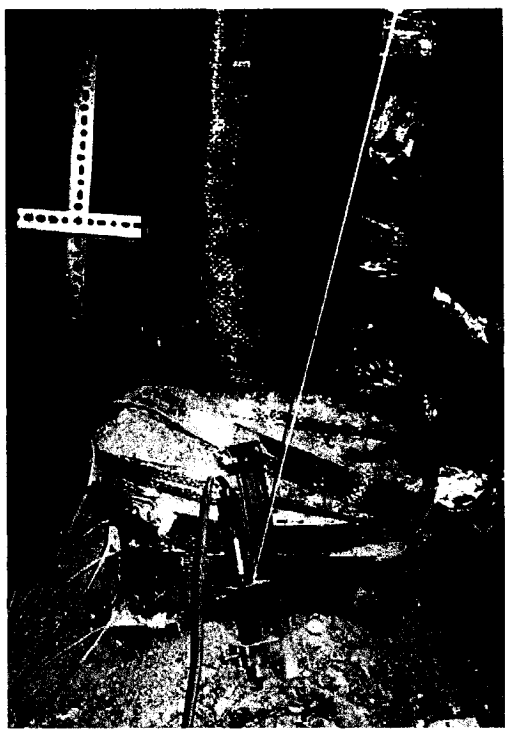

(d) At 10% Drift

Fig. C.5 – Extent of Damage for Column RS-1 at Different Stages of Testing

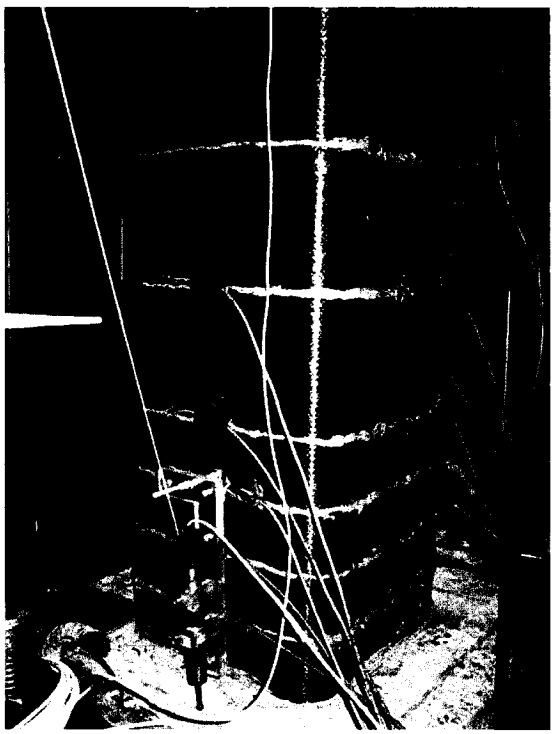

(a) At 3% Drift

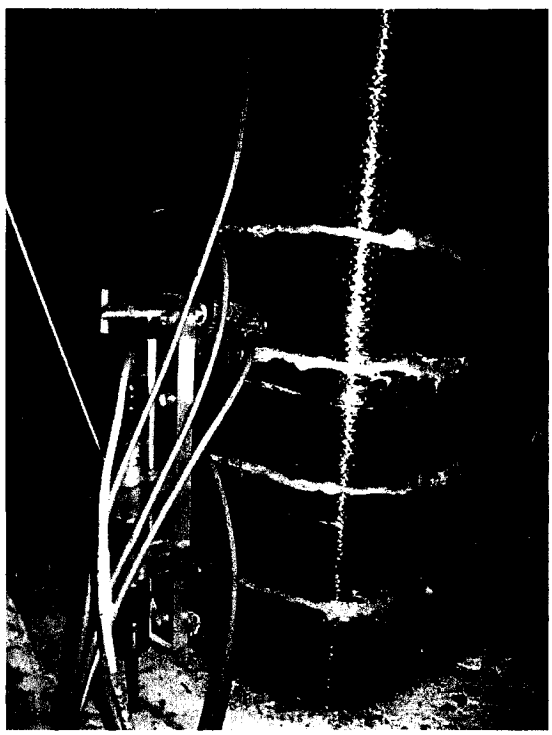

(b) At 6% Drift

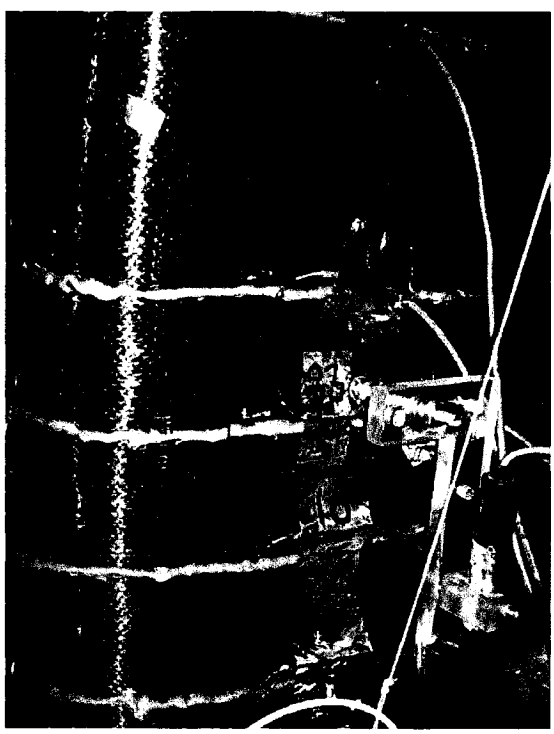

(c) At 8% Drift

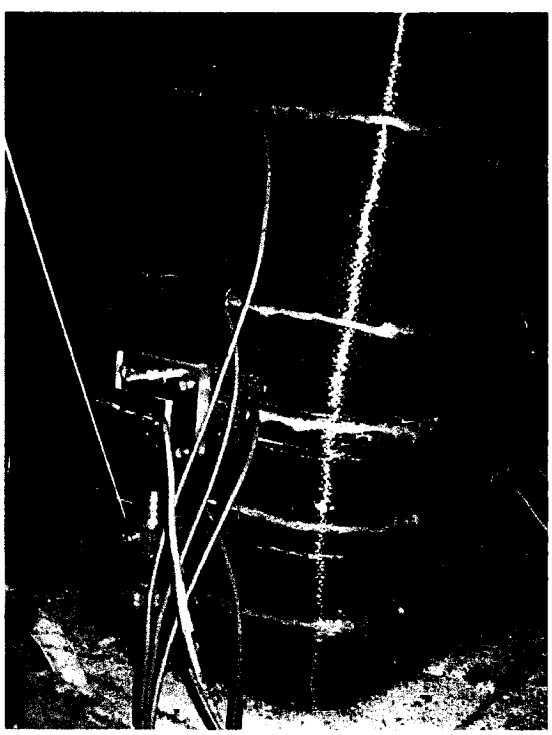

(d) At 9% Drift

Fig. C.6 – Extent of Damage for Column RS-2 at Different Stages of Testing

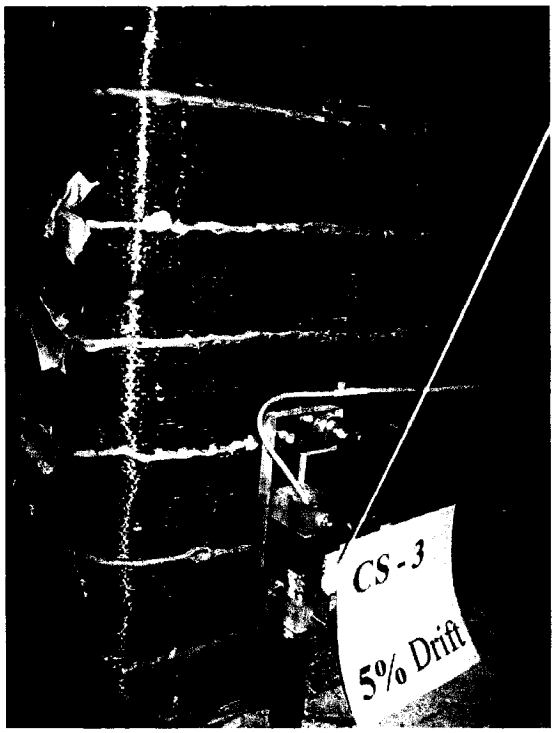

(a) At 5% Drift

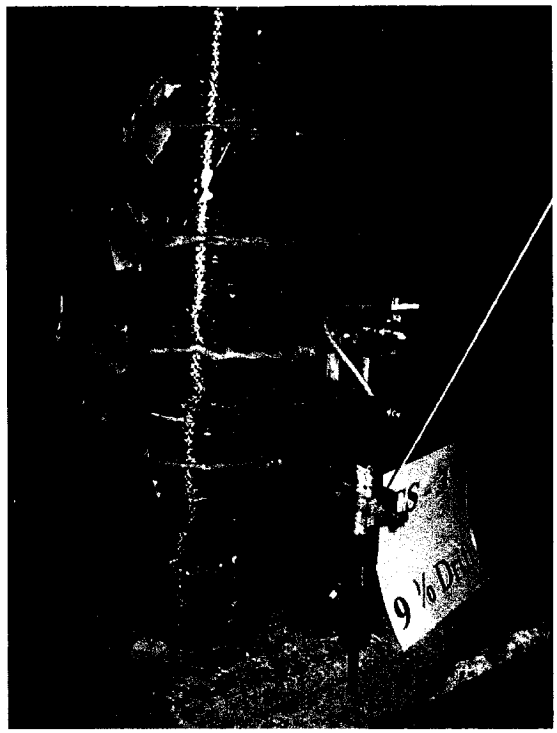

(b) At 9% Drift

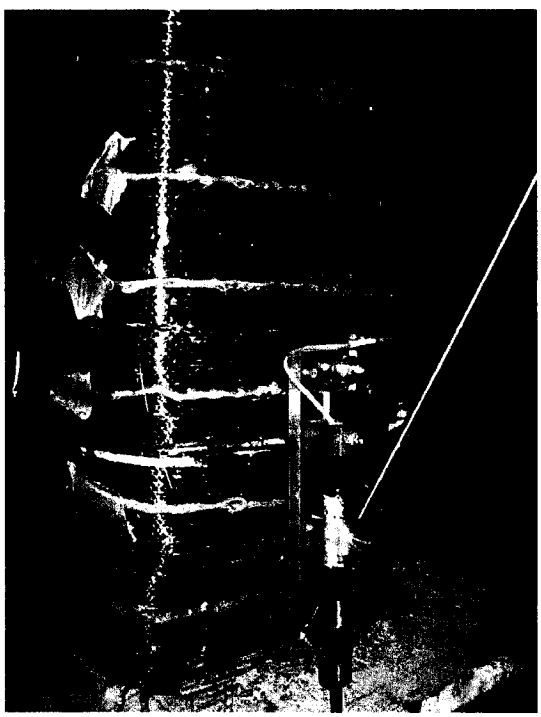

(c) At 11% Drift

(d) At 12% Drift

Fig. C.7 – Extent of Damage for Column RS-3 at Different Stages of Testing

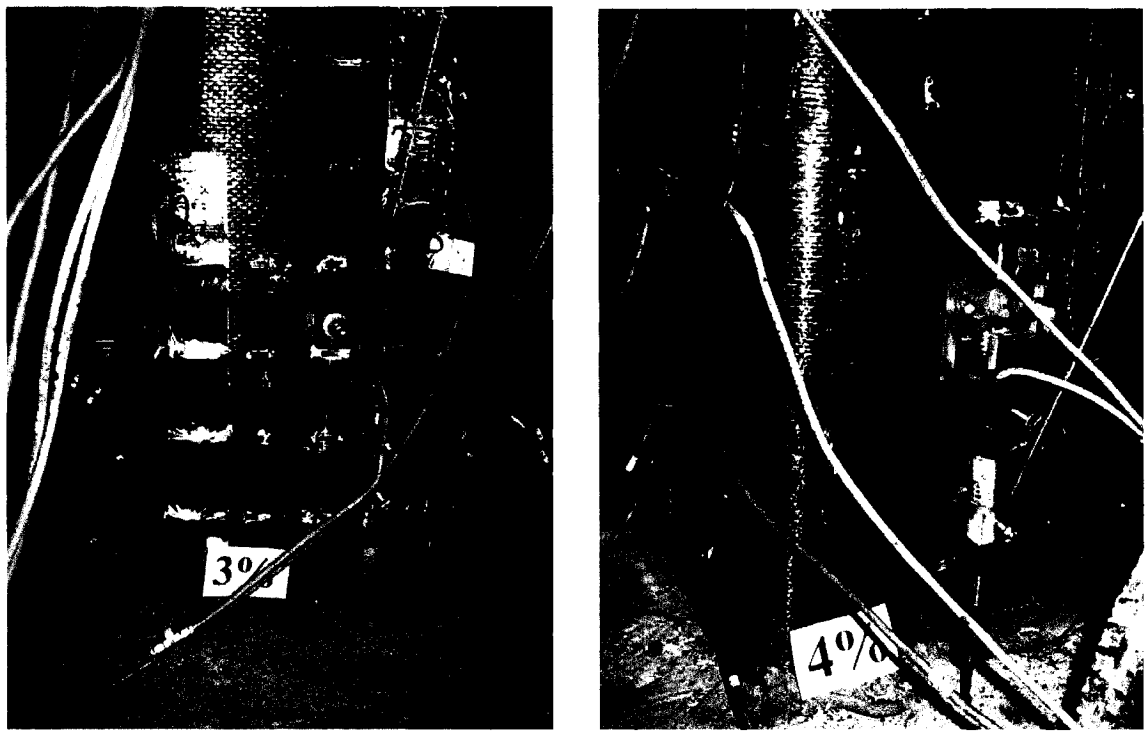

(a) At 3% Drift (b) At 4% Drift

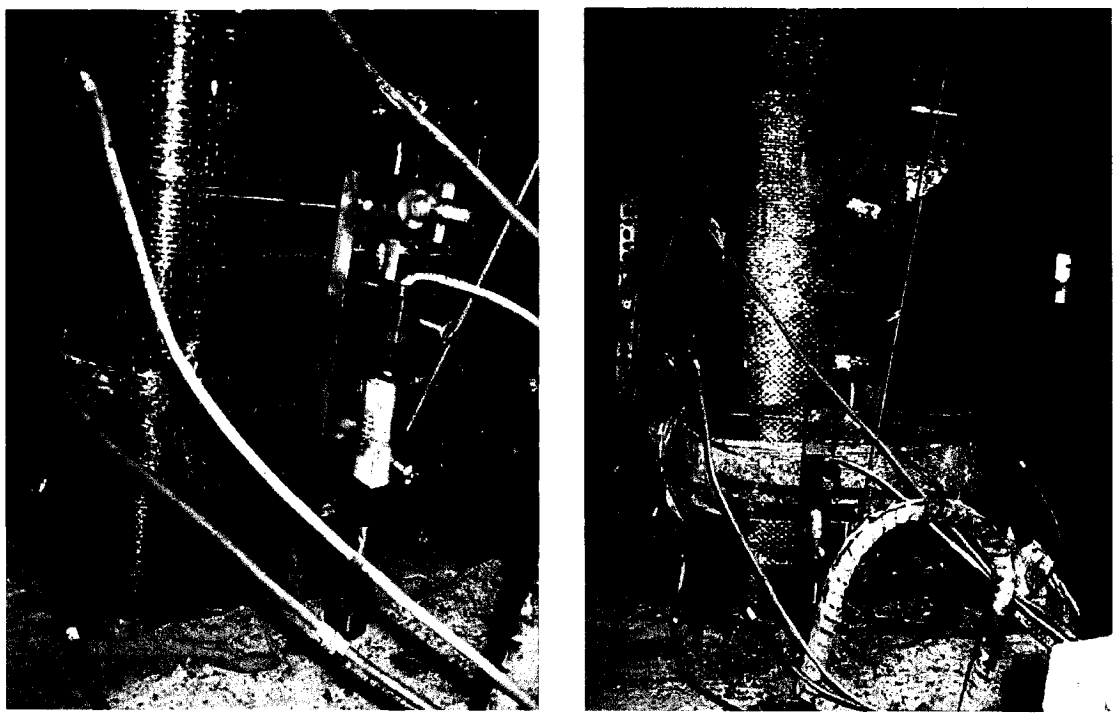

(c) At 5% Drift (d) At 6% Drift

Fig. C.8 – Extent of Damage for Column RS-4 at Different Stages of Testing

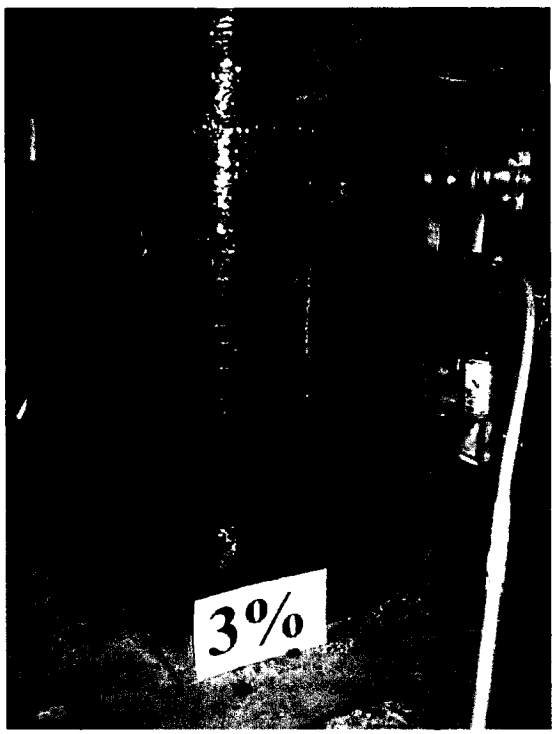

(a) At 3% Drift

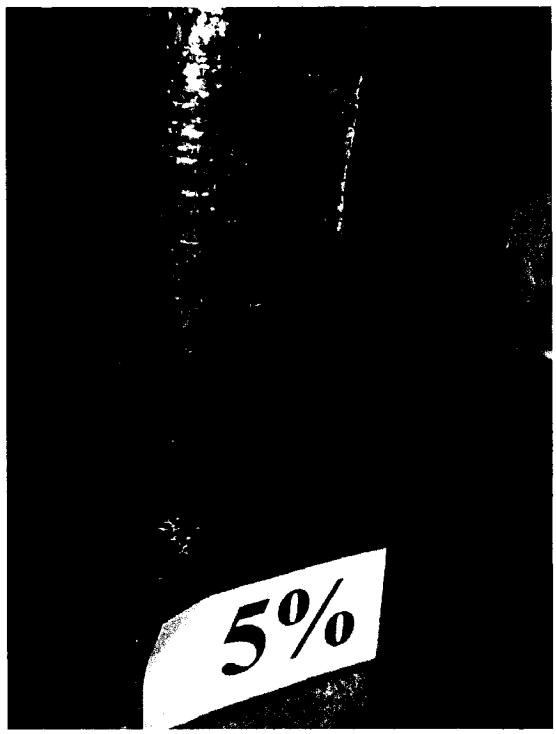

(b) At 4% Drift

(c) At 6% Drift

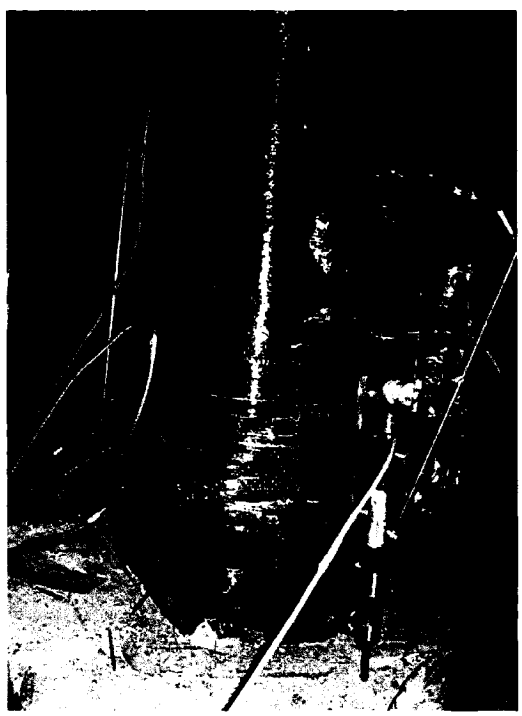

(d) At 6% Drift

Fig. C.9 – Extent of Damage for Column RS-5 at Different Stages of Testing

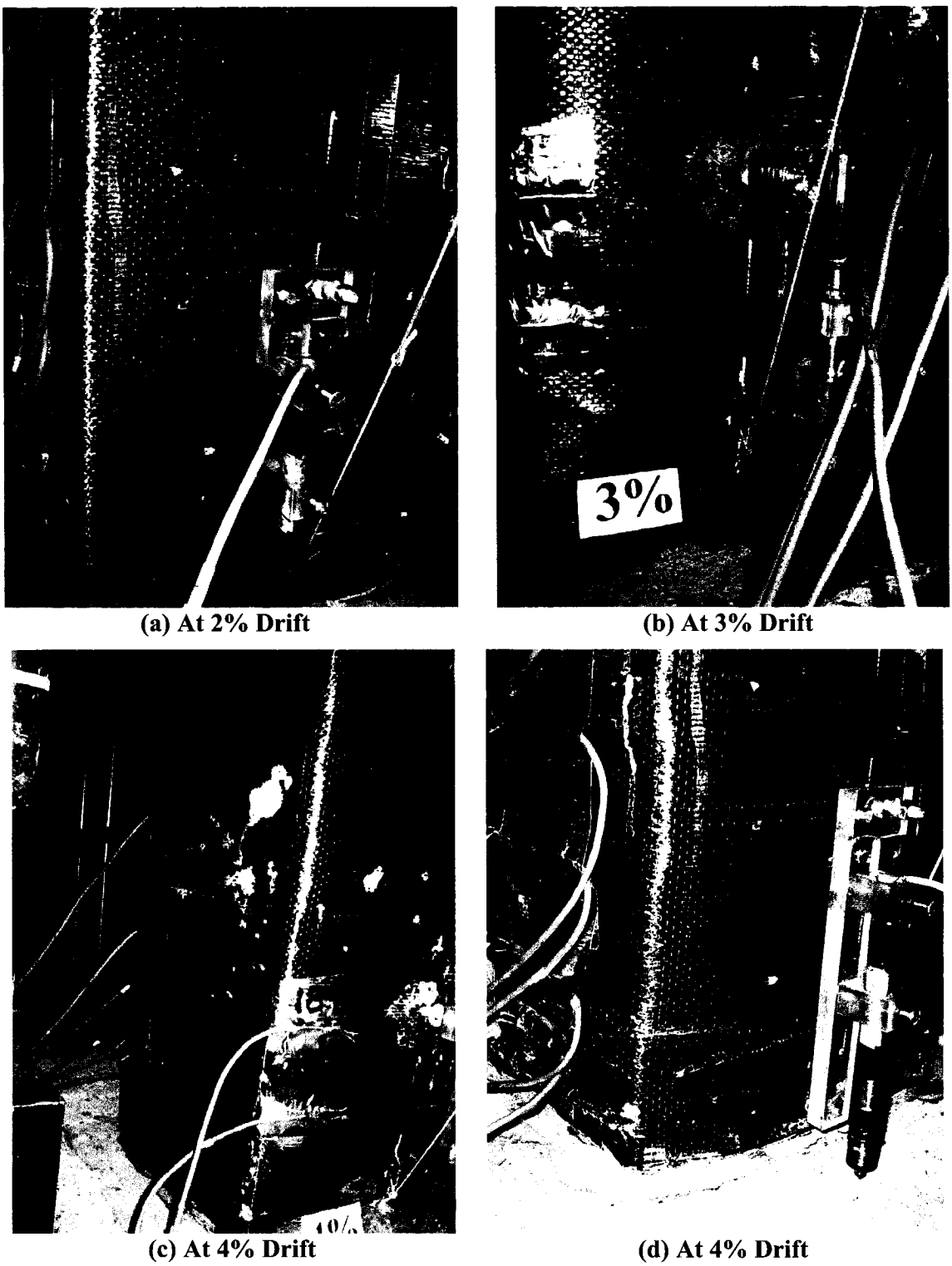

(a) At 2% Drift (b) At 3% Drift

(c) At 4% Drift (d) At 4% Drift

Fig. C.10 – Extent of Damage for Column RS-6 at Different Stages of Testing

Appendix D

Additional Recorded Test Data

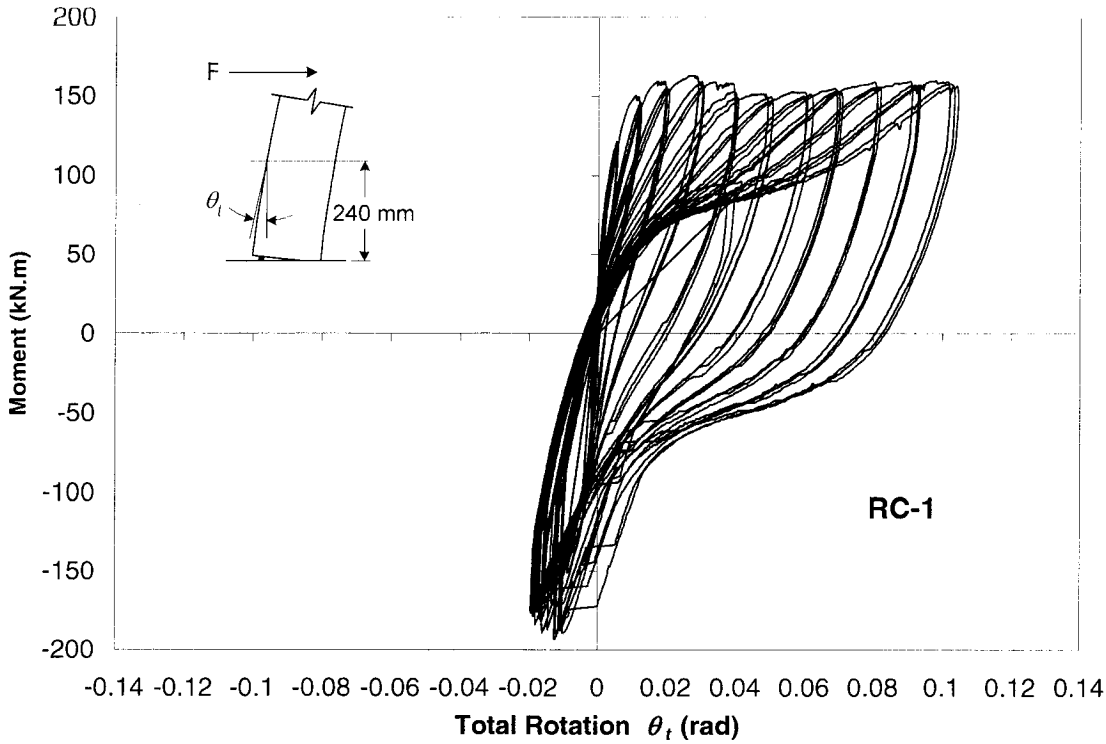

Fig. D.1 – Base Moment-Total Rotation Relationship for Column RC-1

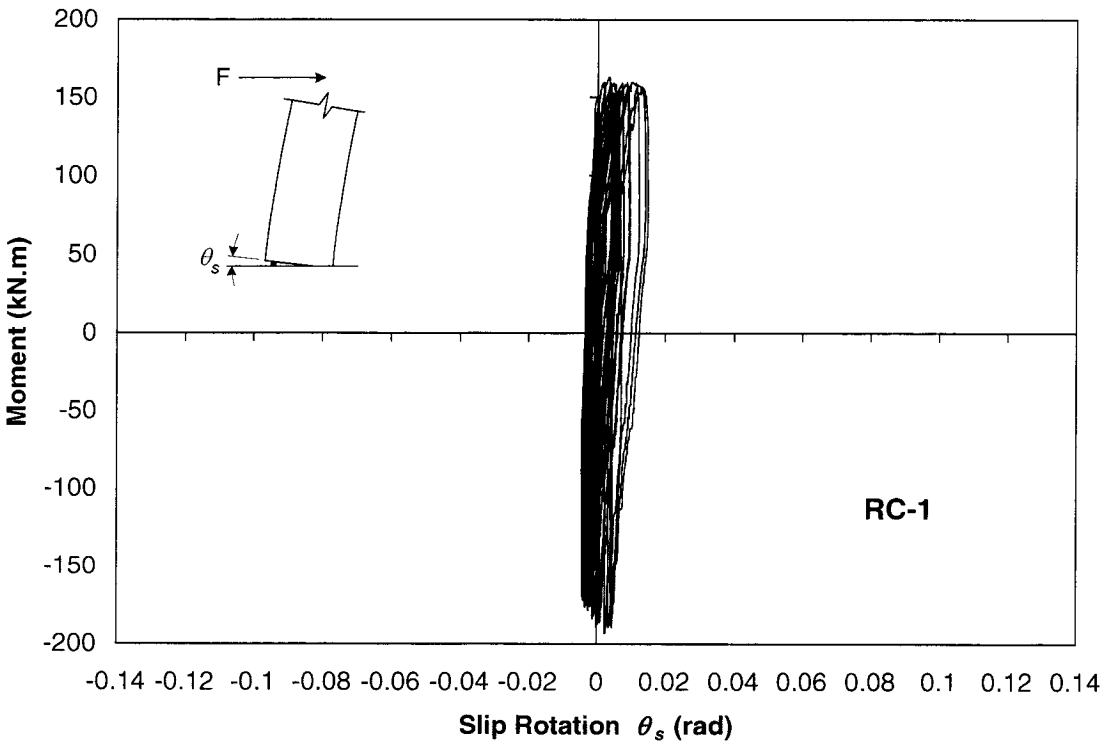

Fig. D.2 – Base Moment-Slip Rotation Relationship for Column RC-1

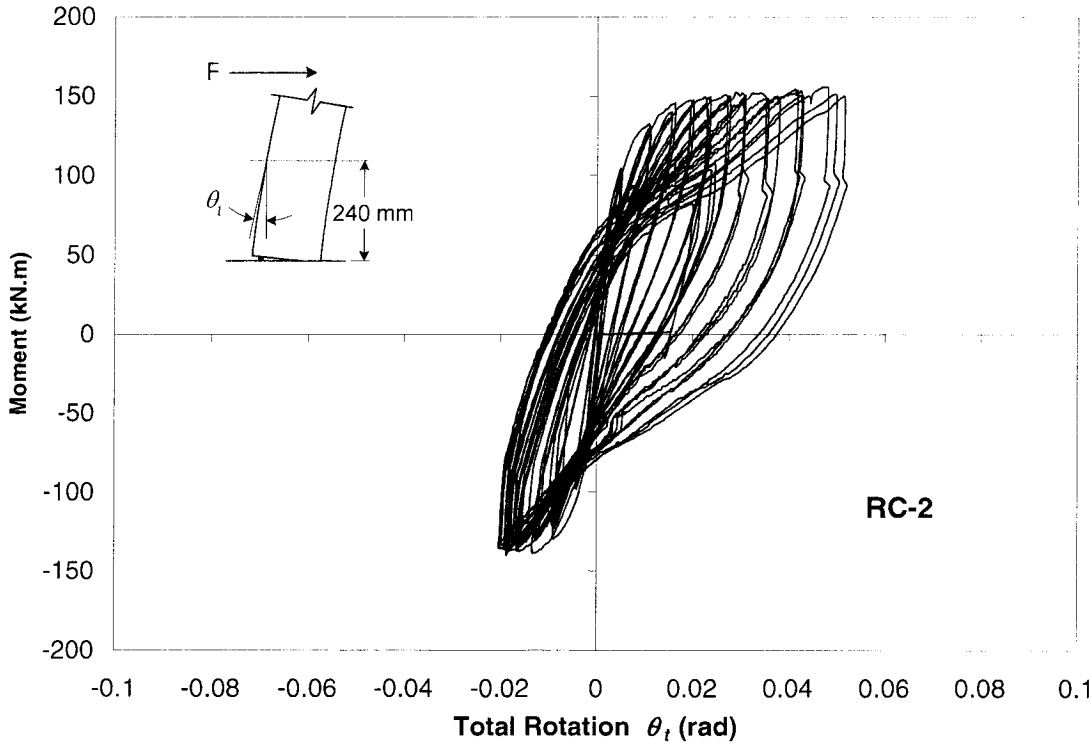

Fig. D.3 – Base Moment-Total Rotation Relationship for Column RC-2

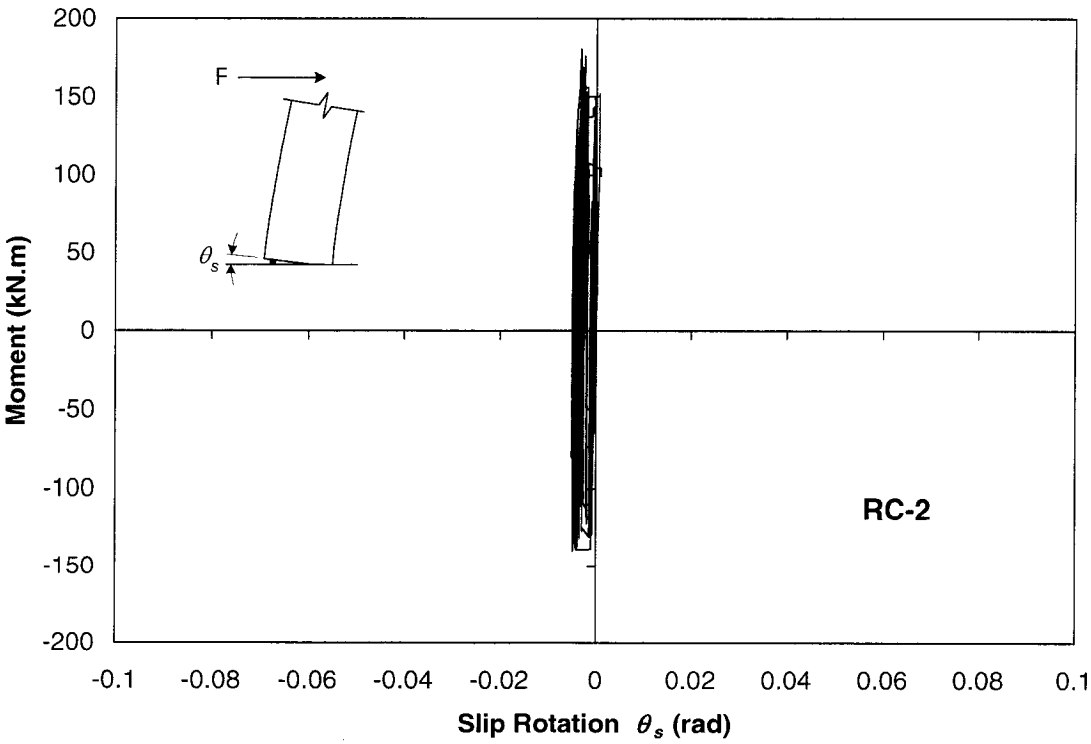

Fig. D.4 – Base Moment-Slip Rotation Relationship for Column RC-2

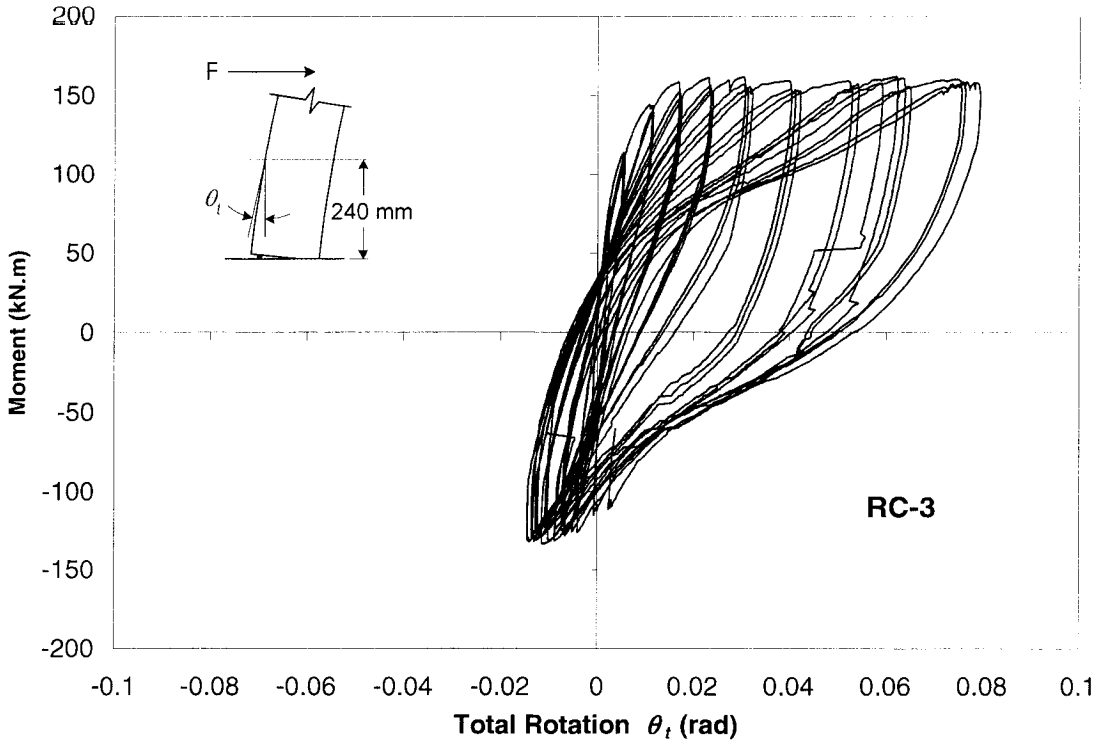

Fig. D.5 – Base Moment-Total Rotation Relationship for Column RC-3

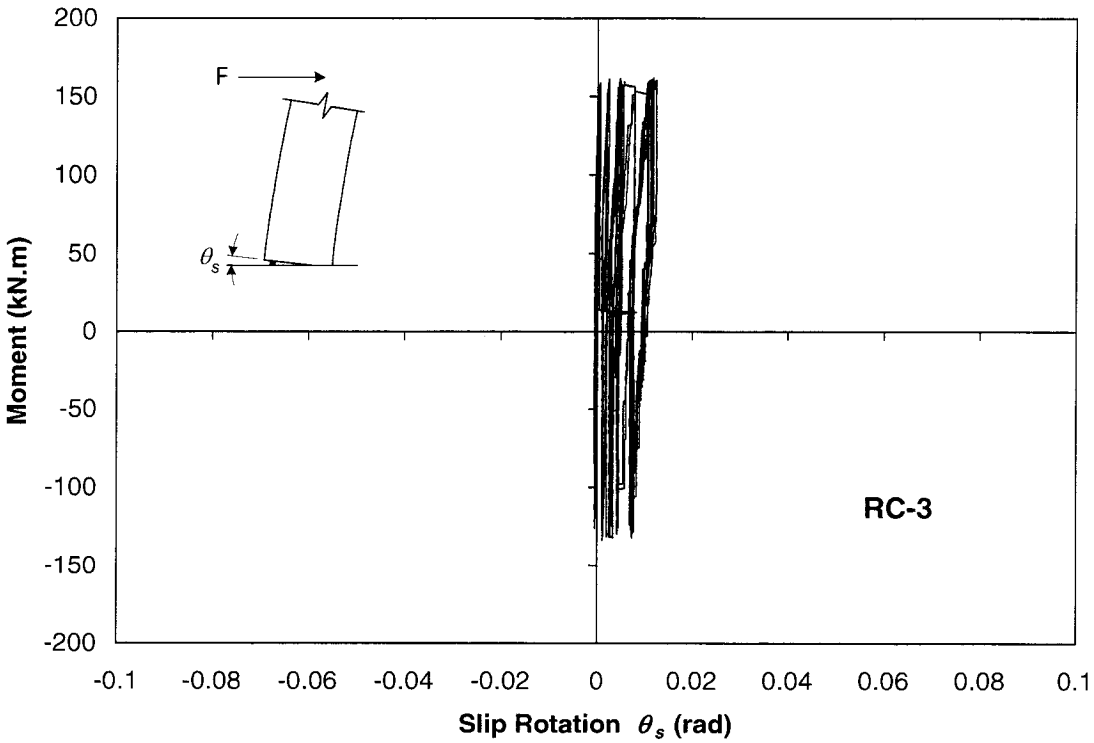

Fig. D.6 – Base Moment-Slip Rotation Relationship for Column RC-3

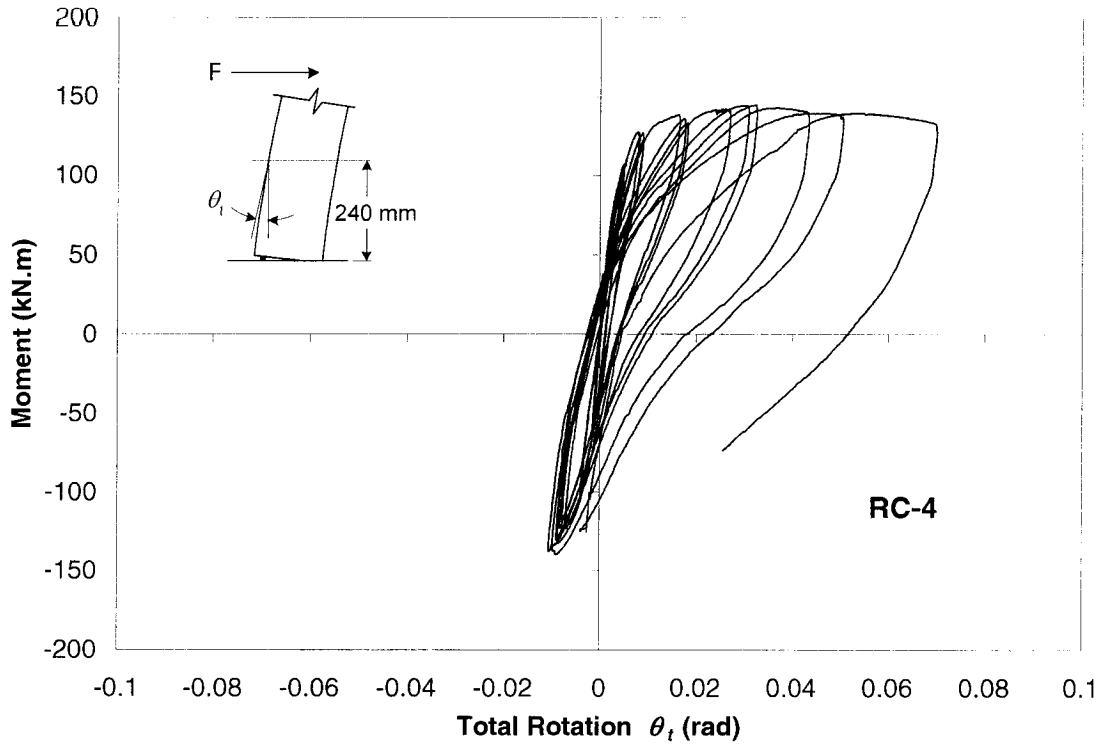

Fig. D.7 – Base Moment-Total Rotation Relationship for Column RC-4

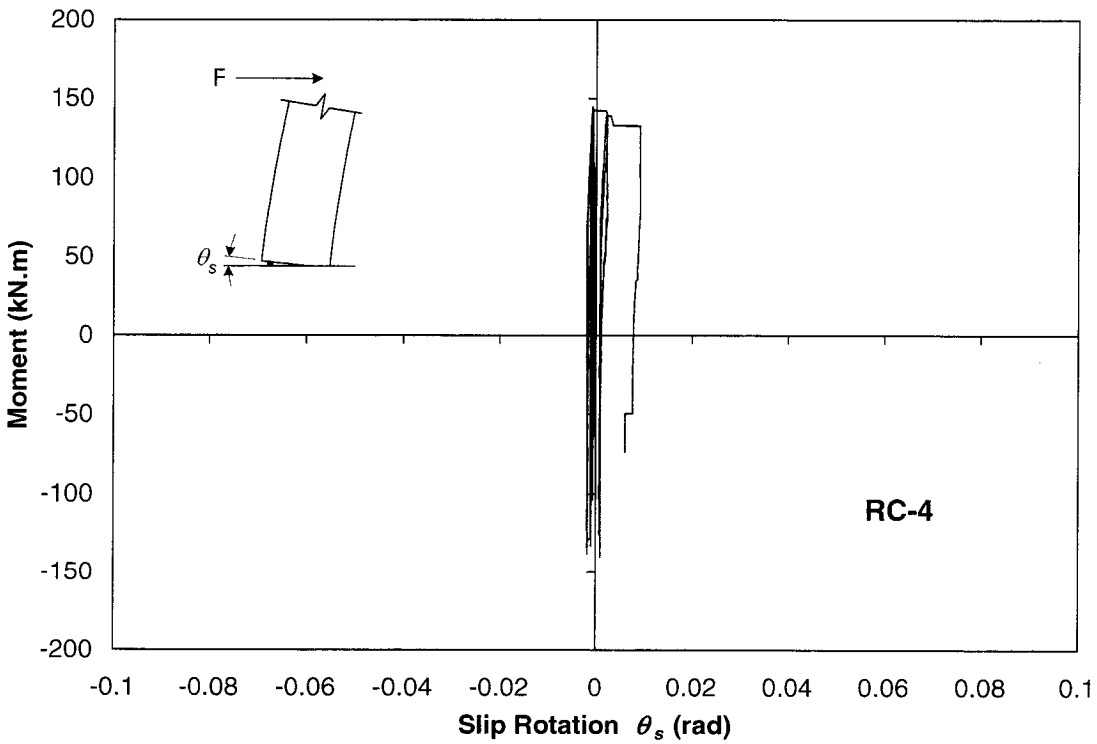

Fig. D.8 – Base Moment-Slip Rotation Relationship for Column RC-4

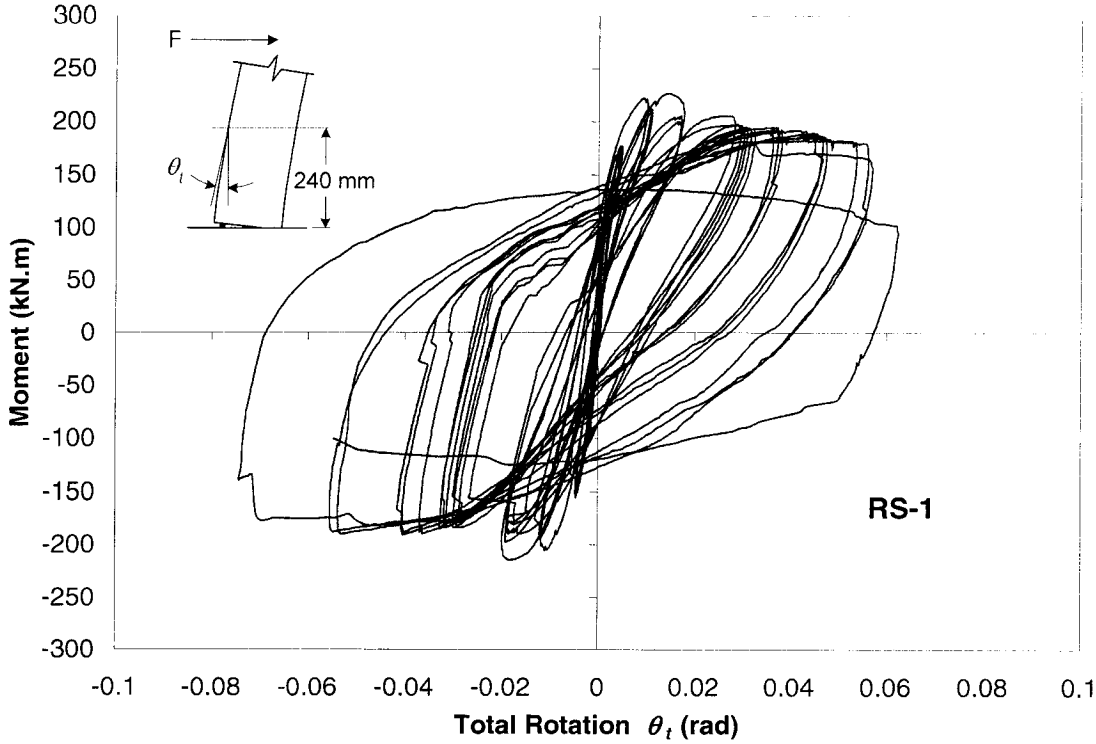

Fig. D.9 – Base Moment-Total Rotation Relationship for Column RS-1

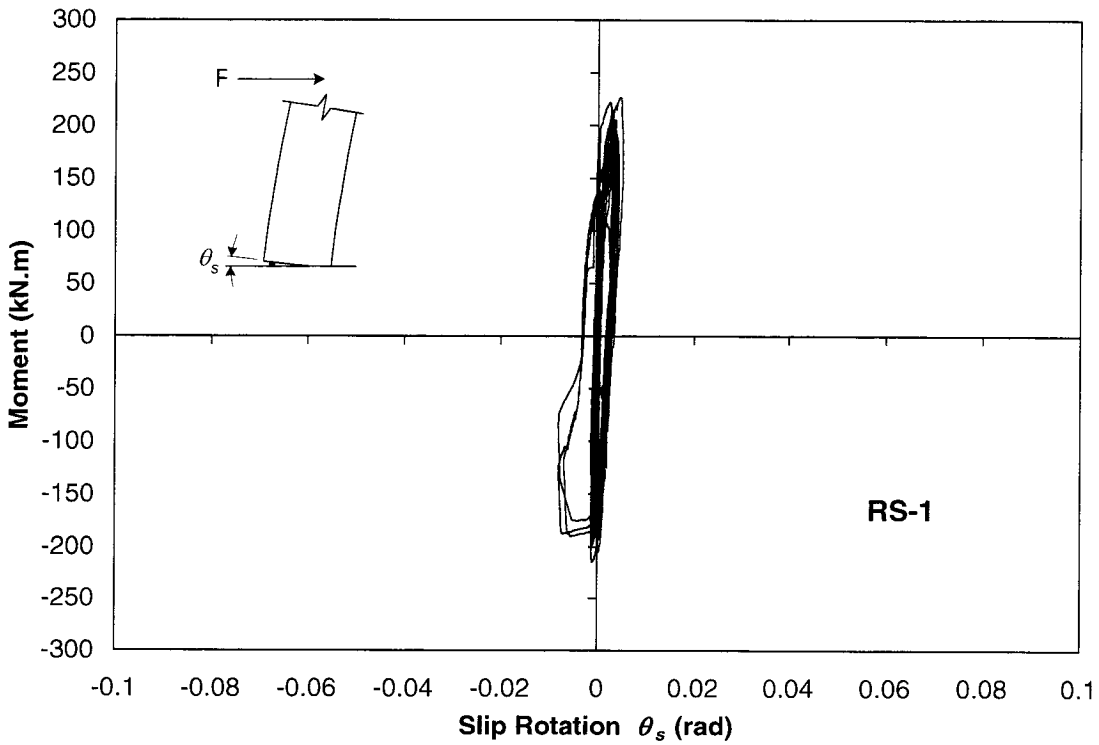

Fig. D.10 – Base Moment-Slip Rotation Relationship for Column RS-1

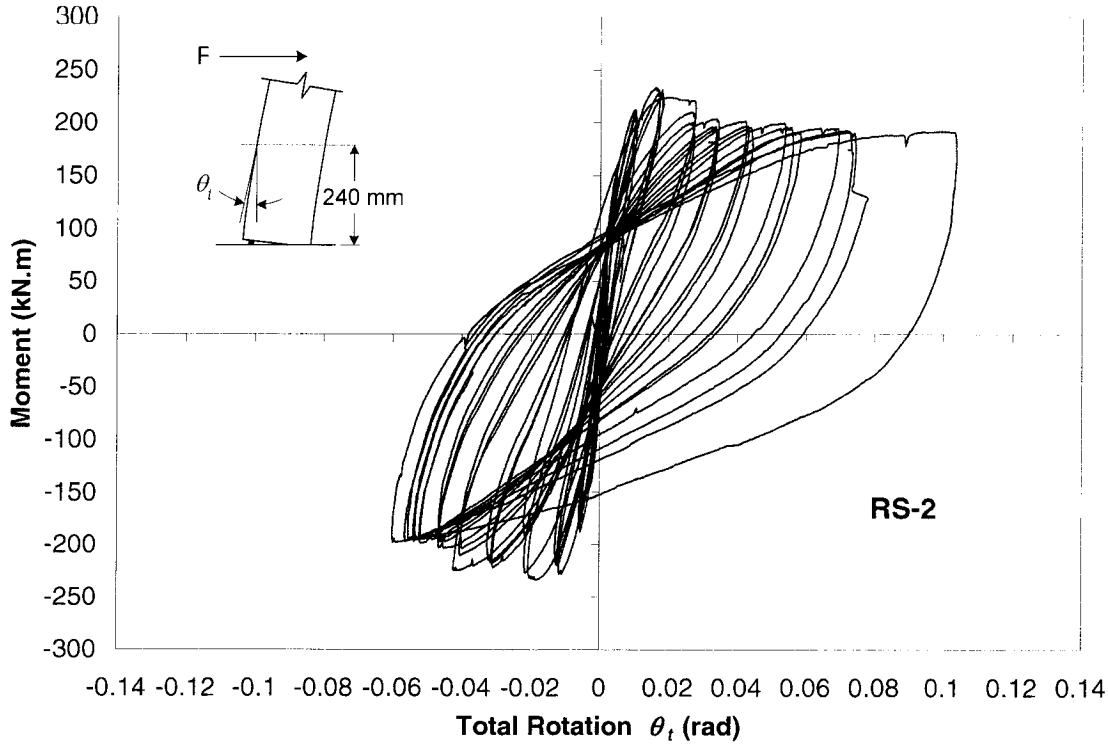

Fig. D.11 – Base Moment-Total Rotation Relationship for Column RS-2

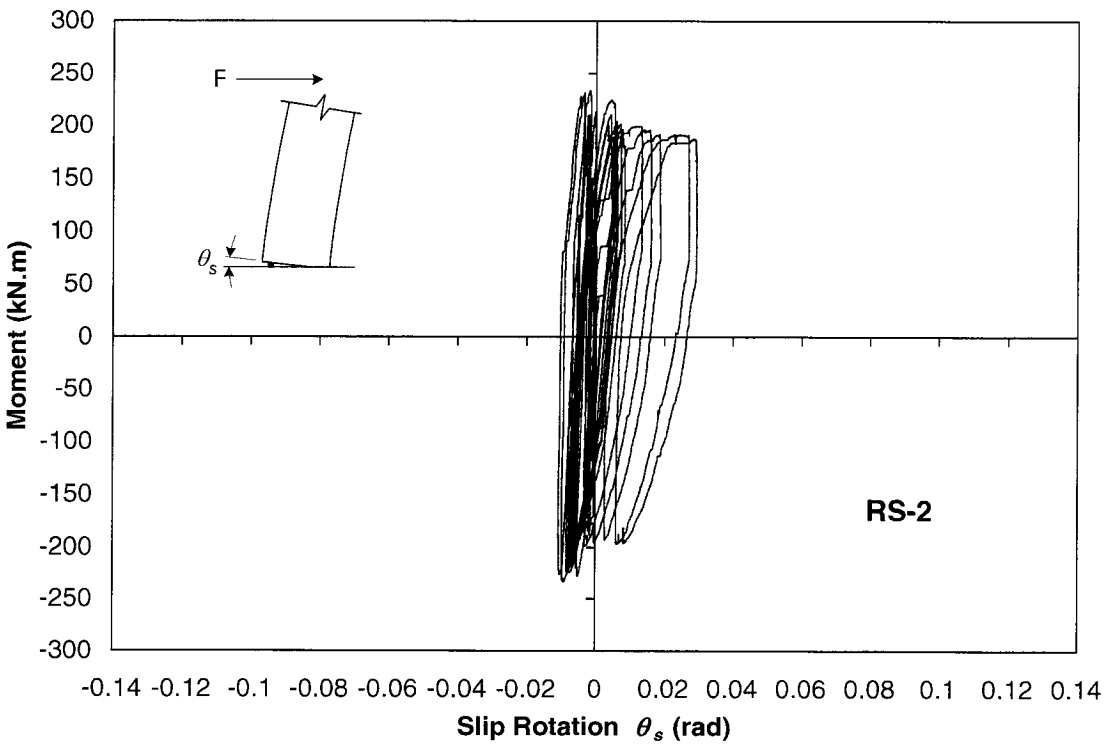

Fig. D.12 – Base Moment-Slip Rotation Relationship for Column RS-2

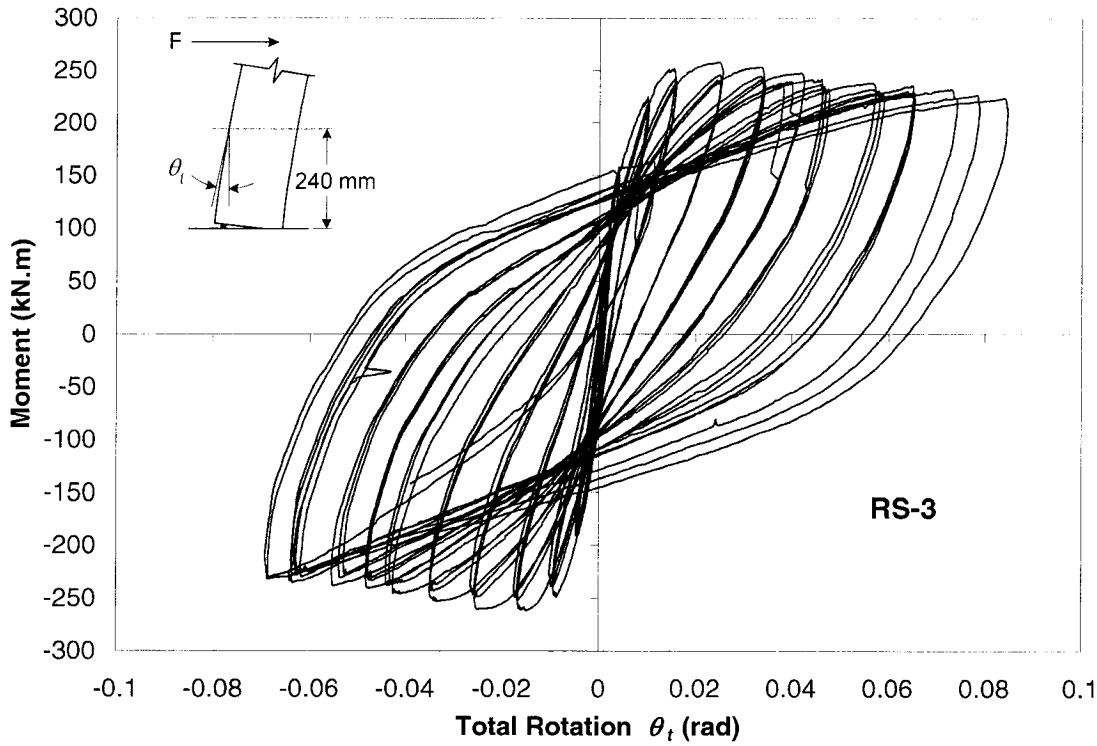

Fig. D.13 – Base Moment-Total Rotation Relationship for Column RS-3

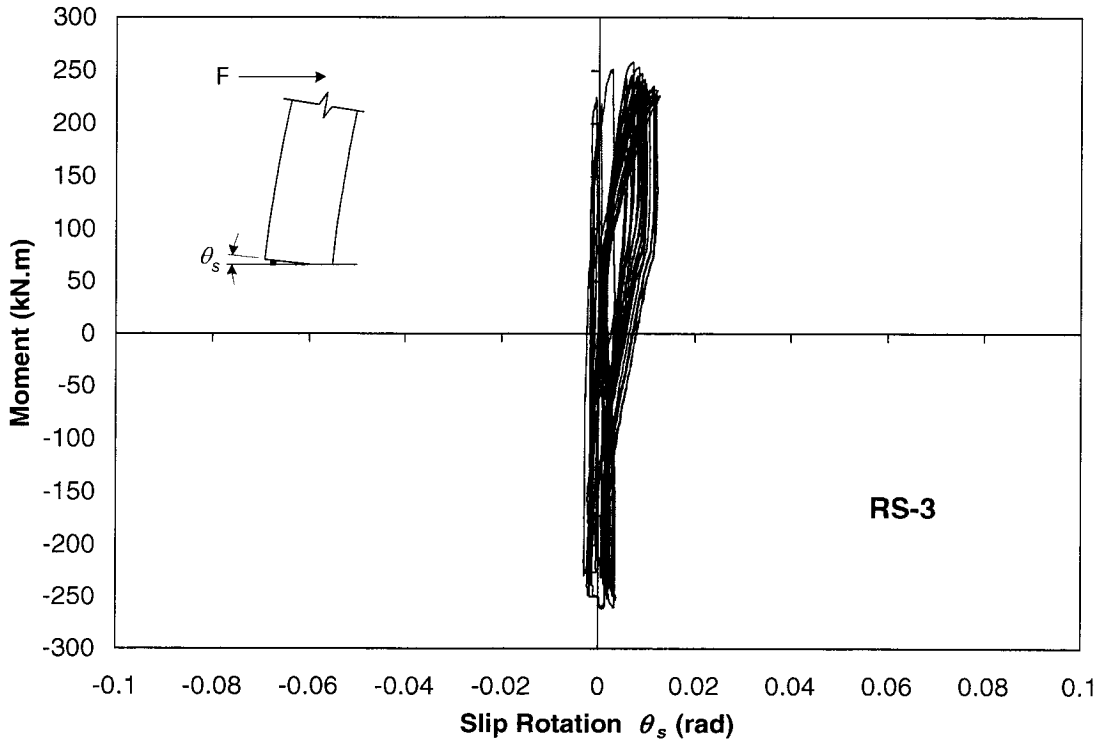

Fig. D.14 – Base Moment-Slip Rotation Relationship for Column RS-3

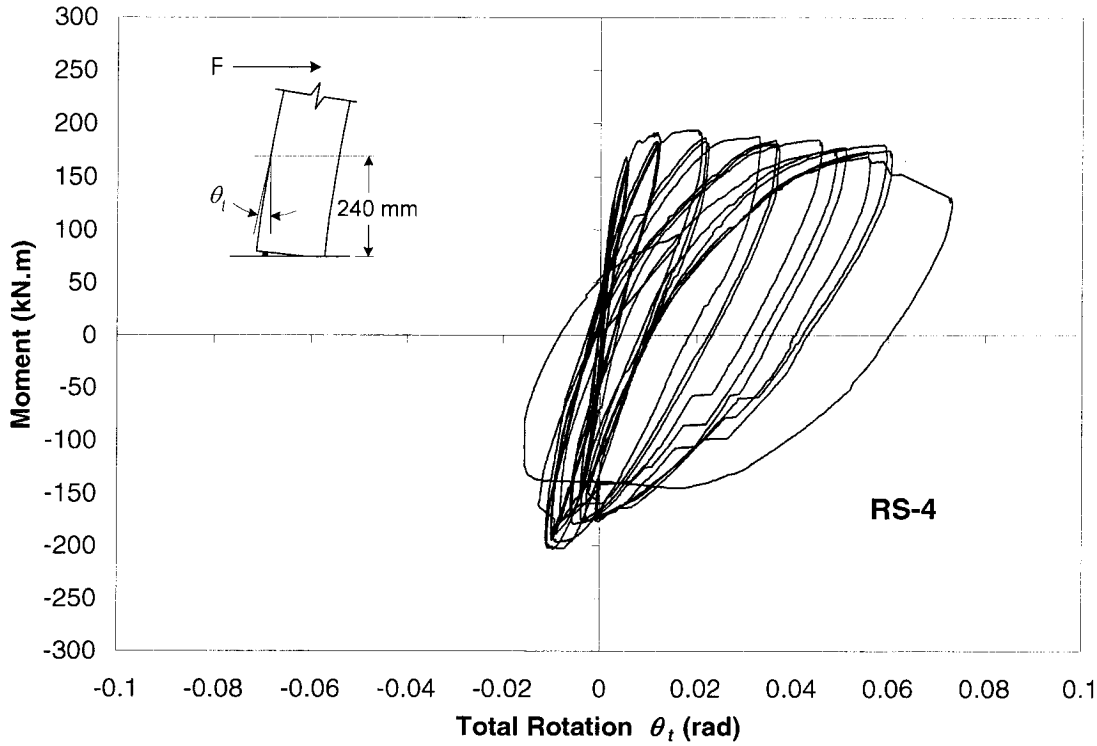

Fig. D.15 – Base Moment-Total Rotation Relationship for Column RS-4

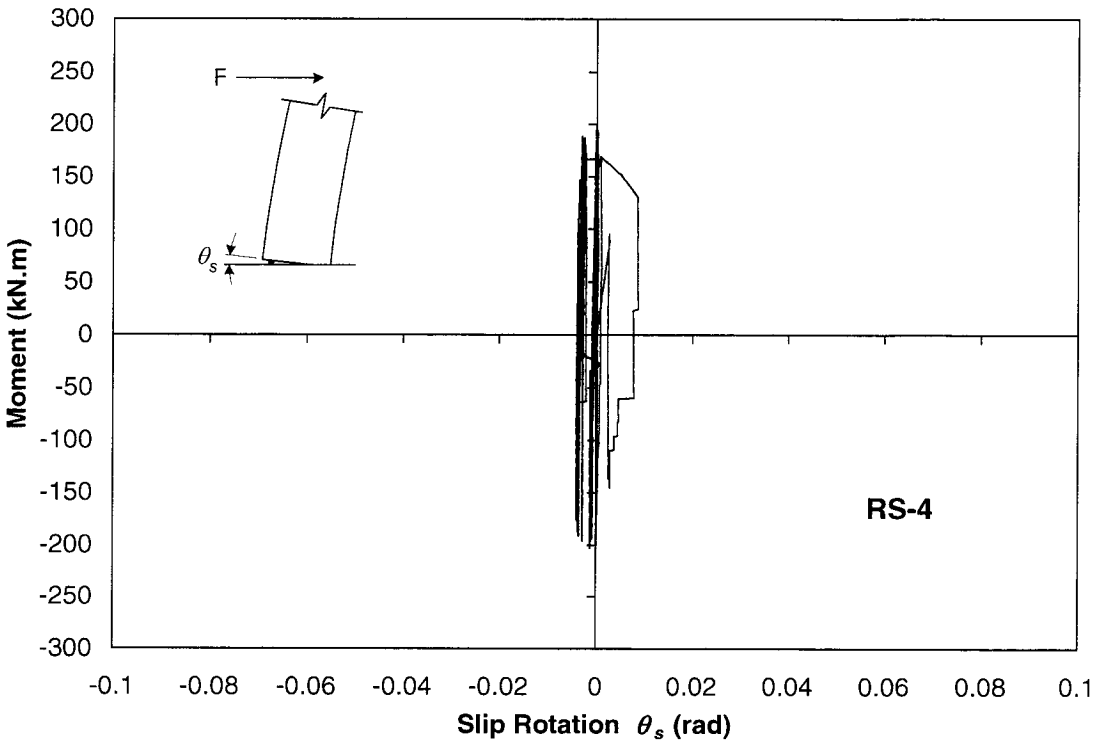

Fig. D.16 – Base Moment-Slip Rotation Relationship for Column RS-4

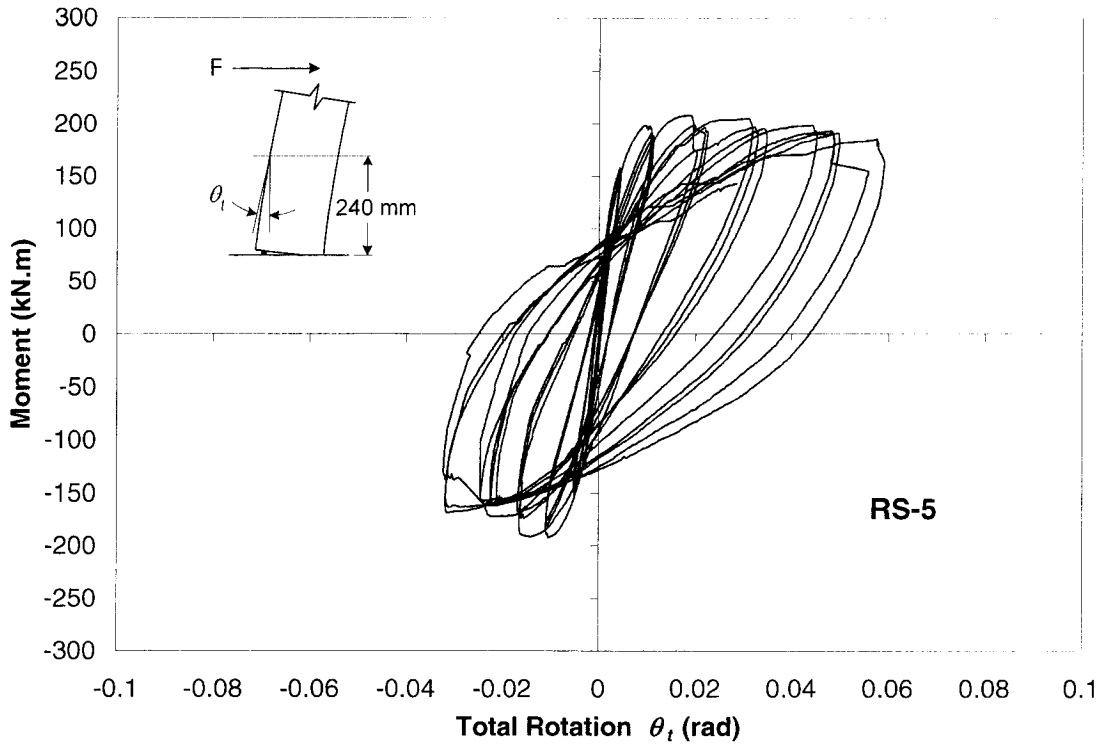

Fig. D.17 – Base Moment-Total Rotation Relationship for Column RS-5

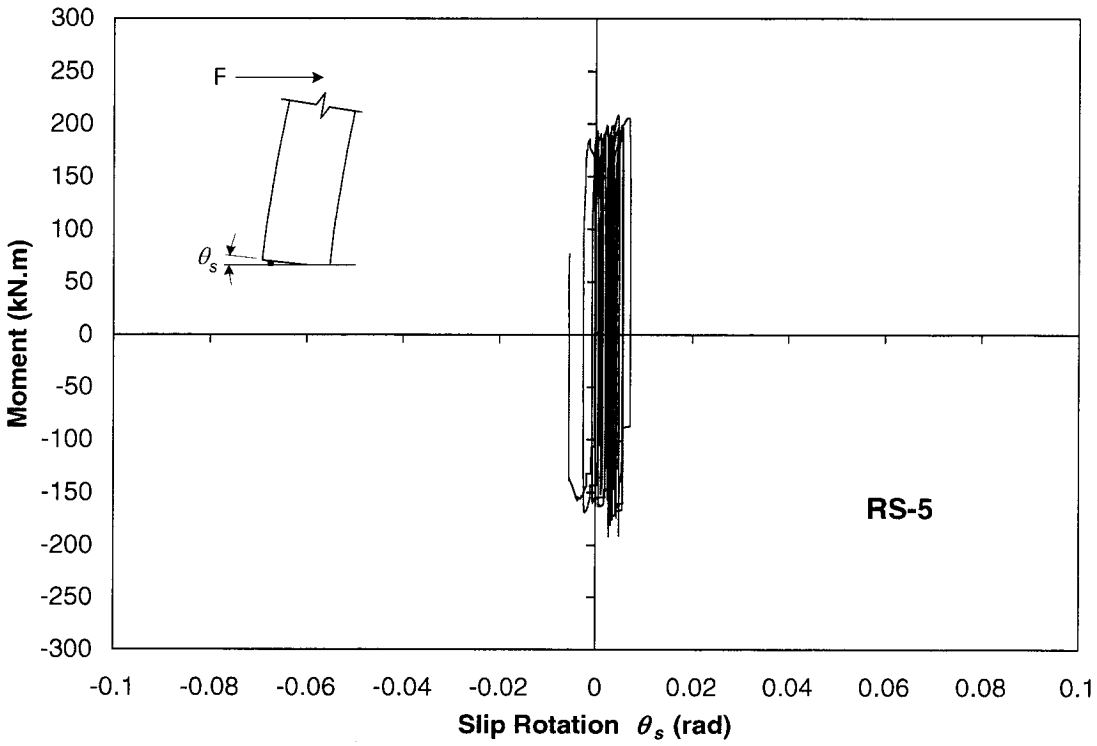

Fig. D.18 – Base Moment-Slip Rotation Relationship for Column RS-5

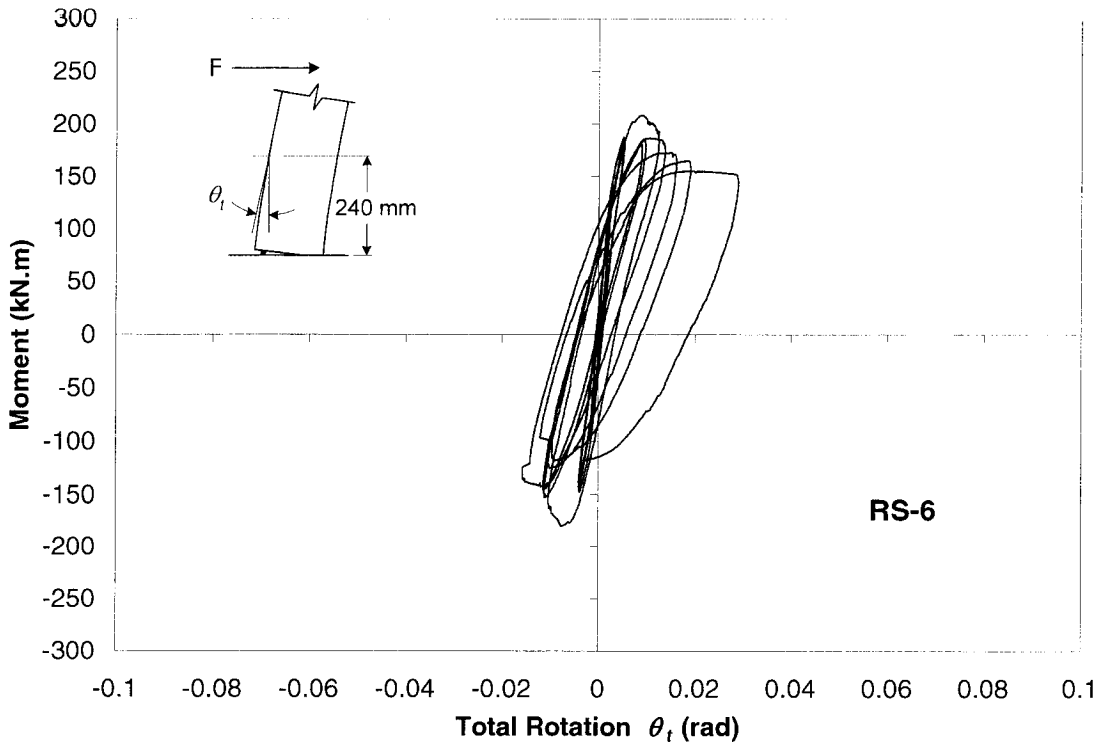

Fig. D.19 – Base Moment-Total Rotation Relationship for Column RS-6

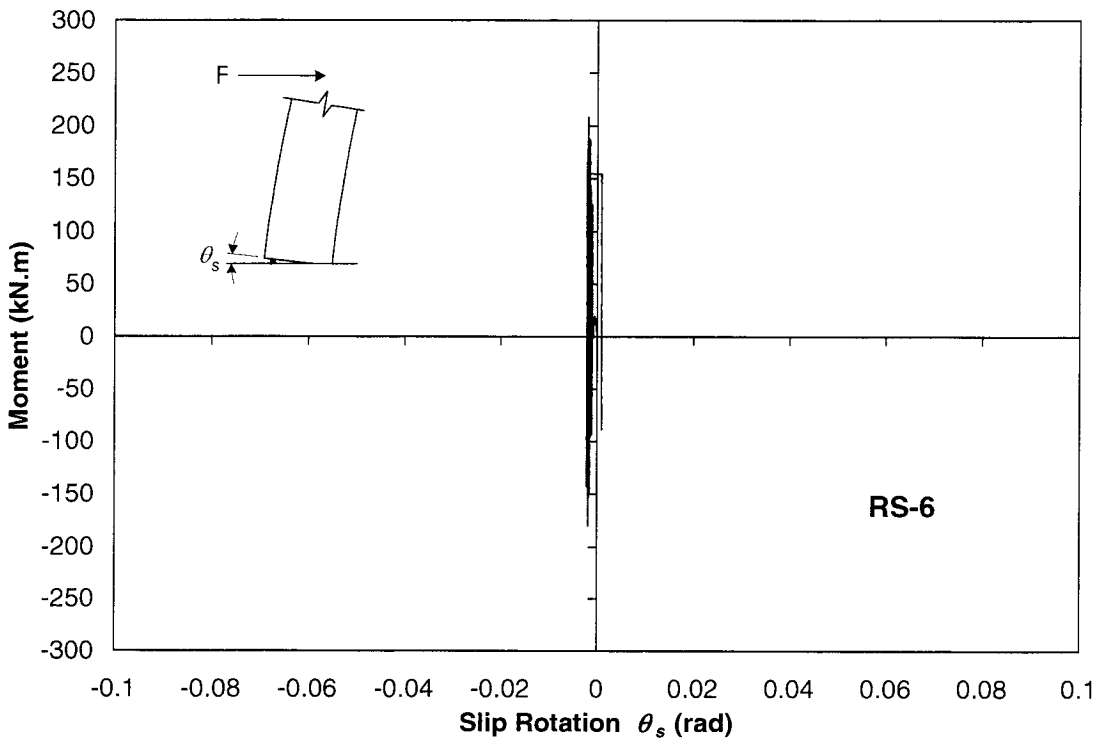

Fig. D.20 – Base Moment-Slip Rotation Relationship for Column RS-6

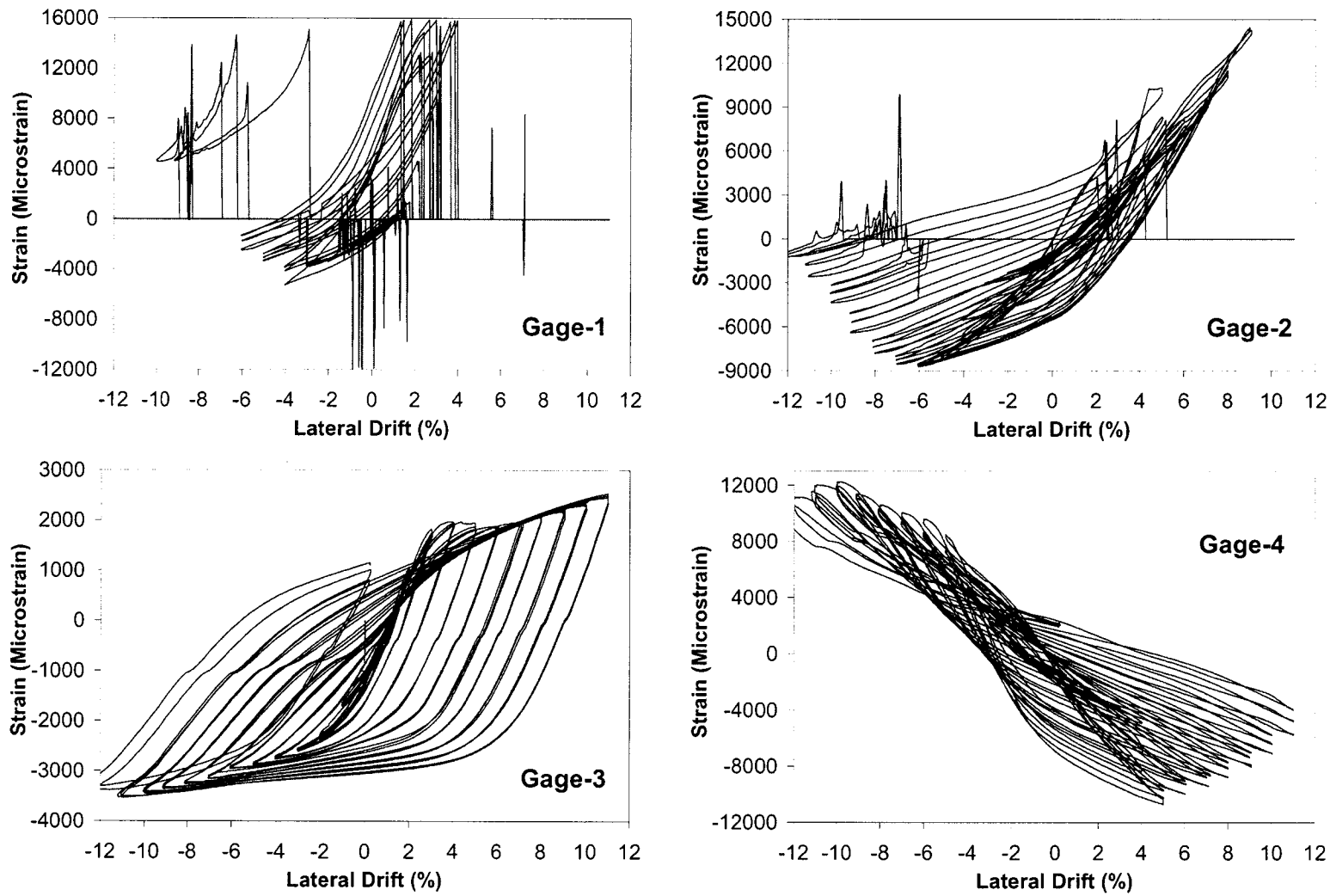

Fig. D.21 – Strain Distribution in Longitudinal Reinforcement of Column RC-1

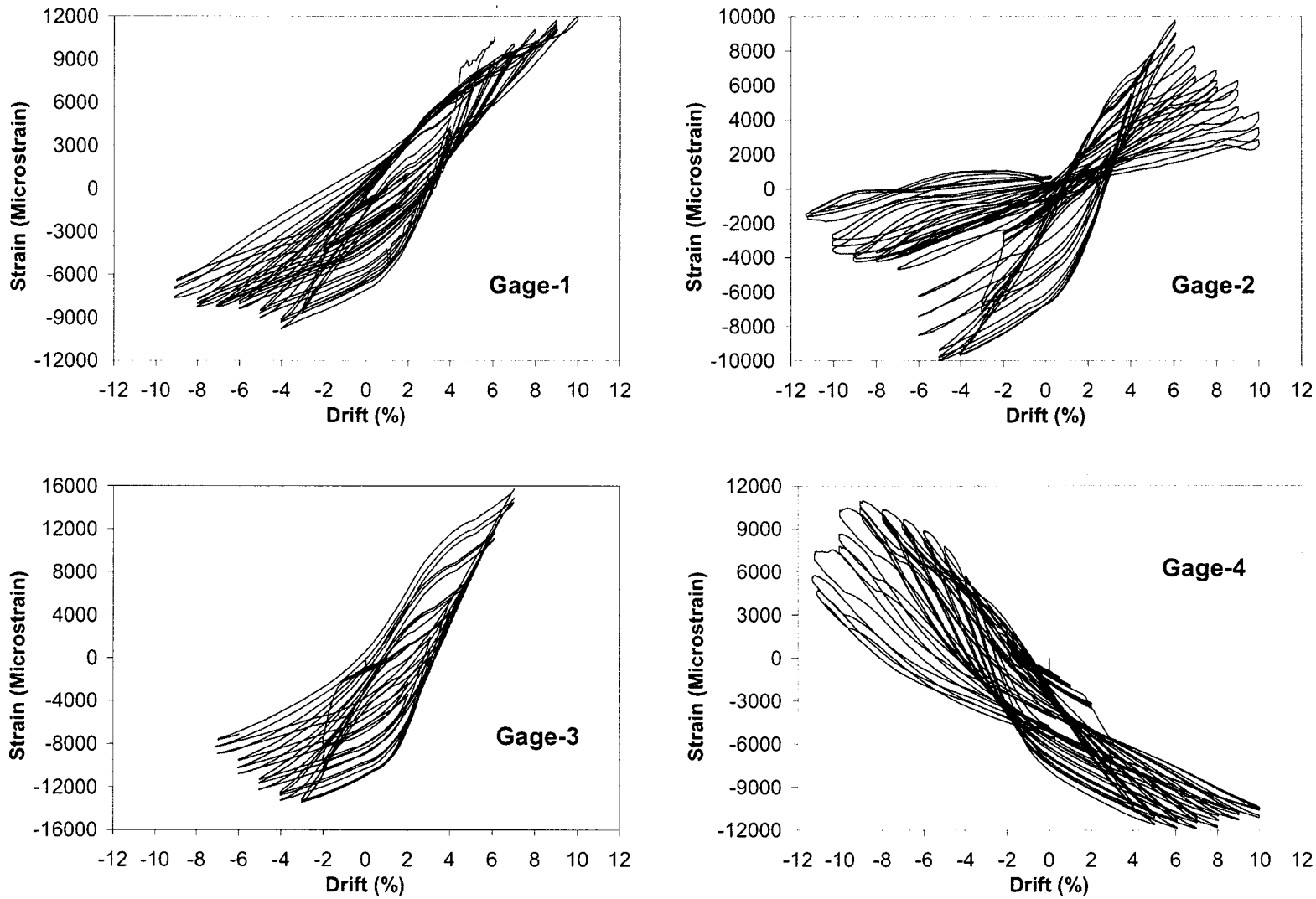

Fig. D.22 – Strain Distribution in Longitudinal Reinforcement of Column RC-2

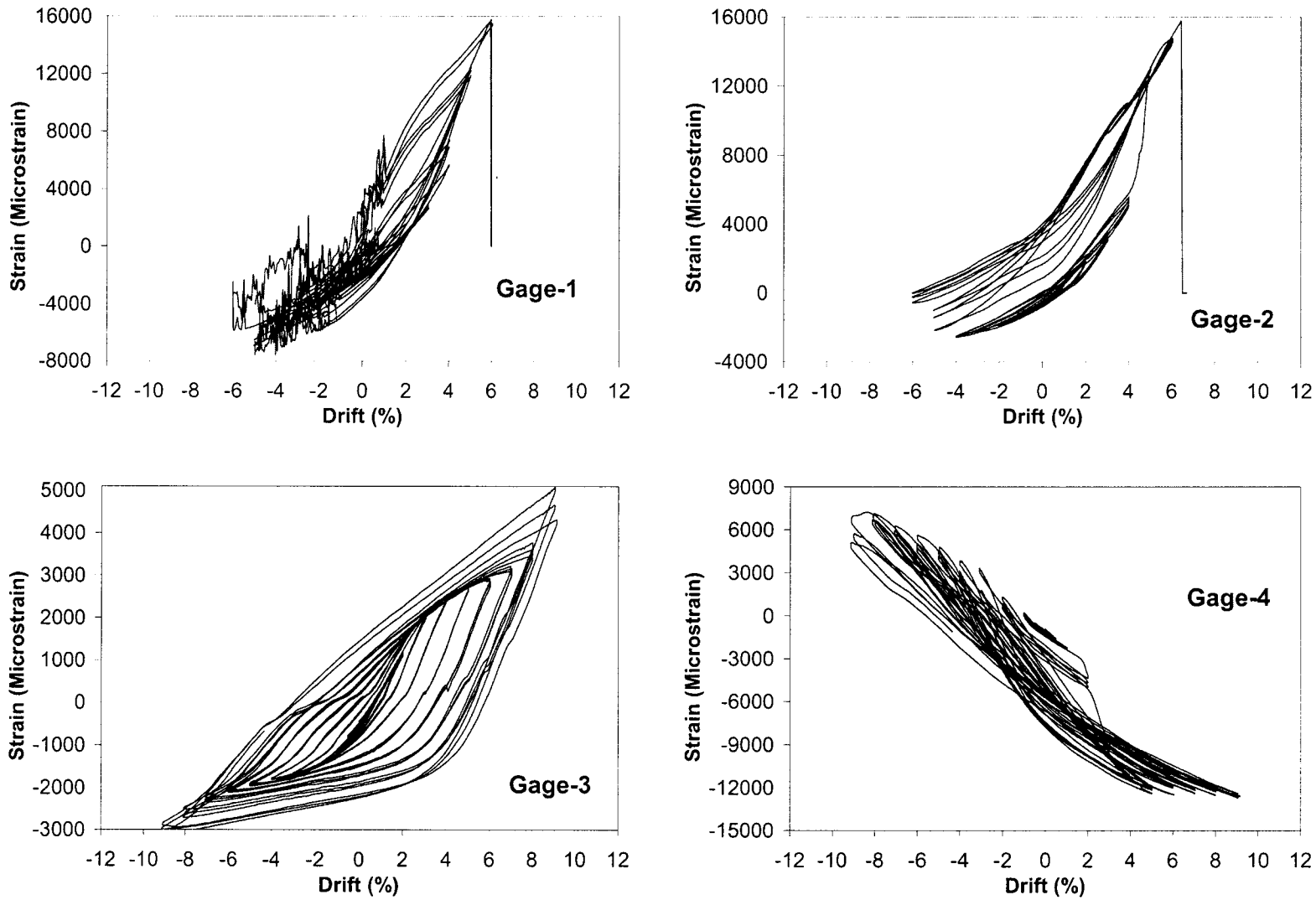

Fig. D.23 – Strain Distribution in Longitudinal Reinforcement of Column RC-3

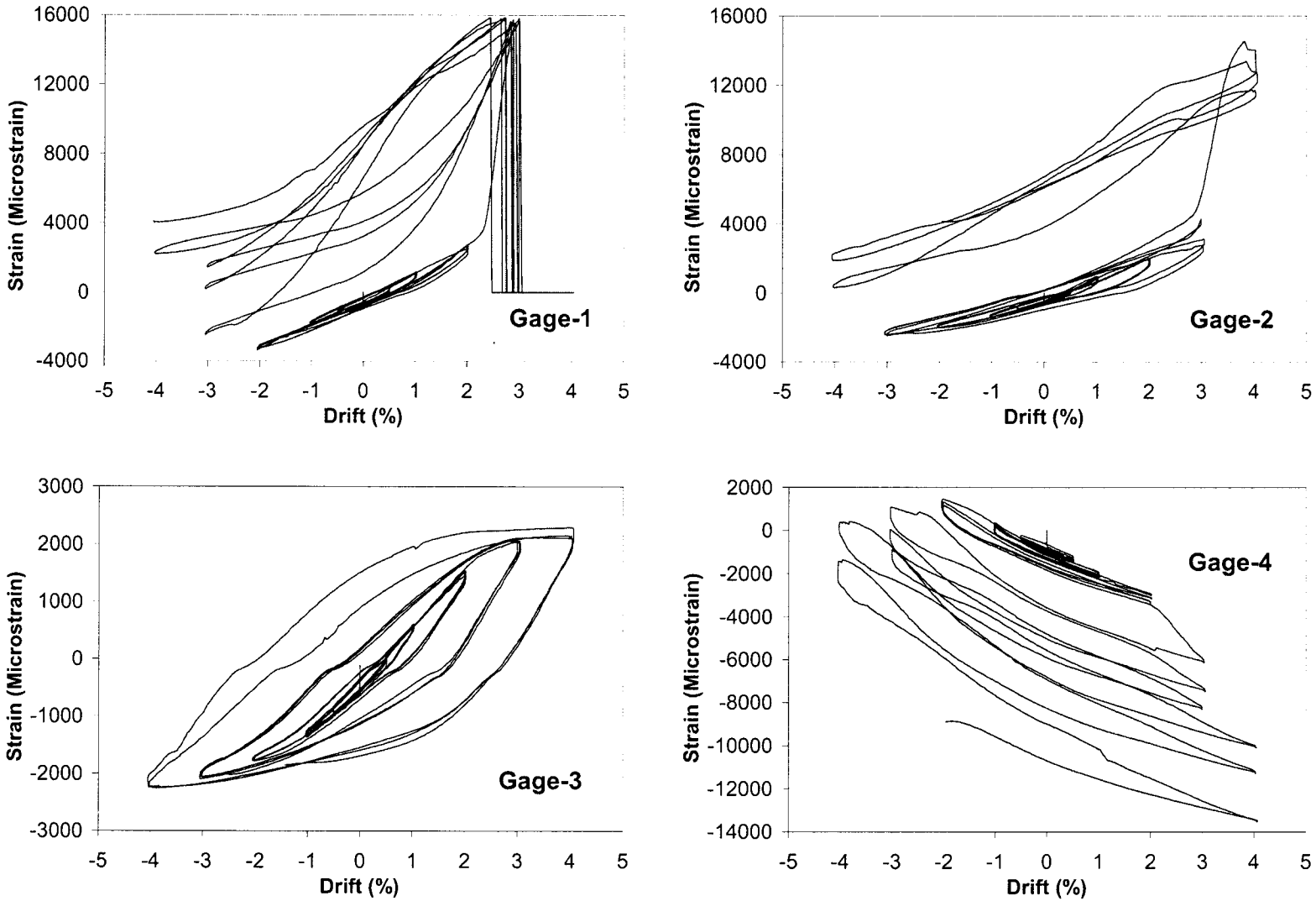

Fig. D.24 – Strain Distribution in Longitudinal Reinforcement of Column RC-4

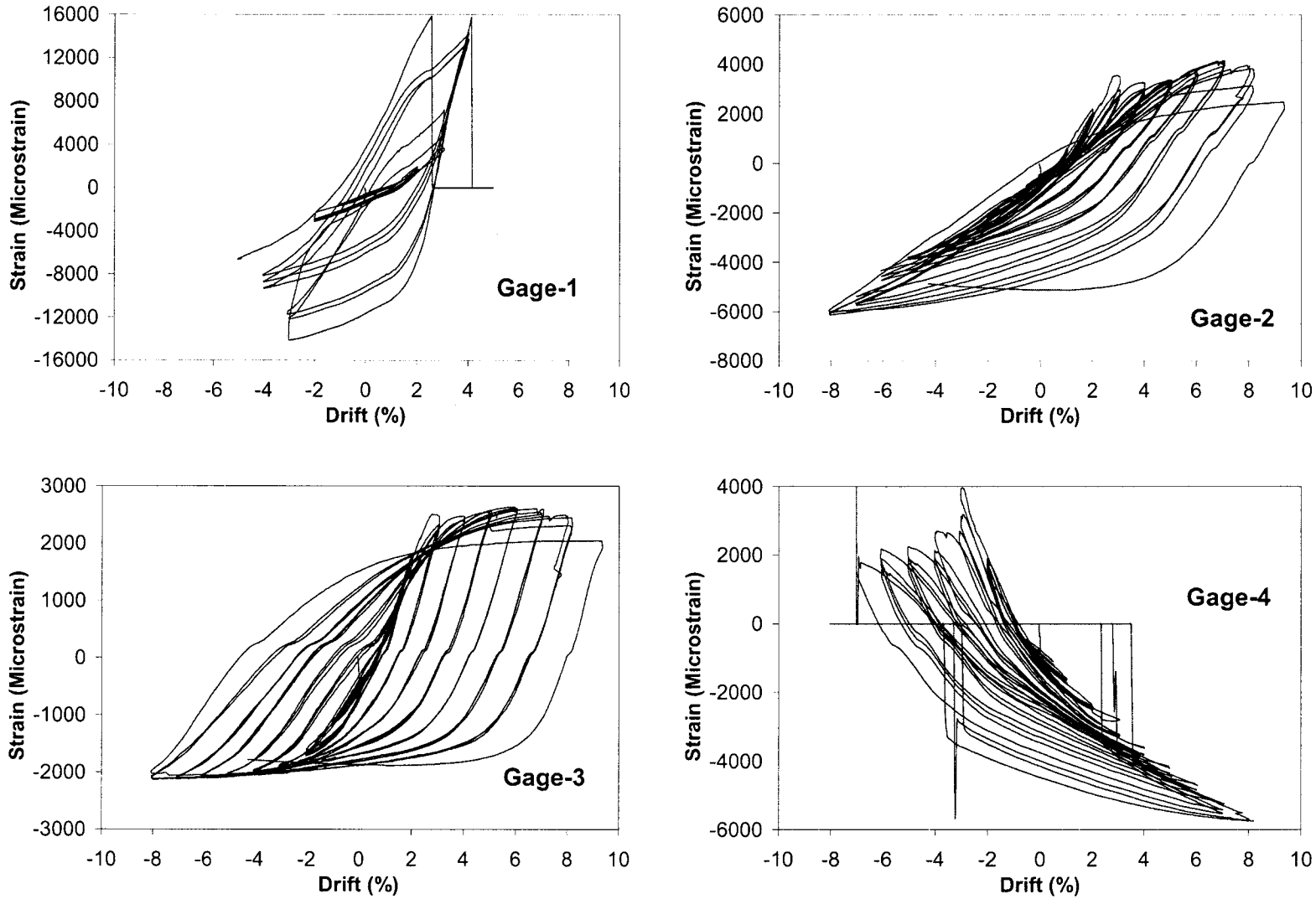

Fig. D.25 – Strain Distribution in Longitudinal Reinforcement of Column RS-1

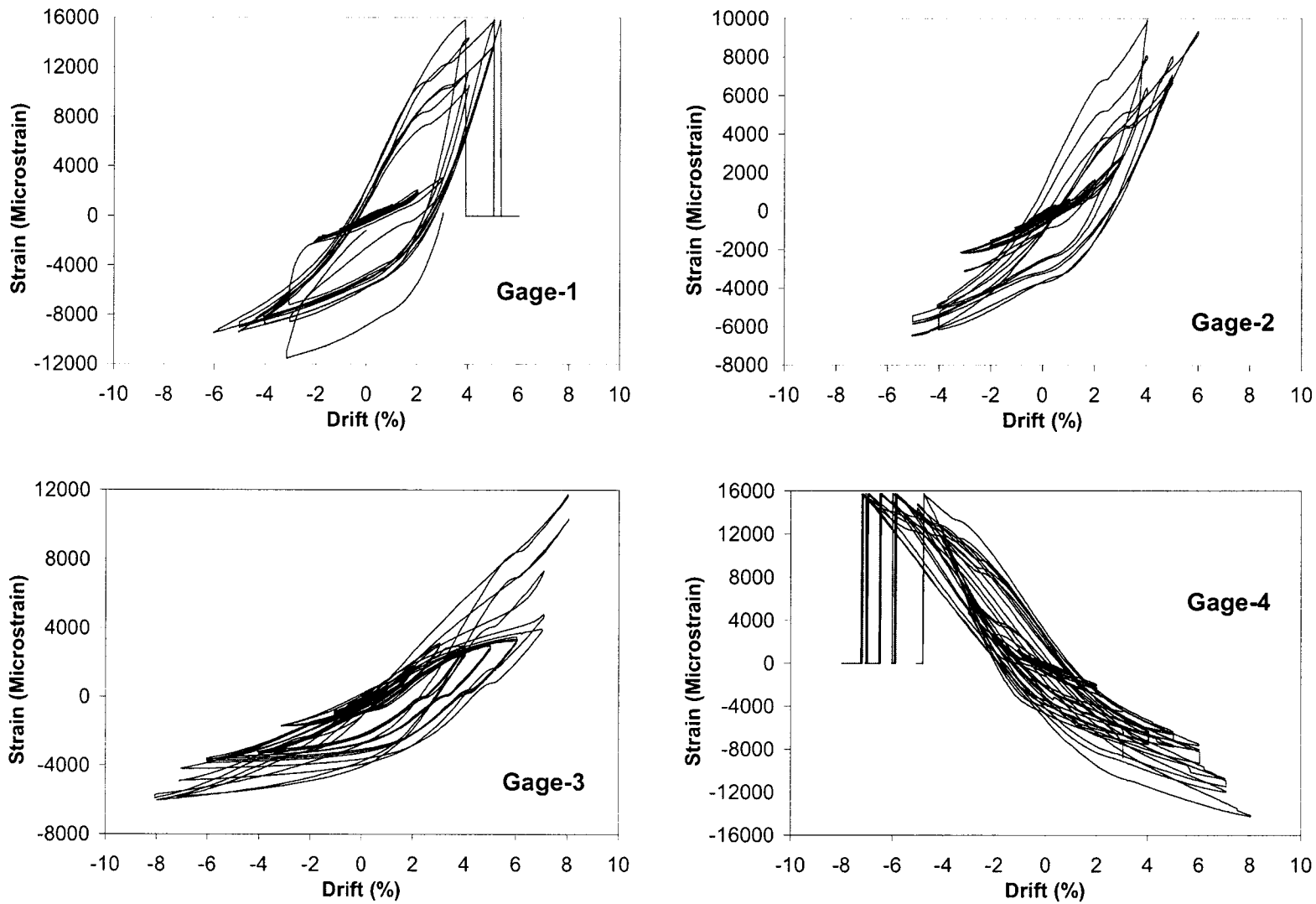

Fig. D.26 – Strain Distribution in Longitudinal Reinforcement of Column RS-2

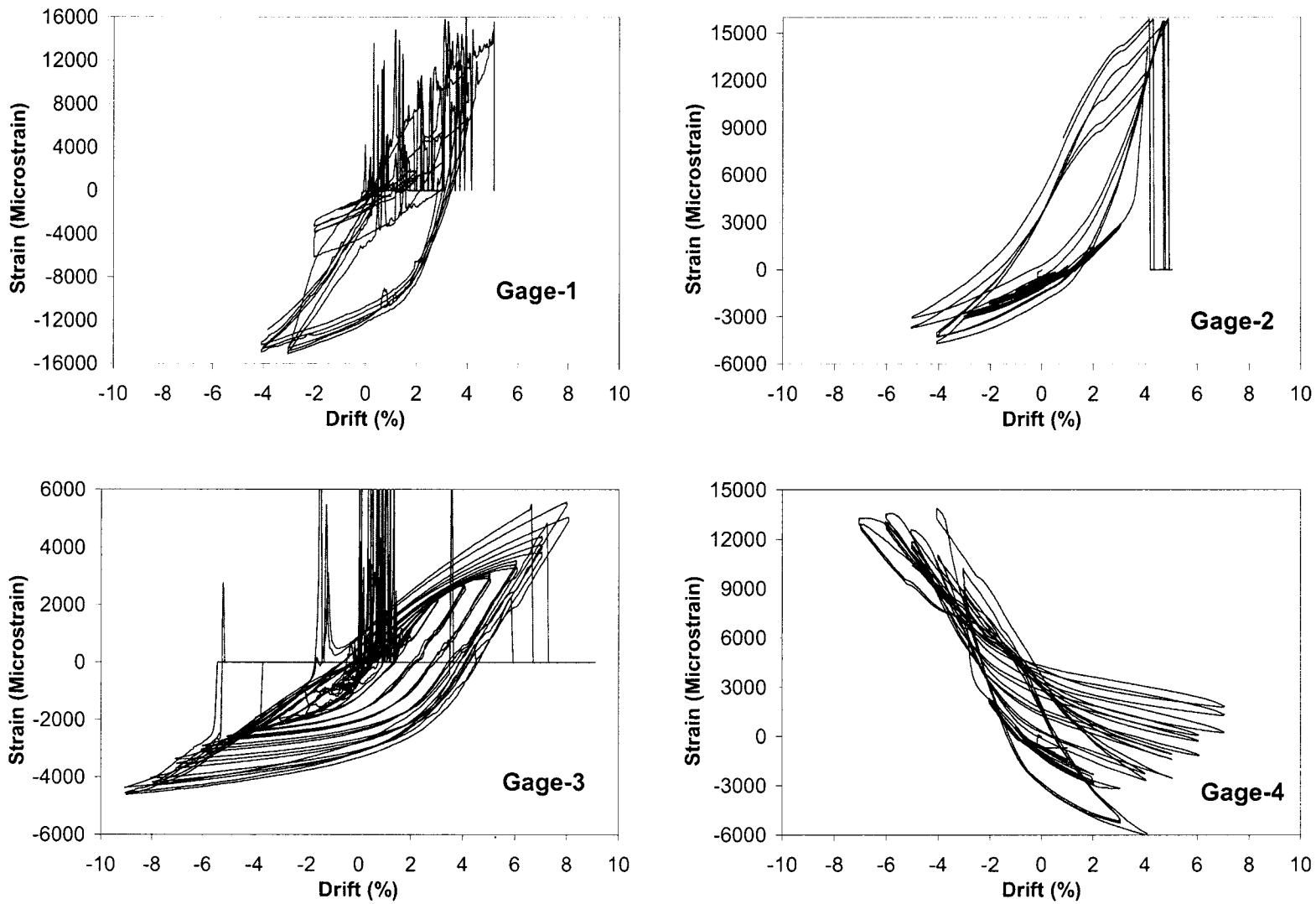

Fig. D.27 – Strain Distribution in Longitudinal Reinforcement of Column RS-3

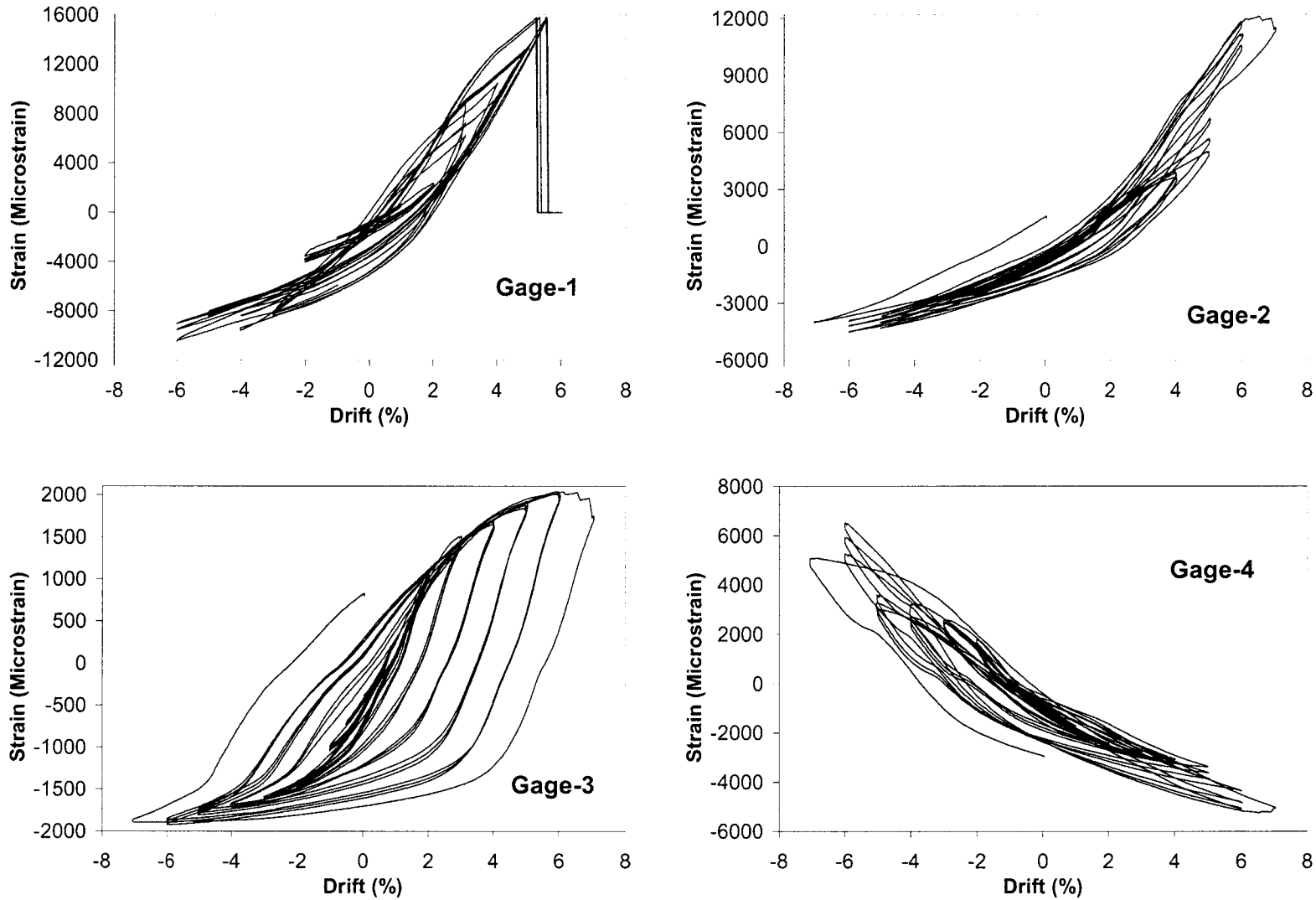

Fig. D.28 – Strain Distribution in Longitudinal Reinforcement of Column RS-4

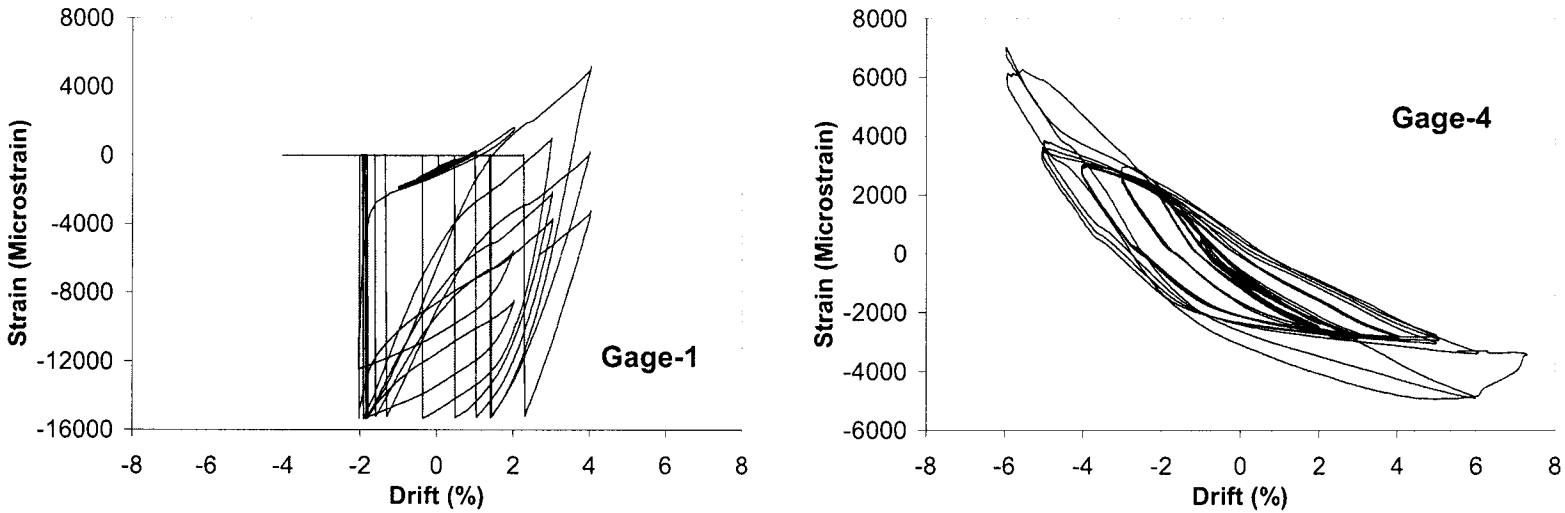

Fig. D.29 – Strain Distribution in Longitudinal Reinforcement of Column RS-5

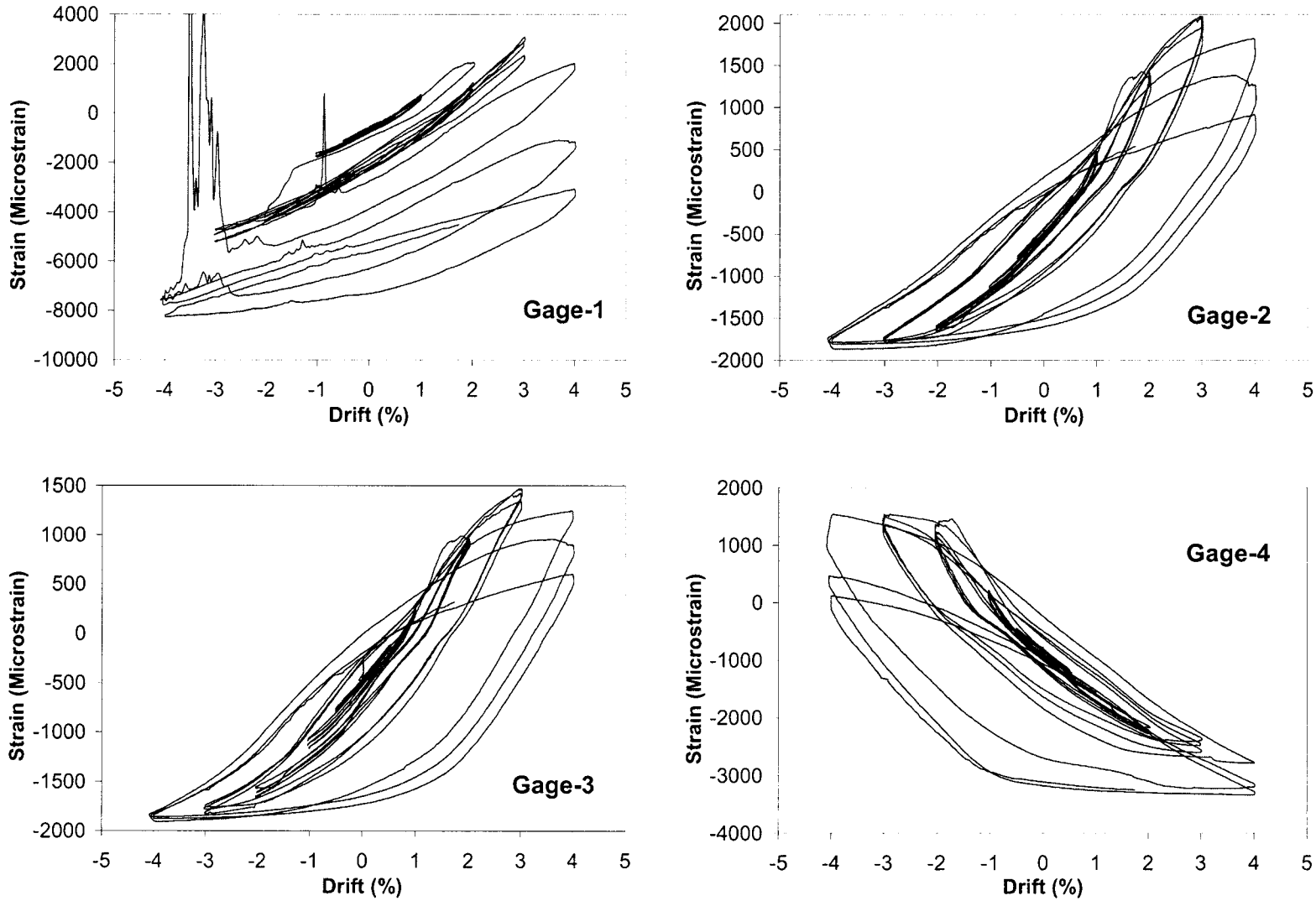

Fig. D.30 – Strain Distribution in Longitudinal Reinforcement of Column RS-6

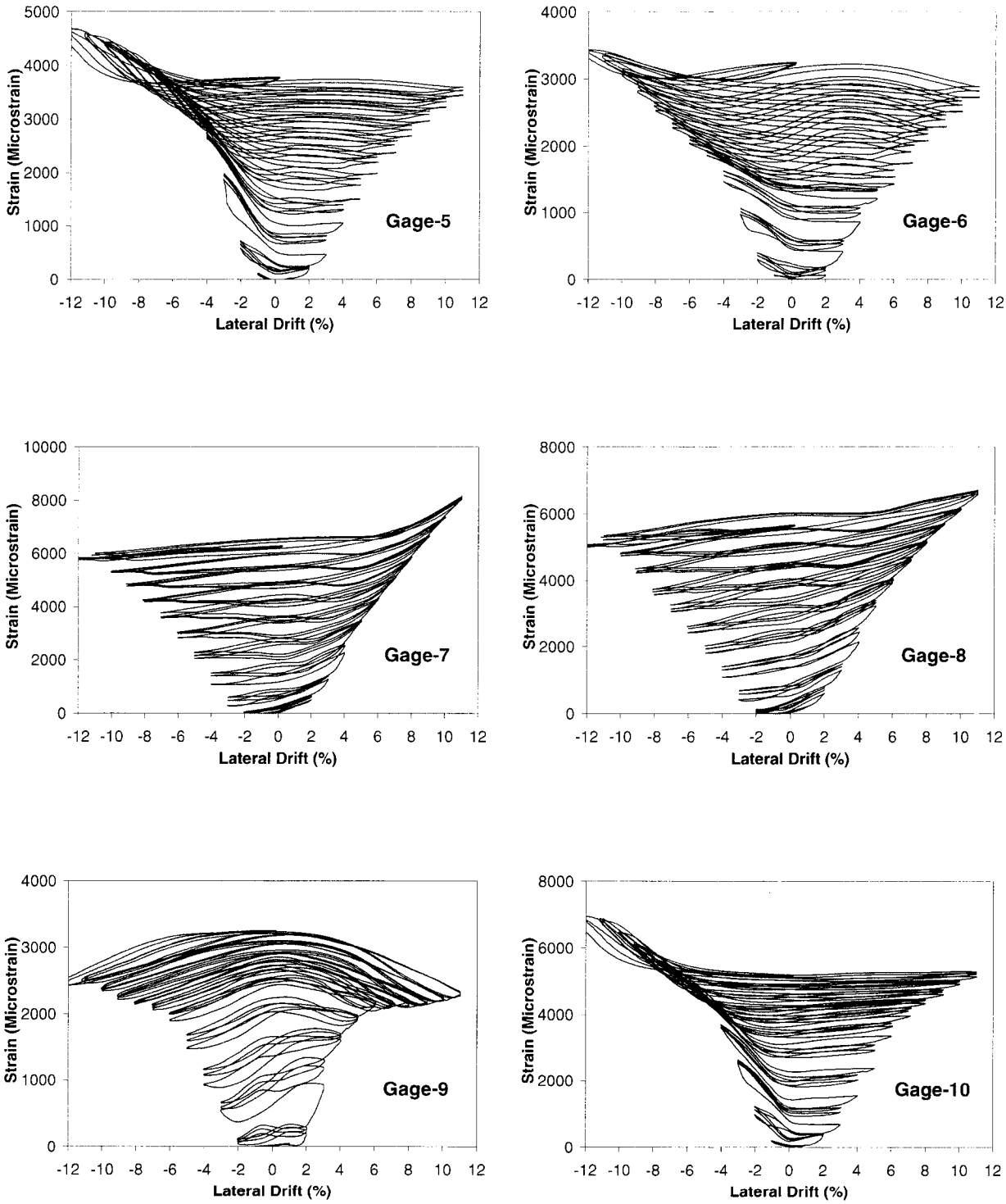

Fig. D.31 – Variation of transverse strain on the FRP Casing of Column RC-1

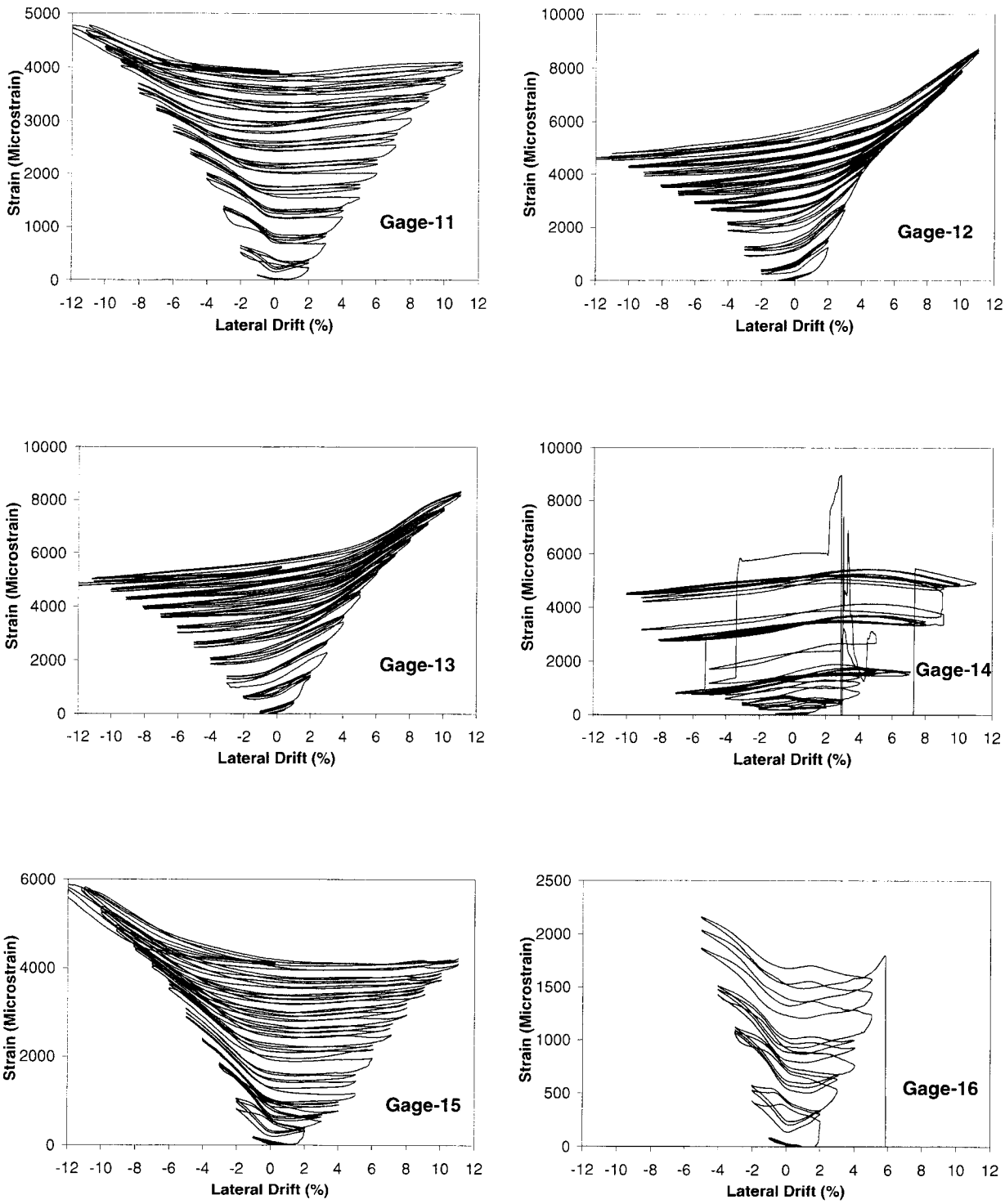

Fig. D.31 – Cont'd

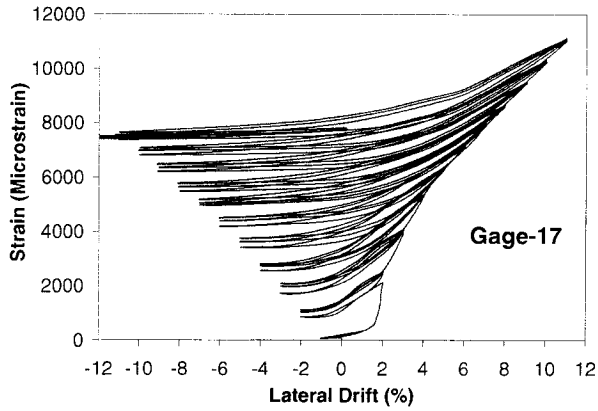

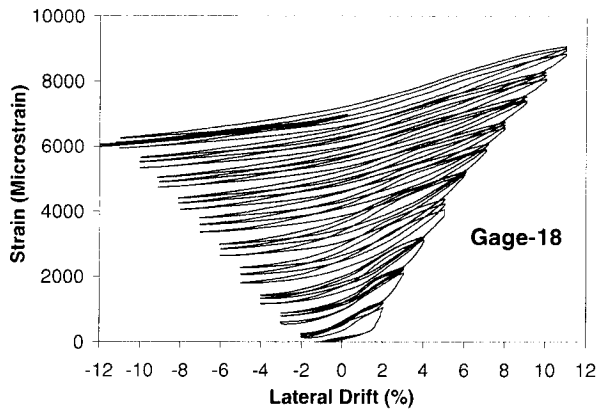

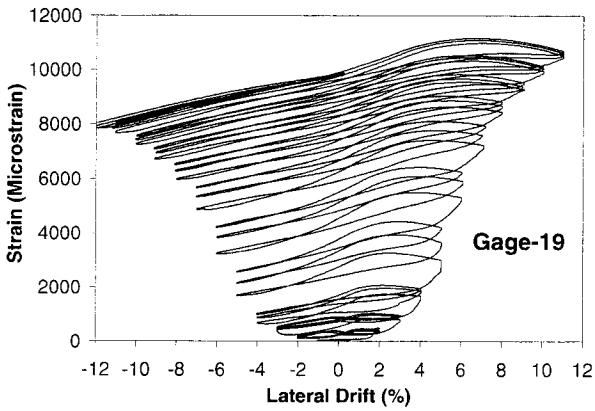

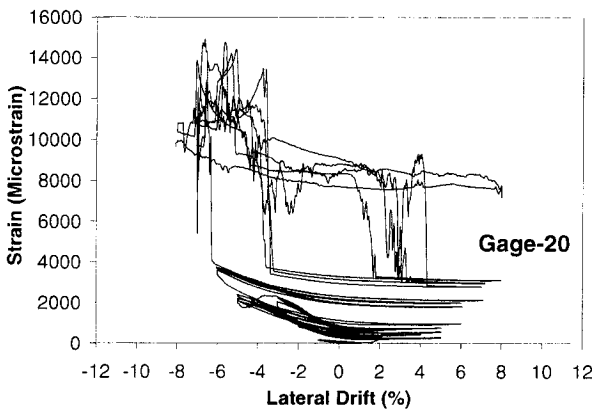

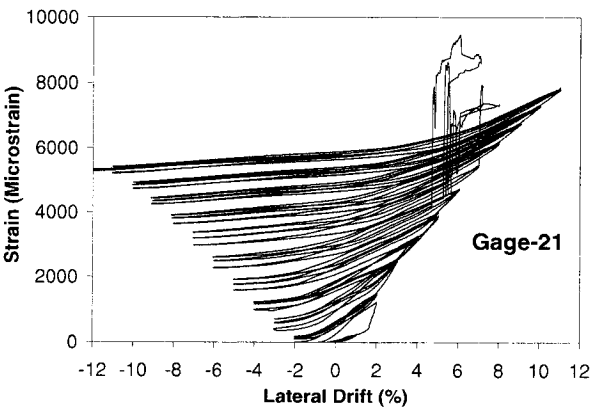

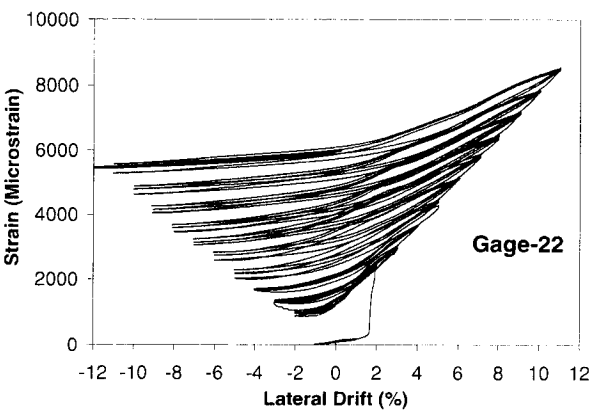

Fig. D.31 – Cont'd

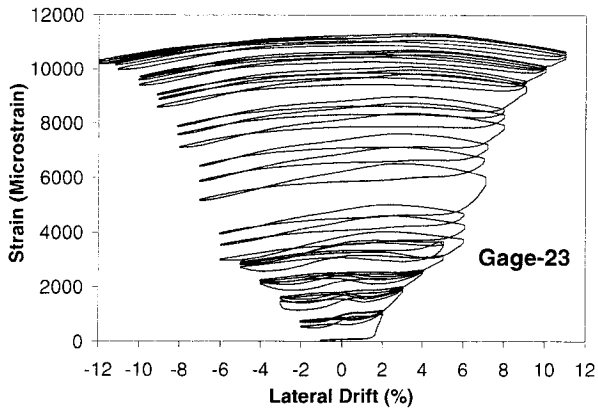

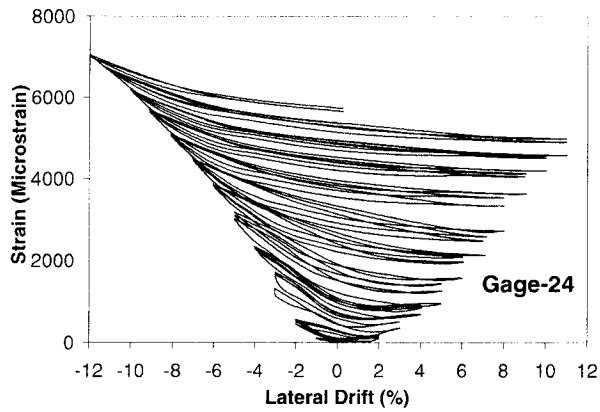

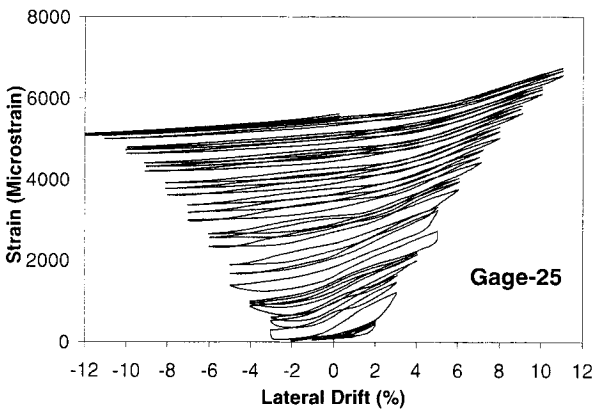

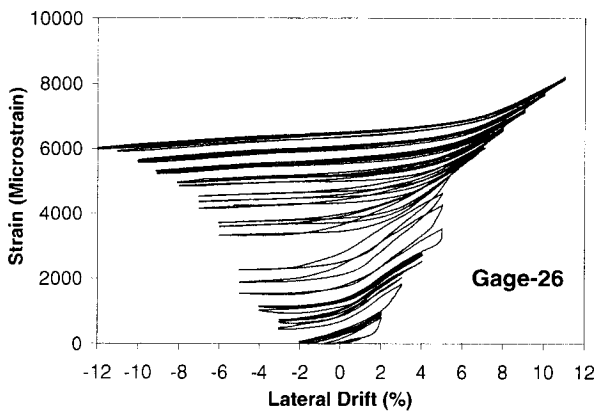

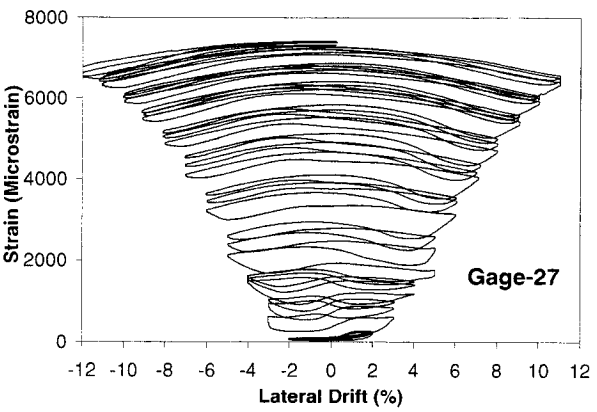

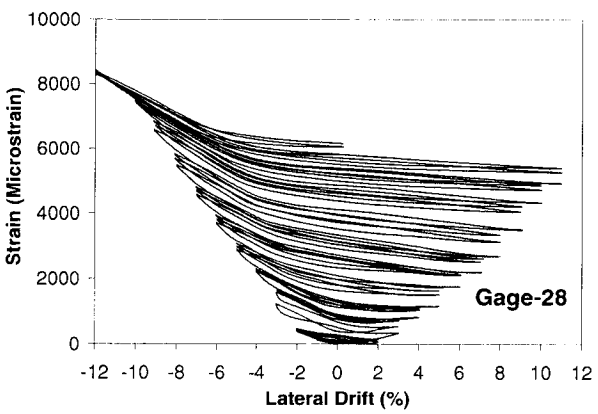

Fig. D.31 – Cont'd

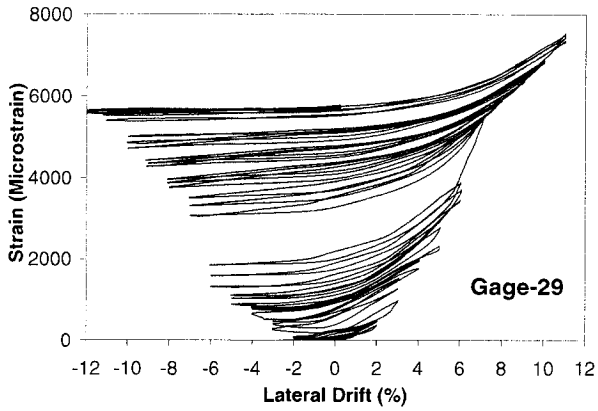

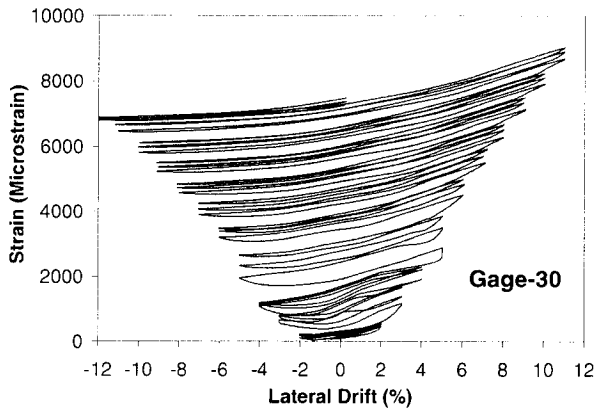

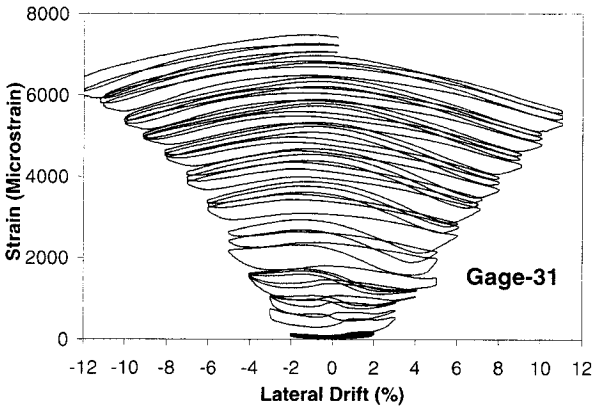

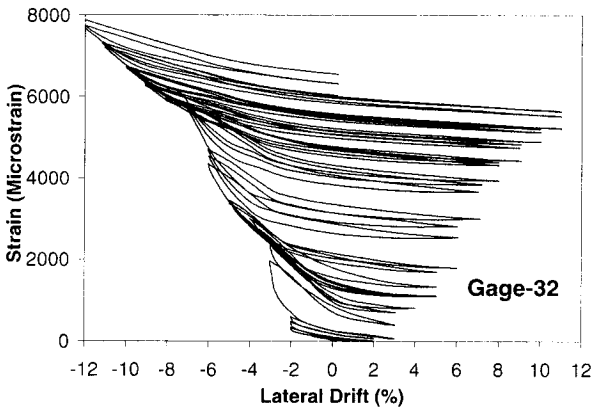

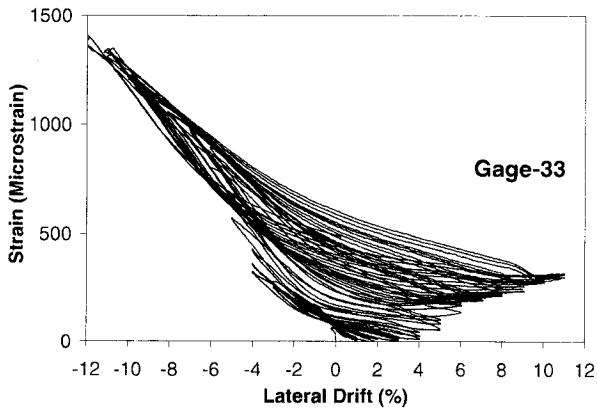

Fig. D.31 – Cont'd

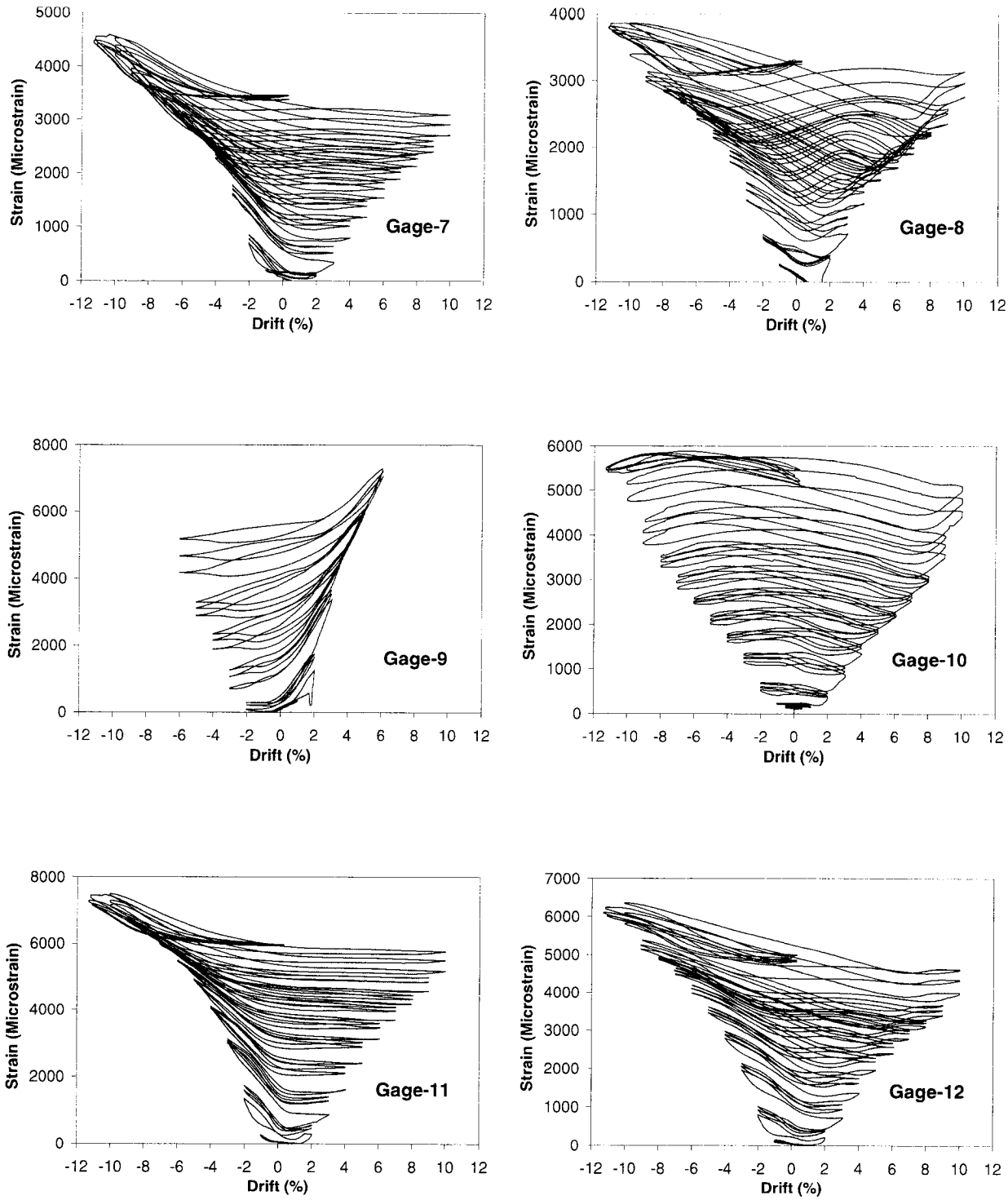

Fig. D.32 – Variation of transverse strain on the FRP Casing of Column RC-2

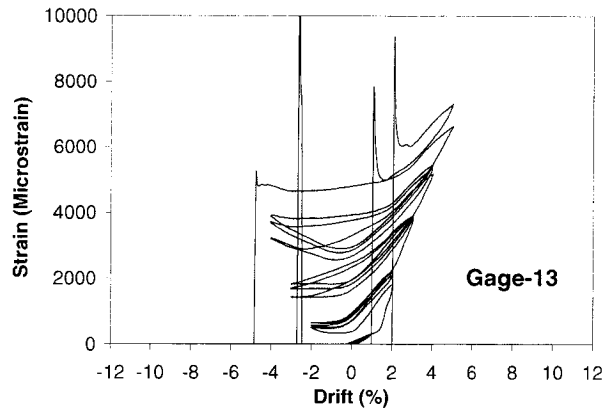

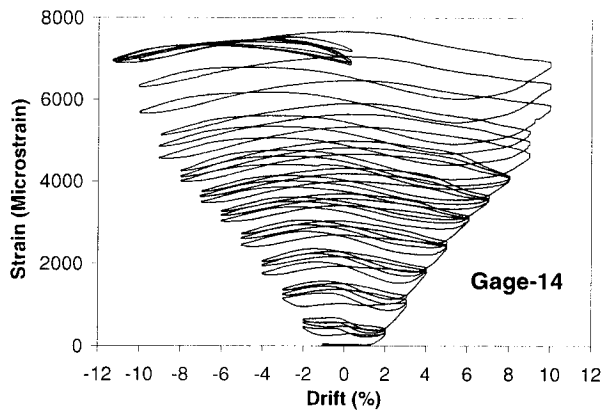

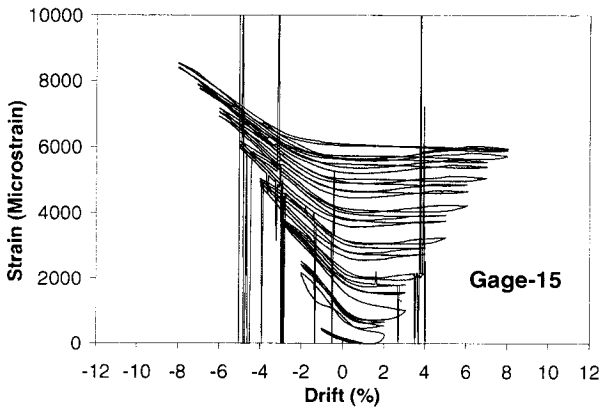

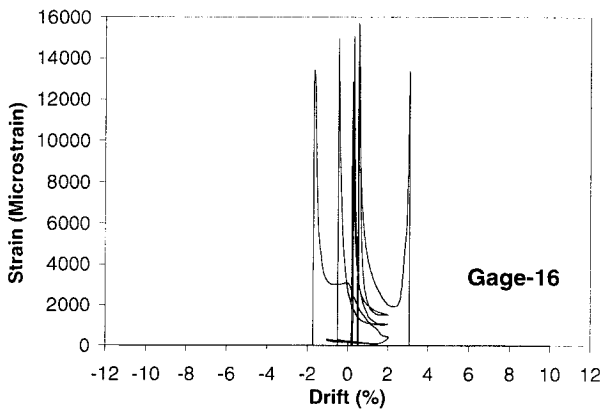

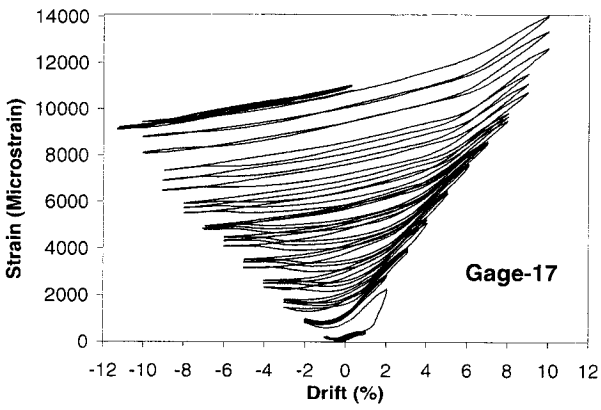

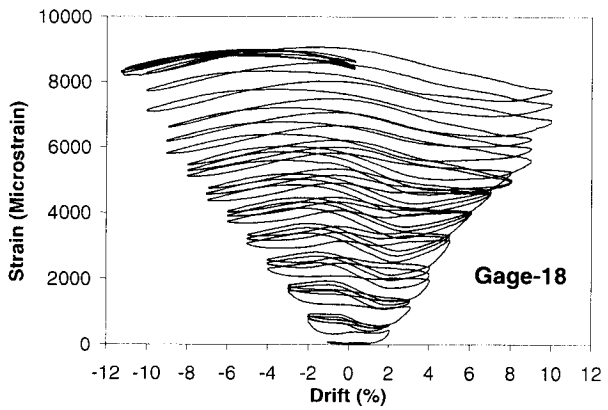

Fig. D.32 – Cont'd

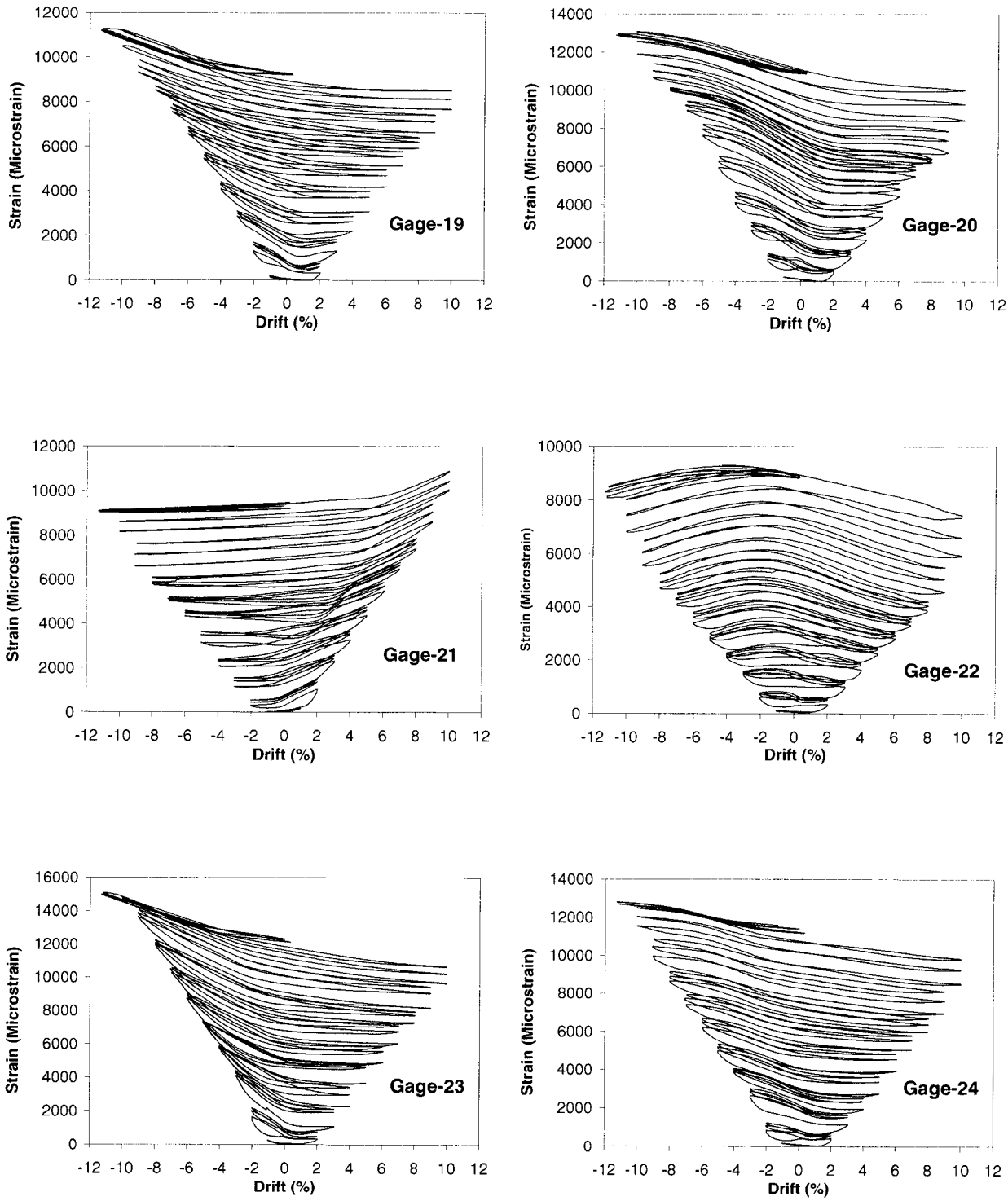

Fig. D.32 – Cont'd

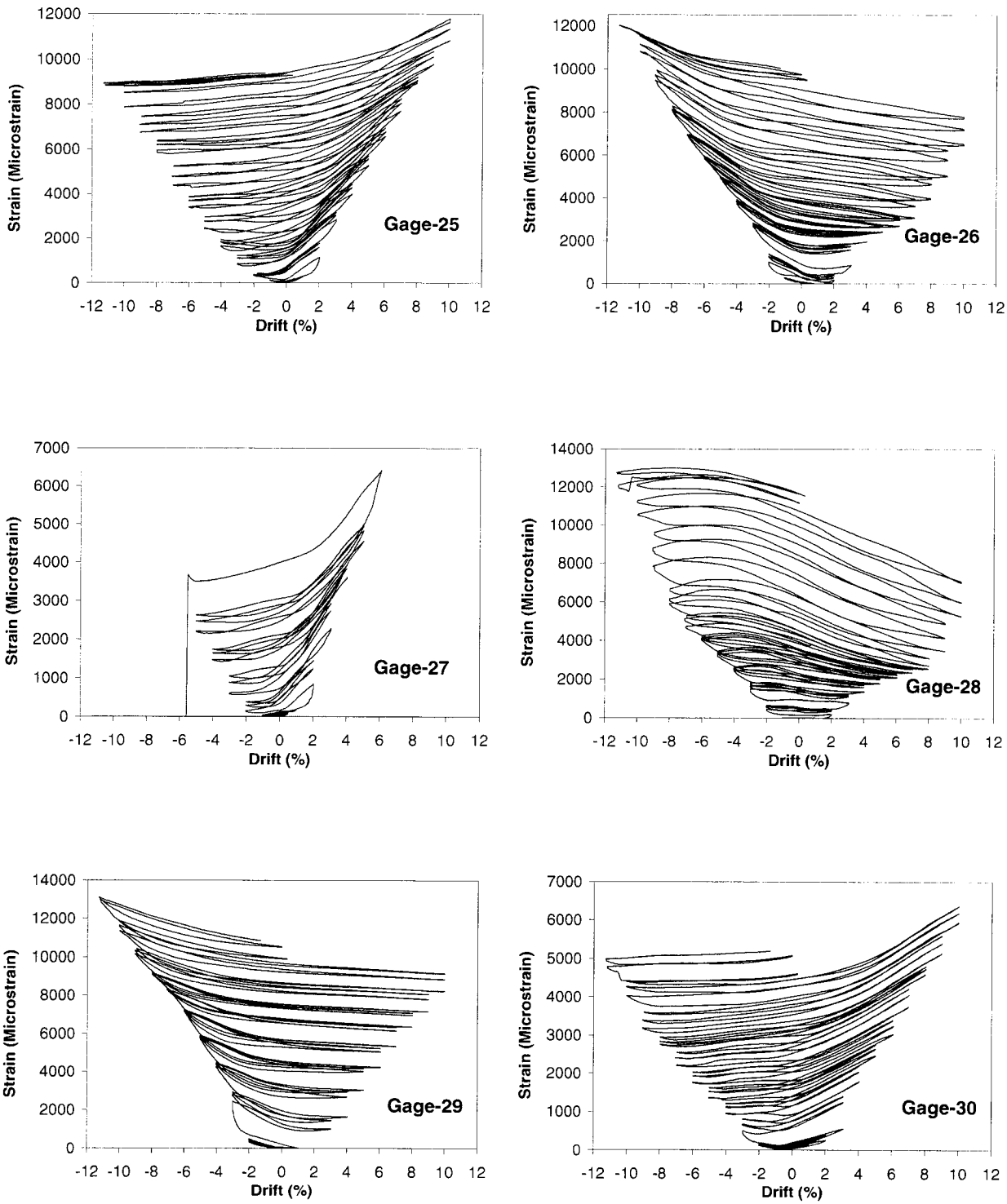

Fig. D.32 – Cont'd

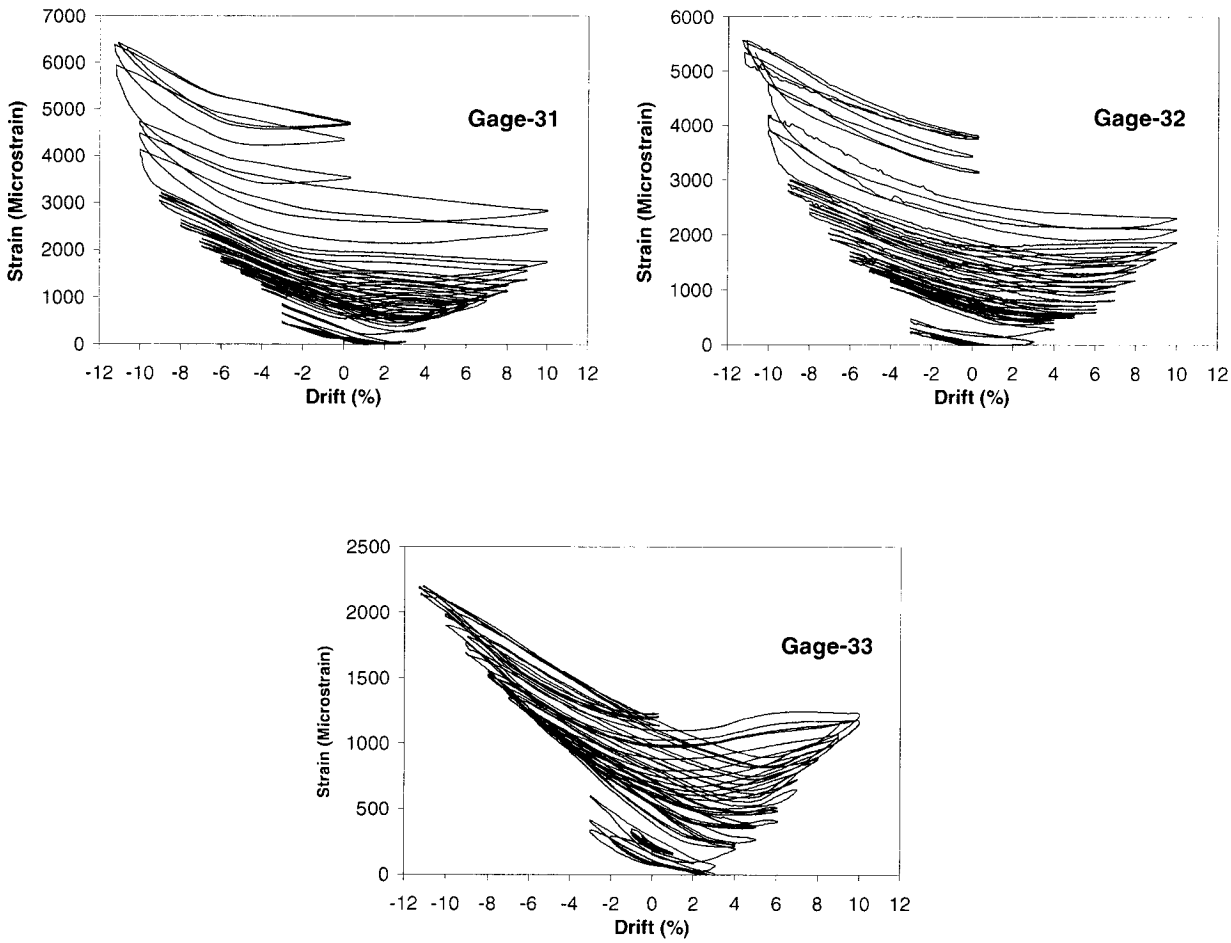

Fig. D.32 – Cont'd

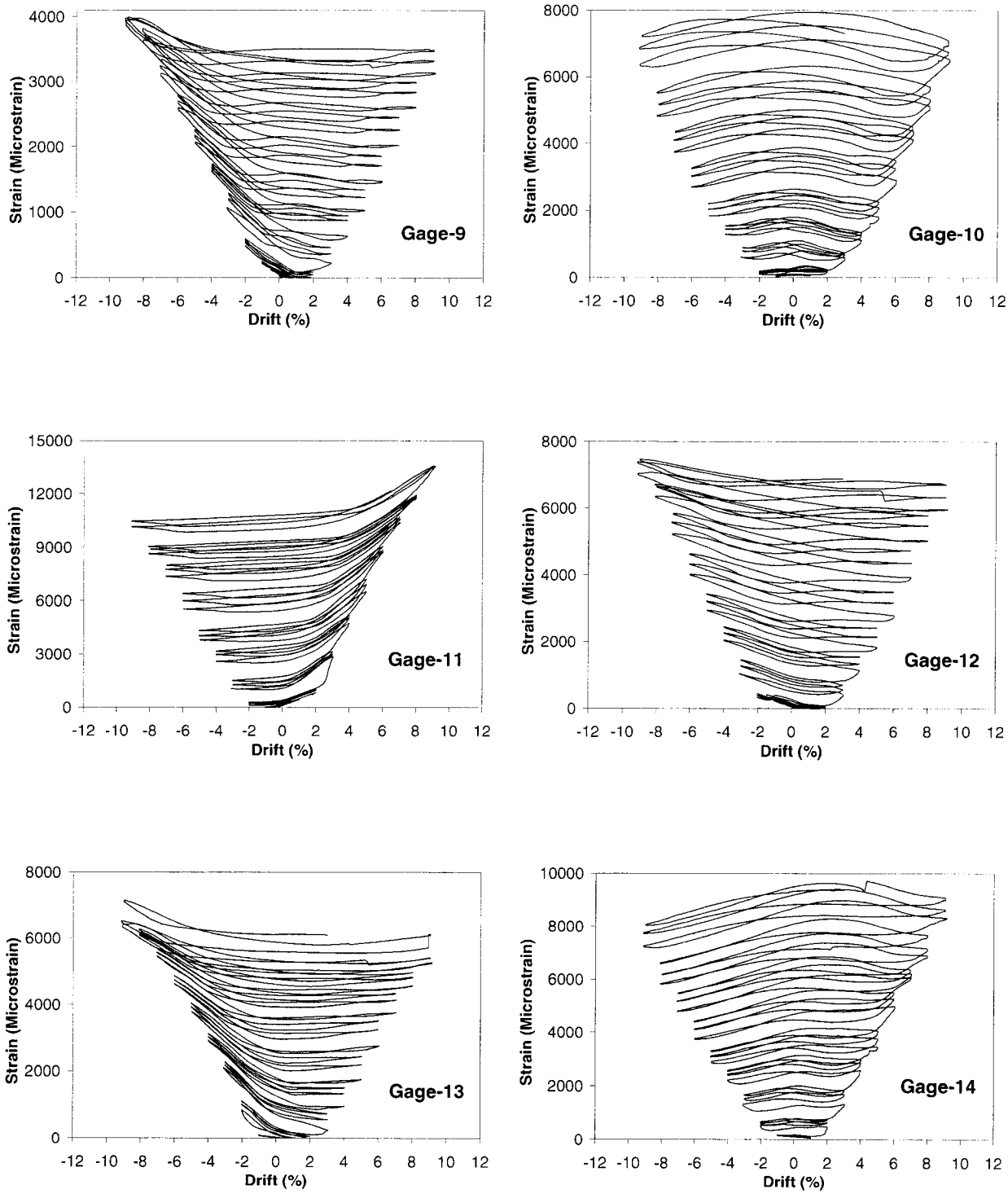

Fig. D.33 – Variation of transverse strain on the FRP Casing of Column RC-3

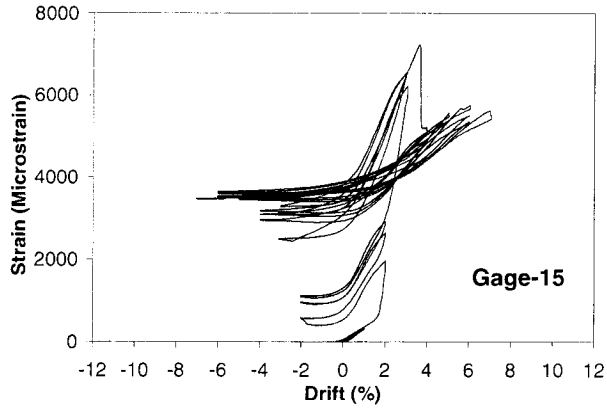

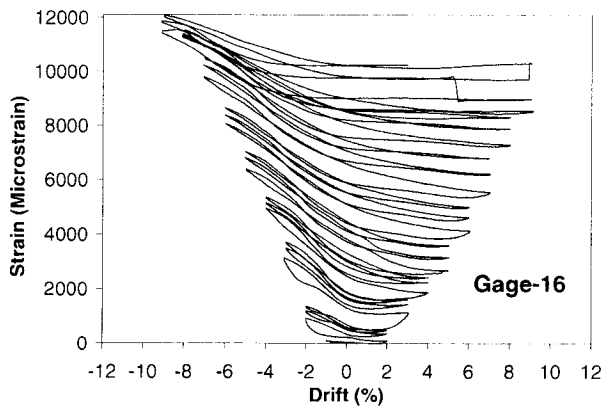

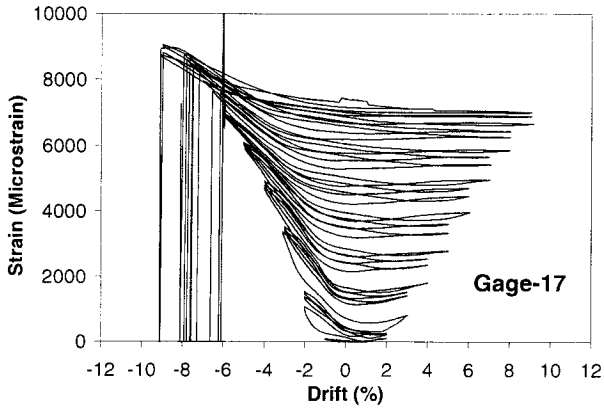

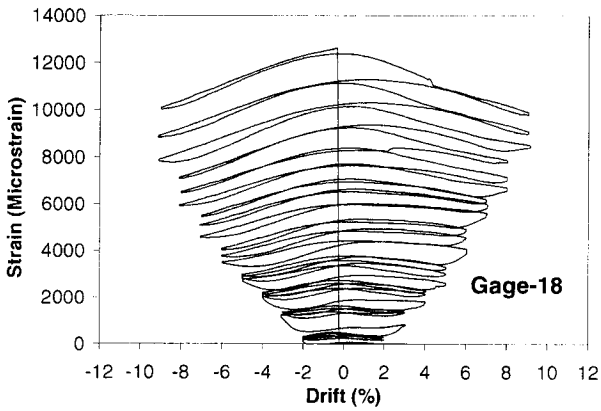

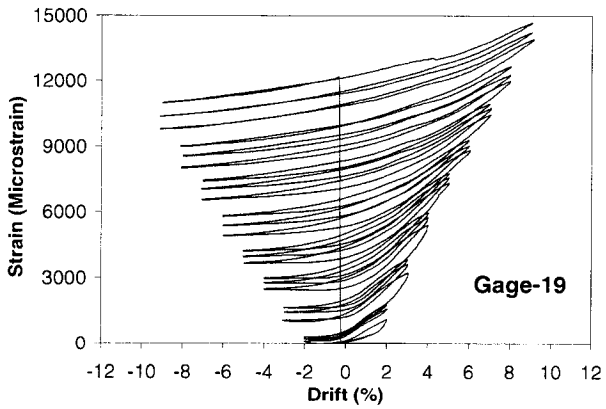

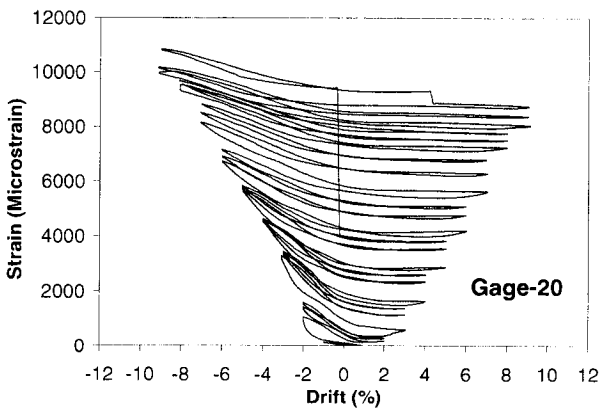

Fig. D.33 – Cont'd

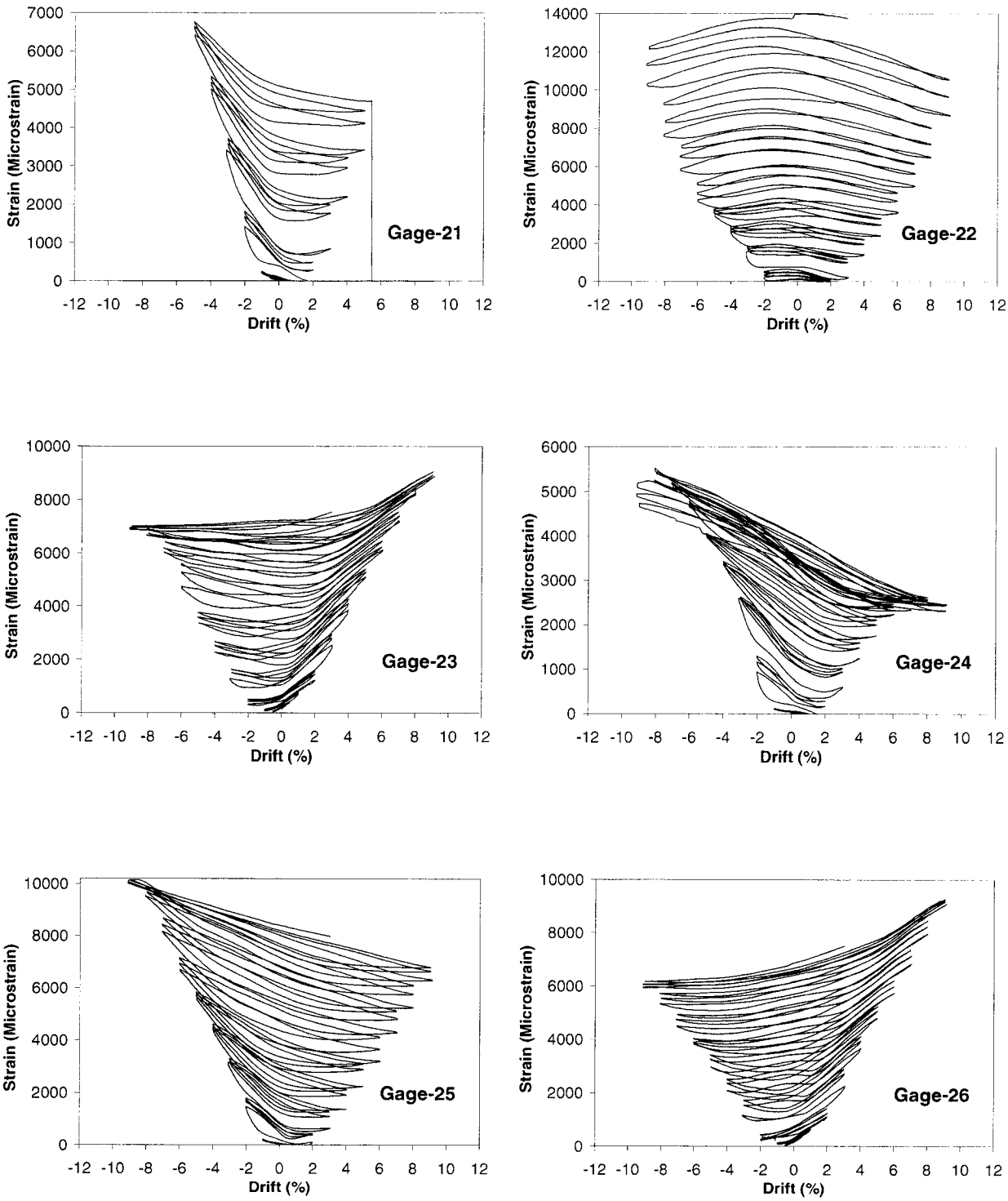

Fig. D.33 – Cont'd

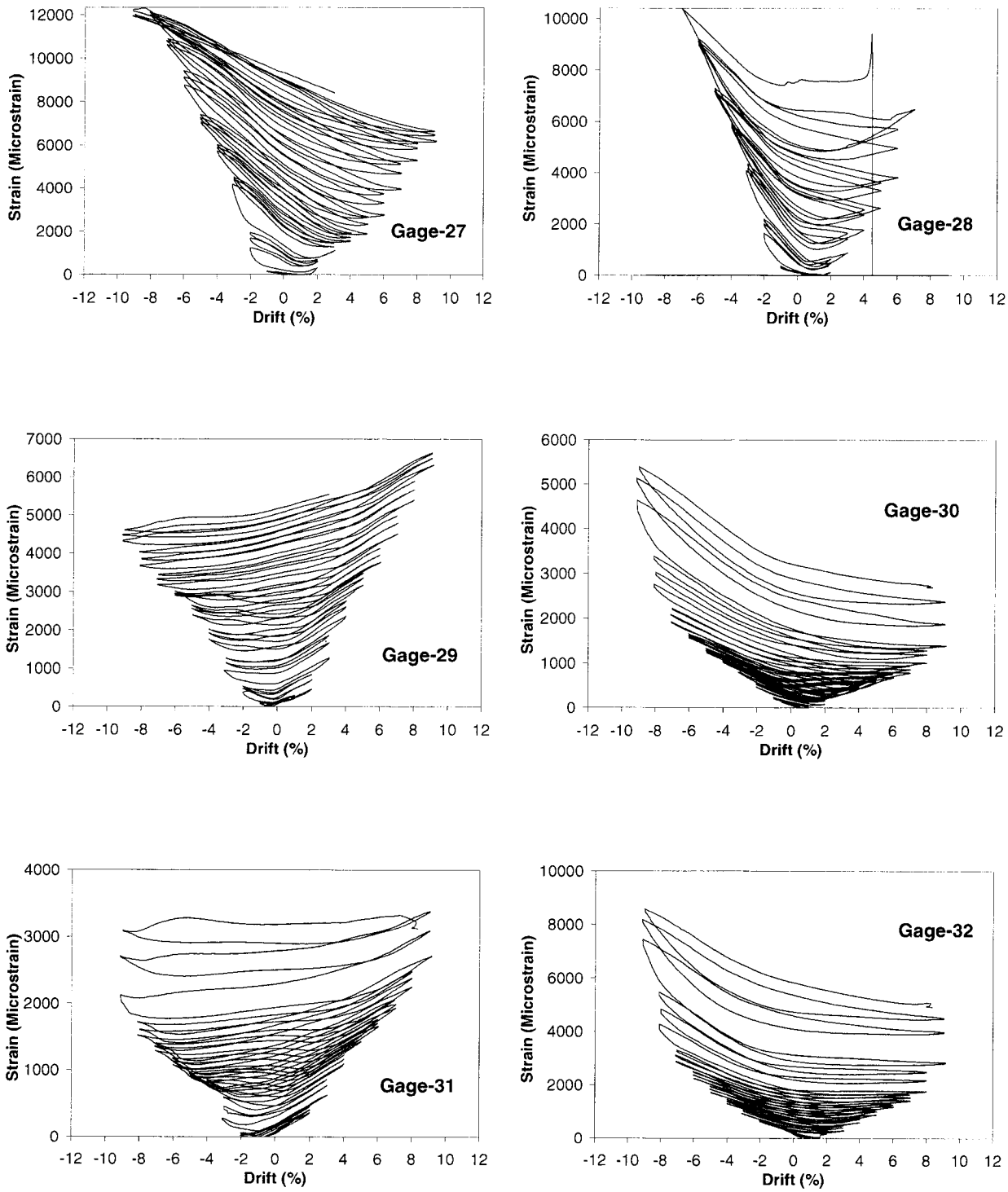

Fig. D.33 – Cont'd

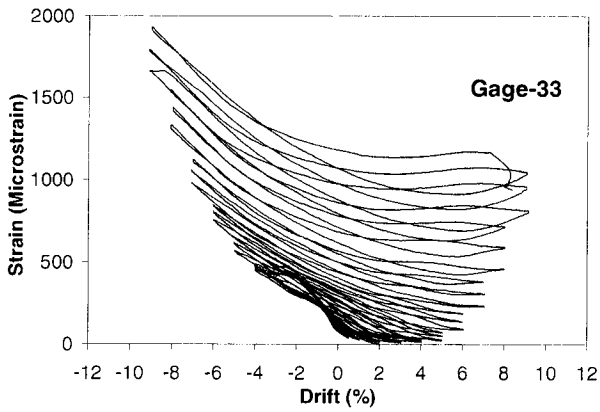

Fig. D.33 – Cont'd

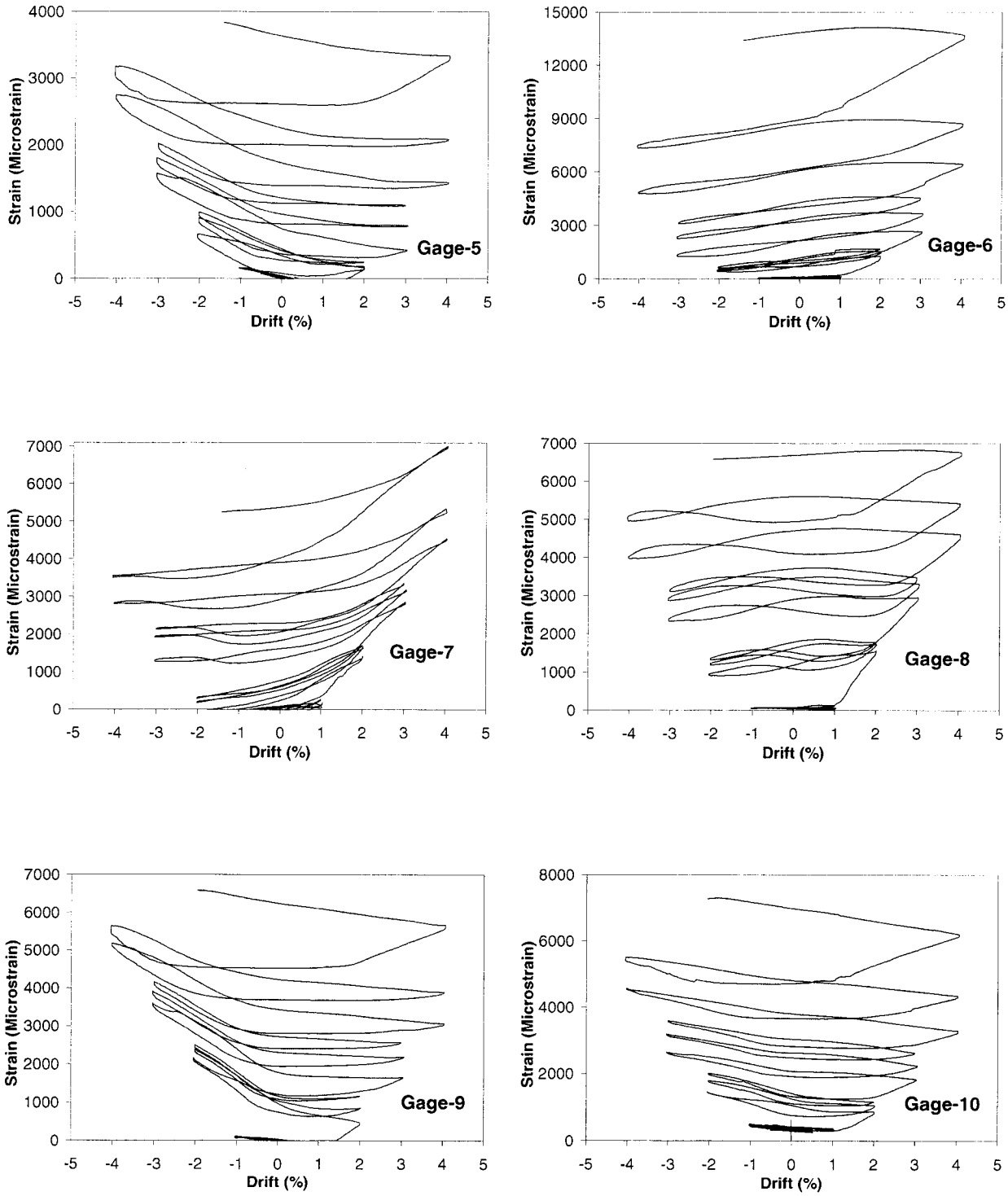

Fig. D.34 – Variation of transverse strain on the FRP Casing of Column RC-4

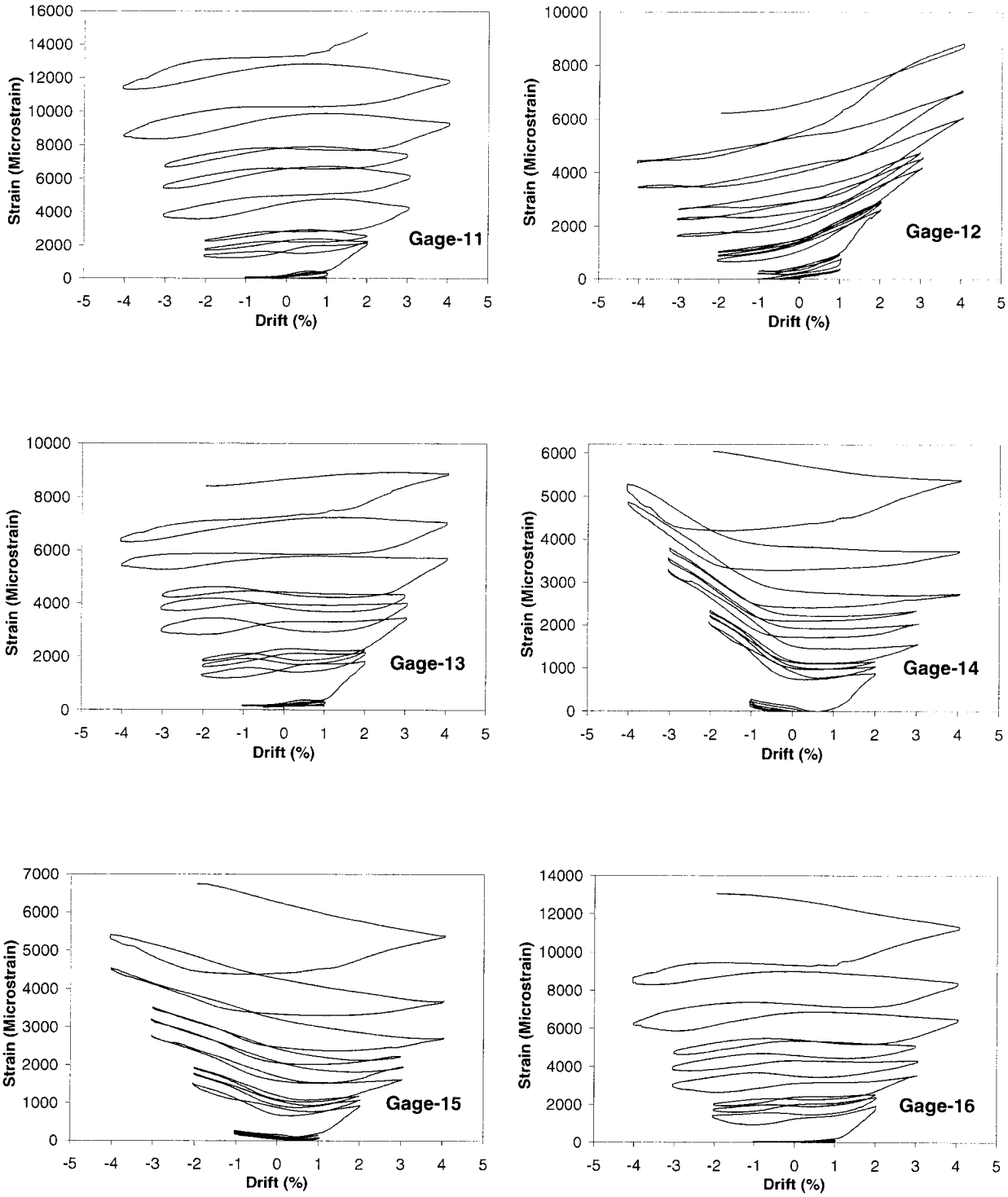

Fig. D.34 – Cont'd

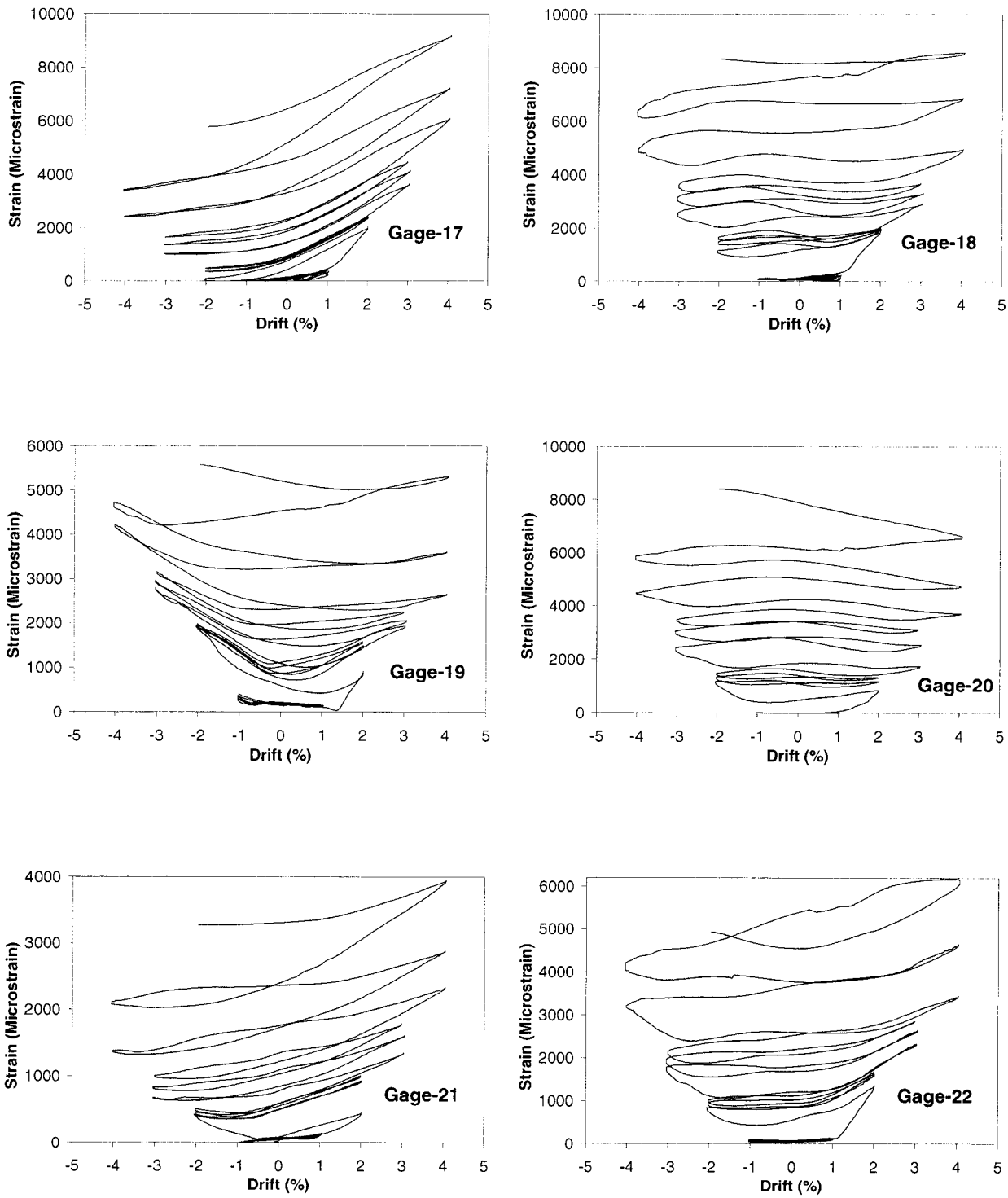

Fig. D.34 – Cont'd

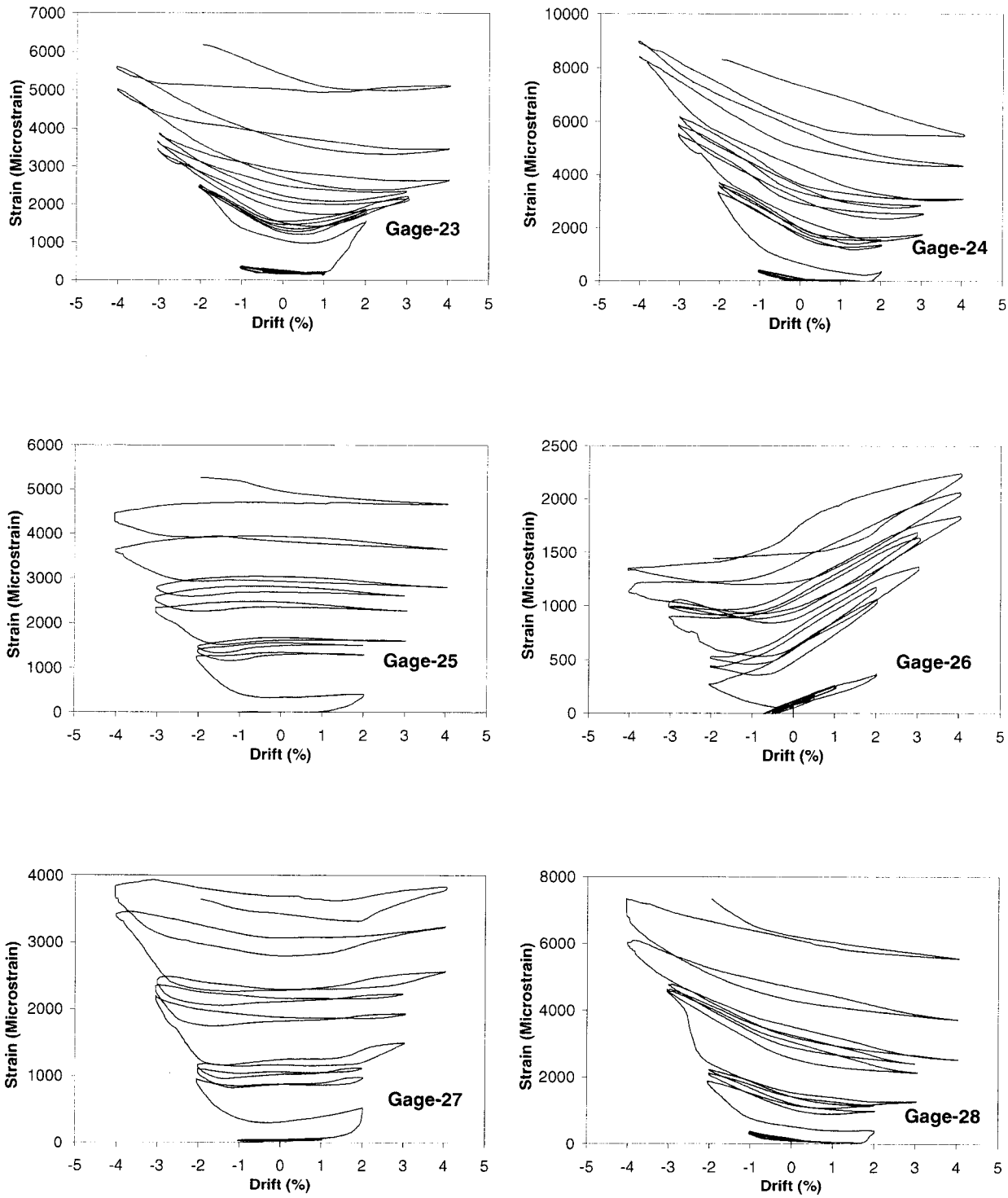

Fig. D.34 – Cont'd

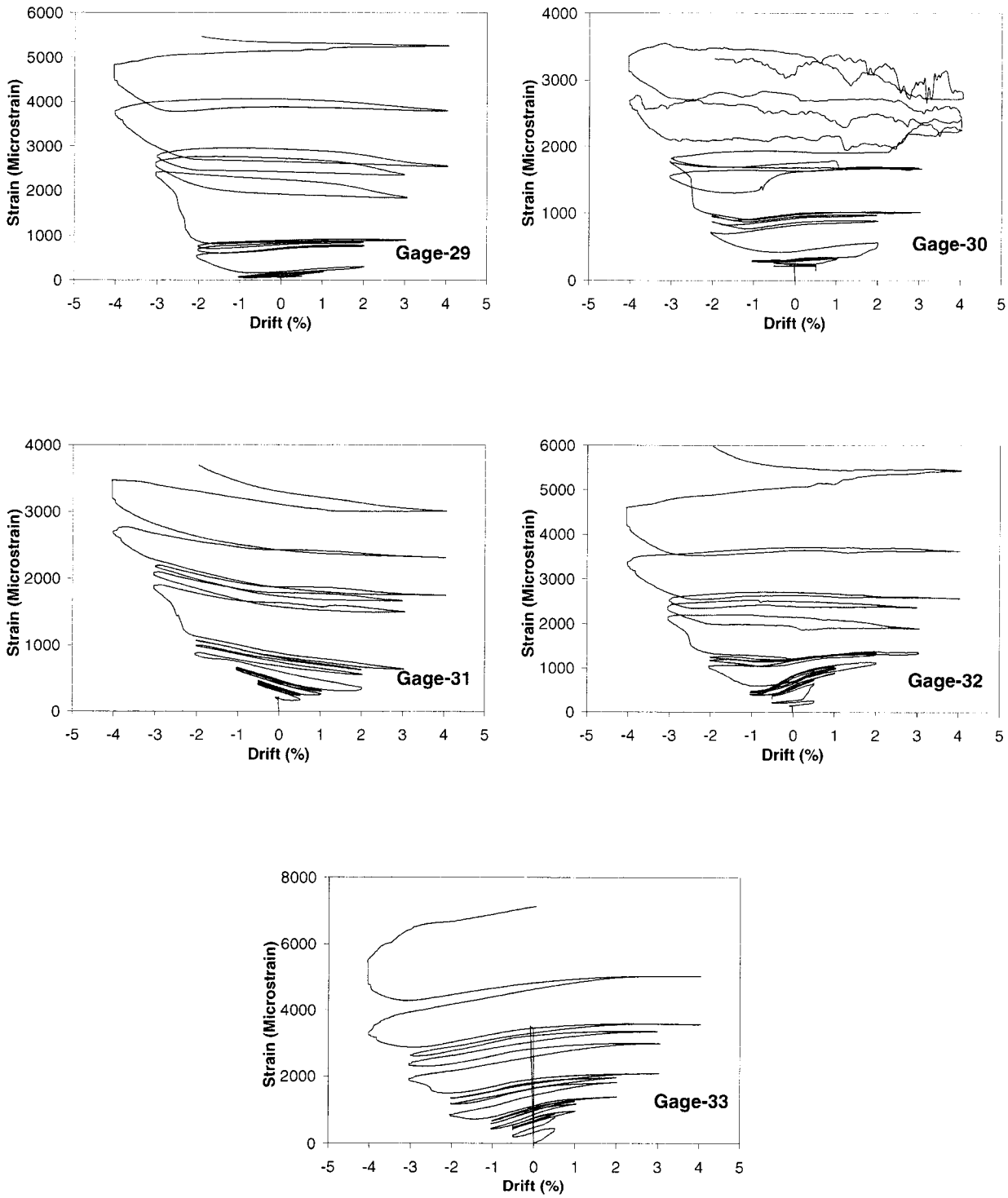

Fig. D.34 – Cont'd

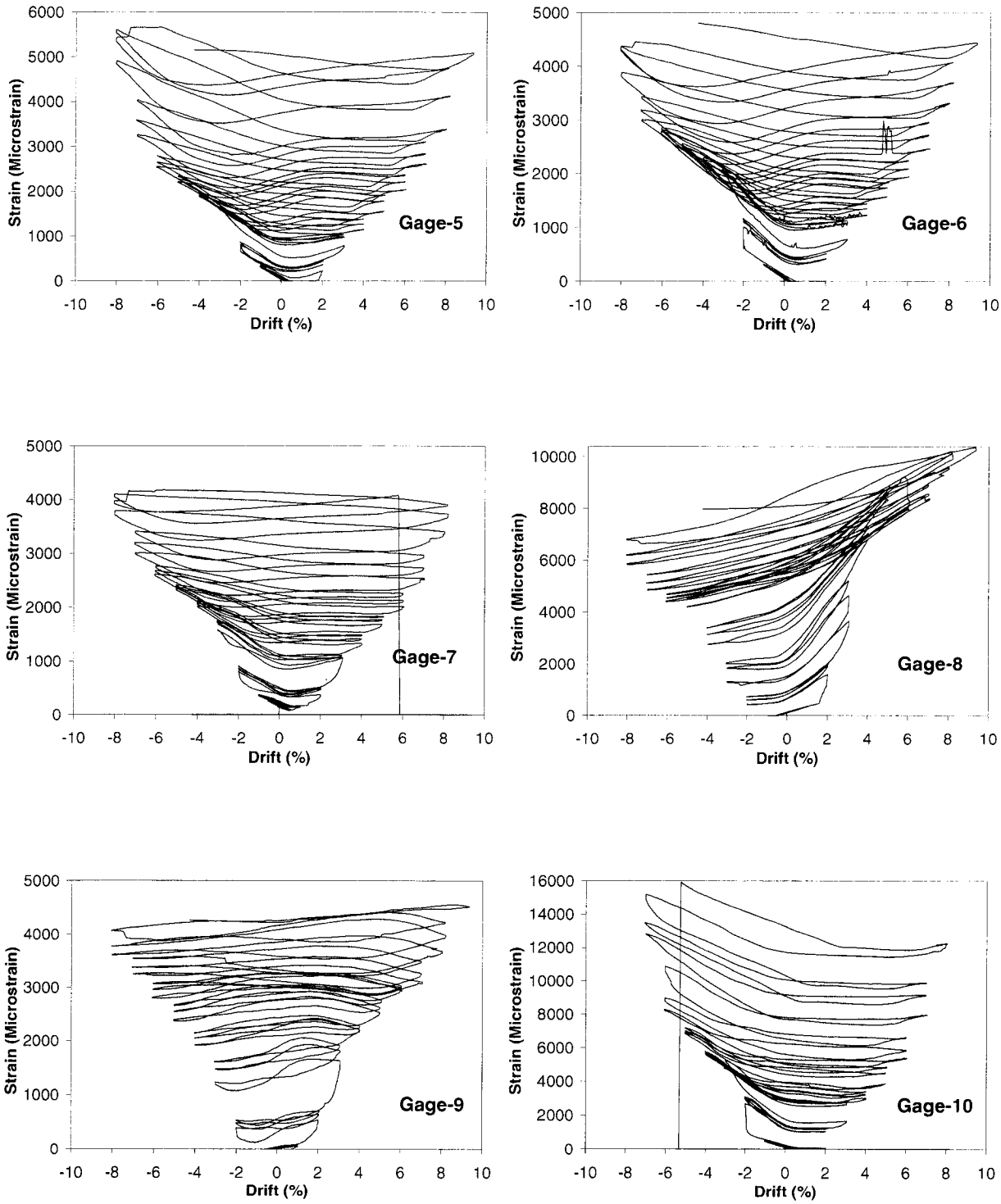

Fig. D.35 – Variation of transverse strain on the FRP Casing of Column RS-1

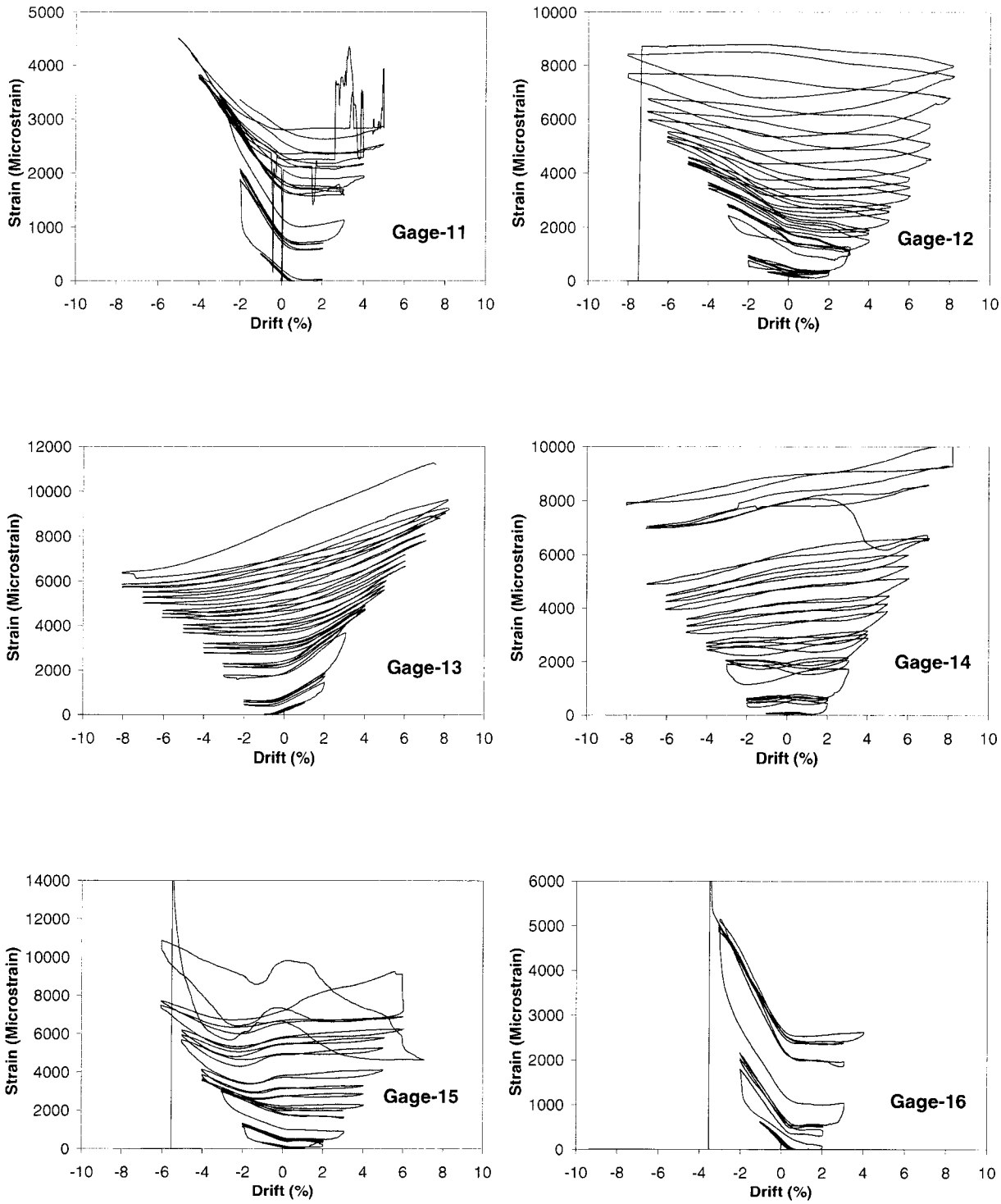

Fig. D.35 – Cont'd

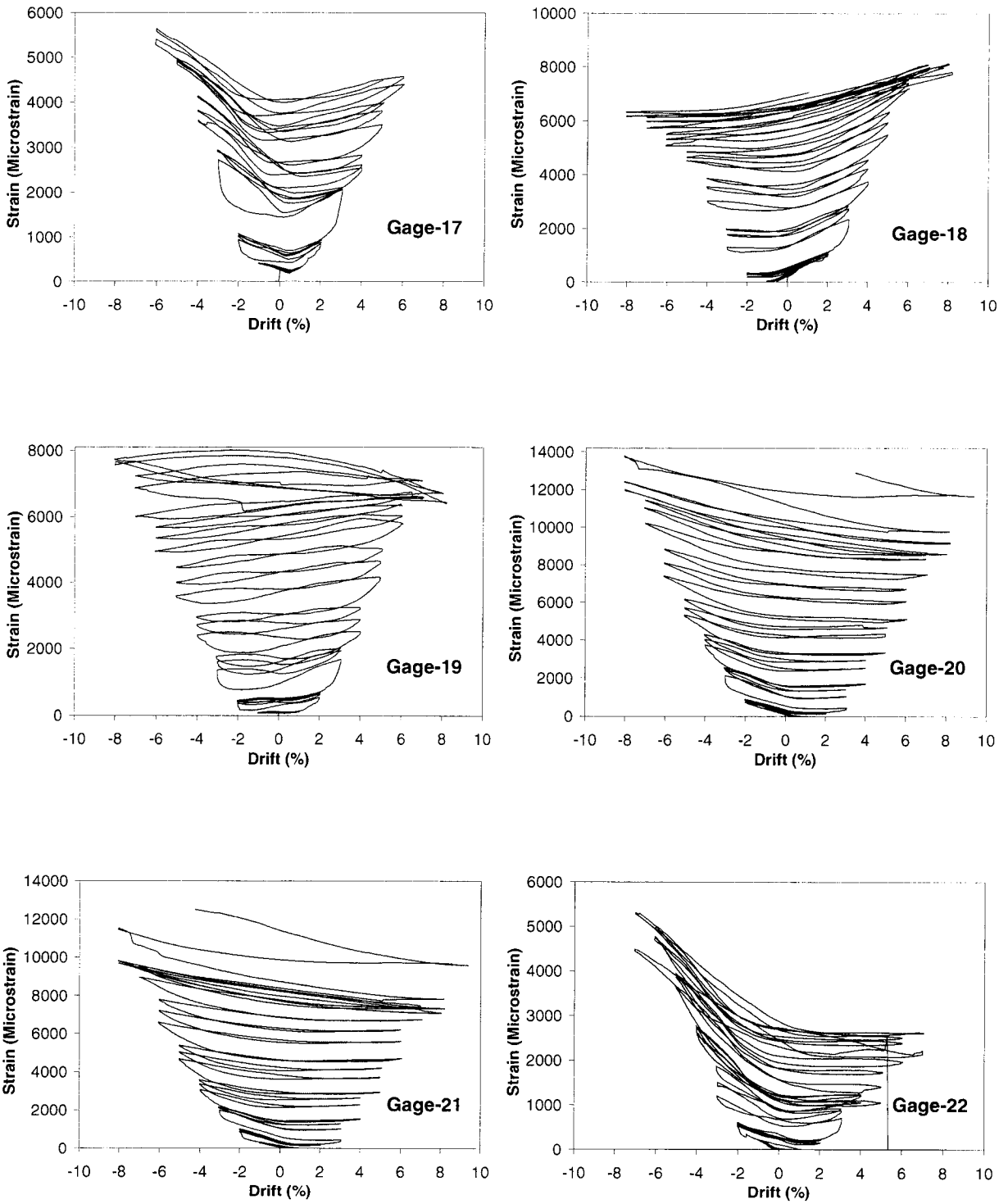

Fig. D.35 – Cont'd

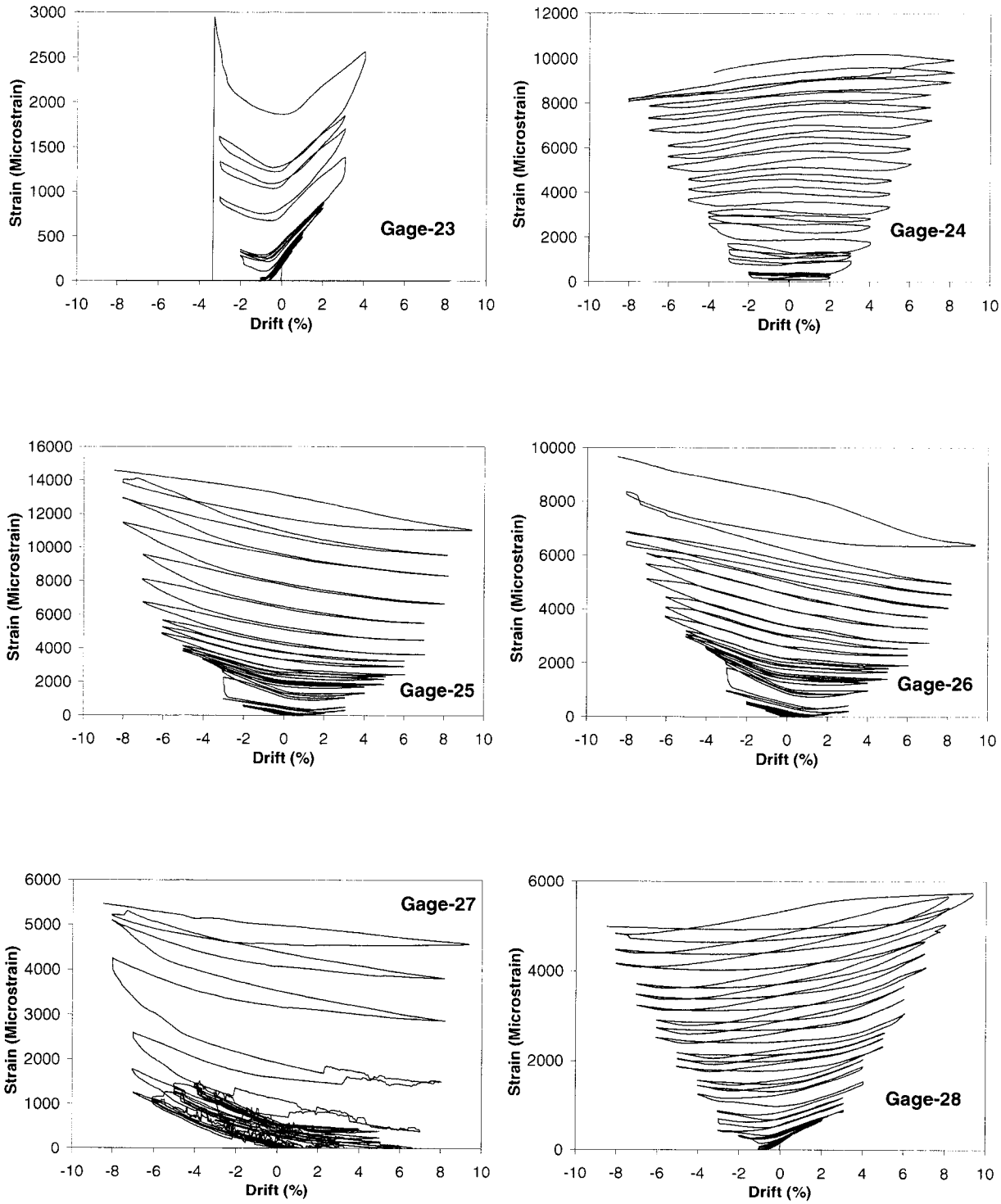

Fig. D.35 – Cont'd

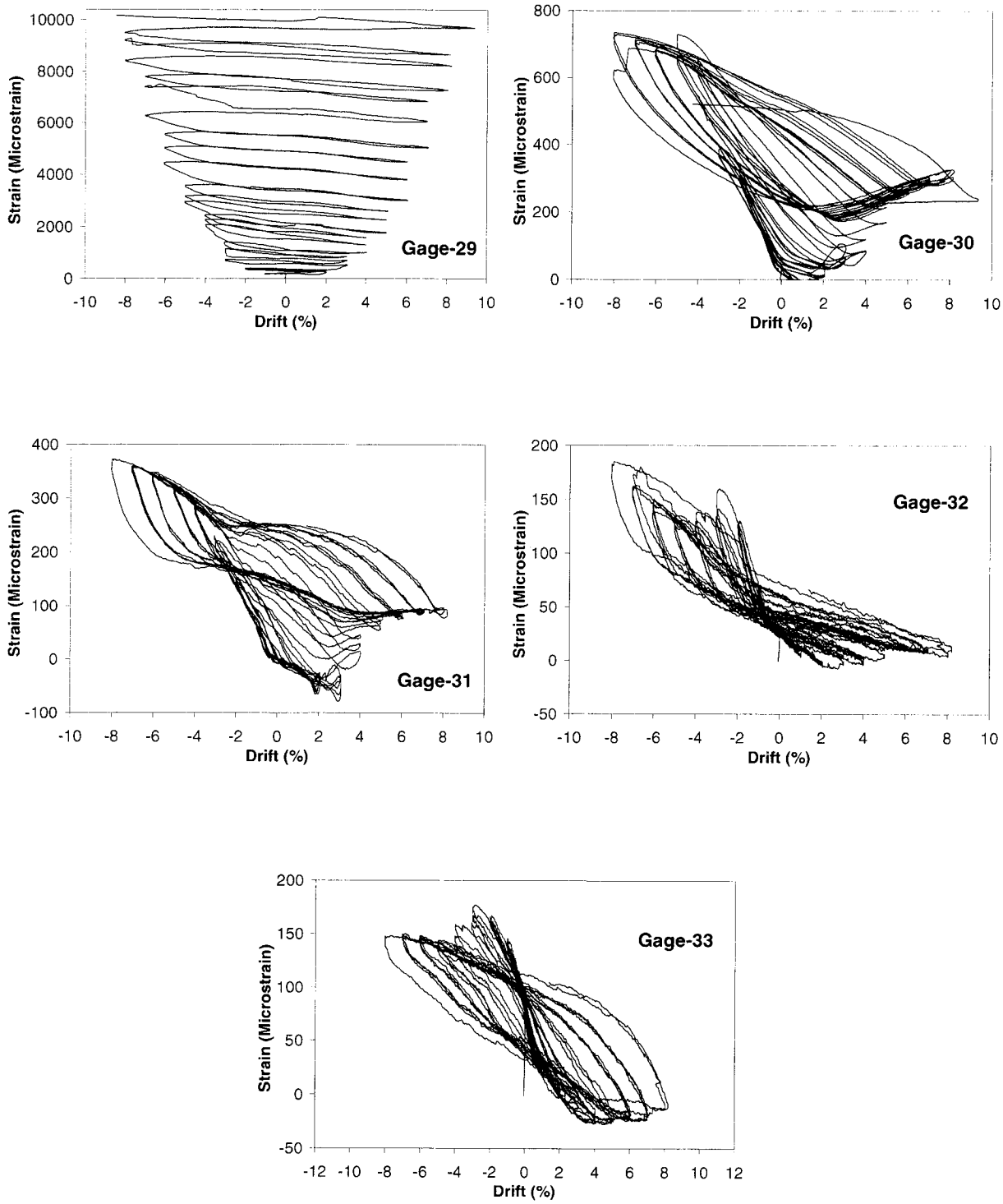

Fig. D.35 – Cont'd

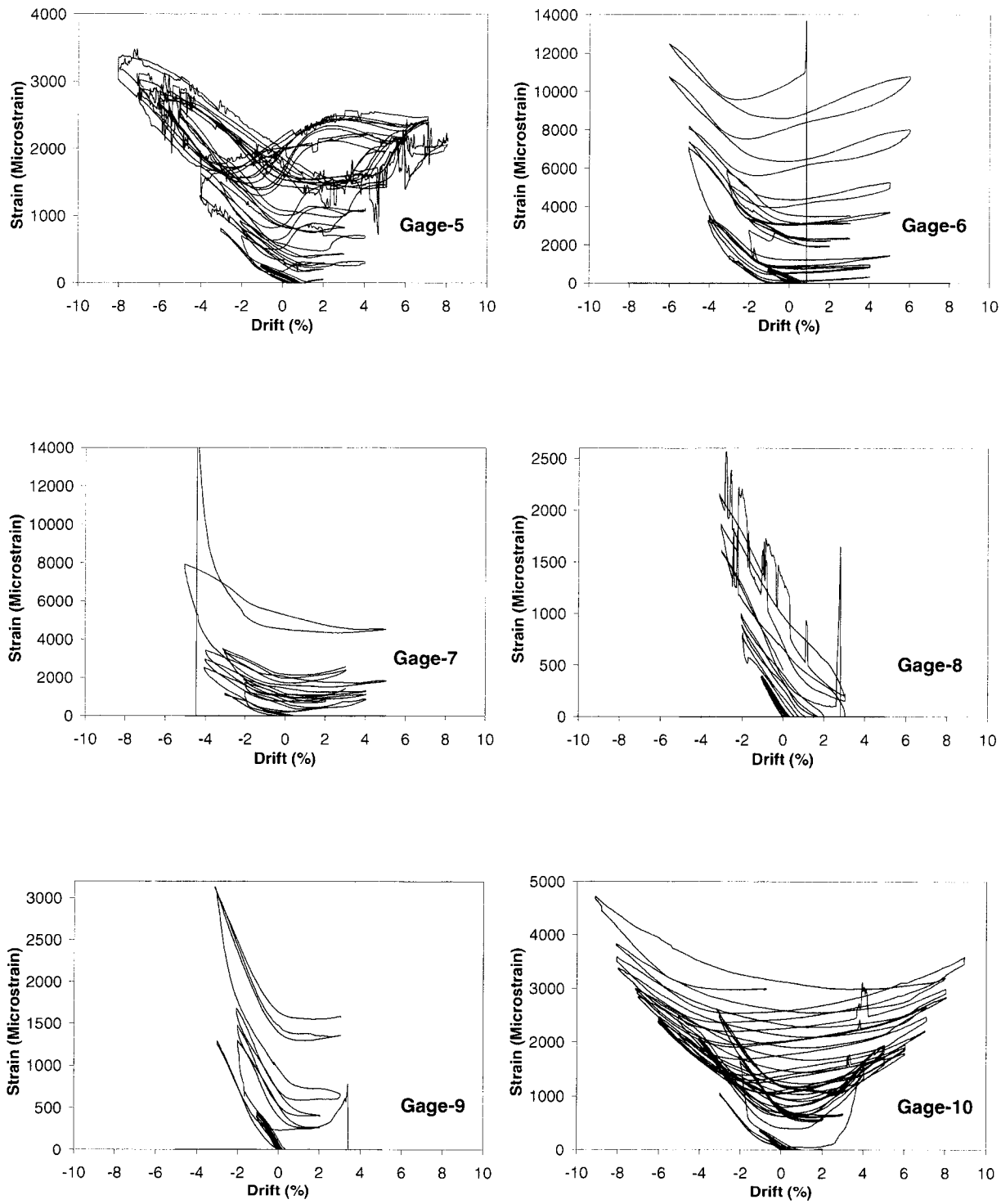

Fig. D.36 – Variation of transverse strain on the FRP Casing of Column RS-2

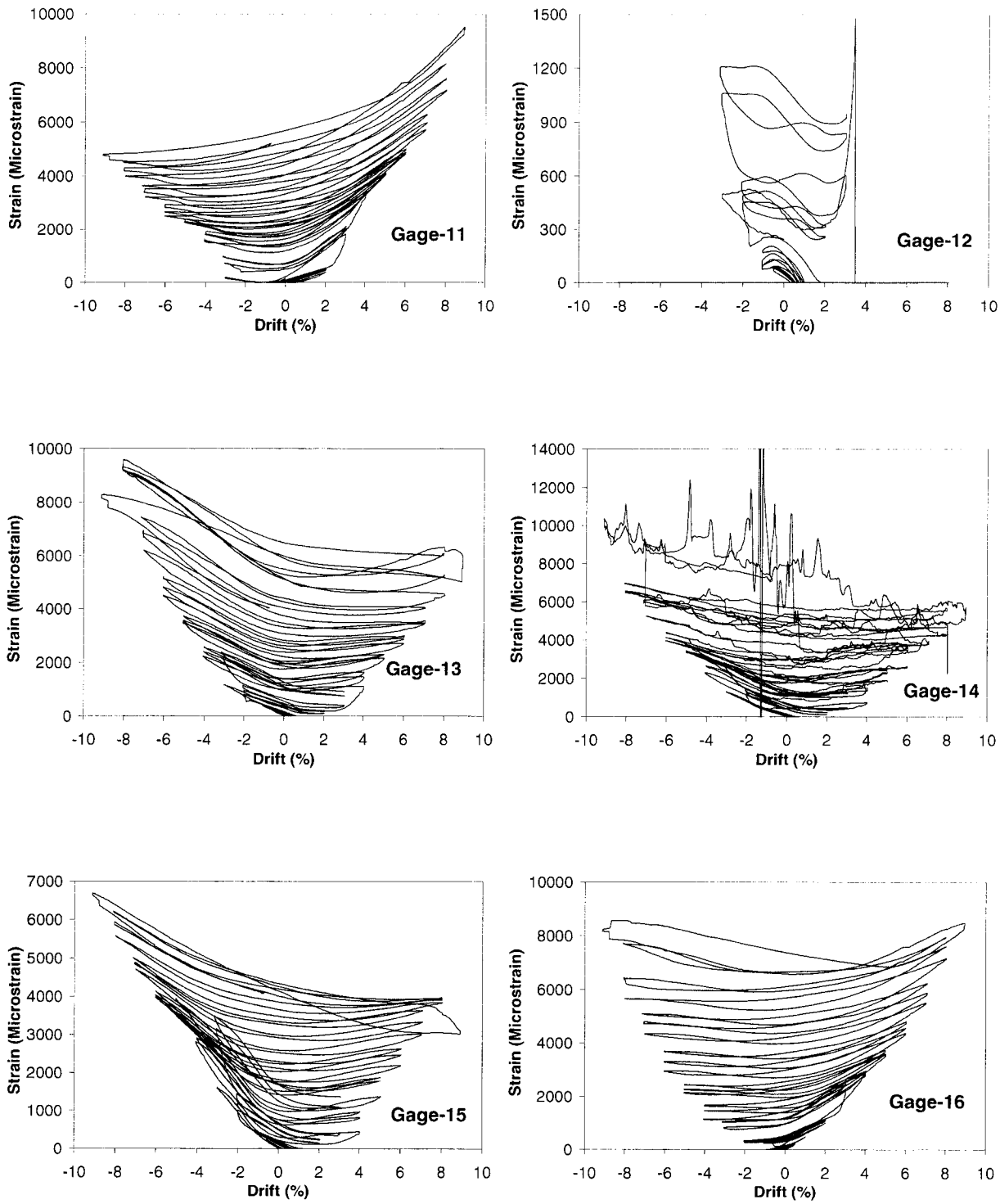

Fig. D.36 – Cont'd

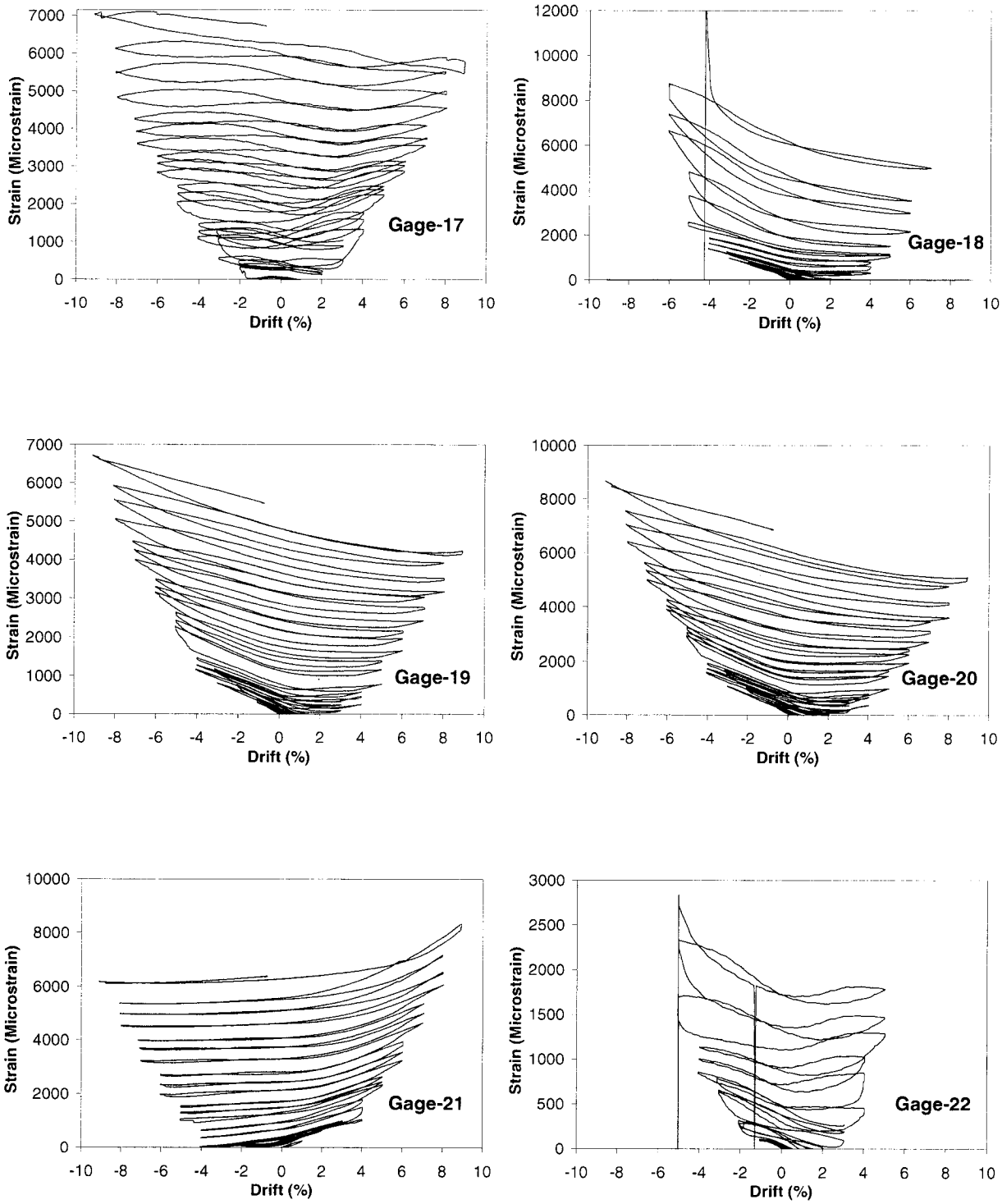

Fig. D.36 – Cont'd

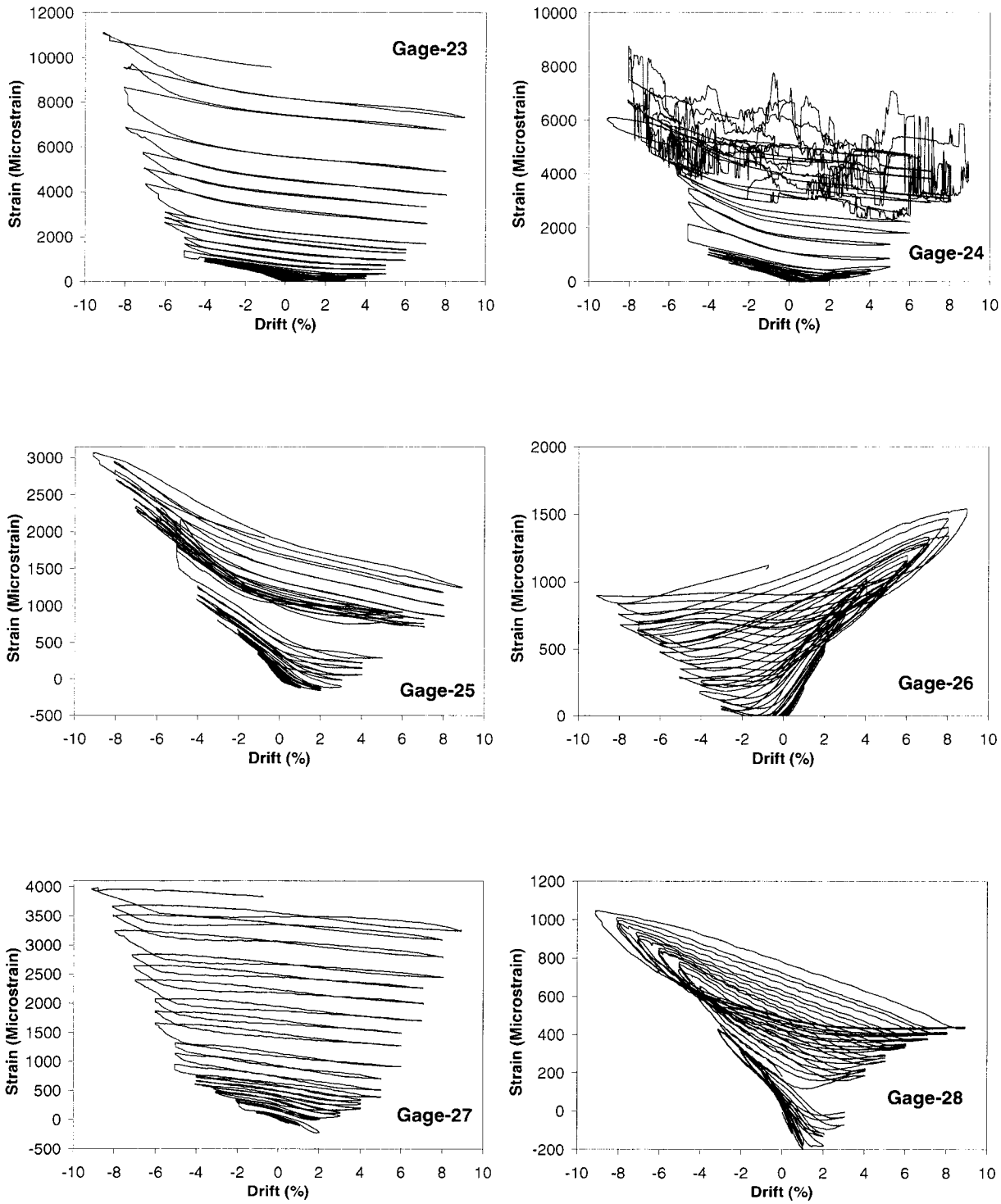

Fig. D.36 – Cont'd

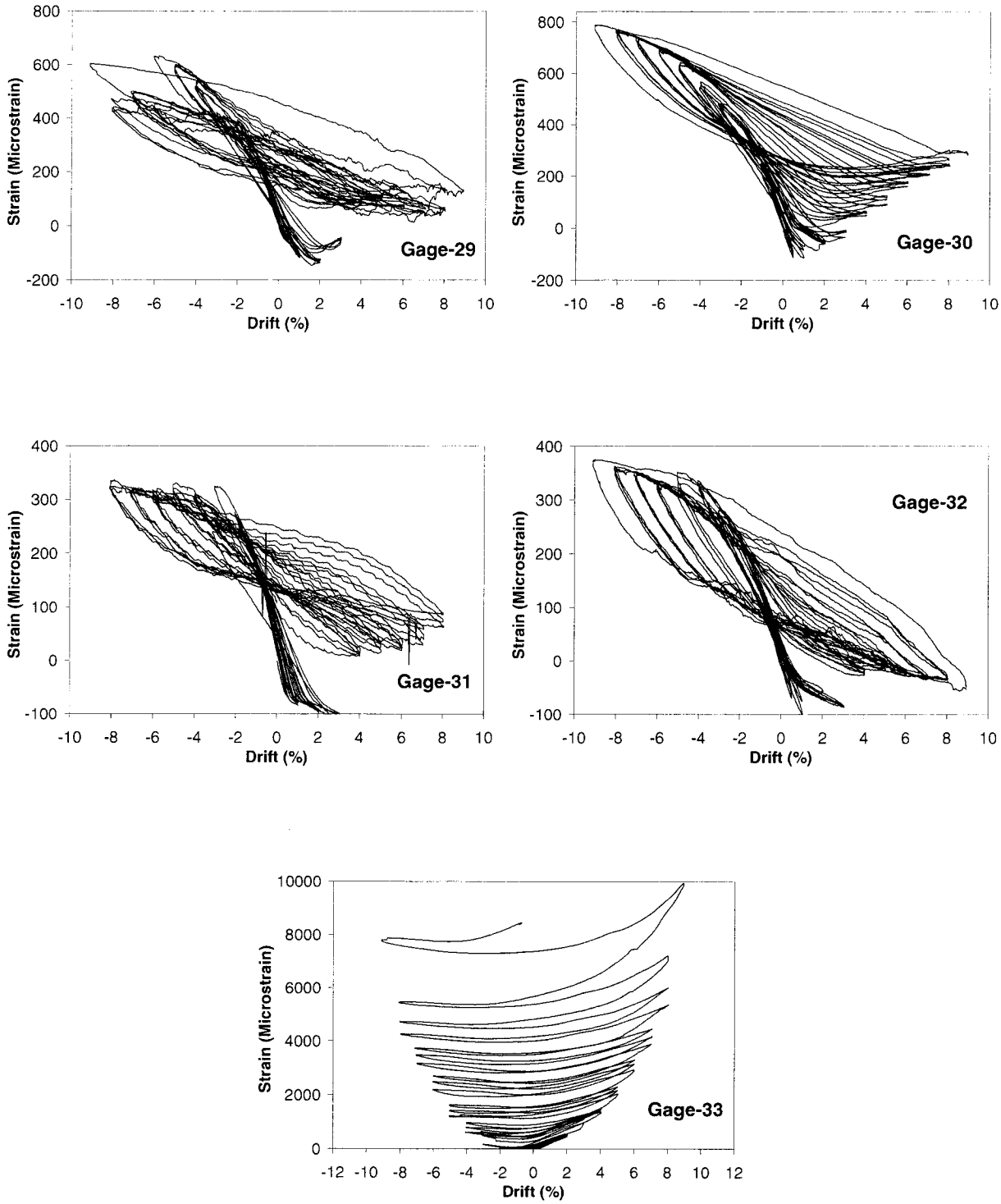

Fig. D.36 – Cont'd

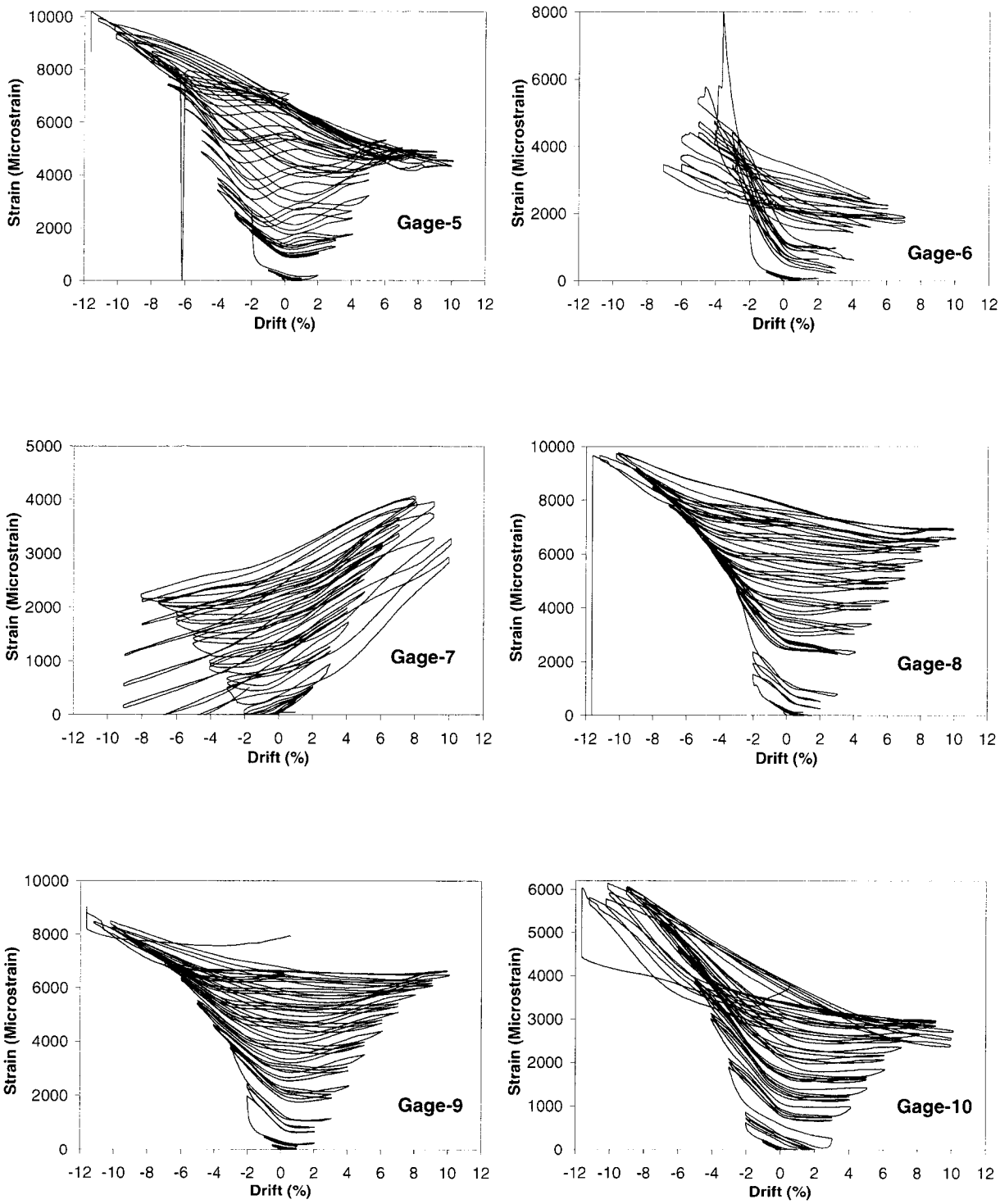

Fig. D.37 – Variation of transverse strain on the FRP Casing of Column RS-3

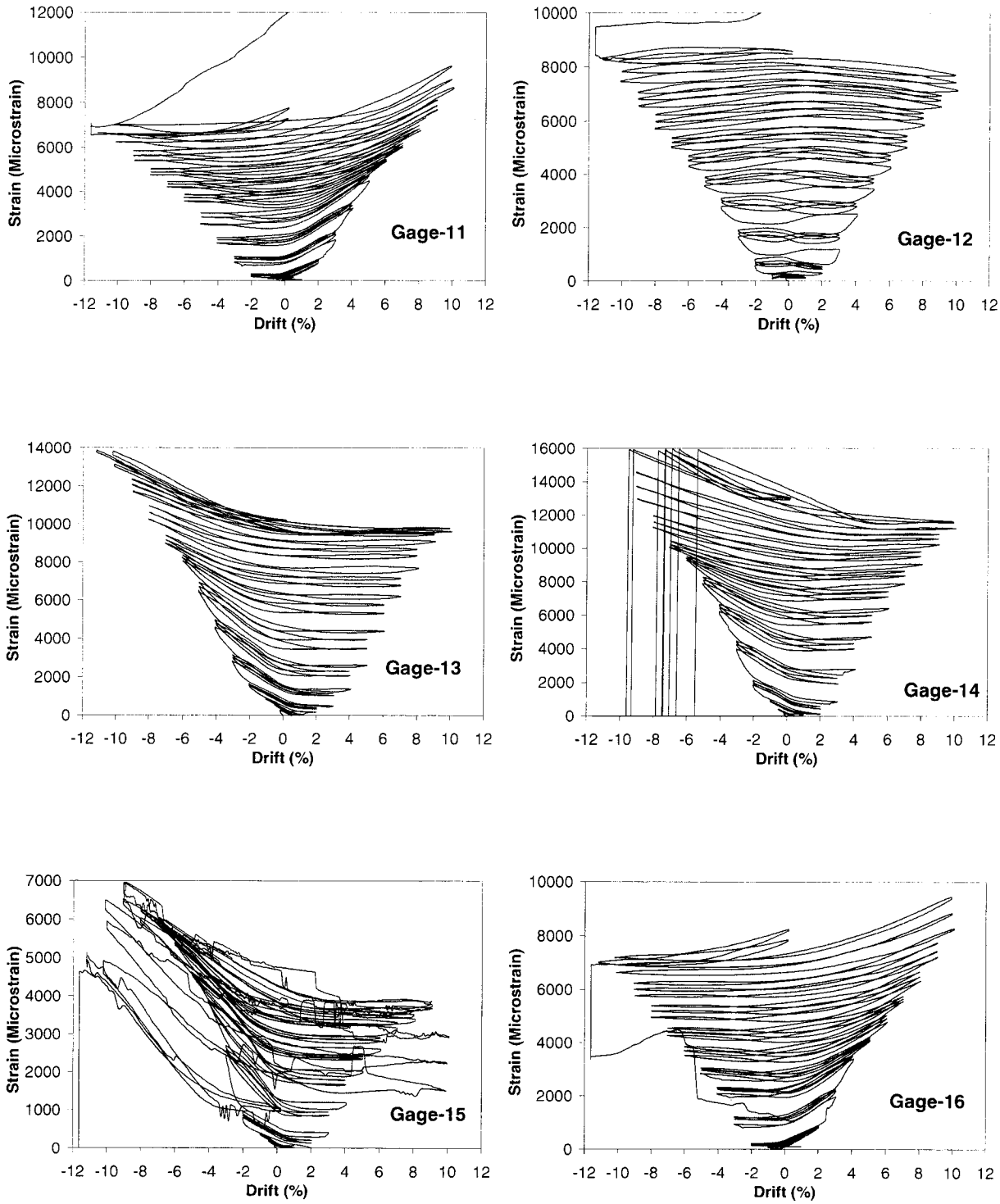

Fig. D.37 – Cont'd

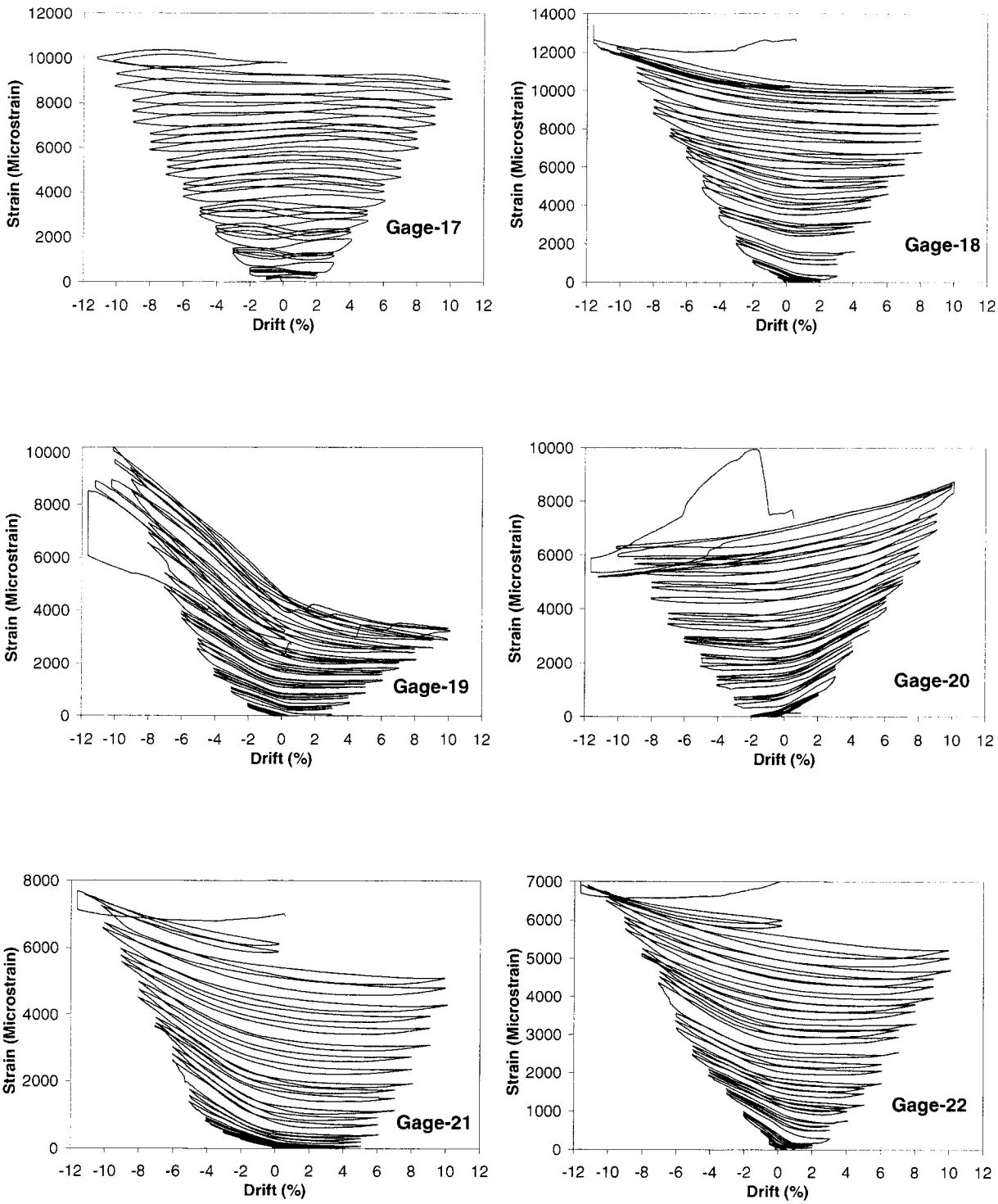

Fig. D.37 – Cont'd

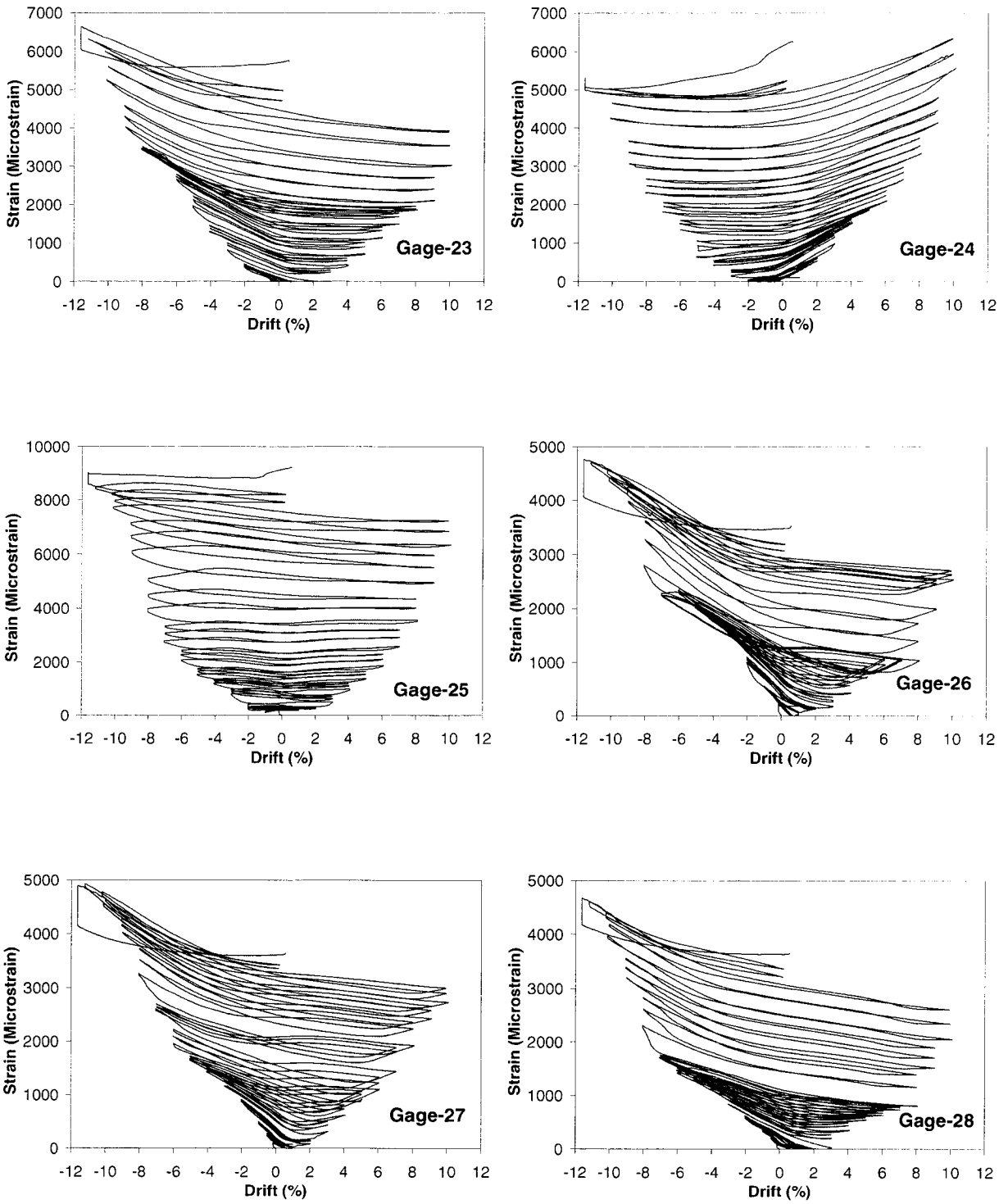

Fig. D.37 – Cont'd

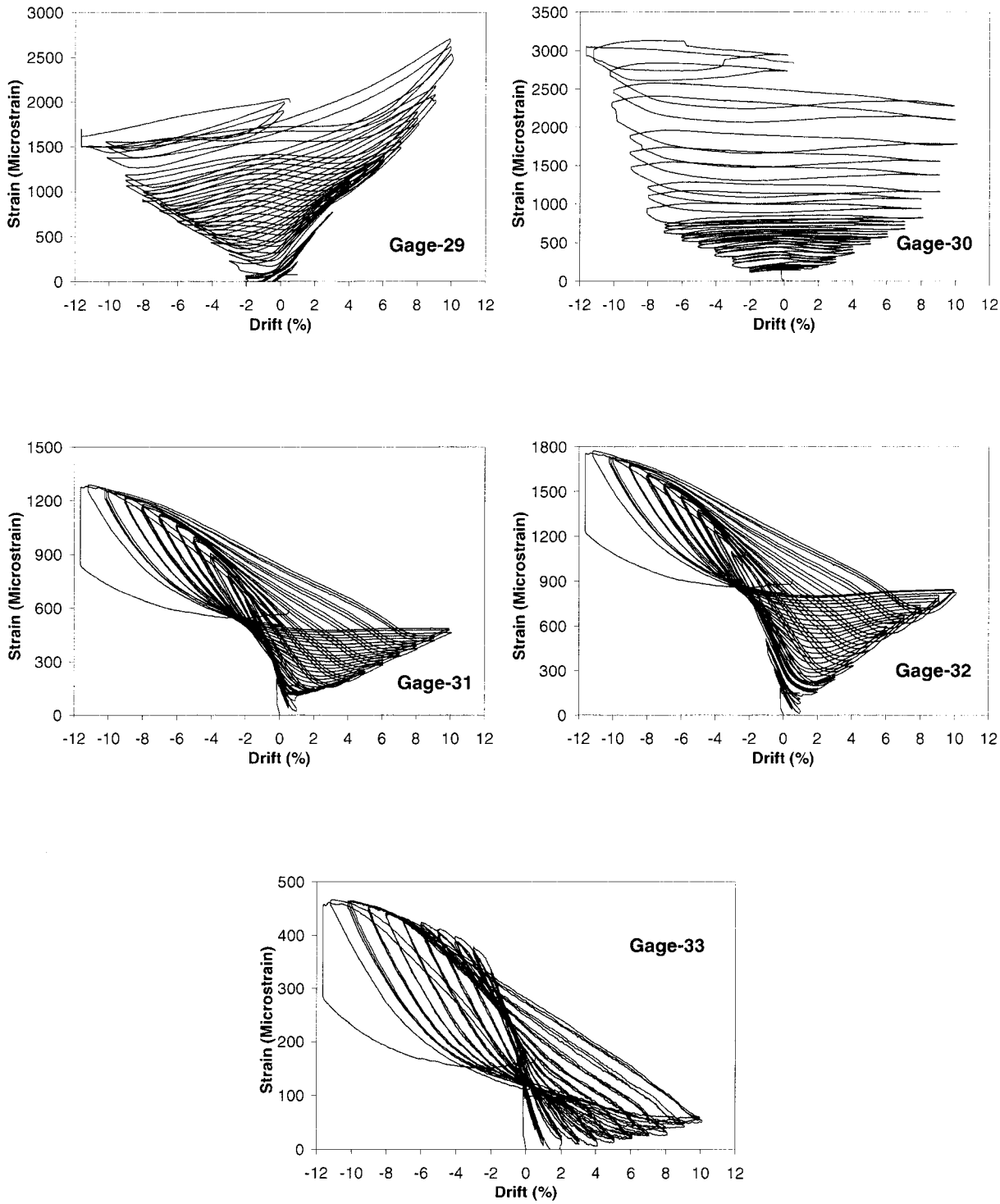

Fig. D.37 – Cont'd

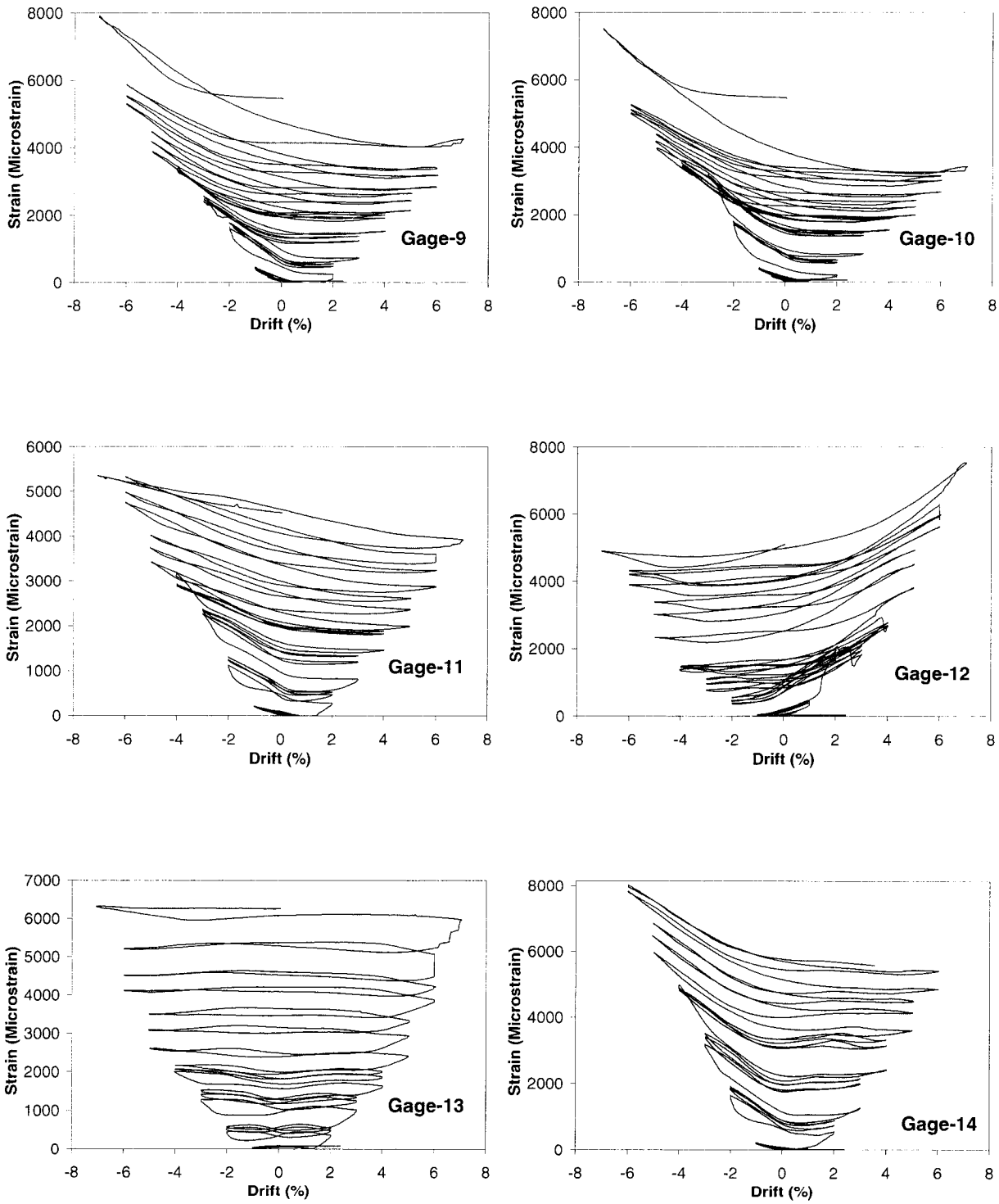

Fig. D.38 – Variation of transverse strain on the FRP Casing of Column RS-4

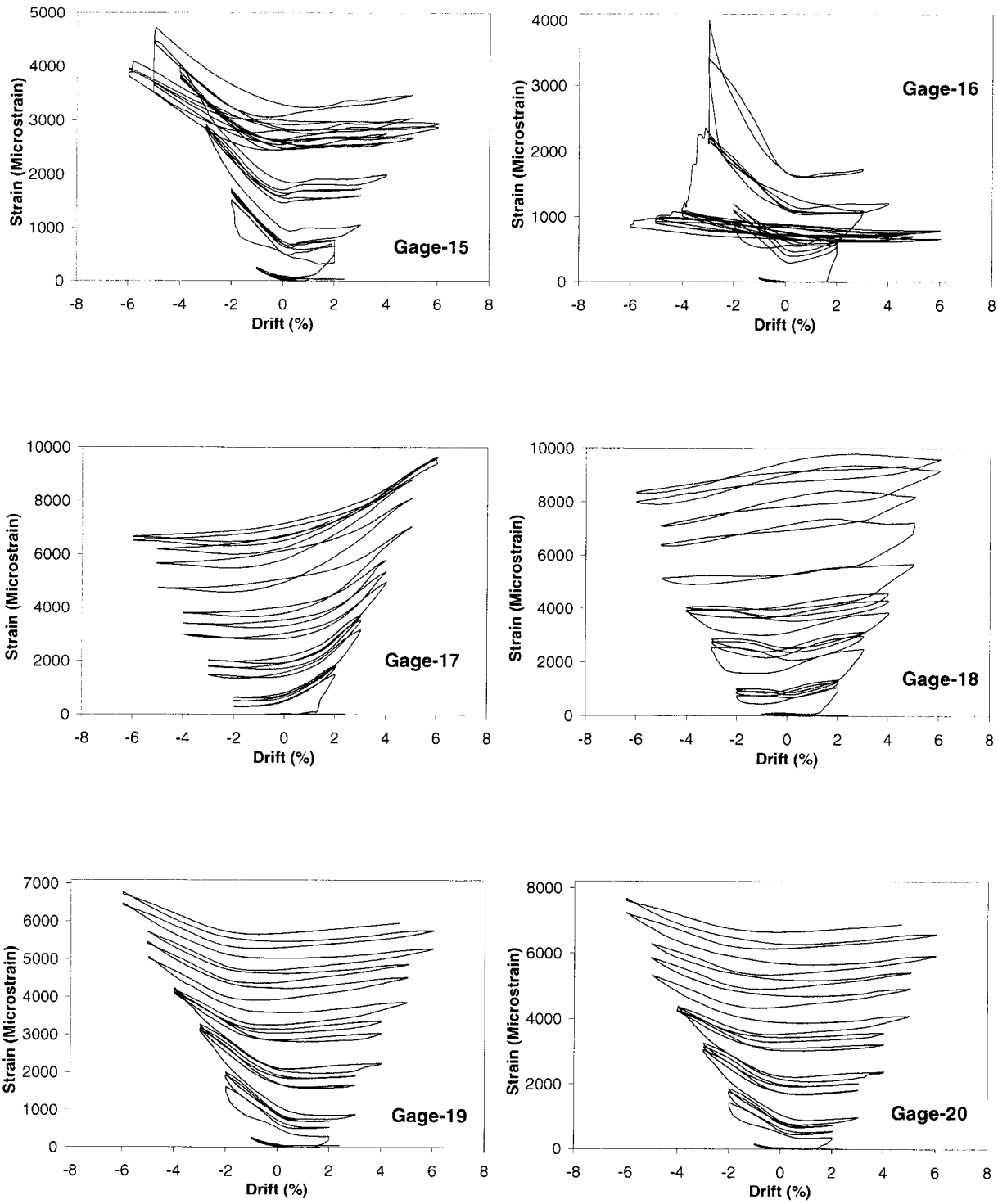

Fig. D.38 – Cont'd

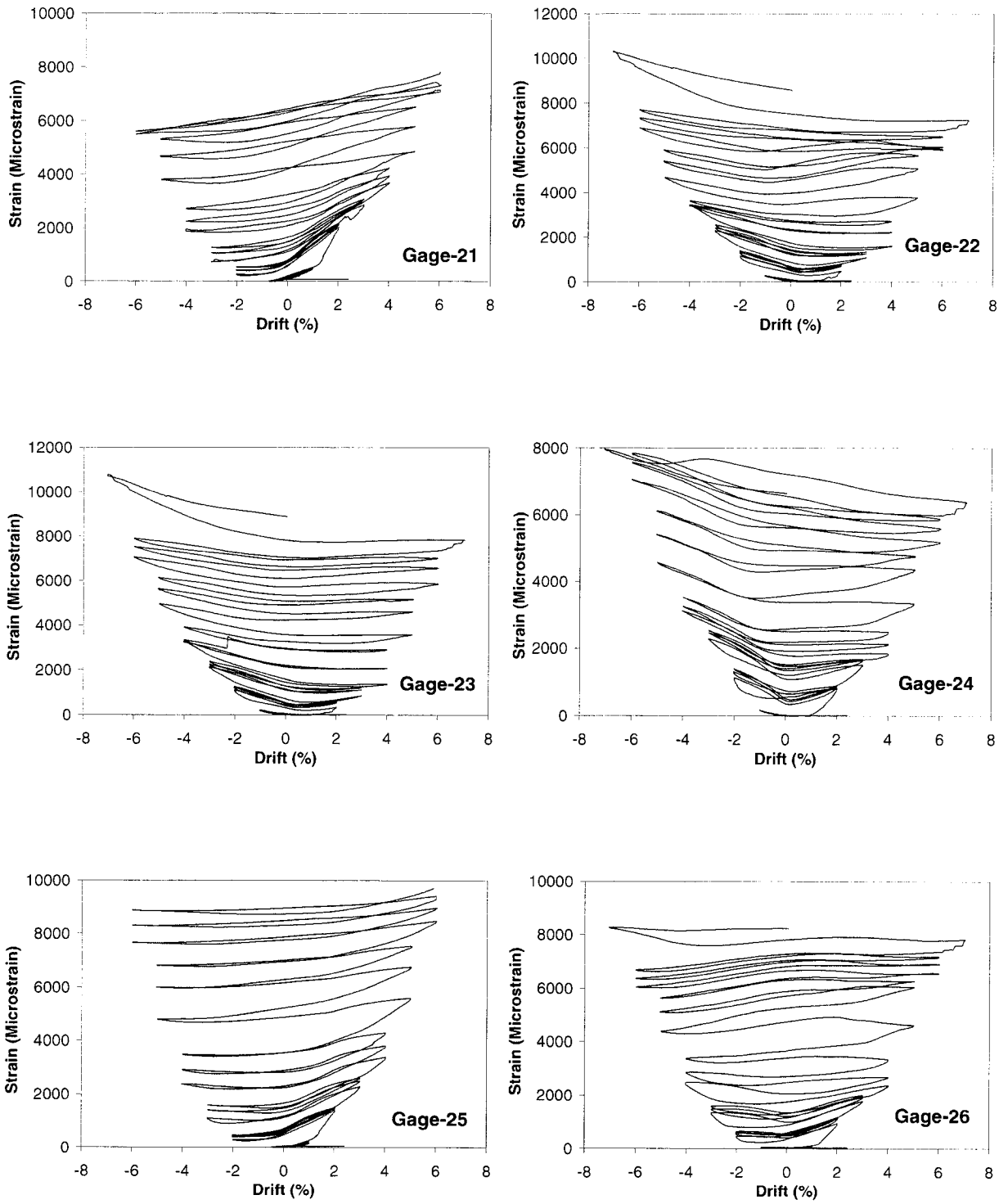

Fig. D.38 – Cont'd

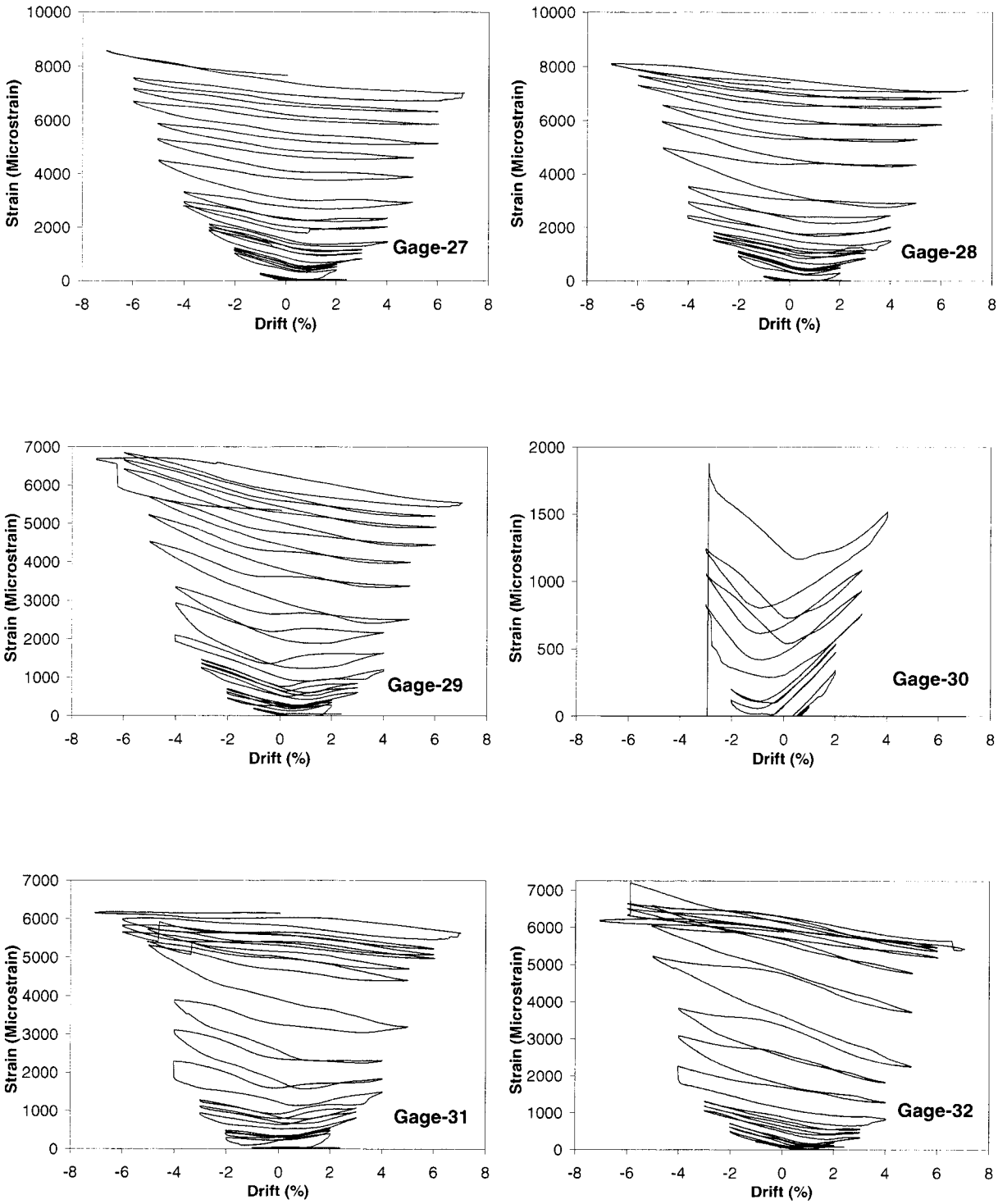

Fig. D.38 – Cont'd

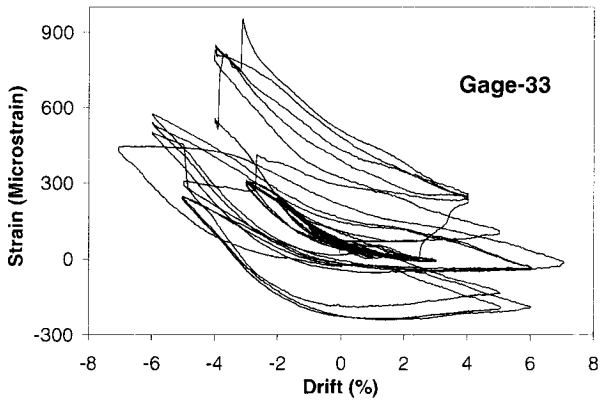

Fig. D.38 – Cont'd

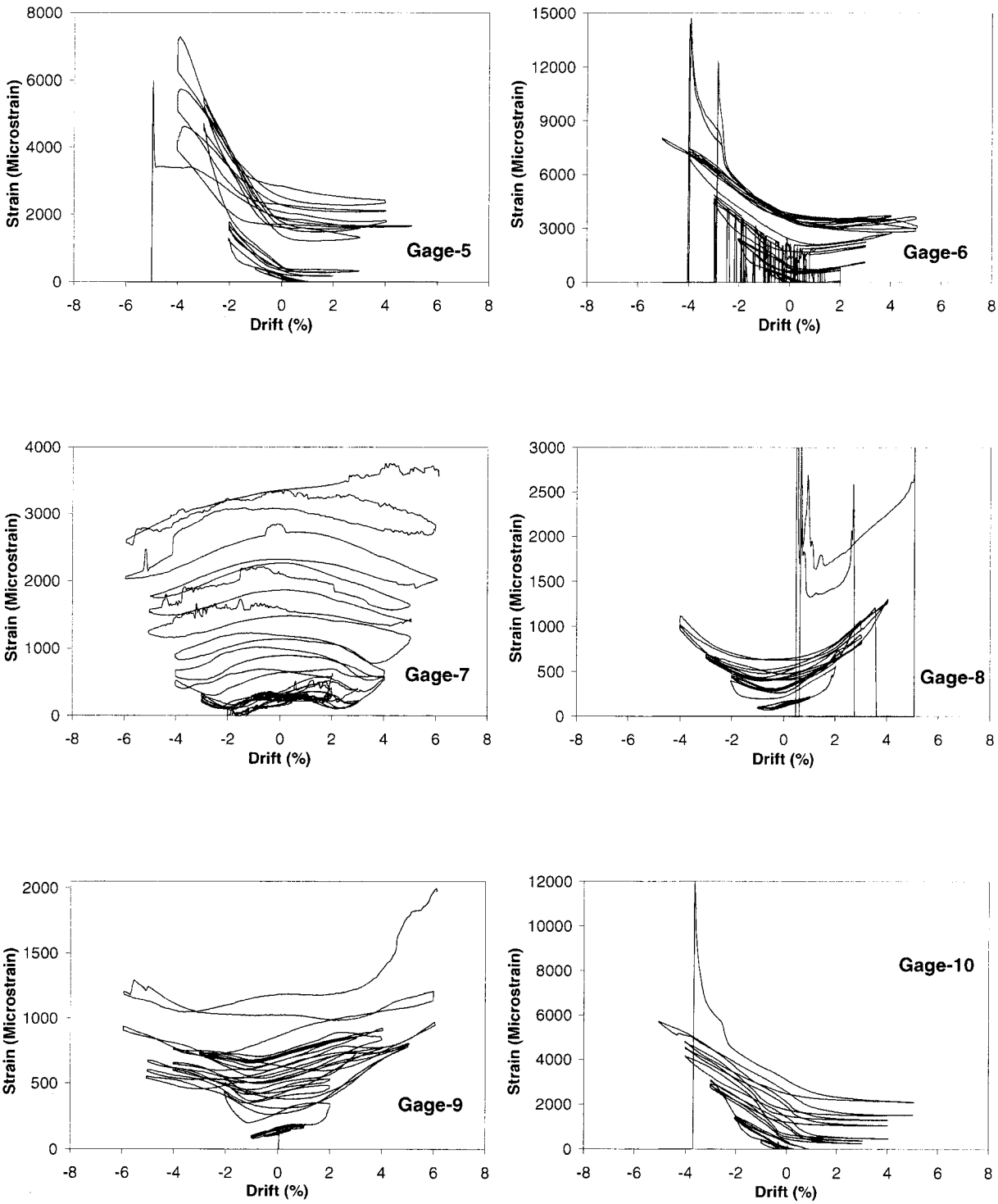

Fig. D.39 – Variation of transverse strain on the FRP Casing of Column RS-5

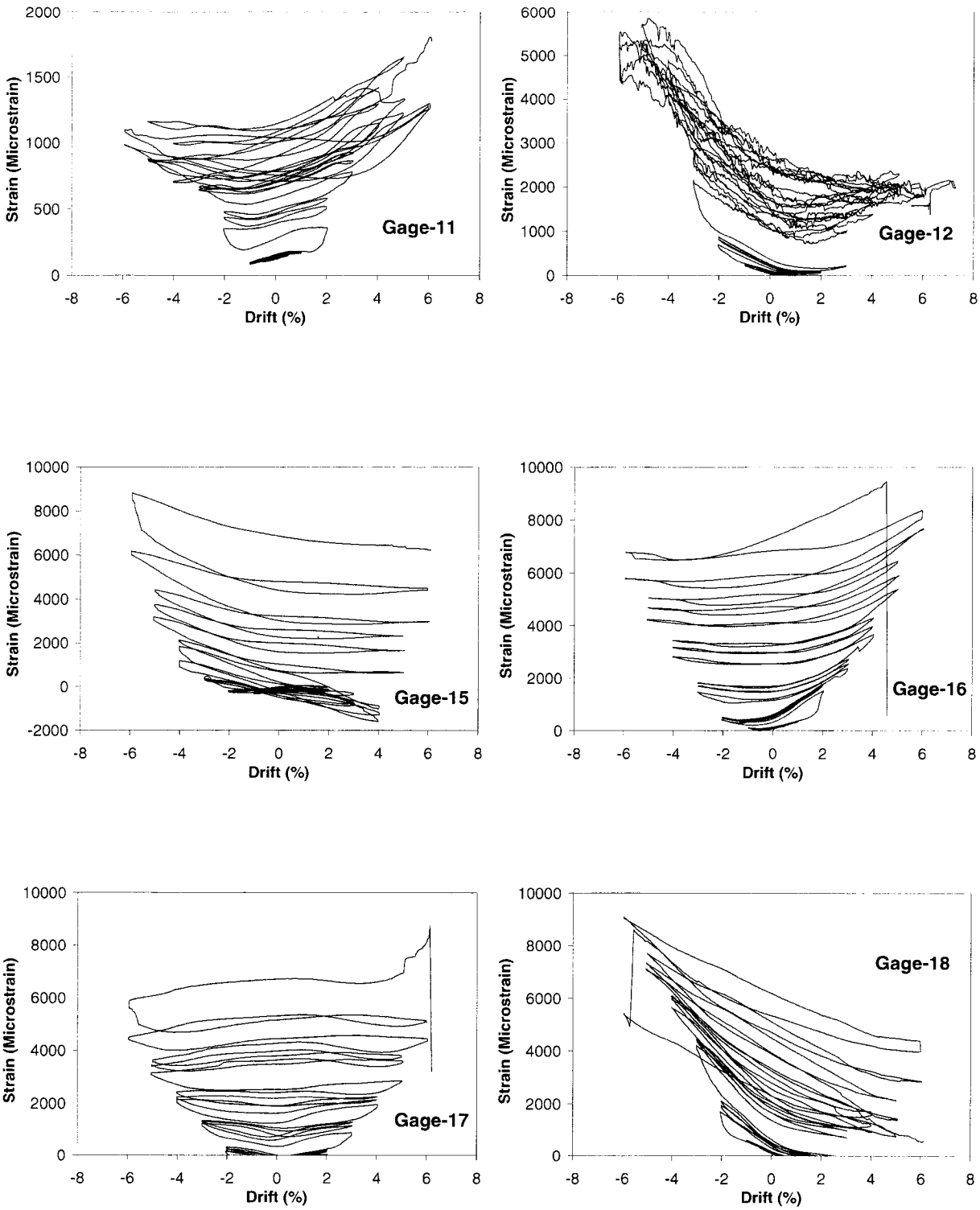

Fig. D.39 – Cont'd

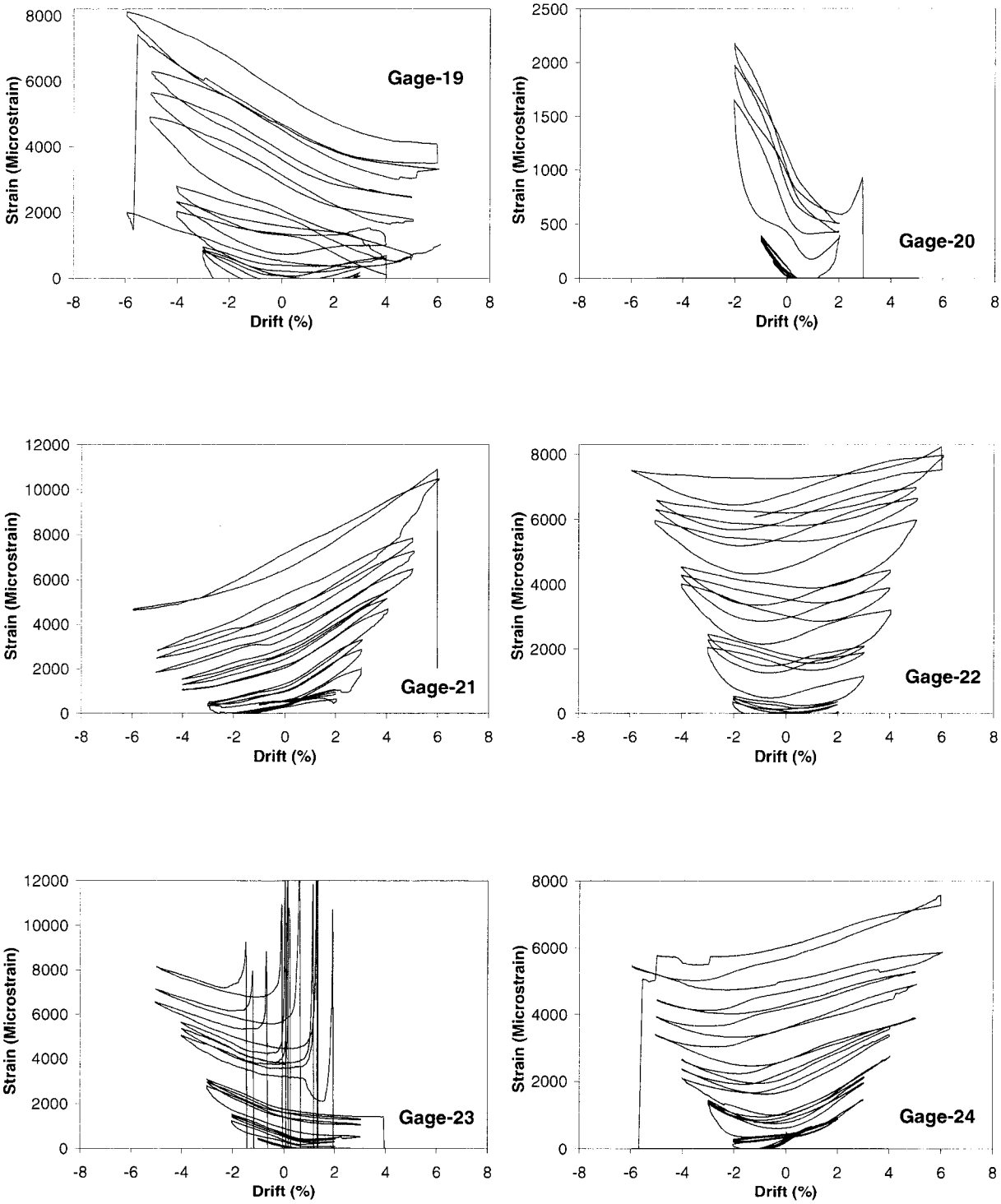

Fig. D.39 – Cont'd

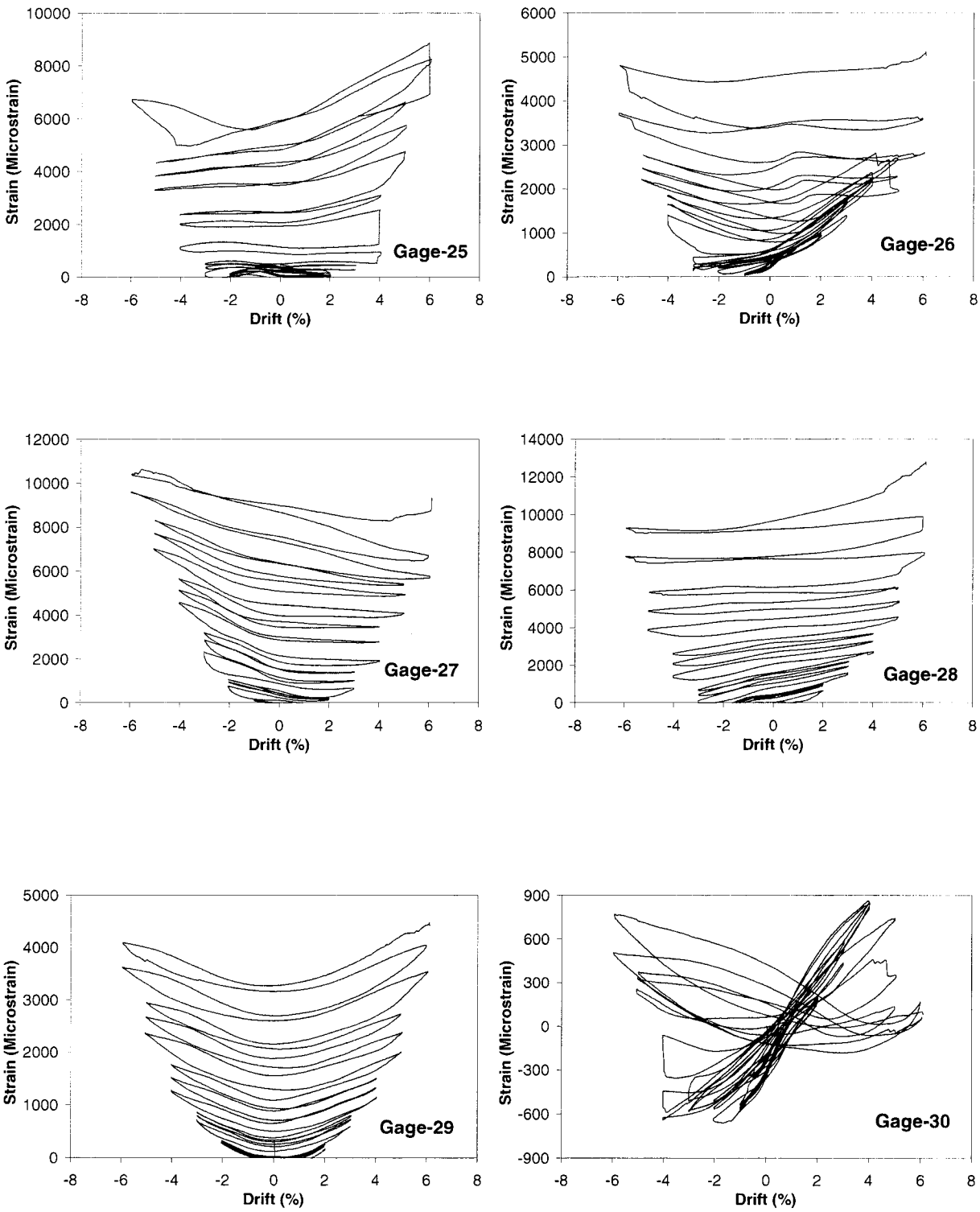

Fig. D.39 – Cont'd

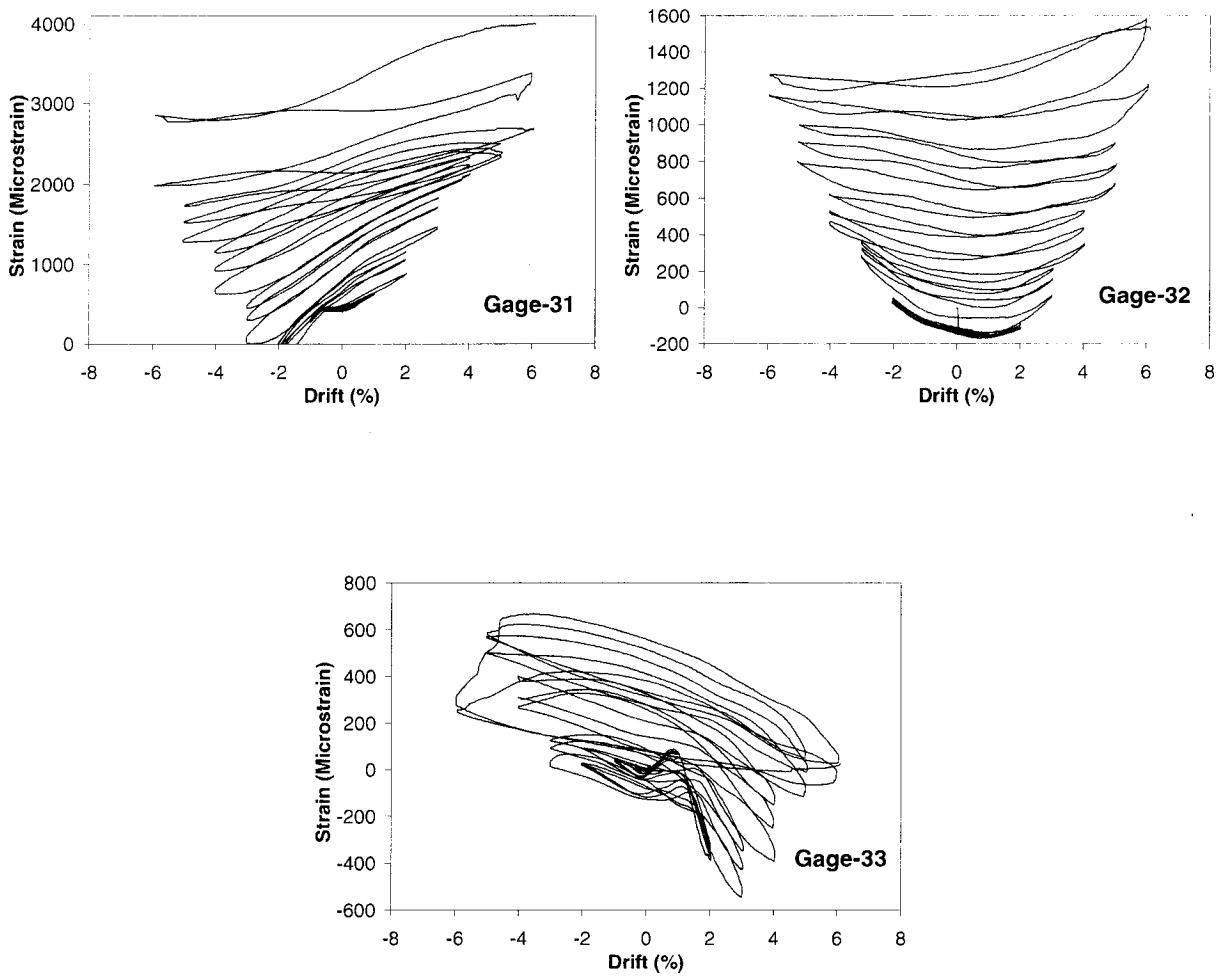

Fig. D.39 – Cont'd

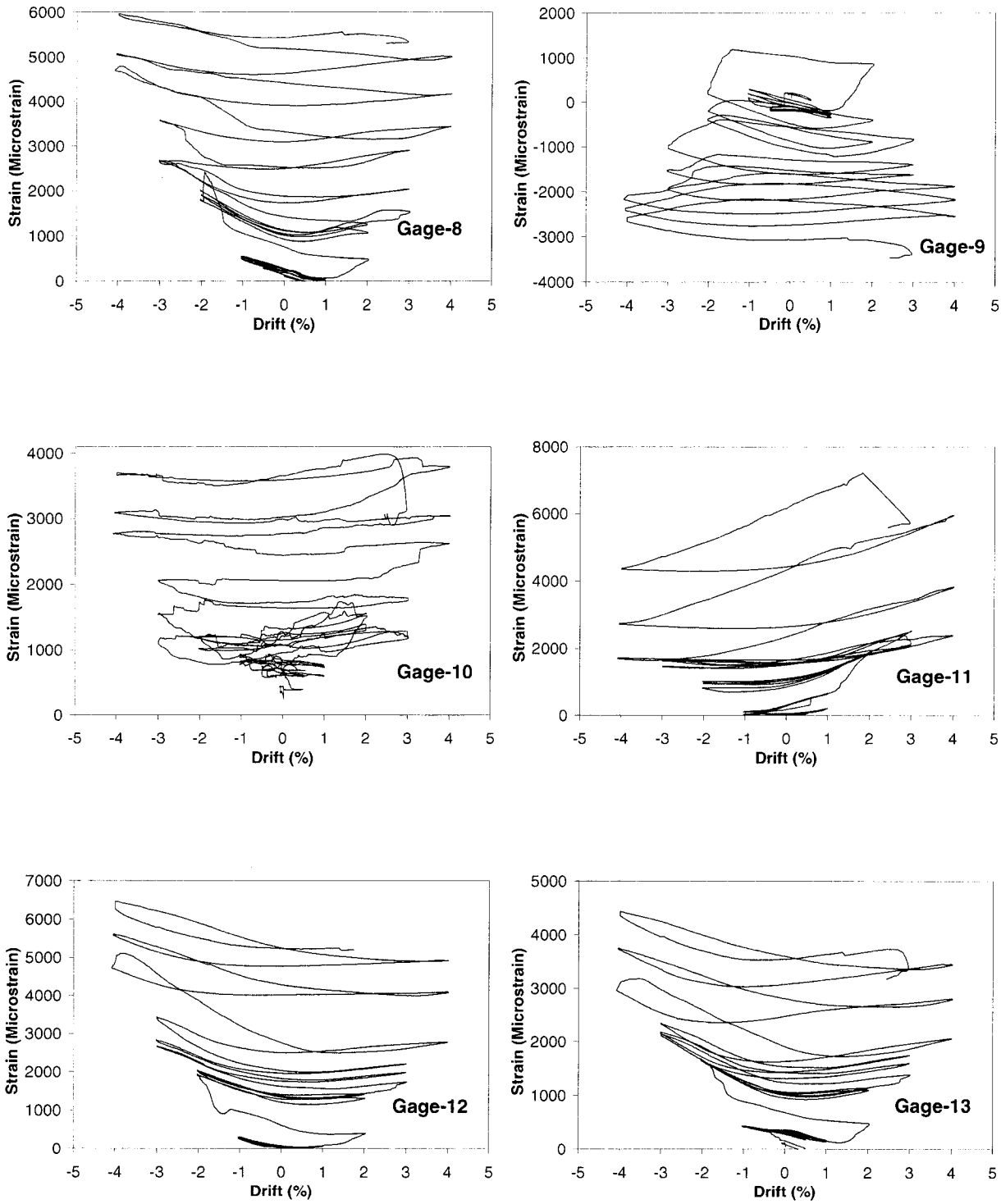

Fig. D.40 – Variation of transverse strain on the FRP Casing of Column RS-6

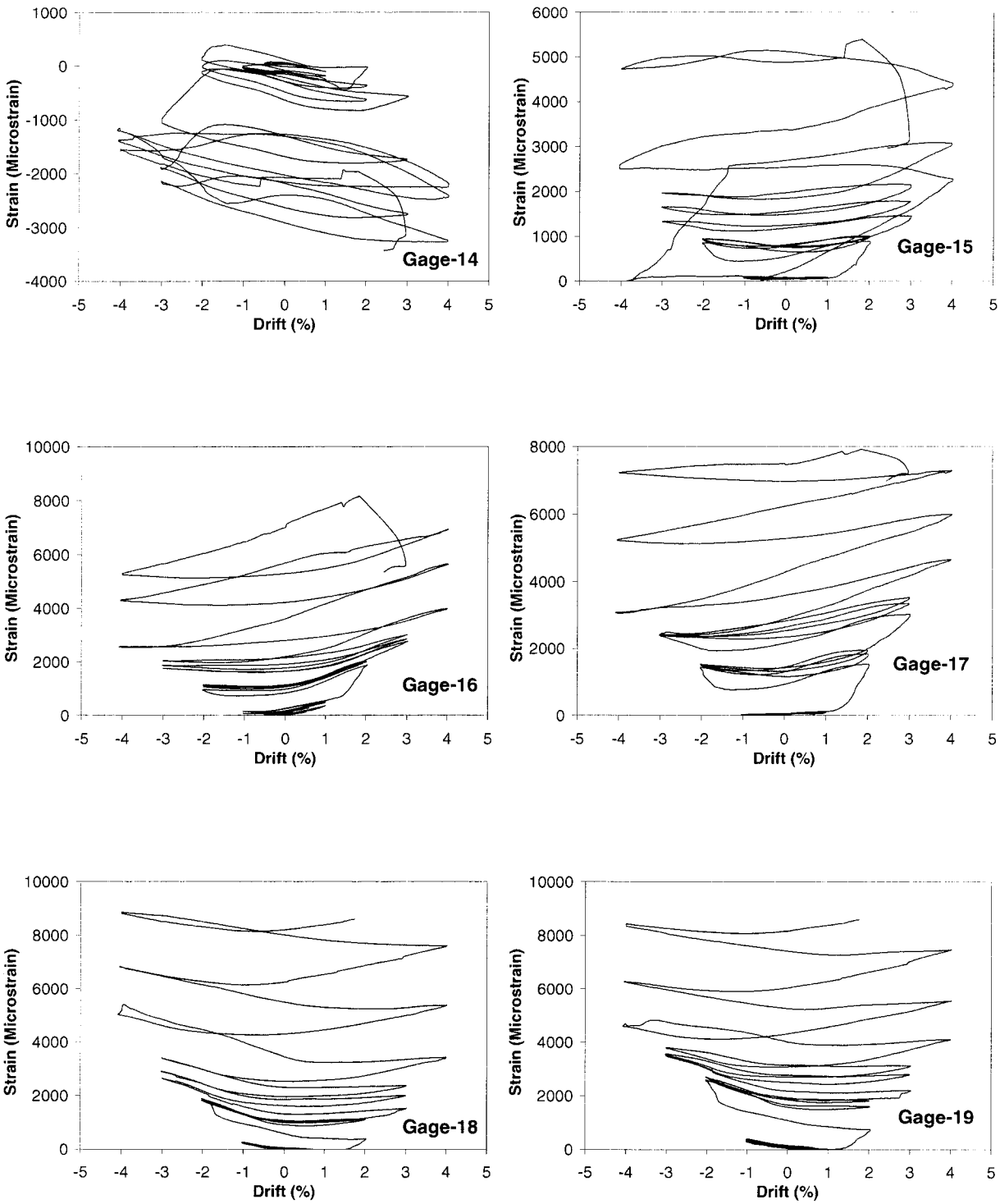

Fig. D.40 – Cont'd

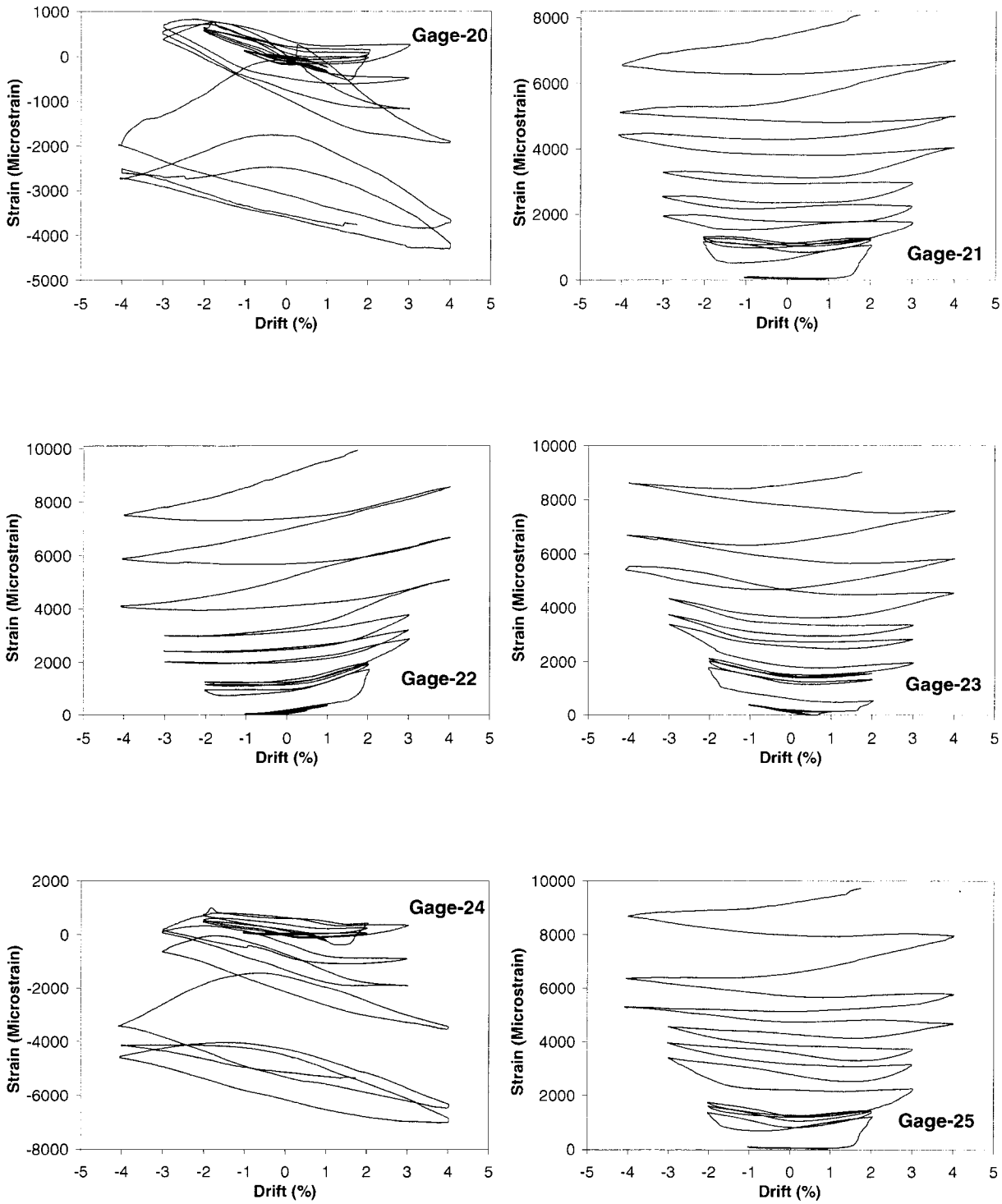

Fig. D.40 – Cont'd

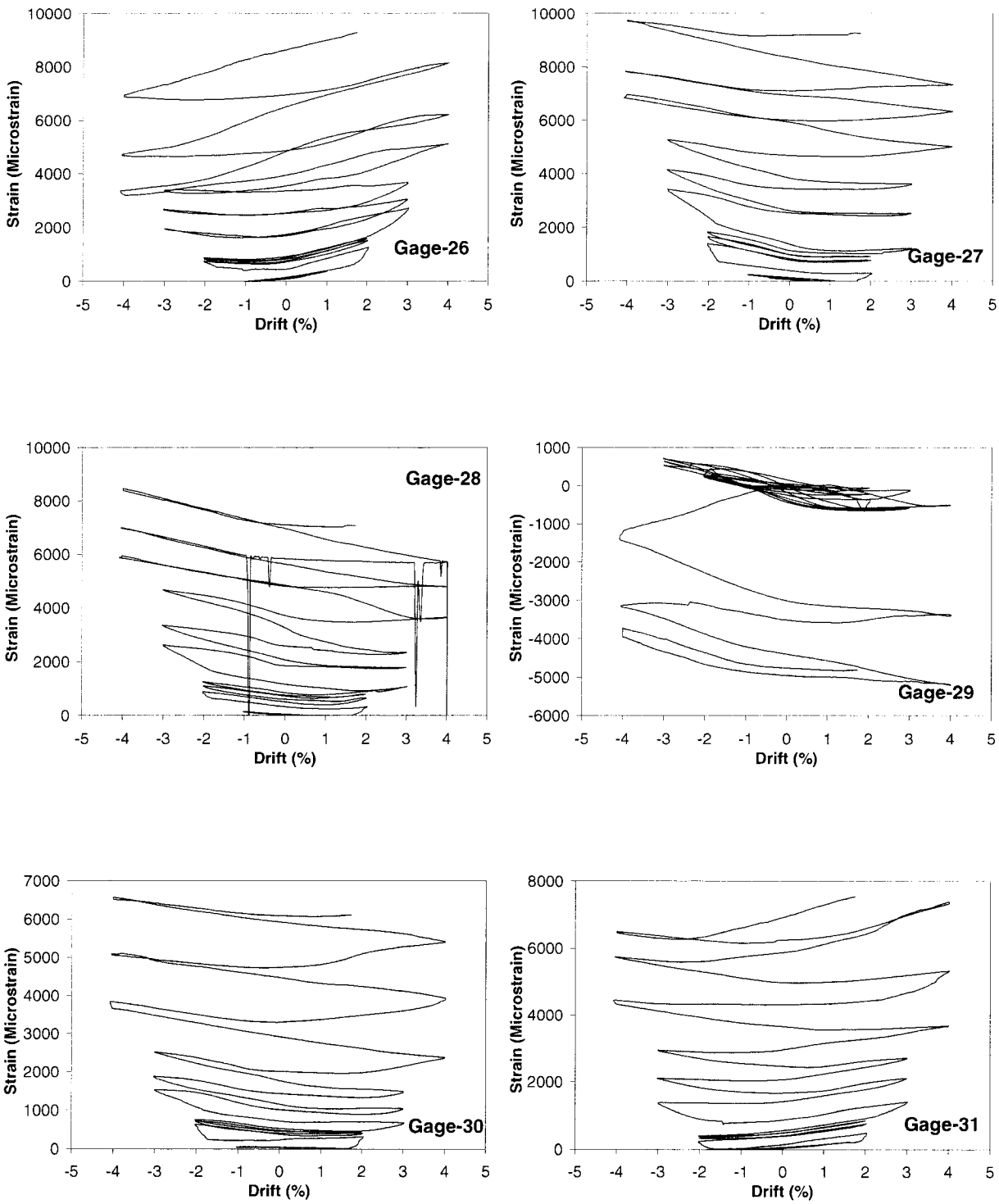

Fig. D.40 – Cont'd

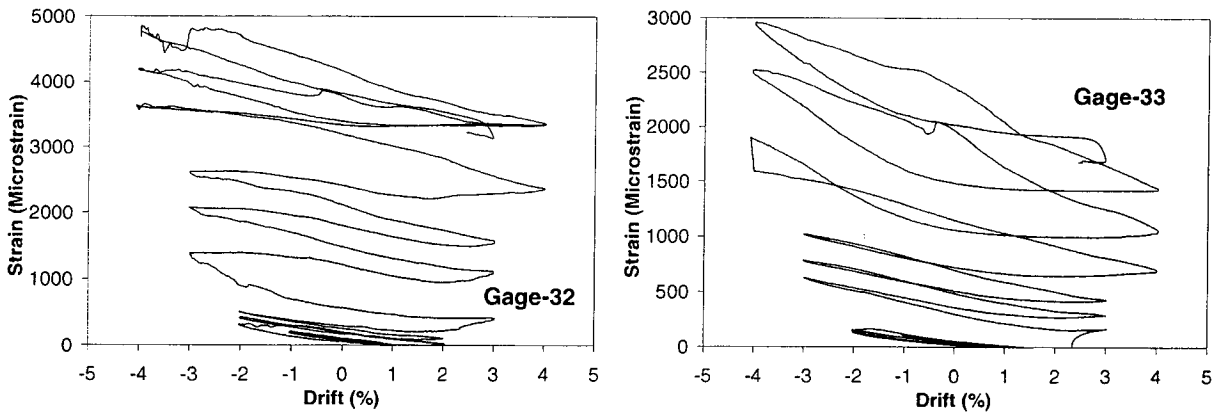

Fig. D.40 – Cont'd